The regulation of pharyngeal pouch morphogenesis by TBX1 and FGF signalling in the endoderm

Jackson, Abigail Laura

Awarding institution:
King's College London

The regulation of pharyngeal pouch morphogenesis by TBX1 and FGF signalling in the endoderm

A thesis submitted for the degree of Doctorate of Philosophy at King's College London

2012

Abigail Laura Jackson

King's College London
The Dental Institute
Department of Craniofacial Development and Stem Cell Biology

Table of Contents

List of tables

List of Figures

Abbreviations

A-P	Anterior -posterior
BMP	Bone morphogenetic protein
bp	Base pairs
Cyp26	Cytochrome p450, family 26
$ddH_2 0$	Double distilled water
DEPC	Diethyl pyrocarbonate
D-V	Dorsal-ventral
E	Days of embryonic development
EtBr	Ethidium bromide
EtOH	Ethanol
FGF	Fibroblast growth factor
FGFR	Fibroblast growth factor receptor
Fgf8cHet^{Sox17}	*Sox17$^{icre/+}$;Fgf8$^{flox/+}$*
Fgf8cKO^{Sox17}	*Sox17$^{icre/+}$;Fgf8$^{flox/-}$*
F3;8cHet^{Sox17}	*Sox17$^{icre/+}$;Fgf3$^{flox/+}$;Fgf8$^{flox/+}$*
F3cHet;F8cKO^{Sox17}	*Sox17$^{icre/+}$;Fgf3$^{flox/+}$;Fgf8$^{flox/-}$*
F3cKO;F8cHet^{Sox17}	*Sox17$^{icre/+}$;Fgf3$^{flox/-}$;Fgf8$^{flox/+}$*
F3;8cKO^{Sox17}	*Sox17$^{icre/+}$;Fgf3$^{flox/-}$;Fgf8$^{flox/-}$*
H-E	Haematoxylin-Eosin
HRP	Horseradish peroxidase
Sox17^{icre}	*Sox17-2A-iCre*
IHC	Immunohistochemistry
ISH	*in-situ* hybridisation

kb	Kilo base
MABT	Maleic acid buffer with Tween-20
MeOH	Methanol
ME-KO	*Mesp1$^{cre/+}$;Tbx1$^{flox/-}$*
min(s)	Minute(s)
NTMT	Sodium (Na) chloride- Tris-Magnesium-Tween-20 buffer
O/N	Overnight
PA	Pharyngeal apparatus
PBS	Phosphate buffered saline
PBT	PBS with Tween-20
PCR	polymerase chain reaction
PE-KO	*Foxg1$^{cre/+}$;Tbx1$^{flox/-}$*
PFA	Paraformaldehyde
PSE-KO	*Ap2alphaIRES$^{cre/+}$;Tbx1$^{flox/-}$*
rpm	Revolutions per minute
RA	Retinoic acid
R1;R2cHet^{Sox17}	*Sox17$^{ice/+}$;Fgfr1;$^{flox/+}$;Fgfr2;$^{flox+-}$*
R1cKO;R2cHet^{Sox17}	*Sox17$^{ice/+}$;Fgfr1;$^{flox/-}$;Fgfr2;$^{flox/+}$*
R1cHet;R2cKO^{Sox17}	*Sox17$^{ice/+}$;Fgfr1;$^{flox/+}$;Fgfr2;$^{flox/-}$*
R1;R2cKO^{Sox17}	*Sox17$^{ice/+}$;Fgfr1;$^{flox/-}$;Fgfr2;$^{flox/-}$*
Spry1;Spry2;Tbx1cHet^{Sox17}	*Sox17$^{ice/+}$; Spry1 $^{flox/+}$;Spry2 $^{flox/+}$;Tbx1$^{flox/+}$*
Spry1;Spry2cHet; Tbx1cKO^{Sox17}	*Sox17$^{ice/+}$; Spry1 $^{flox/+}$;Spry2 $^{flox/+}$;Tbx1$^{flox/-}$*
S	Somite stage
SEM	Standard error of the mean

SDS	Sodium dodecyl sulphate
SHH	Sonic Hedgehog
SSC	Standard saline citrate
TBST	Tris buffered salts with Tween-20
Tbx1cHet^{Sox17}	*Sox17$^{ice/+}$;Tbx1$^{flox/+}$*
Tbx1cKO^{Sox17}	*Sox17$^{ice/+}$;Tbx1$^{flox/-}$*
TE	Tris-EDTA buffer
Tris	Tris hydroxymethylaminomethane
Tween-20	Polyoxyethylenesorbitan monolaurate
v/v	Volume/volume
w/v	Weight/volume

Acknowledgements

Firstly I would like to thank Dr Albert Basson for giving me the opportunity to work in his lab, for his patience and advice and for providing me with the opportunity to pursue such an interesting project. I have been lucky enough to study for my PhD in a department that not only has state-of-the-art facilities but also state-of-the-art people! Chris, Martin, Sharon and Angela – I know the lab and department would fall apart without you all. Angela - I would have fallen apart many a time without your comforting words and secret stash of chocolate! Triona, Jacqui and Harriet - thank you for your understanding, your friendship and all your help over the past four years. In particular I would like to thank the current and past members of the Basson lab, you have made my PhD - I could not have asked for better people to work alongside. Kieran, Mohi, Hagen and Yurichio - you have been the life and soul of many a night/lab trip out; thank you for making me laugh so much. Samantha, Jenny, Subreena and Tian - I could dedicate a page of thanks to each of you. You are amazing scientists. More importantly you are amazing people, no one could ask for better friends.

Finally I would like to thank my family, all of whom have been incredibly supportive and encouraging throughout my PhD. Gramps, Granddad and Grandma - I wish you could have seen what I have achieved, I know you would have been proud. Mum, Dad and Edmund - I couldn't have done this without you; I am beyond lucky to have such a wonderful family. Chris - you are my rock, thank you. This is for us. Always.

Abstract

The pharyngeal apparatus is comprised of a series of pharyngeal arches that are defined by the evagination of endodermal pouches toward the ectoderm. Whilst the transcription factor *T-box 1* (*Tbx1*) and the *Fibroblast growth factor 8* (*Fgf8*) are both required for caudal pouch formation, a role for these factors in the endoderm during pouch morphogenesis has not been confirmed. The observation that *Fgf8* expression is lost in *Tbx1* homozygous null mutant embryos has lead to the hypothesis that FGF8 functions directly downstream of TBX1 during pouch formation. To test this hypothesis the *Sox17-2A-icre* line was used to delete *Fgf8*, *Fibroblast growth factor receptor 1* (*Fgfr1*) and *Fibroblast growth factor receptor* 2 (*Fgfr2*) and *Tbx1* in the endoderm, and analyse the development of the pouches and their derivatives. In all embryos with an endoderm specific deletion of *Tbx1*, the caudal PA remained un-segmented as caudal pouches 3 and 4 do not form. The deletion of endodermal *Tbx1* severely reduced the expression of *Fgf8* in the endoderm; however, the expression of Fibroblast Growth Factor (FGF) signalling readouts was maintained. All rostral and caudal pouches are present in embryos with an endoderm specific deletion of *Fgf8*, indicating that the loss of *Fgf8* alone from this epithelium is not sufficient to disrupt the process of pouch evagination. The compound deletion of *Fgfr1* and *Fgfr2* from the endoderm did not prevent pouch evagination but did cause 3rd pouch hypoplasia and the rostral pouches to fuse. These data indicate that FGF signalling downstream of *Fgfr1* and *Fgfr2* and *Tbx1* are important for pouch formation but that they are likely to function in parallel pathways within the endoderm. Further data suggests that TBX1 may be acting in an FGF independent manner to control the polarity of actin within the endodermal epithelia. Overall this data reveals that both cell signalling and actin polarity must be tightly regulated within the endoderm for the pharyngeal pouches to form correctly.

Chapter 1

Introduction

1.1 Overview of the pharyngeal apparatus

All vertebrate species have a segmented body plan (Maroto et al., 2012). Segmentation is the process of dividing an area of tissue into smaller sections, a process that is often reiterated many times during development. Many examples of segmentation are visible along the anterior-posterior (A-P) axis of the vertebrate embryo's body, from the hindbrain to the somites at the posterior tip of the embryo's trunk (Alexander et al., 2009; Tumpel et al., 2009). A classic, well understood, example of segmentation is somitogenesis, the process of forming successive pairs of somites from the un-segmented paraxial or presomitic mesoderm (PSM) (Maroto et al., 2012). The division of the PSM into somites compartmentalises the embryo's trunk along its A-P axis, enabling a multitude of derivatives to differentiate from this tissue, including vertebrae, skeletal muscle, and dermis (Maroto et al., 2012). The modularity of the vertebrate body is key to the evolution and diversity of vertebrates, as alterations to the process of segmentation can dramatically change the embryos body plan (Carroll, 2001). For example, the dramatic increase in somite number in snakes' bodies enabled their limbless bodies to remain mobile (Gomez and Pourquie, 2009).

The pharyngeal apparatus (PA) is another example of a segmented structure in the vertebrate embryo whose modularity has altered during evolution (Graham, 2001). The PA is a transient structure common to all chordates that is comprised of a series of metameric segments, the pharyngeal arches, segregated by the out pocketing of the pharyngeal endoderm (the pharyngeal pouches) (Graham, 2001). A reduction in the number of pouches is evident in Amniotes, relative to the more primitive Gnathostomes. The reduction and diversification of the pharyngeal pouches during Amniote evolution was likely an adaptive advantage to the

amniotes during their transition to land (Graham, 2001) however, the loss of pharyngeal pouches during development is disadvantageous (see section 1.2).

Pharyngeal pouches are formed as cells of the pharyngeal endoderm migrate laterally toward the pharyngeal ectoderm (Graham, 2001; Graham, 2003). The pharyngeal pouches develop as part of a greater structure, the PA. Superficially the PA appears as iterative bulges flanking the embryo's head in an area between the primitive heart (ventrally) and the rhombomeres of the hindbrain (dorsally), (see Fig 1a). The PA is identifiable from embryonic day of development (E) 8.5 until E11.0 when the majority of this transient structure has become incorporated into structures essential for postnatal survival (see section 1.1.1) (Tamarin and Boyde, 1977). Despite the transient presence of the PA, the structure is complex and its correct development is essential for embryonic viability.

A longitudinal cross-section reveals that the apparatus is composed of six cell types; ectoderm, mesoderm and endoderm and cranial neural crest cells (CNCC) that differentiate into mesenchyme and endothelial cells (see Fig 1b). Each 'bulge', defined as a pharyngeal arch, is covered in an external ectodermal epithelium and is populated by CNCC from the mid and hindbrain that form the arch ectomesenchyme (Graham, 2001; Graham, 2003). A core of mesodermal cells forms within each arch, adjacent to the pharyngeal arch artery (PAA). CNCC also contribute to the PAAs, differentiating into smooth muscle cells that line each vessel. The innermost tissue of the PA is the endodermal epithelium that lines the pharyngeal arches, separating them from the pharyngeal cavity (Graham, 2003; Graham et al., 2004). Finger-like projections of pharyngeal endoderm, the pharyngeal pouches, divide the mesenchymal tissue of the PA as they evaginate laterally toward the ectoderm (Graham, 2001; Graham, 2003). When the

evaginating endoderm contacts the invaginating ectoderm, individual arches are segregated and become defined as separate entities. In mouse and man five pharyngeal arches (I-IV and VI) and four pharyngeal pouches (pp1-4) form along the A-P axis of the embryo's body (see Fig 1a and 1b) (Graham, 2001).

In a manner akin to digit formation there is a temporal and positional requisite for correct development of the PA over 3 axes; anterior-posterior [A-P], ventral-dorsal [V-D] and proximal-distal [P-D]. However, the PA has to co-ordinate the integration of a much higher number of individual cell types, not just ectoderm and mesenchyme, as is the case for digit development (Graham, 2003; Tickle, 2006). Signalling between and within all cell types must be tightly regulated to ensure the PA and its derivatives develop appropriately (Graham et al., 2004). It is becoming apparent that the pharyngeal endoderm plays a prominent, key role in the patterning of the pharyngeal arches and has the ability to influence the development of multiple cell types within the PA (Graham et al., 2004).

Fig 1a

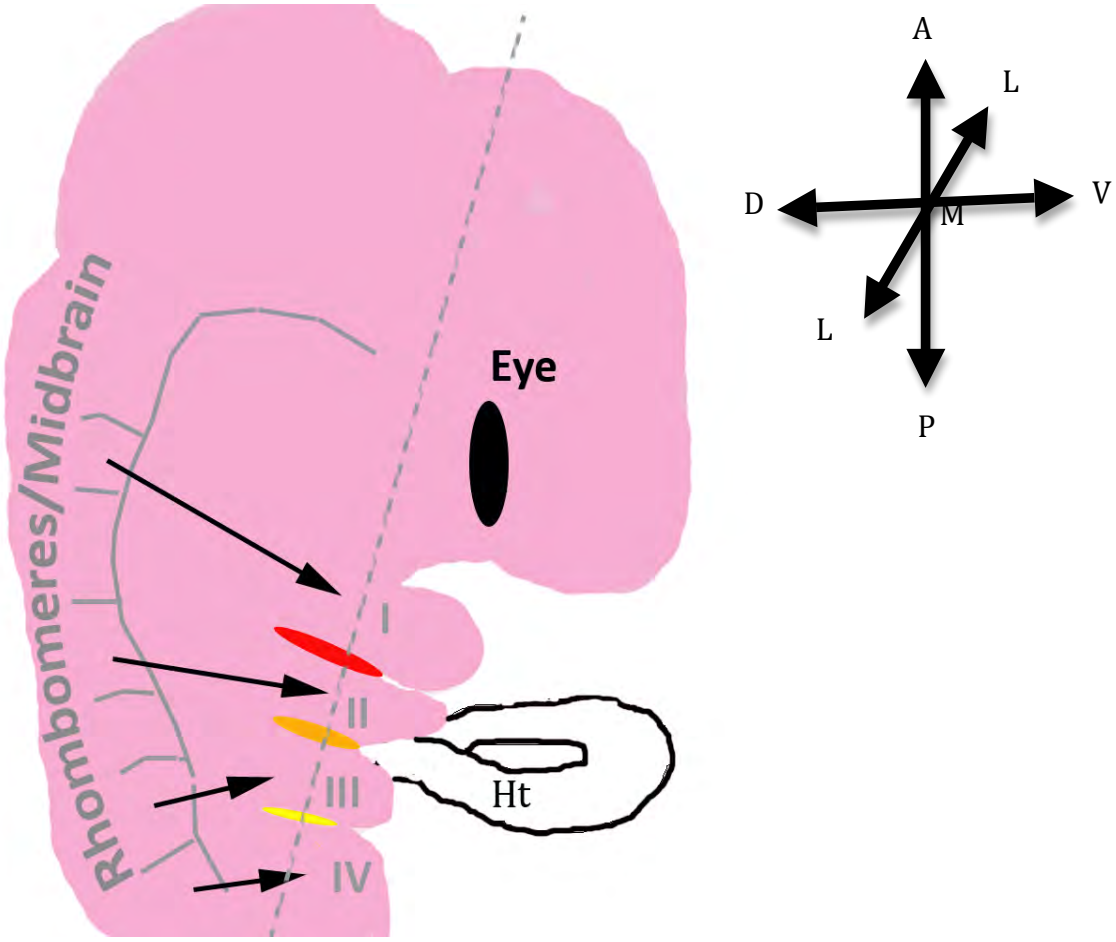
Rhombomeres/Midbrain
Eye
I
II
III
IV
Ht
A
L
D
V
M
L
P

Fig 1b


A
D
L
L
M
A
V
P
I
II
III
IV
VI
pp1
pp2
pp3
pp4

Fig 1a. A schematic of an E9.5 mouse embryo viewed from the side, adapted from Graham 2001, depicting the pharyngeal apparatus. The pharyngeal aches appear as bulges forming between the heart (ht) ventrally and the rhombomeres/midbrain dorsally in a position caudal to the eye. Three pharyngeal pouches can be distinguished externally at this stage of mouse development and are highlighted in colour in the schematic to aid identification: red = 1st pharyngeal pouch, orange = 2nd pharyngeal pouch, yellow = 3rd pharyngeal pouch. Each arch (I to IV) is defined and segregated by the formation of a pharyngeal pouch. Arrows represent cranial neural crest migrating into the arches from the midbrain and rhombomeres of the hindbrain (see Fig 3 for a summary of the CNCC streams). Arrows to the right of the schematic determine the orientation of the schematised embryo; A = anterior, P = posterior, L = lateral, M = medial, V= ventral, D = dorsal. The grey dashed line through the pharyngeal apparatus represents the level/position of the schematic section displayed in Fig 1b.

Fig 1b: A schematic of a frontal section cut through the pharyngeal apparatus of a vertebrate embryo adapted from Graham, 2003. Each of the six cell types within the PA are distinguished by a different colour, highlighting the complexity of this structure. Red = endoderm; light brown = cranial neural crest derived pharyngeal mesenchyme; yellow = mesodermal core of the arch, purple = cranial neural crest and mesodermally derived pharyngeal arch artery, green = ectoderm. Each pharyngeal pouch is labelled from anterior to posterior, (1-4, pp, colour coded in the same way as Fig 1a). The arches are labelled as I-IV and VI over the anterior-posterior axis of the pharyngeal apparatus. Pharyngeal arch VI and pharyngeal pouch 4 are labelled in the cross-section but not in the whole mount schematic of the pharyngeal apparatus because these structures are not easily identified in E9.5 mouse embryos viewed in whole mount. Arrows to the left of the schematic determine the orientation of the schematised embryo; A = anterior, P = posterior, L = lateral, M = medial, V= ventral, D = dorsal.

1.1.1 The pharyngeal endoderm

Anatomical studies, including those conducted as early as the 19th Century, have documented the development of the pharyngeal pouches in various species of vertebrate embryos, including the pig, rat and in humans (Badertscher, 1915; Kingsbury, 1915; Rogers, 1927). The fundamentals of pouch morphogenesis, such as the A-P evagination of the pharyngeal endoderm that defines a series of pharyngeal arches to generate a basic pattern of facial development, is relative between the species. However, subtle differences exist between the size and patterning of pouches between vertebrate species and in the derivatives they form, (Badertscher, 1915; Kingsbury, 1915; Rogers, 1927; Grevellec and Tucker, 2010). The origin and number of parathyroid organs are one example of such differences. The parathyroid is formed from the 3rd pouch in the mouse embryo, whereas two parathyroid organs develop in the chick embryo, one from the 3rd pouch and one from the 4th pouch (Grevellec and Tucker, 2010). A recent paper by Grevellec et al. suggests the location of parathyroid development in the pharyngeal endoderm may be regulated by a SHH mediated repression of the presumptive parathyroid marker *Glial cells missing homolog 2* (*Gcm2*) (Grevellec et al., 2011). This thesis utilises mouse embryos to study the mechanisms that regulate mammalian pouch morphogenesis, thus the text below details the pertinent points of this process in this species.

The definitive endoderm is established during gastrulation as cells of the epiblast (an epithelial structure formed at E4.0) migrate through and exit the primitive streak (PS) (Zorn and Wells, 2009). Lineage tracing experiments have determined that the order the cells leave the PS partially determines their fate. The medial and lateral anterior-definitive endoderm (and axial mesoderm) exits the PS first. Cells

that egress later from the streak form the posterior definitive endoderm. A number of genes are also essential for the specification of endoderm at blastula and gastrula stages of development, such as *Nodal*, as reviewed by Grappin-Botton et al. (Grapin-Botton, 2008; Zorn and Wells, 2009). The anterior and posterior subtypes of definitive endoderm both contribute to the formation of the primitive gut tube that by stage E8.0 is regionalised and extends from the 1st branchial arch to the hindgut (Tremblay and Zaret, 2005; Franklin et al., 2008). The posterior portion of this endodermal tube can be divided into the hindgut (which generates the large intestine) and the midgut, (which generates the small intestine). From the anterior portion of the endodermal tube the foregut will give rise to the lungs and liver, the stomach, biliary system and the pancreas; each organ forms by budding out of the endodermal tube (Tremblay and Zaret, 2005). At the most rostral position of the gut tube the pharyngeal pouches emerge. As with all derivatives of the anterior gut tube the pouches are initially identifiable as areas of endodermal 'out-pocketing'.

During the transient period of pharyngeal pouch development (E8.5-E11.0) the 'out pocketing' or evagination of the pharyngeal endoderm generates four pharyngeal pouches, described in detail below (Tamarin and Boyde, 1977). Time-lapse photography of evaginating endodermal cells in zebrafish embryos depicts the lateral movement of the cells away from the midline of the embryo (after their initial coalescence here), (Crump et al., 2004). This is in agreement with the description of endodermal evagination inferred from histological and topographical analysis of fixed PA tissue. In addition to evaginating laterally the pharyngeal endoderm must become constrained to form a narrow slit-like morphology. In chick embryos this process has found to require a network of actin

cables enriched along the apical side of the evaginating endoderm (Quinlan et al., 2004). Exposing the pharyngeal endoderm of a chick embryo to cytochlasin D, (a context dependent inhibitor of actin polymerisation), prevents the formation of actin supracables in this epithelia (Cooper, 1987). Depending on the time of exposure (prior to or during pouch evagination) the cytochlasin D exposed pouches form but do so with a splayed or convoluted morphology (Quinlan et al., 2004). It is hypothesised that the actin supracables in the endoderm act to constrain and support the epithelium as it evaginates, giving this process directionality.

Post-E8.5 in an area posterior to the telencephalon and anterior to the embryonic heart, the evagination of the pharyngeal endoderm begins (Tamarin and Boyde, 1977). Over the next four days of development endodermal 'out-pocketing' is initiated sequentially along the A-P axis of the embryo. By E9.0 the first pouch is evident as a prominent groove that defines the now enlarged 1st arch anteriorly and the 2nd arch posteriorly, the 2nd pouch is just emerging. Half a day later the 2nd arch has enlarged and appears more distinct as the 2nd pouch anterior to it lengthens laterally and narrows (Tamarin and Boyde, 1977). At E9.5 the evagination of the third pouch has also begun. Between E10.0 and E10.5 the 4th pouch evaginates from the endoderm in close proximity to the 3rd pouch, the 3rd and 4th arch (defined by the caudal pouches) are less pronounced than the rostral arches (Tamarin and Boyde, 1977). By E11.5 all the pharyngeal pouches have contacted the ectoderm giving the arches identity and shape that is permissive to CNCC, ectoderm and mesodermal cell differentiation. The caudal arches evident at E10.5 are masked at E11.5 by the posterior outgrowth of the caudal ectoderm (the cervical sinus) (Tamarin and Boyde, 1977). Post E11.5 the four pharyngeal

pouches and the five pharyngeal arches (1st – 4th and 6th arch, the 5th arch does not form in mammals) of the PA have begun to metamorphose into the various primordia to which they contribute (see Fig 3 and Table 1 for an overview of structure derived from aspects of the PA) (Tamarin and Boyde, 1977).

The pharyngeal endoderm gives rise to endocrine organs of the postnatal embryo. The thyroid forms from a ventral segment of *Nkx2.1* positive endoderm, proximal to the 2nd pharyngeal pouch and opposing the aortic sac (Biddinger and Ray, 1993; Manley and Capecchi, 1995). The thymus forms from *Forkhead box N1*, (*Foxn1*) positive cells (visible at E11.5) in the ventral posterior aspect of the 3rd pharyngeal pouch (Gordon et al., 2001). The parathyroid cells arise from a complementary dorsal-anterior aspect of the third pouch in mice that is marked from E9.5 by *Glial cells missing homolog 2 (Drosophila)* (*Gcm2*), expression (Gordon et al., 2001). At approximately E12.5 the parathyroid and thymus prymordia detach from the endoderm of the pharynx and migrate caudally (Blackburn and Manley, 2004; Grigorieva and Thakker, 2011). The thymus migrates most caudally to its final location above the heart and the parathyroid migrates to an area lateral to the thyroid in the neck (Blackburn and Manley, 2004; Grigorieva and Thakker, 2011). In mouse embryos the ultimobranchial bodies (UBs) arise from the 4th pharyngeal pouch (Kusakabe et al., 2006). By E12.5 the UBs have begun to grow ventral-laterally, as they migrate caudally (Kusakabe et al., 2006). They reach the thyroid around E13.5/14.0 and are fused to the thyroid by E14.5. Post E14.5 cells of the UB disseminate through the thyroid, giving rise to an even coverage of calcitonin cells (C-cells) by E19.0 (Kusakabe et al., 2006).

Whilst the stages of pharyngeal pouch development are well documented, the mechanisms controlling this process are not well understood. A number of signalling cascades are known to affect murine pouch morphogenesis but a requirement for these cascades in the endoderm during pouch formation has not been established (see section 1.3). In addition to forming endocrine organs, the pharyngeal pouches also influence the development of adjacent non-endodermal cells within each arch, as discussed below. Understanding how pharyngeal pouch morphogenesis is regulated will improve our understanding of how the PA develops as a whole.

Fig 2

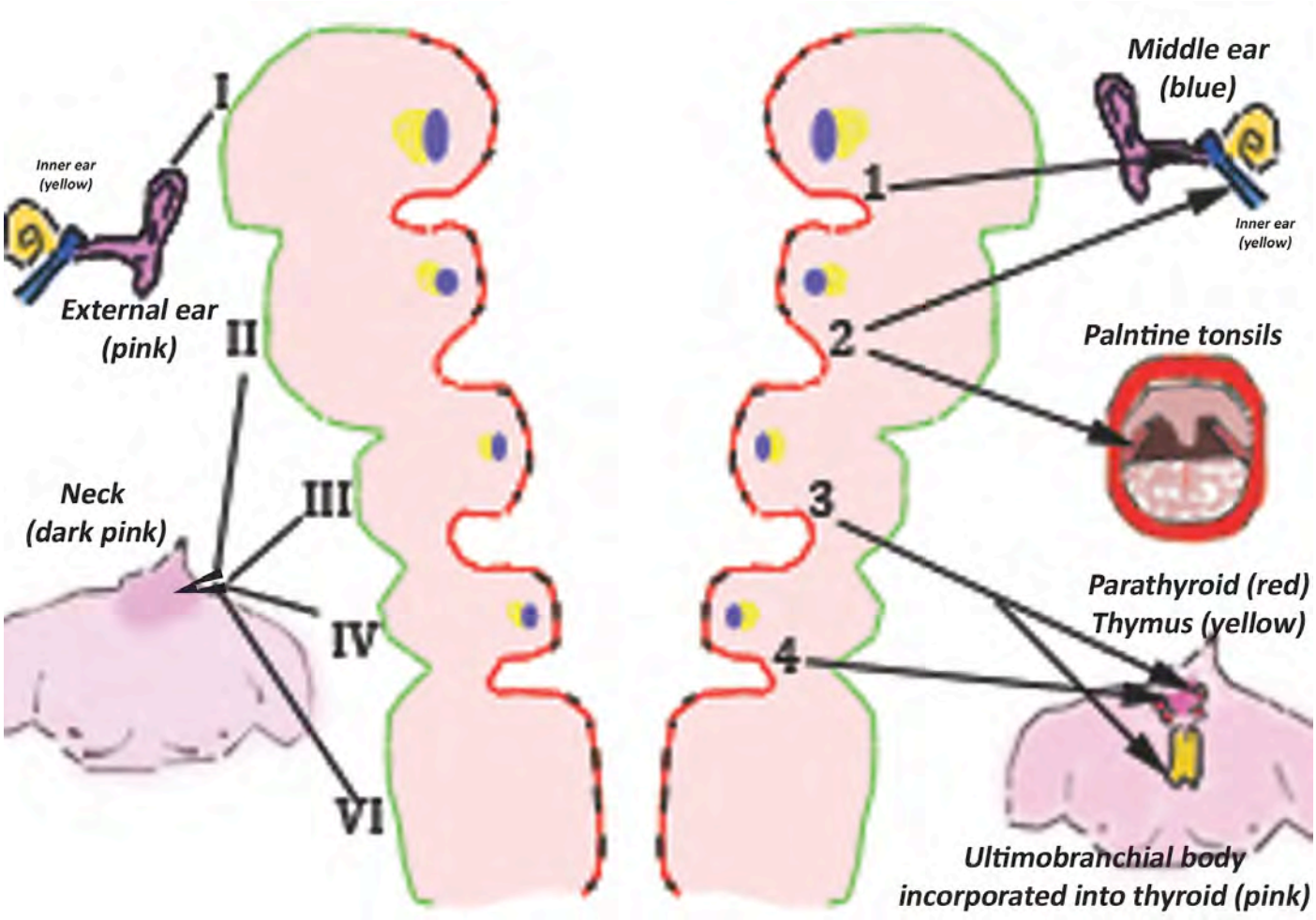

Fig 2 Identifies an overview of anatomical structures present in the postnatal mouse that are derived from specific pharyngeal arches and pouches within the pharyngeal apparatus of the embryonic mouse. Is a schematic of a frontal section cut through the pharyngeal apparatus of a mouse embryo, (adapted from Yamagishi and Srivastava et al. 2003b), identifying the overt postnatal structures that are contributed to by the pharyngeal pouches (images on the right) and pharyngeal arch clefts (images on the left). The 1st pouch and the 2nd pouch, respectively, give rise to the tympanic membrane and the Eustachian tube, which are structures of the middle ear (highlighted in blue in the schematic of the ear that also depicts the outer ear in pink and inner ear in yellow). The palatine tonsils are also derived from the second pouch. The thymus (large yellow organ in the chest) and the parathyroid glands (red circles observed in the lateral aspects of the thyroid [depicted as a pink bow shaped organ in the chest]) are both derived from the third pouch. The ultimobrachial bodies, which contribute to the thyroid (pink organ observed in the chest lying above they thymus), are derived from the 4th pharyngeal pouch in the mouse. The most anterior cleft, formed by the 1st arch, gives rise to the external acoustic meatus of the external ear (depicted in pink in the schematic of the ear). The posterior clefts of arches II-VI fuse to form aspects of the postnatal neck. Specific cell types of the pharyngeal apparatus are coloured in a similar manner to Fig 1a and b; red = endoderm, red broken by black lines is the 'inter-pouch endoderm'; pink = cranial neural crest derived pharyngeal mesenchyme; yellow = mesodermal core of the arch, purple = cranial neural crest and mesodermally derived pharyngeal arch arteries, green = ectoderm.

Table 1. Details, in table format, the postnatal derivatives in the mouse that arise from individual pharyngeal arches within the embryonic pharyngeal apparatus.

Arch number	Thoracic vessels (derived from pharyngeal arch arteries [purple in 2a])	Musculature (derived from pharyngeal mesoderm [yellow in 2a])	Skeletal derivatives (derived from cranial neural crests [see Fig 3])	Nerves (derived from cranial neural crests [see Fig 3] and ectoderm, [green in Fig 2a])
I	Maxillary artery.	Muscles of mastication (temporalis, masseter, and pterygoids).	Middle ear ossicles (malleus, incus). An aspect of the jawbone formed from Meckel's cartilage.	Trigeminal nerve which enables sensation in the face and motor control over functions such as mastication.
II	Stapedia and Hyoid artery.	Muscles enabling facial expression.	Middle ear ossicle (Stapes). Hyoid cartilage elements support the laryngeal, pharyngeal and tongue musculature enabling a wide range of movement..	Facial nerve that innervates the muscles controlling facial expression and transmits signals of taste from the tongue to the brain.
III	Internal carotid artery.	Stylopharyngeus musculature enabling the lifting of the larynx and pharynx, which in turn facilitates swallowing.	Hyoid cartilage elements.	Glossopharyngeal has several functions including innervating the parotid gland (a salivary gland).
IV	Right subclavian artery. Aorta.	Laryngeal and pharyngeal musculature that form a passage way for food and air in the throat.	Laryngeal cartilage elements within the throat.	Vagus innervates almost all the organs from the neck to the colon and transmits information from these targets to the central nervous system.
VI	Ductus arteriosus	Intrinsic muscles of larynx.	Laryngeal cartilages.	Vagus nerve.

1.1.2 The Pharyngeal Mesoderm

The pharynx is populated by cells of the splanchnic mesoderm, which coalesce to form a core within each of the pharyngeal arch (Tzahor and Evans, 2011). The pharyngeal mesoderm gives rise to cranial muscles and contributes to the formation of the vessels of the heart, such as the aorta (Tzahor and Evans, 2011). The aorta is derived from a primitive conduit present early in gestation, the outflow tract (OFT) and is contributed to by CNCC and mesodermal cells (Kirby and Waldo, 1995; Xu et al., 2004). The myocardium of the OFT is mesodermally derived, it forms from an area of splanchnic mesoderm caudal to the pharynx (defined as the secondary heart field, SHF) that gives rise to cardiomyocyte precursors (Waldo et al., 2001). The OFT myocardium acts as a primitive valve whose contraction within the OFT enables blood to circulate from the right ventricle to the aortic sac. Defects in the morphogenesis or septation of the OFT result in defects of the aorta. The current view is that the development of the craniofacial muscles and the aorta is regulated tissue-specifically by the pharyngeal mesoderm, although the role of the pharyngeal endoderm has not definitively been ruled out (Zhang et al., 2006).

In contrast, there is evidence that signalling from mesodermal cells can perturb pharyngeal pouch formation. TBX1 is a T-box transcription factor that is essential to the formation of the caudal PA (see 1.3.1.4). Zhang et al. demonstrated that the loss of *Tbx1* expression from the mesoderm, (using the MESP1^{Cre} that has mesodermal activity in a *Tbx1* heterozygous background), results in caudal pouch aplasia (Zhang et al., 2006). Re-activation of *Tbx1* expression in mesodermal cells was sufficient to rescue 2nd pouch formation and partially rescue 3rd and 4th pouch hypoplasia in *Tbx1* hypomorphs. Interestingly, however, the pouch phenotype of

embryos deficient of mesodermal *Tbx1* (*Mesp1*$^{cre/+}$;*Tbx1*$^{\Delta E5/flox}$ embryos, here after referred to as *M-KO* [mesodermal *Tbx1* knock out]embryos), is different to that of embryos homozygous null for the *Tbx1* allele, *Tbx1*^{tm1Bld} (referred to as Tbx1$^{-/-}$ embryos from here after). *M-KO* embryos form a hypoplastic 4th pouch but do not form a 2nd pouch, the converse is true of *Tbx1*$^{-/-}$ embryos (Zhang et al., 2006). The difference in pouch phenotypes and the observation that reactivation of *Tbx1* expression in mesodermal cells is not sufficient to fully rescue pouch defects suggests that other sources of *Tbx1* also play a role in pouch evagination.

1.1.3 The Cranial Neural Crest Cells

In contrast to the pharyngeal mesoderm, the CNCC that infiltrate the PA appears to be greatly influenced by the pharyngeal endoderm. There are four main steps in Cranial Neural Crest Cells (CNCC) development: 1) Induction; 2) Epithelial to Mesenchymal transition (EMT); 3) Migration; 4) Differentiation (Cordero et al., 2011).

A multitude of genetic components govern the steps of CNCC development that researchers are compiling into a gene network hierarchy (Sauka-Spengler and Bronner-Fraser, 2008). The genetic requirements for each step are too complex to discuss here (they are reviewed by Sauka-Spengler and Bronner-Fraser) (Sauka-Spengler and Bronner-Fraser, 2008). However, it is of interest to this thesis to note that the pharyngeal endoderm plays a role in the development of the CNCC. The first two steps of CNCC development occur within or in close proximity to the neural tissue from which they are derived; i.e. the midbrain and rhombomeres of the hindbrain (Graham et al., 2004). As such, the pharyngeal endoderm does not

appear to influence these processes. Once the CNCC have acquired the characteristics of a migratory cell, they move in distinct streams to appropriate locations within the PA and differentiate (Cordero et al., 2011).

The most anterior stream of CNCC, the trigeminal crest, emanate from rhombomeres 1 and 2 of the hindbrain and from the midbrain. The trigeminal stream migrates ventrally and ingresses under the ectoderm into the first pharyngeal arch (Serbedzija et al., 1992; Graham et al., 2004). Within the 1st arch CNCC differentiate to produce elements of the jaw and middle ear such as the incus (i.e. skeletal elements), and neurones of the trigeminal ganglion. The hyoid bone of the neck and the stapes of the ear are skeletal structures derived from the CNCC of the 2nd arch (Graham et al., 2004; Santagati et al., 2005). Differentiation of the 2nd arch CNCC into neuronal cell types generates the distal axons of the facial ganglion. The CNCC that locate to the 2nd arch initially emanate from the 4th rhombomere, migrating to the 2nd arch as the hyoid stream (Serbedzija et al., 1992; Graham et al., 2004). The most posterior CNCC stream, the post-otic stream, populates all the remaining caudal arches (3,4 and 6). This caudal stream of cells delaminates from rhombomeres 6 and 7 of the hindbrain (i.e. those caudal to the otic vesicle) (Serbedzija et al., 1992). A multitude of structures are derived from the post-otic CNCC, unsurprisingly, as they populate three separate branchial arches (Graham et al., 2004). In addition to neuronal and skeletal cell types the CNCC also contribute to each of the PAA as smooth muscle cell and as aspects of the OFT and the heart, for example, the neural crest cells of the 6th PAA are defined as cardiac NCC because they specifically contribute to the cardiac cushion of the heart (Vincentz et al., 2005) (See Fig 3 which gives an overview of the trajectories of each stream of crest cells).

Migrating CNCC were thought to induce segmentation and impose identity on the PA. However, in the past decade the importance of the pharyngeal endoderm to CNCC migration and differentiation has begun to emerge (Graham et al., 2004). Evolutionary data has shown that basal chordates, which lack a jaw and CNCC, still develop a segmented, regionalised PA in the absence of CNCC (Graham, 2001). Experimental data has confirmed that in the absence of the CNCC, patterned pharyngeal pouch morphogenesis occurs (Veitch et al., 1999). Genes such as *Bmp7* and *Pax1* were maintained and restricted to their correct endodermal expression domains within the pouches of chick embryos where CNCC had been ablated (Veitch et al., 1999). This data indicates that CNCC are not required for the segmentation of patterning of the pharyngeal endoderm.

The pharyngeal endoderm has also been found to play a role in directing CNCC differentiation, the 4th step in CNCC development. Zebrafish deficient in the (S1P) type 2 receptor (*s1pr2*) display ectopic or reduced Meckel's cartilage, which is derived from CNCC in the mandibular half of the 1st arch (Balczerski et al., 2012). This defect correlated with either a shift or reduction in the expression of *sonic hedgehog* (*shh*) in the anterior pharyngeal endoderm and the same trend observed in the expression of *fibroblast growth factor 8* (*fgf8*) within the ectoderm. It was found that transplantation of wild type endoderm into the *s1pr2* mutants rescued the Meckel's cartilage defects (Balczerski et al., 2012).

Although the pharyngeal endoderm influences CNCC development it is also evident that the CNCC are not passive once they enter the PA. Each stream of CNCC expresses a different repertoire of genes that sensitises or de-sensitises the cells to signalling from adjacent tissues i.e. the endoderm (Couly et al., 2002). Moreover

the interaction between different cell types of the PA is often reciprocal. As such there is evidence that the CNCC can affect the regionalisation of the pharyngeal pouches once they have formed. This is evident in the 3rd pouch of mouse embryos homozygous null for *Pax3* (*Splotch* mutants). The 3rd pouch of *Splotch* mutant's forms but does not pattern appropriately into presumptive parathyroid and thymus expression domains (Conway et al., 1997; Griffith et al., 2009). The expanded thymus progenitor domain is attributed to the CNCC deficiencies of *Splotch* mutants, as *Pax3* is only expressed in this cell type (Conway et al., 1997; Griffith et al., 2009).

Fig 3

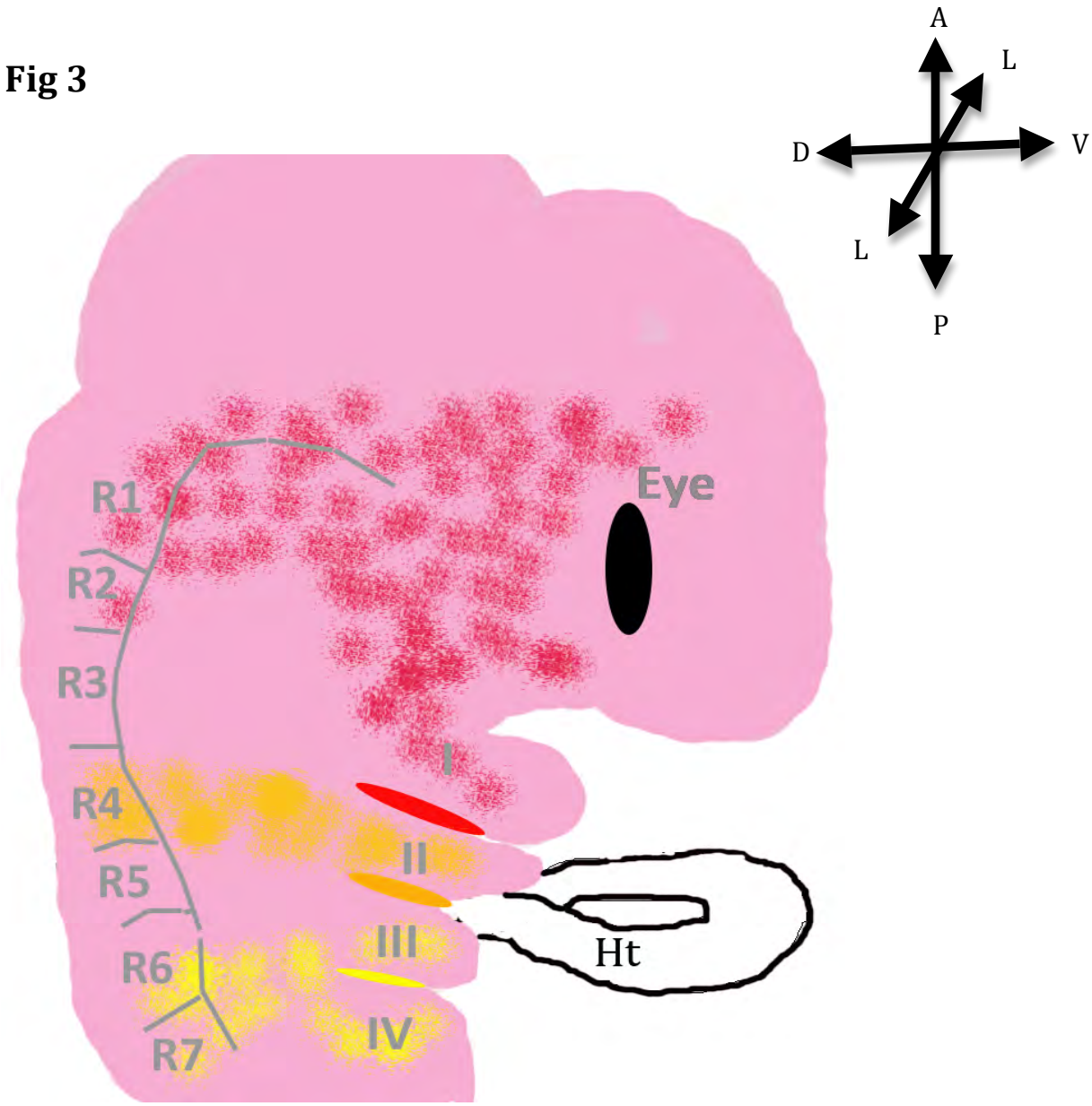

Fig 3: An overview of the trajectories of neural crest streams, (adapted from Graham, 2003)**.** The migration of CNCC from the rhombomeres to the pharyngeal arches occurs in specific streams. The trajectory of each stream is distinguished using different colours. The 1st arch is populated by CNCC derived primarily from the rhombomeres 1 and 2 (highlighted in red). CNCC from rhombomere 4 migrate into the 2nd arch (highlighted in orange). The caudal arches are populated by the post-otic crest that emanates from rhombomeres 6 and 7 (highlighted in yellow). Annotations: Heart (ht), Rhombomeres (Rh), Red oval= 1st pharyngeal pouch, orange oval = 2nd pharyngeal pouch, yellow oval = 3rd pharyngeal pouch. Pharyngeal arches labelled I to IV. Arrows to the right of the schematic determine the orientation of the schematised embryo; A = anterior, P = posterior, L = lateral, M = medial, V= ventral, D = dorsal.

1.1.4 The pharyngeal ectoderm

Mirroring the evagination of the pharyngeal endoderm is the (less pronounced) invagination of the pharyngeal ectoderm (Grevellec and Tucker, 2010). The fusion of the invaginating ectoderm with the lateral tip of the evaginating endodermal pouch forms an epithelial border that defines each pharyngeal arch (Quinlan et al., 2004). The invaginating ectoderm of the 1st arch forms a cleft that, with the 1st pouch, generates the external auditory meatus (EAM), a portion of the canal of the external ear (Mallo and Gridley, 1996). The 2nd, 3rd and 4th clefts of the pharyngeal ectoderm become incorporated into the cervical sinus (an expansion of the 2nd arch) that does not appear to give rise to any structures (Rogers, 1927). Although some genes important for the formation of the EAM, such as *Tbx1*, are known the tissue specific requirements for the formation of the clefts are not. Medical conditions characterised by defects in branchial clefting illustrate the importance of ectodermal invagination during development (Bajaj et al., 2011). It would be interesting to determine whether the pharyngeal endoderm induces ectodermal cleft formation as it does the formation of the epibranchial placodes in ectoderm proximal to the PA.

Placodes are regions of ectodermal thickenings that give rise to the sense organs and neurones. The sensory organs, the ears, eyes and nose develop from the otic, lens and olfactory placodes, respectively (i.e. the sensory placodes) (Ladher et al., 2010). Distal elements of the cranial ganglia are derived from the neurogenic placodes (that also includes the lateral line in aquatic embryos): the Vth arises from the trigeminal, the VIIIth (auditory) from the otic and the VIIth (facial), IXth (glossopharyngeal), Xth (vagal) from the epibranchial placodes (Ladher et al.,

2010). The cranial nerves are of dual origin and their proximal elements are derived from CNCC (see section 1.1.3).

The epibranchial placode consists of three individual thickenings (the geniculate, petrosal and nodose in order of position along the A-P axis of the embryos body) of ectoderm located dorso-caudally to the ectodermal clefts (described above) (Ladher et al., 2010). Development of the epibranchial placode requires:

1) Induction of placode cell identity, akin to the induction of the CNCC, induction of this placode is thought to be driven by signals from the hindbrain and the cephalic mesoderm that are in close proximity to the forming pre-placodal regions (Nechiporuk et al., 2007).

2) Commitment to a neuronal cell type. After induction the placodal cells adopt a neurogenic fate (as neuroblast cells) and delaminate through the basal membrane toward the hindbrain. It has been found that neuroblast cells from the epibranchial placode, in the chick, are committed to generate a specific ganglion before delamination (Blentic et al., 2011). Begbie et al. found that *Bmp7* from the pharyngeal endoderm was capable of inducing neuronal commitment within ectodermal explants. Only explants cultured with endoderm or BMP7 expressed the epibranchial marker *Phox2a* and produced neurones (Begbie et al., 1999), thus proving that the pharyngeal endoderm controls the neuronal commitment of the epibranchial placode. Data from more recent zebrafish studies support the findings of the seminal paper from Begbie et al. For instance, endodermal pouches do not form in *sox23* mutants, and although the epibranchial placodes form they are unable to initiate neurogenesis (marked by *neurogenin1* expression) (Holzschuh et al., 2005). These defects can be rescued by the transplantation of 'wild type' endodermal cells into *sox23* deficient mutants. Fgf3, Bmp2 and Bmp5 have all

been proposed as endodermally derived signalling molecules that are required for epibranchial placode neurogenesis in the zebrafish (Holzschuh et al., 2005; Nechiporuk et al., 2005).

3) Migration and simultaneous formation of the proximal cranial nerves that innervate the hindbrain has been shown to be dependent on the hindbrain target tissue and the CNCC emigrating from this region (Begbie and Graham, 2001; Blentic et al., 2011).

Understanding the mechanisms that control the formation of the pharyngeal pouches and the structures they influence is not just interesting from a developmental context but is also relevant to the understanding of a number of congenital syndromes that are characterised by defects of PA derivatives.

1.2 DiGeorge syndrome

Microdeletions of Chromosome 22q11 are the cause of a number of syndromes that all share a similar aetiology, the 22q11 syndromes (McDonald-McGinn and Sullivan, 2011). Digeorge syndrome (DGS), Velocardiofacial syndrome (VCFS), CATCH 22 syndrome, (Cardiac defects, Abnormal facies, Thymic hypoplasia, Cleft palate, and Hypocalcaemia) and Conotruncal anomaly face syndrome (CTAF) are all classified as 22q11 deletion syndromes (Shprintzen et al., 1981; Burn et al., 1993; Driscoll et al., 1993; Wilson et al., 1993). As the names VCFS and CTAF suggest, the common afflictions suffered by 22q11 deletion patients are craniofacial dysmorphia and cardiac defects (Driscoll et al., 1993). DGS is also characterised by immune deficiencies as the patient's thymus is aplastic or hypoplastic (Ryan et al., 1997; Scambler, 2000). The frequency of these congenital syndromes is relatively high, (1 in 3000 to 1 in 4000 live births), hence understanding the basis of the pathogenesis underlying these syndromes is of great importance (McDonald-McGinn and Sullivan, 2011).

DGS was first characterised in 1965 by the clinician Dr Angelo DiGeorge who described thymus and parathyroid agenesis in a group of children (Finley et al., 1977). Most of the structures affected in patients with DGS originate embryonically from the PA (see Table 2), as such the syndrome was often termed pharyngeal pouch syndrome (Vesterhus et al., 1975; Wurdak et al., 2006). Defects of structures that are not derived from the PA also manifest in DGS patients, for example patients may develop multi-cystic kidneys and renal atresia. In addition, low IQ and psychosis can persist in individuals with DGS, these mental defects are possibly due to poor development of the cerebellum (Ryan et al., 1997; McDonald-McGinn and Sullivan, 2011).

In the 1980's many DGS patients were found to have a Chromosome 22 karyotype, characterized by monosomy from unbalanced translocations and/or interstitial deletions (Driscoll et al., 1993). Further cytogenetic analysis pinpointed a segment on the long arm of Chromosome 22, 22q11.2, which typically caused DGS (Driscoll et al., 1993; Scambler, 2000). Over 35 genes have subsequently been mapped to this 'typically deleted region' (TDR) on Chromosome 22q11.2. The penetrance of all DGS defects between individuals is highly variable, as is the degree of severity. This suggests that DGS may be caused by defects in multiple genes within the TDR or by defects in genetic modifiers outside the TDR that are perturbed by the translocation/mutations within the TDR (Carey et al., 1990; Scambler, 2000). Currently the loss of *TBX1*, a gene found within the TDR, is the main candidate for a genetic cause of DGS (Scambler, 2010).

The 22q11 region affected in DGS was found to map to mouse Chromosome 16 (MU16) (Galili et al., 1997). There are some differences in gene synteny between the two species, but to a large extent gene organisation is maintained between 22q11 and MU16 (Sutherland et al., 1998). Lindsay et al. utilised this genetic synteny and created mouse lines with a deletion (*Df1)* or reciprocal duplication (*Dpl)* in a 1.2MB region on MU16 (Lindsay et al., 1999). The D*f1/+* animals analysed at E11.5 had absent or severely reduced 4th PAAs that resulted in thoracic vessel defects, such as interrupted aortic arch type B (IAA-B), at E18.5 (Lindsay et al., 1999). These data indicated that the deletion of gene(s) in the *Dfl* segment are likely to be the cause of thoracic vessel defects that are present in DGS (Chieffo et al., 1997). Supporting this prediction was the observation that deleting one allele of *Tbx1* generated embryos with PAA defects that are the cause of thoracic vessel

defects observed in DGS (and in *Dfl/+* mice), i.e. IAA-B (Prescott et al., 2005). Embryos homozygous null for *Tbx1* (*Tbx1*$^{-/-}$ embryos) developed the full complement of DGS phenotypes (see Table 2). Despite differences in the threshold of *TBX1* that causes DGS defects in mouse and man (hemizygosity of *TBX1* causes DGS in humans, whereas the same defects only arise in mice homozygous null for *Tbx1* in the mouse), some cohorts of DGS patients were found to have mutations in *TBX1* (Stoller and Epstein, 2005).

Table 2: A summary of the defects that manifest in DGS patients and their origin within the PA (adapted from

DGS defect	**Pharyngeal element the structure is derived from**
Otolaryngeal abnormalities, cleft palate and cleft lip	1st pharyngeal arch defect
Otolaryngeal abnormalities, otitis media a middle ear defect and low set ears an external ear defect	1st and 2nd pharyngeal arch defects
Cranial nerve palsies	CNCC/placodal cranial nerve defect
Craniofacial dysmorphia due to skeletal or musculature defects	Mesodermal/ CNCC defects of various arches
Parathyroid hypoplasia/aplasia with associated hypocalcaemia.	3rd pharyngeal pouch defect
Thymus hypoplasia/aplasia with associated immune deficiencies.	3rd and 4th pharyngeal pouch defect
Malformation of the great vessels of the heart.	Pharyngeal arch artery defects, primarily associated with the 4th PAA.
Cardiac defects; defects in the division of the aorta and the formation of the cardiac cushions of the heart	Out flow tract/cardiac NCC defect.

1.3 Genes and signalling cascades that affect the formation of the pharyngeal pouches

1.3.1 *T-box 1* (*Tbx1*)

One of the distinguishing features of *Tbx1*$^{-/-}$ embryos is the lack of pouch formation and thus arch formation caudal to the 1st pharyngeal pouch and arch. This identifies TBX1 as a key regulator of pharyngeal pouch morphogenesis, discussed further in section 1.3.1.3d. However, the mechanisms and interactions by which TBX1 regulates PA development are still not fully understood some 90 years after the first T-box protein, BRACHYURY, was discovered (Korzh and Grunwald, 2001).

1.3.1.1 TBX1 structure

Central to the function and characterisation of TBX1 and its family member is the T-domain, containing the T-box motif, a 17-26kDa protein domain required for DNA binding. This domain has been maintained in all T-box proteins throughout the 600 million year period of metazoan evolution, indicative of the functional importance this domain conveys (Agulnik et al., 1996; Minguillon and Logan, 2003). Kispert, amongst other researchers, helped to determine that the T-Box domain, located in the N-terminal of the protein, has DNA binding activity (Kispert et al., 1995). The T-box recognises a 20bp palindromic sequence in target genes, the *T-consensus* motif. To initiate trans-activation or repression of transcription T-box proteins also require domains in their C-terminal (Kispert et al., 1995).

The conserved motif of the T-box was a key tool in identifying other T-box proteins both between species and within the same species (Agulnik et al., 1996). To date

17 T-box genes, classified into 5 subfamilies (*Brachyury*, *T-brain*, *Tbx1*, *Tbx2* and *Tbx6*), have been identified in the mouse and human genome. *Tbx1* is part of the *Tbx1* subfamily, which also includes *Tbx12*, *Tbx18*, *Tbx20* and *Tbx22* (Minguillon and Logan, 2003). There are two splice forms of *Tbx1* in humans that produce an mRNA transcript with either 9 or 10 exons (Chieffo et al., 1997). The main difference observed between TBX1 other T-box proteins whose structures have been solved is in the 'dimerization' region. The crystal structure predicts that TBX1 binds the palindromic *T-consensus* site as two monomers that connect via the bound DNA, rather than binding DNA directly as a TBX1 dimer (El Omari et al., 2011). In addition to its role as a classic transcription factor, TBX1 is also able to regulate signalling independently from its transcriptional function. TBX1 regulates BMP signalling by competitively binding to SMAD1, thus interfering with BMP4-SMAD1 binding and the downstream SMAD1-SMAD4 interactions (Fulcoli et al., 2009). The competitive binding of SMAD1 also occurs in TBX1 proteins that lack a T-box domain. Interestingly, the F148Y mutation of *TBX1* (found in DGS patients) maps to the T-box domain, but disrupts a residue at the surface of the protein. This data suggests that the perturbation of TBX1 mediated protein-protein interactions may underlie the DGS syndrome phenotype (El Omari et al., 2011).

1.3.1.2 *Tbx1* expression

Tbx1 expression in the mouse is first detected in the rostral mesoderm of the egg cylinder at E7.5. Two days later *Tbx1* is almost exclusively expressed within the craniofacial region (e.g. within the otic vesicle, the PA and the hindbrain) (Chapman et al., 1996). Later in gestation *Tbx1* expression is detected in structures that are re-iterated, segmented or branching, for instance, the tooth buds, rib cartilages and the lung buds (Chapman et al., 1996). Chapman noted that the

expression patterns of *Tbx1-Tbx6* were, on the whole, localised to areas where 'inductive interactions' are taking place (Chapman et al., 1996). This trend is exemplified by the expression pattern of *Tbx1* in the PA between E8.5 and E10.5. *Tbx1* is expressed in all cell types of the PA apart from the CNCCs: the mesodermal core of the pharyngeal arches, the endothelium of the PAA and the ectodermal and endodermal pharyngeal epithelia (Vitelli et al., 2002; Zhang et al., 2005). Interestingly, *Tbx1* expression is extensive in the evaginating pharyngeal endoderm of the caudal most forming pouch. For example, at E9.5 *Tbx1* expression is confined to the distal tip of the 1st and 2nd pouches pharyngeal pouches, whereas *Tbx1* expression is visible throughout the just forming 3rd pouch (Garg et al., 2001; Vitelli et al., 2002).

1.3.1.3 A requirement for *Tbx1* in the development of the PA

The dynamic, widespread expression of *Tbx1* within the PA is a predictor of its importance to the formation of this structure and accounts for the extensive defects observed in the PA and PA derivatives of *Tbx1*$^{-/-}$ embryos.

1.3.1.3a Defects in the development of the pharyngeal mesoderm caused by a loss of *Tbx1*

Musculature derived from mesodermal cells of the caudal arches is unable to form in *Tbx1*$^{-/-}$ embryos because of the distorted morphology of the caudal PA (i.e. the muscles of the pharynx and larynx). In the rostral arches mesodermal cells are unable to express *Tbx1*-dependent myogenic regulatory factors such as *Myf5,* consequently hypoplastic mandibular muscles develop in *Tbx1*$^{-/-}$ embryos (Kelly et al., 2004; Grifone et al., 2008). Loss of *Tbx1* also results in hypoplasia of the distal portion of the OFT. Hypoplasia of the OFT of *Tbx1*$^{-/-}$ embryos is partially attributed

to defects in the expansion of cardiomyocyte precursors that arise from the splanchnic mesoderm of the SHF (Xu et al., 2004). Defects in the growth and septation of the OFT affect the formation of the aorta and cause cardiac defects such as persistent truncus arterious (PTA) (Bajolle et al., 2006). PTA is evident in the embryo as a single vessel arising from the heart. This cardiac defect occurs because septation of the aorta has failed, preventing the segregation of pulmonary and systemic aspects of the heart and thus the circulatory system (Kirby et al., 2008).

1.3.1.3b Defects in the development of the pharyngeal ectoderm caused by a loss of *Tbx1*

The distal aspects of IXth and Xth cranial nerves derived, respectively, from the petrosal and nodose epibranchial placodes, are fused in *Tbx1*$^{-/-}$ embryos (Vitelli et al., 2002). The functional consequence of this fusion for the tongue, carotid sinus and carotid body, which are innervated by the IXth and Xth cranial nerves, has not been assessed, (Ladher et al., 2010). However, the aberrant development of the Xth cranial nerve in *Tbx1*$^{-/-}$ embryos results in a loss of vagal nerve innervation of the stomach (Calmont et al., 2011).

1.3.1.3c Defects in the development of the CNCC caused by a loss of *Tbx1*

Although CNCCs do not express *Tbx1* the loss of this gene from the surrounding niche severely perturbs CNCC migration into and differentiation within the pharyngeal arches. In *Tbx1*$^{-/-}$ embryos streams of *Crabp1* expressing CNCC are merged and often ectopic as they migrate towards the PA; *Dlx2* marked CNCC are

absent from the caudal PA (Vitelli et al., 2002). These CNCC defects impact upon the normal development of cranial nerves, craniofacial skeletal elements and pharyngeal arch arteries. Neurofilament staining reveals that the proximal projections *Tbx1*$^{-/-}$ embryos cranial nerves are also fused to one another (Vitelli et al, 2002). Abnormal fusion of the Vth cranial nerve with the VIIth/VIIIth cranial nerve is attributed to the ectopic migration of the hyoid CNCCs (*Hoxa2/Sox3* positive), that enter the 1st arch. The aberrant migration of the CNCC into the rostral arches also perturbs the formation of the CNCC derived skeletal elements of the middle and outer ear (Mallo and Gridley, 1996). In *Tbx1*$^{-/-}$ embryos the 2nd arch derived ossicle, the stapes, is aplastic and the first branchial arch derived ossicle, the incus, is hypoplastic (Moraes et al., 2005). Defects in CNCC that populate the caudal PA affect the formation of the 3rd, 4th and 6th pharyngeal arch arteries, none of which are able to form in *Tbx1*$^{-/-}$ embryos (Lindsay et al., 2001). Although the lack of arch morphology is the primary cause of the caudal PAA aplasia, CNCC also differentiate into smooth muscle cells of the PAA, a process that is perturbed by the loss of one allele of *Tbx1* (Zhang et al., 2005).

1.3.1.3d Defects in the development of the pharyngeal endoderm caused by a loss of *Tbx1*

The dynamic pattern of *Tbx1* expression in the pharyngeal endoderm indicates that *Tbx1* may be required within the endoderm to regulate pharyngeal pouch morphogenesis. Certainly the loss of *Tbx1* prevents the evagination of the pharyngeal endoderm caudal to the 1st pouch (Jerome and Papaioannou, 2001). As such, the organs that normally metamorphose from the pharyngeal endoderm are aplastic or hypoplastic in *Tbx1*$^{-/-}$ embryos. Thyroid development is initiated normally in *Tbx1*$^{-/-}$ embryos and the precursor domain is of correct size and place

in the pharyngeal endoderm, likely because *Tbx1* is normally only weakly expressed in this domain (Liao et al., 2004; Fagman et al., 2007). However, thyroid hypoplasia and hemiagenesis manifests in embryos absent of *Tbx1* expression. These thyroid defects are partially attributed to the thyroid primordium's inability, in a *Tbx1* devoid environment, to associate with the surrounding vasculature. The vasculature with which the thyroid should associate has been shown to influence the growth, lobulation and migration of the gland, (Liao et al., 2004; Fagman et al., 2007). Aplasia of the 4th pouch in *Tbx1*$^{-/-}$ embryos also contributes to the thyroid hypoplasia because C-cells derived from the UB are unable to form if this most caudal pouch is absent during development (Liao et al., 2004). Similarly, aplasia of the 3rd pouch in *Tbx1*$^{-/-}$ embryos prevents the thymus and parathyroid from developing (Jerome and Papaioannou, 2001; Liao et al., 2004).

It is difficult to determine from an analysis of *Tbx1*$^{-/-}$ embryos whether TBX1 has tissue specific roles during PA development. As discussed in section 1.1, the pharyngeal endoderm can influence the development of non-endodermal cells in the PA and thus the structures they contribute to later in gestation. It is possible that caudal pouch aplasia is caused by the loss of *Tbx1* expression from the endoderm and that this in turn perturbs the development of the adjacent pharyngeal tissues. To elucidate this, first the requirement and role of TBX1 in the endoderm during pharyngeal pouch outgrowth needs to be established. The generation of mouse lines that drive the deletion of *Tbx1* in a defined spatial or temporal manner have enabled researchers to address the tissue specific role of TBX1 at different time points in development. In all cases 'Cre-loxP' technology has been used to delete genetically engineered *Tbx1* alleles in which critical exons, such as the T-box containing exon 5, are flanked by *loxP* sites (Xu et al., 2004;

Arnold et al., 2006). CRE enzymes recognize the *lox-P* sites and act to recombine and thus delete the exons that are essential to the function of TBX1 (Ray et al., 2000). By driving the expression of *Cre* with a cell-specific promoter it is hoped that the activity of the CRE enzyme and thus the deletion of the 'floxed' target gene is restricted (Feil, 2007). Whilst a number of tissue specific *Cre* lines are available, a requirement for *Tbx1* in the endoderm has still not been established.

1.3.1.4 Dissecting the tissue specific requirements for *Tbx1* during pharyngeal pouch development

The deletion of *Tbx1* using $WNT1^{Cre}$, (the name is derived from the genes *Wingless* and *Integrase-1*; this enzyme is only active in CNCC) does not recapitulate any phenotypes of the $Tbx1^{-/-}$ embryos, including caudal pouch aplasia (Kochilas et al., 2002). This finding was in agreement with the observation that *Tbx1* is not expressed in the CNCC (Garg et al., 2001; Vitelli et al., 2002). Thus, TBX1 in the endoderm, ectoderm or mesoderm, or in a combination of all three of these tissue types, must regulate pharyngeal pouch morphogenesis.

Pharyngeal pouch defects have not been documented in embryos that are unable to express *Tbx1* in the ectoderm, ($Ap2alphaIRES^{cre/+};Tbx1^{flox/-}$ embryos named as *PSE-KO* embryos from here onward) (Calmont et al., 2009; Randall et al., 2009). However, thymus hypoplasia does manifest in *PSE-KO* embryos (Randall et al., 2009). It is likely that the documented defects of CNCC migration into the pharyngeal arches of *PSE-KO* embryos accounts for the hypoplasia of this endocrine organ. However, until pouch morphogenesis is analysed and noted as normal in the *PSE-KO* mutants, a role for ectodermal *Tbx1* in pouch development cannot be completely excluded (Calmont et al., 2009).

Surprisingly, a MESP1^{Cre} (*Mesodermal posterior 1 homolog*) driven recombination of *Tbx1* within mesodermal cells results in non-cell autonomous endodermal pouch defects, (Zhang et al., 2006). The 2nd and 3rd pouches of *M-KO* embryos were aplastic (hence so were the majority of thymi examined) and the 4th was hypoplastic. Conversely, the reactivation of *Tbx1* in the mesoderm in a *Tbx1* hypomorphic background partially rescued the pouch abnormalities; embryos develop a hypoplastic 3rd and 4th pouch and a normalised 2nd pouch (Zhang, 2006). However, the thymic defects are not rescued by the mesodermal reactivation of *Tbx1*, indicating that *Tbx1* is required in the pharyngeal epithelia during thymus organogenesis. The partial rescue of pouch morphogenesis by the reactivation of mesodermal *Tbx1* expression was surprising and illustrates that *Tbx1* in the mesoderm influences pouch (Zhang et al., 2006). However, it is uncertain whether the low level of *Tbx1* transcription from the hypomophic-*Tbx1* allele, combined with mesodermal *Tbx1* expression, is enabling pouch morphogenesis to proceed, rather than expression from mesoderm alone.

The *Foxg1cre* line has been used to drive the deletion of *Tbx1* specifically in the endoderm (*Foxg1$^{Cre/+}$;Tbx1$^{flox/-}$* now referred to as *PE-KO* embryos) (Arnold et al., 2006). As expected, the *PE-KO* embryos recapitulated the endodermal defects of *Tbx1$^{-/-}$* embryos. Surprisingly, *PE-KO* mutants also phenocopy the non-endodermal defects observed in *Tbx1$^{-/-}$* mutants, such as the loss of the muscles of mastication (Arnold et al., 2006). Whilst the use of FOXG1^{Cre} (*Forkhead box G1*), on the Swiss-Webster (S-W) genetic background attenuates any non-endodermal activity, on other backgrounds this driver induces recombination in multiple cell types within the PA (Zhang et al., 2005). The NKX2.5^{Cre} (*Nk2 homoeobox* 5) induces

recombination of *Tbx1* within discreet domains of the 3rd and 4th pharyngeal pouches and results in 4th arch and thymus hypoplasia. Severe endodermal defects were not observed in these mutants because the endodermal domains of *Nkx2.5* and *Tbx1* only partially overlap in the caudal pouches (Xu et al., 2004). Moreover, the deletion of *Tbx1* from mesodermal domains, where *Nkx2.5*^{Cre} is expressed in addition to the endoderm, may also contribute to the pouch defects observed (Moses et al., 2001). As such, the role *Tbx1* plays in the endoderm during pouch morphogenesis and indeed in the development of non-endodermal structures within the PA is still questioned.

It is clear that to elucidate the role of TBX1 specifically in the endoderm a *Cre* line that is highly efficient at recombining *Tbx1* specifically throughout the pharyngeal endoderm is required. In addition, *Tbx1*-dependent signalling molecules and cellular processes that regulate pouch outgrowth within the endoderm also need to be identified. Signalling cascades that may be able to fulfil this role are discussed below.

1.3.2 The FGF signalling cascade

Members of the Fibroblast Growth Factor (FGF) signalling cascade are expressed in the endoderm and their deletion affects pouch morphogenesis (discussed below). As such signalling from this cascade within the pharyngeal endoderm may be able to regulate pouch morphogenesis.

1.3.2.1 FGF structure and function

Fibroblast growth factors (FGFs) are a group of signalling molecules that in mouse and man are comprised of 22 genes (Dorey and Amaya, 2010). FGFs function as ligands that, on binding to their target receptor, activate a signalling cascade that can regulate a number of cellular mechanisms, including; proliferation, differentiation, cell survival and even cell death (Dorey and Amaya, 2010).

The high degree of conservation between *Fgf* transcripts and the expansion of the FGF family through evolution highlights the importance of this signalling cascade (Ornitz and Itoh, 2001). Phylogeny and sequence homology studies have divided the 22 FGF ligands into 7 subfamilies determined by the similarities in their nucleotide and amino acid sequences. The families are grouped as follows: FGF1/2, FGF4/5/6, FGF3/7/10/22, FGF9/16/20, FGF8/17/18, FGF15/19/21/23 and FGF11/12/13/14 (Itoh and Ornitz, 2004). As amino acid sequences are indicative of protein function, FGFs with similar functions and characteristics are logically grouped together. Each group also tends to be

characterised by the FGF protein's ability to function as intracrine, paracrine or endocrine factors (Itoh and Ornitz, 2011). Paracrine FGFs are the most numerous consisting of FGF/1/2/5, FGF3/4/6, FGF7/10/22, FGF8/17/18 and FGF9/16/20 subfamilies. Predominantly, the N-terminal peptides are cleaved from the paracrine FGFs and secreted from the cells in which they were synthesised (Revest et al., 2000; Tulin and Stathopoulos, 2010). The ability of paracrine FGFs to act extracellularly enables the ligands to bind to cell surface tyrosine kinase FGFRs on neighbouring cells, activating FGF signalling non-cell autonomously (Revest et al., 2000; Scholpp and Brand, 2004). Despite differences in their mode of signalling, FGF members all have a conserved core structure that identifies them as an FGF protein.

Vertebrate FGFs are 17 to 34kDa proteins consisting of variant N- and C- termini that flank a highly invariant section – the 'conserved core'- which permits an FGF to function as a signalling molecule (Ornitz, 2000; Dorey and Amaya, 2010). Typically the conserved core consists of 12 beta-strands, that on folding to a tertiary structure (a B-trefoil shape), appears almost pyramidal, (Zhu et al., 1991; Ornitz and Itoh, 2001). Amino acids within the conserved FGF core have been identified as sites required for FGF receptor (FGFR) binding and independent sites for heparin/heparan sulfate proteoglycan binding (Plotnikov et al., 2000). Unlike other tyrosine kinase receptor ligands, FGFs exist as monomers rather than dimers and, if not present in excess, require other factors such as heparan sulfate (HS) to facilitate receptor binding (Mohammadi et al., 2005).

Four *Fgfr* genes have been identified in mouse and man, (*Fgfr1-4*). Each *Fgfr* transcript is comprised of three domains; an extracellular ligand binding domain, a transmembrane domain and a tyrosine kinase domain that is located intracellularly, (Itoh and Ornitz, 2004). Within the C-terminal of the protein (the extracellular ligand binding domain in the *Fgfr* mRNA) there are three immunoglobulin-like (Ig) domains that all function in ligand binding. The alternate splicing of exons in the Ig-like III domain generates FGFR isoforms type - IIIa, -IIIb and –IIIc, which appear to have distinct expression patterns (Groth and Lardelli, 2002). Whilst isoforms -IIIa are not known to function in FGF signalling, isoforms –IIIb and –IIIc are restricted, respectively to epithelial and mesenchymal tissue types (Orr-Urtreger et al., 1993). In addition to regulating FGF signalling in a tissue specific manner, alternative splicing of the *Fgfr* transcripts also regulates the binding affinity between a ligand and its cognate receptor, (Yeh et al., 2003; Beenken et al., 2012). For instance, the splicing event that occurs in *Fgfr2* to form FGFR2(III)b retains and reveals the amino acid Ser-315 in the receptors D3 binding domain. Ser-315 forms strong, highly specific hydrogen bonds with the Asp-76 amino acid in the ligand FGF10 (and other FGF7 family members) (Yeh et al., 2003). Consequently, interchanging Ser-315 for the relative D3 amino acid in FGFR2(III)c, (alanine-315) drastically reduces the binding affinity between FGFR2(III)b and FGF7 (Wang et al., 1995).

The crystal structures of many FGF-FGFR-HS structures have now been solved revealing that these factors interact in a 2:2:2 conformation to induce signalling (Plotnikov et al., 2000). Upon the trans-autophosphorylation of tyrosine residues within the intracellular domain of the FGFR (induced by FGF ligand binding),

many downstream intracellular pathways are activated (Thisse and Thisse, 2005). Specific signalling pathways are activated when intracellular proteins are recruited to specific, (now phosphorylated), recognition motifs within the receptor, (Thisse and Thisse, 2005).

The Ras/Map Kinase pathway is one of three major cascades stimulated downstream of activated FGFRs (see Fig 4), the other two being the PLCg pathway and the PI3K/PKB pathway (Dorey and Amaya, 2010). Signal transduction is induced by the (activated) FGFR-dependent phosphorylation of the membrane-anchored docking protein, FGFR substrate 2α (FRS2α) (Kouhara et al., 1997). The tyrosine phosphorylation of FRS2α facilitates the binding of a GRB2-SOS complex (Clark et al., 1992; Lowenstein et al., 1992). This step initiates the Ras-Raf-MEK-MAP kinase (ERK1/2) phosphorylation cascade, which is catalysed by the exchange of GDP for GTP on RAS via SOS (a nucleotide exchange factor) (Thisse and Thisse, 2005). Phosphorylated MAP kinase is able to enter the nucleus where it phosphorylates and complexes with transcription factors such as the Ets domain containing factors ERM and PEA3 (Janknecht et al., 1996; Sharrocks, 2001). This initiates the transcription of FGF target genes, including *Erm* and *Pea3* themselves, and regulates FGF dependent cellular functions (Raible and Brand, 2001; Thisse and Thisse, 2005). The protein kinase C pathway has been implicated in cell migration, the Akt pathway is associated with cell survival and proliferation is linked to the Ras/ERK pathway. FGF signalling is controlled at many levels in each pathway (Dorey and Amaya, 2010). One way FGF signalling can be attenuated is through the FGF-dependent transcription of negative feedback regulators, such as the *Sprouty* (*Spry*) genes

(Thisse and Thisse, 2005). SPROUTY proteins are able to inhibit FGF signalling at various places in the signalling cascade, including the binding of SPRY2 binding to the Src homology domain of GRB2 which inhibits this proteins interaction with FRS2α (Hanafusa et al., 2002; Thisse and Thisse, 2005). The PLCg pathway has also been outlined in Figure 4 because this pathway is mentioned later within this thesis during a discussion about the link between FGF signalling and the actin cytoskeleton, in reference to a study by Sai et al.

Fig 4

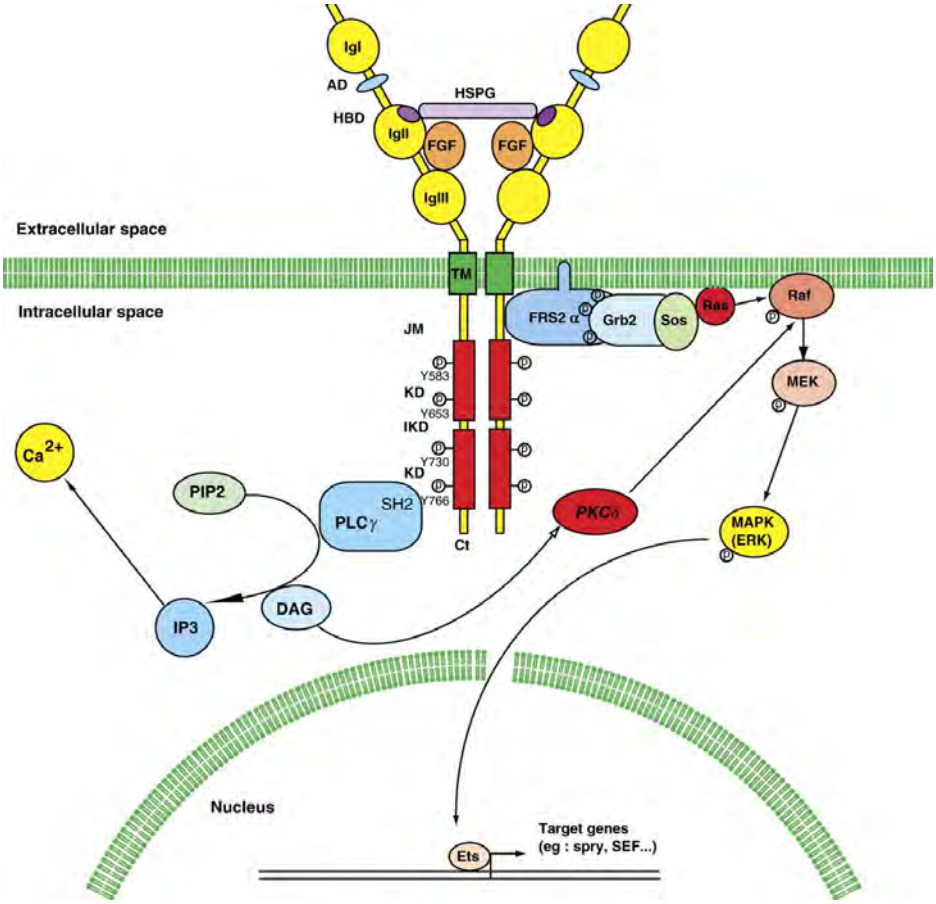

Fig 4. A summary of the Ras/Map Kinase pathway of the FGF signalling cascade, taken from Thisse and Thisse, 2005. Phosphorylated FGFRs enable the recruitment of Grb2 to phosphorylated Frs2α. The Ras-Raf-MEK-MAP kinase (ERK1/2) phosphorylation cascade is initiated by the conversion of Ras bound GDP to GTP, facilitated by SOS. The subsequent phosphorylation steps culminate with MAPK entering the nucleus and activating transcription factors such as the Ets protein *Pea3*. The expression of the *Ets* genes can also be induced by the PLCg pathway (activated downstream of FGFR dimerization). The latter pathway is facilitated by PLCg which, by virtue of catalysing the conversion of the phosphatidtylinositol lipid, PIP2, to Inositol tri-phosphate (IP3) and the secondary messenger DAG (diacylglycerol) activates Protein Kinase C (PKC). In the otic epithelium, activation of the PLCg pathway also induces the activation of Phospho-Myosin Light Chain that maintains actin polarity within this tissue.

1.3.2.2 A number of FGF ligands are expressed within the pharyngeal endoderm during PA development

A number of *Fgf* ligands are expressed in the pharyngeal endoderm during PA development, indicating that they may be able to function in this epithelium (via the activation of FGF signalling) to drive or regulate pouch formation.

The loss of *Fgf10* affects the development of some of the endodermally derived endocrine organs. The thyroid is absent and the thymi are reduced in size in embryos homozygous null for *Fgf10*, (*Fgf10*$^{-/-}$ embryos) (Ohuchi et al., 2000). However, unless pouch morphogenesis is regulated non-cell autonomously by *Fgf10* that is expressed in the mesoderm of the caudal arches, it is unlikely that the endocrine gland aberrancies of *Fgf10*$^{-/-}$ embryos arise as a result of pharyngeal endoderm defects. For, *Fgf10* is predominantly expressed in the mesoderm and mesenchyme of the pharyngeal aches and is only expressed within the endoderm of the 1st pharyngeal pouch (Kelly et al., 2001).

Fgf15 is expressed more extensively in the pharyngeal endoderm than *Fgf10*. Expression of *Fgf15* is detected in the pharyngeal endoderm from approximately E8.25 (at the 10s somite stage of development) and is maintained in the posterior half of each pouch throughout PA development (Trokovic et al., 2005; Vincentz et al., 2005). The loss of *Fgf15* results in defects of the cardiac cushion (and thus OFT defects), due to a reduced number of CNCC entering the aortic sac from the 6th PAA at E11.5 (Vincentz et al., 2005). However, no pouch defects have been described in embryos homozygous null for *Fgf15* (*Fgf15*$^{-/-}$ embryos).

The expression domains of *Fgf3* and *Fgf15* in the pharyngeal endoderm overlap

largely in the posterior half of each pouch at E9.5 (Vincentz et al., 2005; Aggarwal et al., 2006). Moreover, akin to *Fgf15*$^{-/-}$ mutants, embryos homozygous null for *Fgf3,* (*Fgf3*$^{-/-}$ embryos), are not reported to have pouch defects. However, structures within the PA influenced by the endoderm are perturbed by the loss of *Fgf3*. For instance, chick embryos exposed to *Fgf3* antisense oligodeoxynucleotides were not able to form the nodose placode, nor the vagal ganglion that this placode gives rise to (Culbertson et al., 2011). Moreover, thymus hypoplasia was also detected in *Fgf3*$^{-/-}$ embryos, the cause of which, in contrast to *Fgf10*$^{-/-}$ embryos, may be due to the loss of *Fgf3* from the endoderm of the 3rd pouch (Aggarwal et al., 2006).

The expression domain of *Fgf8* overlaps with *Fgf3* and *Fgf15* at E9.5 within the pharyngeal endoderm (Vincentz et al., 2005; Aggarwal et al., 2006). As the pharyngeal pouch matures and narrows, *Fgf8* becomes restricted laterally toward the tip of the pouch, as observed in the 1st and 2nd pouches at E9.5 (Crossley and Martin, 1995). However, in contrast to *Fgf3* and *Fgf15*, reducing *Fgf8* expression in development perturbs pharyngeal pouch morphogenesis. Mice homozygous null for (*Fgf8*$^{-/-}$ embryos) fail to gastrulate properly, therefore to analyse the role of *Fgf8* post-gastrulation, embryos that have a significant reduction in the level of *Fgf8* expression were generated (*Fgf8* hypomorphs) (Sun et al., 1999). A hypomorphic allele was created by the CRE mediated insertion of a neomycin resistance expression cassette (flanked by *frt* sites) between the floxed exons (2 and 3) of the *Fgf8* allele (Meyers et al., 1998). *Fgf8* mild hypomorphs only form an aplastic 3rd pouch, resulting in the 3rd and 4th arches appearing fused (Frank et al., 2002). In 50% of the mutant embryos thymus aplasia was observed, in the remaining 50% the thymi were ectopic and hypoplastic with only 20% of the

'normal' T-cell numbers being obtained from the lobes that formed (Frank et al., 2002). In severe *Fgf8* hypomorphs pharyngeal pouch defects were more extensive, in keeping with a greater loss in *Fgf8* expression (Abu-Issa et al., 2002). At E9.5 the 1st and 2nd pouches of severe *Fgf8* hypomorphs form but appear splayed, rather than 'slit-like', and fused to one another. By E10.5 a very hypoplastic 3rd pouch is present but the loss of *Pax1* expression, that normally outlines the pouch, makes identification difficult (Abu-Issa et al., 2002). In accordance with the disorganised 1st and 2nd pouch formation the rostral arches appear hypoplastic.

Fgf8 is a secreted ligand that is expressed in the mesenchyme, ectoderm and endoderm of the PA, thus it is possible that non-cell autonomous sources of *Fgf8* could play a role in pouch morphogenesis. To confirm which sources of *Fgf8* are required for pouch morphogenesis, as is the case for *Tbx1,* mouse lines that carry tissue specific deletions of *Fgf8* have been utilised.

1.3.2.3 Dissecting the tissue specific requirements for *Fgf8* during pharyngeal pouch development

Although *Fgf8*-severe hypomorphs display a reduction in the amount of CNCC migrating into the caudal PA, this defect is not cell-autonomous because *Fgf8* is not expressed in the CNCC (Abu-Issa et al., 2002). The deletion of *Fgf8* from the mesoderm (*Mesp1*$^{Cre/+}$;*Fgf8*$^{flox/-}$ embryos) causes OFT hypoplasia and PAA defects (Park et al., 2006; Watanabe et al., 2010). Pouch formation was not assessed in the *Mesp1cre;Fgf8*$^{flox/-}$ embryos. Interestingly, however, although arch and pouch development was not analysed in detail, *Mesp1cre;Fgf8*$^{flox/-}$*Fgf10*$^{+/-}$ embryos are described as having hypoplastic 2nd and 3rd arches (Watanabe et al., 2010). Thus, the role of FGFs in the mesoderm during pouch formation remains unclear.

Similarly, *Islet1*$^{Cre/+}$*Fgf8*$^{flox/-}$ embryos, that are deficient of *Fgf8* in the anterior heart field and endoderm, are described as having hypoplastic arches, however neither arch nor pouch development was analysed in detail (Park et al., 2006).

An analysis of *Ap2alphaIRES*$^{cre/+}$*;Fgf8*$^{flox/-}$ embryos, that are deficient for *Fgf8* in the ectoderm, indicated that *Fgf8* in the outer pharyngeal epithelium is not required for pouch formation nor endocrine organ formation (Macatee et al., 2003). *Ap2alphaIRES*$^{cre/+}$*;Fgf8*$^{flox/-}$ mutants were not documented as having pharyngeal pouch defects or significant defects in thymi or parathyroid development (Macatee et al., 2003). In contrast, the thymi and parathyroid's of *Hoxa3*$^{Cre/+;}$*Fgf8*$^{flox/-}$ embryos were hypoplastic and/or ectopic (in addition some embryo's parathyroid lobes were also aplastic), (Macatee et al., 2003). HOXA3^{Cre} drives *Fgf8* ablation in the endoderm and ectoderm caudal to the 2nd arch and pouch. As the ectodermal deletion of *Fgf8* did not generate significant endocrine gland defects, this data indicates that *Fgf8* within the endoderm, (at least the caudal endoderm), is required for 3rd pouch derived endocrine gland formation (Macatee et al., 2003). Whether there is a requirement for *Fgf8* in the endoderm during pouch formation was not addressed in the *Hoxa3*$^{Cre/+;}$*Fgf8*$^{flox/-}$ mutants.

The dynamic expression of *Fgf8* throughout the pharyngeal endoderm combined with the disorganised pouch morphogenesis of severe *Fgf8* hypomorphs indicates that *Fgf8* may be required in the endoderm for pouch formation. A lack of data analysing pouch formation in conditional *Fgf8* mouse lines that recombine *Fgf8* only in non-endodermal cells prevents a role for *Fgf8* in the mesoderm and ectoderm during pouch outgrowth from being discounted. Furthermore, a conditional mutant line in which *Fgf8* is efficiently deleted through the entire

pharyngeal endoderm (rather than in small domains of pharyngeal endoderm) is required to determine whether endodermal *Fgf8* is required during pouch morphogenesis.

1.3.2.4 FGF receptor 1 is required for pharyngeal pouch morphogenesis

It is likely that the reduction of *Fgf8* expression within the PA of *Fgf8*-hypomorphs results in a loss of FGFR mediated signalling. *Fgfrs 1-3* are all expressed within the PA (Walshe and Mason, 2000). Mice homozygous null for *Fgfr3* survive to term but have malformed skeletons (Deng et al., 1996). *Fgfr1* homozygous null and *Fgfr2* homozygous null embryos both die early in development as FGF signalling through these receptors is required, respectively, during gastrulation and implantation (Deng et al., 1994; Yamaguchi et al., 1994; Arman et al., 1998). Despite their overlapping expression domains within the PA, pouch morphogenesis has only been analysed (or documented) in *Fgfr1* deficient mice (*Fgfr1* hypomorphs). Although it has been demonstrated that the *Fgfr2* isoform, *Fgfr2-IIIb* is required for the stroma of the thymi to proliferate, an earlier role for FGFR2-IIIb in 3rd pouch morphogenesis has not been analysed (Dooley et al., 2007).

Mice hypomorphic for *Fgfr1* were generated by insertion of a neomycin cassette into either exon 7 or exon 15 of the *Fgfr1* allele, (respectively, *Fgfr1*$^{n7/n7}$ and *Fgfr1*$^{n15/n15}$ embryos) resulting in a reduction in the level of *Fgfr1* transcription to 20% of the level normally produced (Partanen et al., 1998). Surprisingly, only rostral pouch formation was affected *Fgfr1*$^{n7/n7}$ embryos (from here on referred to as *Fgfr1* hypomorphs) with the 1st and 2nd pouches appearing splayed and fused (Trokovic et al., 2003; Trokovic et al., 2005). Concordant with rostral pouch

phenotype, the 2nd arch of the *Fgfr1* hypomorphs was hypoplastic with only the distal region identifiable at E10.5 (Trokovic et al., 2003; Trokovic et al., 2005). The absence of the proximal arch coincided with a loss of CNCC migrating to this area and high levels of apoptosis in a region adjacent to the malformed 2nd arch (Trokovic et al., 2003). However, a CNCC specific deletion of *Fgfr1*, mediated by WNT1^{Cre}, did not recapitulate the 2nd pharyngeal arch hypoplasia of the *Fgfr1* hypomorphs. Conversely, reactivating *Fgfr1* expression in the CNCC of *Fgfr1* hypomorphs could not rescue the 2nd arch hypoplasia (Trokovic et al., 2003). Trokovic et al. propose that the loss of FGF signalling in the ectoderm of *Fgfr1* hypomorphs, (at stages preceding the outgrowth of the hypoplastic 2nd arch) underlies the 2nd arch defects (Trokovic et al., 2003; Trokovic et al., 2005). However, it is possible that the loss of endodermal FGF signalling and/or the perturbed endoderm morphology underlies the 2nd arch hypoplasia. The reduction of *Fgfr1* produces a relatively localised pharyngeal pouch defect when compared to the pharyngeal pouch defects of severe *Fgf8* hypomorphs. Thus, it is possible that FGF8 may also signal through other receptors during pouch morphogenesis, such as FGFR2.

1.3.2.5 FGF8 is hypothesized to act downstream of TBX1 within the endoderm during pouch formation

The caudal pouch aplasia of *Fgf8* hypomorphs and *Tbx1*$^{-/-}$ embryos indicates that both genes are required for pouch formation. The overlapping domains of *Fgf8* and *Tbx1* expression in the endoderm of the caudal most forming pouch suggests that both factors may function in the endoderm during pouch morphogenesis (Vitelli et al., 2002). Furthermore, the loss of *Fgf8* expression specifically in the endoderm of *Tbx1*$^{-/-}$ embryos indicates that FGF8 may act downstream of TBX1 in the endoderm

during pouch formation (Vitelli et al., 2002). Lastly, *Fgf8* and *Tbx1* act epistatically during the formation of endocrine glands derived from the pharyngeal endoderm (Vitelli et al., 2002). An increase in the incidence of thymus hypoplasia is reported in *Fgf8;Tbx1*$^{+/-}$ embryos relative to *Tbx1*$^{+/-}$ embryos. Moreover, thyroid hypoplasia manifests when *Fgf8* is deleted from *Tbx1* positive cells and is partially rescued by driving *Fgf8* transcription in *Tbx1* expression domains (Lania et al., 2009). Whether FGF8 and TBX1 function within the same endodermal pathway to regulate pouch morphogenesis has yet to be determined.

In addition to the FGF signalling cascade, there are a number of signalling cascades that affect pouch morphogenesis and appear to be regulated by, or are regulators of, TBX1 within the PA. Whether the proposed interactions with TBX1 are endoderm specific has not been determined.

1.3.3 The Retinoic Acid Signalling Pathway

Retinoic acid (RA) is the biologically active form of Vitamin A, (retinol), a compound whose level must be tightly regulated to ensure that viable embryonic development proceeds (Duester, 2008). The level of RA a cell is exposed to can be regulated by coupling the extent of RA synthesis to the extent of RA breakdown. Metabolism of RA is a 3-step process that requires the stepwise conversion of an alcohol (retinol) to an aldehyde (retinaldehyde), which in turn is oxidized to a carboxylic acid (RA) (Kam et al., 2012). RA is deemed the 'biologically active' component of the pathway as it directly binds to retinoic acid receptor (RAR) or retinoid X receptor (RXR) complexes to regulate the transcription of target genes (Kam et al., 2012). In the absence of RA, the receptor complex acts as a transcriptional repressor by binding to specific motifs (retinoic acid response elements, RAREs) within the promoter of a gene (Kam et al., 2012). Once RA binds to the DNA:RAR:RXR complex a conformational change is elicited; the chromatin is relaxed, the transcriptional co-repressors are released and the pre-initiation complex is recruited to enable transcription of the RA signalling target gene (Kam et al., 2012). RA signalling dependent transcription can thus be attenuated by the catabolism of RA. The cytochrome-P450 26-subfamily can achieve the latter through oxidative metabolism that degrades RA into the polar metabolites 4-hydroxy-RA and 4-oxo-RA. Thus, cells expressing the *Cyp26a1*, *Cyp26b1* or *Cyp26c1* will be rendered insensitive to RA signalling (Kam et al., 2012).

1.3.3.1 A requirement for RA signalling during pharyngeal pouch morphogenesis

The level of RA signalling during embryogenesis has been shown to be important for the correct formation of the pharyngeal pouches. RA is synthesised in the

pharyngeal mesenchyme, adjacent to the endoderm, where *Retinaldehyde dehydrogenase 2* (*Raldh2*) is expressed up to the level of the 2nd arch (Niederreither et al., 1997). RA signalling is then elicited in the endoderm by the binding of RA to RAR/RXRs expressed in the pharyngeal endoderm, such as Retinoic acid receptor-ß (RARB) (Niederreither and Dolle, 1998; Matt, 2003). Signalling is restricted to specific areas of pharyngeal endoderm, in part, by the differential expression of RAR/RXRs within the endoderm (Matt, 2003). This results in the pharyngeal pouches having varying sensitivity for RA signalling; broadly the anterior 2 pouches are less sensitive to RA than the posterior pouches.

The first pouch appears to have its own developmental program that does not require RA. As such, even in complete absence of RA the first pouch appears to form normally (Quinlan et al., 2002). However, it is interesting to note that excess RA can inhibit the formation of this pouch and the genes expressed within it. The second pouch is sensitive to the level of RA signalling but in a complex manner. In complete absence of RA, Vitamin A deficient quails only develop a partially formed, but regionally patterned, second pouch (Quinlan et al., 2002). In embryos hypomorphic for *Raldh2* (*Raldh2*$^{neo/-}$ embryos) the second pouch forms normally, presumably because *Raldh1* and *Raldh3* are expressed after E8.5, enabling some RA signalling in the endoderm to occur (Niederreither et al., 2003). Yet, mouse embryos deficient in *RARα1* and *RARß1*, that are expressed exclusively in the caudal PA, develop an expanded of second pouch (Matt, 2003). This indicates that outgrowth of the second pouch is controlled by RA signalling through specific RAR isoforms. Genetic and pharmacological studies have provided evidence to indicate that the 3rd and 4th pharyngeal pouches are highly sensitive to a loss or gain in the level of RA (Dupe et al., 1999; Wendling et al., 2000; Roberts et al., 2005; Roberts et

al., 2006). If RA signalling is inhibited or reduced then the caudal pouches are unable to evaginate (Dupe et al., 1999; Wendling et al., 2000). This is highlighted in *Raldh2*$^{neo/-}$ mutant mice that display thymus and parathyroid aplasia due to lack of third pouch formation (Niederreither et al., 2003).

1.3.3.2 A reciprocal inhibition of *Tbx1* expression and RA signalling is evident in the pharyngeal endoderm during pharyngeal pouch morphogenesis

Caudal pouch aplasia, similar to that exhibited in *Tbx1*$^{-/-}$ embryos, manifests in embryos that lack, or have increased, RA signalling. Data in the literature demonstrates that *Tbx1* expression and RA signalling are mutually inhibitory (Guris et al., 2006). Retinol soaked beads grafted into the pharyngeal pouches of quail embryos results in a decrease in the level of *Tbx1* expression around the bead and VAD quails lack *Tbx1* expression (Roberts et al., 2005). Conversely, the expression of *Raldh2* (an enzyme that synthesises RA), is extended anteriorly in the PA of *Tbx1*$^{-/-}$ embryos (Guris et al., 2006). The latter coincides with a loss in expression of the catabolic enzymes *Cyp26a1, Cyp26b1* and *Cyp26c1* that clear RA (Guris et al., 2006; Roberts et al., 2006). Lastly, *Raldh2* and *Tbx1* have been shown to interact epistatically during the formation of the fourth pouch. The 4th pouch is unilaterally hypoplastic in mice heterozygous null for both *Raldh2* and *Tbx1*, a defect not observed in embryos lacking one allele of either *Raldh2* or *Tbx1* (Ryckebusch et al., 2010).

1.3.4 The Sonic Hedgehog (SHH) pathway

Sonic Hedgehog (*Shh*) is one of three *Hedgehog* (*Hh*) ligand homologues in expressed in mammals, the other two are *Indian hedgehog* (*Ihh*) and *Desert Hedgehog* (*Dhh*) (Bürglin and Kuwabara, 2006). *Hh* was first isolated from a mutagenesis screen in *Drosophila melanogaster* that identified Hh as a key regulator of the spatial organisation of the larva's segmented body-plan (Nusslein-Volhard and Wieschaus, 1980). HH signalling is now recognised as a fundamental to mammalian development. The absence of *Shh* in embryos homozygous null for this allele ($Shh^{-/-}$ embryos) severely perturbs development, resulting in defects of the nervous system (i.e. reduced brain size, specifically the forebrain and absence of the spinal column), skeleton (i.e. absence of digits, and rib cartilages) and of sensory organs (i.e. cyclopia of the eyes and the presence of a single nasal pit contribute to the holoprosencephaly of $Shh^{-/-}$ embryos) (Chiang et al., 1996; Hu and Helms, 1999). As such, the requirement for SHH in the formation of the PA was not immediately investigated despite its evident malformation in *Shh-/-* embryos.

1.3.4.1 SHH signalling

SHH is often found in 'signalling centres' (e.g. the zone of polarising activity in the limb buds) where its activity is essential for the patterning the surrounding tissues (Cohen, 2010). There are three steps in SHH signalling 1) *Post-translational modification of the immature ligand* which involves the SHH peptide being autocatalitically cleaved into two fragments (Lee et al., 1994). The active N-terminal fragment is modified by addition of cholesterol and a palmitoyl group to, respectively, the C-terminus and N-terminus (Beachy et al., 1997; Pepinsky et al.,

1998) 2) *Signal transduction* involves the inhibitory association of Patched (PTCH) with a 7-pass G-protein receptor, Smoothened (SMO), being relieved (Stone et al., 1996; Murone et al., 1999). The latter is achieved when PTCH1 or PTCH2 (which are 12-pass transmembrane receptors) sequester the mature, secreted SHH peptide (Marigo et al., 1996). 3) *Intracellular signalling* is achieved by the phosphorylation of Glioma-associated oncogene transcription factors (GLI1, GLI2 and GLI3) by SMO recruited kinases (Ingham and McMahon, 2001). GLI1 and (generally) GLI2 are transcriptional activators that in an un-phosphorylated form are recruited to the nucleus to initiate transcription (Barnfield et al., 2005). GLI3 in its cleaved form is a transcriptional repressor (Ding et al., 1999). Target genes include those in the SHH transduction pathway, such as *Gli1* and *Ptch1*, thus the SHH pathway is autoregulatory (Ingham and McMahon, 2001).

1.3.4.2 A requirement for SHH during pharyngeal pouch morphogenesis

Shh is present primarily in the medial regions of pharyngeal endoderm (the inter-pouch regions) although it has been identified as an early marker of 2nd pouch formation in chick embryos, despite its absence from the 2nd pouch later in gestation (Garg et al., 2001; Quinlan et al., 2002; Moore-Scott and Manley, 2005). In mouse embryos, by E9.5, *Shh* expression is generally restricted to the inter-pouch regions and is absent from the pharyngeal pouches themselves. For instance, at E9.5 *Shh* is visible in the pharyngeal endoderm caudal to the 3rd pouch (the presumptive 4th pouch domain) but is absent from the 3rd pouch proper (Moore-Scott and Manley, 2005). Despite the absence of *Shh* from the majority of the pharyngeal pouch endoderm, *Shh*$^{-/-}$ embryos display pouch defects (Moore-Scott and Manley, 2005).

At E9.5 pouches the 2nd and 3rd pouches of *Shh*$^{-/-}$ embryos have formed relatively normally but the 1st pouch is severely hypoplastic (Moore-Scott and Manley, 2005). By E10.5 all four pouches of *Shh*$^{-/-}$ embryos were hypoplastic (as were the corresponding arches) and abnormally patterned. For instance, in the absence of *Shh* the expression of *Fgf8 a*nd *Pax1* are up-regulated in the 3rd pouch, relative to the more anterior pouches (Moore-Scott and Manley, 2005). An increase in apoptosis is observed in the pharyngeal mesenchyme of *Shh*$^{-/-}$ embryos (Moore-Scott and Manley, 2005; Yamagishi et al., 2006). In the 1st arch at the least, the increase in apoptosis is correlated to a loss of endodermal *Shh* that is required to drive the expression of *Fgf8* in the 1st arch ectoderm (Haworth et al., 2007). This data indicates that if endodermal SHH plays a role in pouch development it is likely during the regulation of pouch patterning, or indeed in cell survival (which has not been analysed in the endoderm), because pharyngeal pouch formation commences in the absence of *Shh*.

1.3.4.3 SHH regulates *Tbx1* expression in the endoderm during pharyngeal pouch morphogenesis

The observation that; a) *Tbx1* expression was absent from the pharyngeal endoderm of *Shh*$^{-/-}$ embryos at E9.5 and b) is ectopically expressed in the tissue surrounding a SHH coated bead implanted into the PA of chick embryos, suggested that SHH may regulate *Tbx1* expression (Garg et al., 2001). It was subsequently found that SHH may positively regulate *Tbx1* expression in the endoderm via the transcription factor *Forkhead box A2* (*Foxa2*) *(Yamagishi et al., 2003)*. SHH is required for the maintained expression of *Foxa2* and this transcription factor is able to activate a luciferase reporter cloned downstream of the Fox-binding

element (FBE) in the 1.1-kb *Tbx1* enhancer (Yamagishi et al., 2003).

However, it is questionable whether the SHH dependent regulation of *Tbx1* is required for pouch formation. For, the expression domains of *Shh* and *Tbx1* do not overlap in the evaginating pouch endoderm. More significantly, the loss of *Shh* results in a pouch phenotype that is distinct from that which is generated by a loss of *Tbx1;* the rostral pouches are most significantly affected by the loss of *Shh* whereas the caudal pouches are most significantly affected by the loss of *Tbx1* (Jerome and Papaioannou, 2001; Moore-Scott and Manley, 2005). Furthermore, the genetic profile of the caudal endoderm of the two mutants is also distinct. For instance, *Fgf8* expression is absent from the caudal endoderm of *Tbx1*$^{-/-}$ embryos but is maintained in *Shh*$^{-/-}$ embryos pharyngeal endoderm (Vitelli et al., 2002; Moore-Scott and Manley, 2005). Although parathyroid development is absent in both mutants, different mechanisms are attributed to the loss of this endocrine organ. The parathyroid of *Tbx1*$^{-/-}$ embryos fails to develop because the 3rd pouch is aplastic (Liao et al., 2004). In contrast, the 3rd pouch of *Shh*$^{-/-}$ embryos develops but the *Gcm2* domain is lost at the expense of an expanded *Foxn1* domain (Moore-Scott and Manley, 2005).

1.4 Aim of this study

The research presented in the introduction identifies a number of genes expressed within the pharyngeal endoderm that when deleted affect pouch development. However, with the exception of *Tbx1* (which needs confirming), the requirement for these genes within the endoderm during pouch morphogenesis has not been directly examined, only inferred. The aim of this study was to use a new endodermally expressed *Cre* line, the *Sox17-2Ai-Cre* line, to test the requirement for *Tbx1*, *Fgf8* and *Fgf receptors 1* and *2* within the endoderm during pharyngeal pouch development. It was hoped that the data collected would reveal the mechanisms by which *Tbx1* regulates pouch evagination.

Pouch morphogenesis and thymi formation were assessed in $Sox17^{icre/+}Tbx1^{flox/-}$ ($Tbx1cKO^{Sox17}$) embryos to test the inference of Arnold et al. that *Tbx1* is required in the endoderm during pouch and endocrine organ development (Arnold et al., 2006). The formation of PA derivatives that originate from non-endodermal pharyngeal cells (thoracic vessels and external ear) were also analysed in the mutants to address the non-cell autonomous effect endodermal *Tbx1* has during PA development. $Tbx1cKO^{Sox17}$ embryos recapitulated the endodermal defects of $Tbx1^{-/-}$ and *PE-KO* embryos. The next question posed was how does endodermal *Tbx1* regulate pharyngeal pouch evagination? It was hypothesised that *Tbx1* is required in the endoderm during pouch morphogenesis to positively regulate the FGF pathway by inducing the endodermal expression of *Fgf* ligands. Subsequently, *in situ* hybridisation was used to analyse the expression of genes in the FGF signalling cascade endoderm of $Sox17^{icre/+}Tbx1^{flox/-}$ embryos. Surprisingly, only *Fgf8* expression was diminished in the pharyngeal endoderm of these mutants, indicative of a unique, TBX1 dependent role for FGF8 within the endoderm during

pouch formation. To test the role of *Fgf8* within the endoderm during pouch formation *Sox17$^{icre/+}$Fgf8$^{flox/-}$* (*Fgf8cKO^{Sox17}*) embryos were generated. An analysis of the pharyngeal endoderm and thymus formation in the *Fgf8cKO^{Sox17}* embryos revealed that pharyngeal endoderm development appeared to be unaffected by the loss of endodermal *Fgf8*. As FGF signalling (assessed by the expression of *Fgf* readouts) was unperturbed in the endoderm of *Fgf8cKO^{Sox17}* embryos it was reasoned that other FGF ligands within the endoderm may be compensating for the loss of *Fgf8*. The alternative possibility was that FGF signalling is not required in the endoderm during pouch formation.

Thus, the second aim of the study was to verify that FGF signalling is required within the endoderm during pouch morphogenesis. Compound mutants deficient of *Fgf3* and *Fgf8* (*Sox17$^{icre/+}$;Fgf3$^{flox/-}$;Fgf8$^{flox/-}$* embryos) in the endoderm were found to have a low frequency of rostral pouch fusion, detected by whole mount in situ hybridisation for *Pax1*. Deleting *Fgfr1* and *Fgfr2* from the endoderm recapitulated, with full penetrance, the bilateral rostral pouch fusion detected in some *Sox17$^{icre/+}$;Fgf3$^{flox/-}$;Fgf8$^{flox/-}$* embryos and displayed severe 3rd pouch hypoplasia. These pouch defects correlated with a greatly diminished expression of *Fgf* effectors within the pharyngeal endoderm. These results demonstrate that FGF signalling and TBX1 are both required within the endoderm for pharyngeal pouch morphogenesis to proceed 'normally'. However, three pieces of data indicate that FGF signalling and TBX1 function in independent endodermal pathways to regulate pouch morphogenesis: 1) distinct pouch phenotypes are observed in FGF-deficient and Tbx1-deficient endodermal mutants; 2) *Sox17$^{icre/+}$Fgf8$^{flox/+}$;Tbx1$^{flox/+}$* mutant's pouch morphogenesis is no more perturbed than that of *Sox17$^{icre/+}$;Tbx1$^{f/+}$* embryos indicating there is no epistatic interaction

between FGF8 and TBX1 in the endoderm during pouch development; and 3) that genetically reducing the level of FGF signalling regulators (*Sprouty* genes) in the endoderm of *Tbx1cKO*^{Sox17} embryos did not rescue caudal pouch morphogenesis.

The third aim of the study was to determine the mechanism(s) by which TBX1 regulates pouch outgrowth within the pharyngeal endoderm. An expression analysis of the RA signalling cascade (regulated by TBX1) and SHH signalling cascade (a regulator of *Tbx1*) revealed that genes in both cascades were maintained in the pharyngeal endoderm of *Tbx1cKO*^{Sox17} embryos. Multiple genes in each cascade (i.e. *Shh*, *Ptch1, Rarb, Cyp26b1*) displayed an 'un-segmented' expression pattern in the pharyngeal endoderm of the *Tbx1cKO*^{Sox17} embryos. This led to the prediction that the expression changes were secondary to a TBX1-dependent loss of pharyngeal endoderm architecture/structure. To test this prediction the presence and location of cytoskeletal proteins within TBX1-deficient endoderm was analysed. A striking loss in the polarity of the actin cytoskeleton was observed in the pharyngeal endoderm of *Tbx1cKO*^{Sox17} embryos.

Chapter 2

Materials and Methods

2.1 General solutions and reagents

All solutions, unless stated otherwise, were prepared with deionised, double-distilled water (ddH_20) and sterilised by autoclaving. Solutions were treated with 0.01% (v/v) Diethylpyrocarbonate (DepC) for 2 hours minimum, prior to autoclaving if RNase sensitive protocols were carried out. Detergents (tween, triton-X etc.) were added post-autoclaving.

Table 3: Lists the solutions used routinely during experiments

Solution	Reagents	Storage conditions
0.5M Ethylenediaminetetraacetic acid (EDTA), pH8.0	93.1g EDTA disodium salt (Fisher Bp120500), 10g NaOH (VWR 28244.262), add 400ml ddH_2O adjust to pH8.0 with sodium hydroxide (fisher), adjust 500ml with ddH_2O.	Store at RT^{o}C.
Glycerol (x%)	Glycerol (Fisher, G060017) diluted in PBS to required concentration (X%), i.e. 80%	Store at RT^{o}C.
Goat serum (GS)	Goat serum (Sigma) thawed and heat inactivated (HI) at 56^{o}C for 30 minutes.	Store 10ml aliquots, after cooling, at -20^{o}C.
4% (w/v) Paraformaldehyde (PFA)	Paraformaldehyde (Sigma) dissolved in PBS whilst heating to 60^{o}C and stirring.	Store 20ml aliquots, after cooling, at -20^{o}C. Thaw at 37^{o}C and cool

		on ice before applying to embryos.
10x Phosphate buffered saline solution	10x Phosphate buffered saline tablets (Sigma) dissolved in sterile ddH_2O as per manufacturers instructions.	Store at RT^{o}C. Dilute 1:10 with sterile ddH_2O to 1x Phosphate buffered saline solution, (PBS) working solution.
PBT	Tween-20 was added at 0.1% (v/v) to PBS solutions (unless otherwise stated).	Store at RT^{o}C.
PBTX	Triton-x (Sigma) was added at 0.1% (v/v) to PBS solutions (unless otherwise stated).	Store at RT^{o}C.

20% Sodium dodecyl sulphate (SDS)	Sodium dodecyl sulphate (Sigma) dissolved in DepC H_2O.	Store at RT^{o}C.
20x Sodium citrate solution (SSC) pH4.5.	20x Sodium citrate solution (solution purchased from	Store at RT^{o}C.

	Fisher BP13254)	
Tris-HCL pH (X)	Trizma base (Sigma, T1503) dissolve in DepC H_2O, adjusted to desired pH with hydrochloric acid.	Store at RT°C.
Triton X-100	4-(1,1,3,3-Tetramethylbutyl) phenyl-polyethylene glycol, (solution purchased from Sigma, X100)	Store at RT°C.
Tween-20	Polyethylene glycol sorbitan monolaurate, (solution purchased from Sigma, P9416)	Store at RT°C.

2.2 Molecular biology

Centrifuge steps were all carried out on a bench top centrifuge at 13500rpm unless stated otherwise.

2.2.1 Genotyping

2.2.1.1 Genotyping Solutions

Table 4 lists the solutions routinely used during genotyping protocols.

Table 4: General genotyping solutions

Gentle lysis buffer	5ml gelatine (stock 10mg/ml), 25ml 1M KCL (sigma), 1ml 1M $MgCL_2$ (fisher), 22.5ml of 10% IGE-PAL (sigma) and 5ml 1M Tris-HCL pH8.3 bring volume to 500ml with ddH_2O. Autoclave, then upon cooling add 22.5ml of Tween-20, aliquot and store long term at -20°C.
Proteinase K (Invitrogen 25530015)	100mg Proteinase K (PK) added to 5ml RNase free H_2O, freeze 100µl at -20°C.
50x TAE	200ml 0.5M EDTA pH8.0, 114.2ml glacial acetic acid 484g Tris base (Sigma), to 1L ddH_2O.

2.2.1.2 DNA isolation

Ear clips from mouse pups or yolk sacs from embryos were added to 300µl of gentle lysis buffer with 1.5µl of proteinase K (PK, 100µg/ml). Mouse tissue was degraded in a heat-block overnight at 55°C. Post-incubation 300µl of RNase free PCR grade H_2O (molecular grade water, VWR International cat no. 443847D) was added to the genotyping samples. Subsequently the samples were heat inactivated at 90°C for 45 minutes to denature the PK. After cooling, the genotyping samples were spun in a centrifuge for 5 minutes to pellet cell debris, leaving the DNA in solution.

2.2.1.3 PCR Reaction

PCR reactions listed in Table 5 (see below) were set up on ice, the master mix used was dependent on the requirement of the oligonucleotides for additional GC-rich substrate (see Appendix A). 1µl of DNA was added to each 19µl reaction aliquot. The PCR reaction was loaded into a thermocycler PCR machine (Eppendorf Mastercycler) that subjects the mix to a series of heating and cooling steps that result in an amplification of the genomic DNA. In brief the thermocycler PCR amplification steps are as follows, (for specifics of each oligonucleotides PCR see Appendix A). The three steps are repeated for between 30-40 cycles.

Step	Temperature	Time
1) Denaturing (Disassociating double stranded DNA to form single stranded DNA)	94°C	1 minute
2) Annealing (Binding of primers to complementary sequence in the endogenous DNA)	54°C	45 seconds
3) Extension (The polymerase binds to the ends of the double stranded DNA formed by the primer-template duplex and adds additional dNTPs to the sequence.)	72°C	2 minutes

Table 5: Typical PCR master mix reaction

Roche PCR master mix, 19µl/sample total	**Promega PCR master mix, 19µl/sample total**
H_2O (11.7/15.7µl)	H_2O (12.5µl)
G-C Rich buffer (4/0µl) *NB: Some PCR reactions do not require G-C.*	Green buffer (4µl)
$MgCl_2$ (1.2µl)	$MgCl_2$ (2µl)
Primers (x) (1µl)*	Primers (x) (1µl)*
dNTPs (0.15µl)	dNTPs (0.15µl)
Roche Fast start Taq polymerase (0.15µl)	Promega Hot start Taq polymerase (0.15µl)

2.2.1.4 Gel electrophoresis

Gel electrophoresis was used to visualize the products of the PCR reaction. A 1.5% agarose gel was prepared by dissolving 6g of low melting point agarose (Fisher, BP160-100) in 400ml of 1x TAE. After cooling 20µl of ethidium bromide (Sigma, E7637) was added to the molten agarose and the solution was poured into a gel-casting tray. The PCR samples, mixed with 4µl of loading dye (Promega green buffer), and either a 100bp (Fermentas, SM0324) or a 1Kb plus DNA ladder (Invitrogen, 10787018) were loaded onto the set gel. The samples were run through the gel in an electrophoresis tank at 190V in 1x TAE typically for 40 minutes. Using the DNA ladder as a reference, the size of the DNA fragments amplified in the PCR reaction, (that are intercalated with ethidium bromide) were determined after visualizing the gel in an ultraviolet light illuminator.

2.2.2 Protocol for production of an mRNA probe

Note: All steps involving bacterial cells were performed over a Bunsen burner flame under sterile conditions i.e. with sterilized consumables and ethanol sterilized surfaces.

2.2.2.1 Transformation of competent bacterial cells

N.B. Competent cells were kept on ice at all times unless otherwise stated. SOC media and agar plates with antibiotics were warmed to 37°C before use.

Vectors containing a DNA sequence of interest were amplified by driving the plasmid into Novablue *Escherichia coli* (*E. coli*) competent cells (Merck Chemicals Ltd. Cat no.69825-4). 1µg of plasmid DNA was added to a 10µl aliquot of competent cells, (thawed on ice) and incubated for a further 5 minutes on ice. Uptake of the vector by *E. coli* cells was achieved by heat shocking the cell-vector mix for 45 seconds at 42°C. The *E. coli* cells were left to recover on ice for a subsequent 2 minutes. 80µl of SOC media was added to the cells that were then streaked onto agar plates (with the required antibiotic to select for transformed cells). The plates were incubated at 37°C for between 14-16 hours for optimal bacterial growth.

2.2.2.2 Starter culture of transformed bacterial clones

N.B. Bacterial plates may be stored at 4°C (in a bacterial fridge) for up to 4 weeks.

After the overnight incubation single colonies of transformed *E. coli* cells were picked from the seeded bacterial plate using a pipette tip. The pipette tip was ejected into 5ml of LB media (with appropriate antibiotic (typically 50mg/ml) for selection of transformed bacteria). Bacterial cultures were incubated in a

(300rpm) rotating shaker Kuhner Shaker (model no.isf-1-w) at 37^{o}C for between 14-16 hours, to ensure optimal bacterial growth.

2.2.2.3 Large culture of transformed bacterial clones and bacterial stocks

N.B. Bacterial suspensions may be stored at 4^{o}C (in a bacterial fridge) for up to 4 weeks.

After overnight incubation the 5ml 'starter' mini culture of transformed *E. coli* cells were re-homogenised by gently inverting the falcon tube. 1ml of bacterial cells were removed from the starter suspension and ejected into a conical flask containing 200ml of LB media (with 400µl of the appropriate antibiotic (typically 50mg/ml) for selection of transformed bacteria). Bacterial suspensions were incubated in a rotating shaker (300rpm), at 37^{o}C for between 14-16 hours, to ensure optimal bacterial growth. A further 500µl of starter growth culture was removed, mixed with 500µl of 50% glycerol or 7% DMSO to make a bacterial stock and transferred to the -80^{o}C for long-term storage.

2.2.2.4 Maxi-preparation of plasmid DNA

N.B. Bacterial pellets from the centrifuged large culture may be stored at -20^{o}C for up to 1 week once the LB media has been removed.

After an overnight incubation the 200ml 'large' culture of transformed *E. coli* cells were aliquoted into four 50ml falcon tubes of equal weight and spun at 4^{o}C, 5000rpm, for 30 minutes in a large bench top centrifuge. The liquid broth was discarded and the bacterial pellet retained for DNA isolation by maxi-preparation. The extraction of DNA was achieved by following the steps outlined in the Quiagen Maxiprep protocol. In brief, the DNA was re-suspended and homogenized by

adding buffer P1 (containing lyse blue to visualize efficiency of lysis by buffer P2 and100µg/ml of RNase A) to the bacterial pellets and combining to one falcon. Subsequently buffer P2 was added (mixed by gentle inverting to avoid DNA shearing) to achieve bacterial cell lysis. To neutralize the reaction and precipitate genomic DNA and proteins, chilled buffer P3 was added. Supernatant (containing plasmid DNA) from the P3 mix was filtered through a QIAfilter cartidge, into an equilibrated QIAGEN-tip 500 to which the DNA binds. The bound DNA was washed twice with buffer QC to remove any contaminants and then eluted into a 50ml falcon with buffer QF, to which isopropanol was added to precipitate DNA from the solution. After incubation, the DNA was collected using the QIA precipitator that filters the isopropanol and binds the DNA. Finally, the DNA is washed in the QIA precipitator with 70% ethanol and eluted with 1.5ml of buffer TE into an eppendorf (repeating twice to maximize elution). The isolated DNA is stored at -20^{o}C. The optical density (OD) of the maxi-preparation's end product (1µl of prep diluted in 199µl of H_2O or TE) was measured in a spectrophotometer to determine the concentration of the isolated DNA.

2.2.2.5 DNA digest, sequencing and linearization

To confirm that the DNA isolated from the vector by maxi-preparation was the vector carrying the DNA insert of interest, restriction digests were routinely performed. The DNA vector was cut at multiple restriction enzyme (RE) sites. The cutting of the vector by different REs cut the circular vector into linear fragments of DNA of a specific size. The size of the bands resulting from the digest, determined by gel electrophoresis (see 2.2.1.4) should match those detailed on the vector map. To an eppendorf containing 20µg of plasmid, 1µl of the required restriction enzyme(s) was added with 4µl of the appropriate RE buffer and 0.5µl

BSA (if required). Molecular biology grade H_2O was added to bring the total volume to 20µl and the reaction was left to proceed overnight at RT^oC, or, for 2 hours at 37^oC. After the incubation period, 5µl of the reactions end product was removed and imaged by gel electrophoresis with the uncut plasmid to determine if the digest was successful and to determine the size of the cut DNA fragments.

To further confirm that the vector isolated by maxi-preparation contains the DNA insert of interest, an aliquot of the DNA was sent for sequencing. Typically 10µl of DNA (of a concentration between 10-250ng/µl) was sent to DBS Genomics (Durham University) that was sequenced with their universal in-house primers. Commonly either pBluescript T3 (GCA ATT AAC CCT CAC TAA AGG GA), pBluescript/pGEM T7 (GTA ATA CGA CTC ACT ATA GGG CG) or pGEM SP6 (GCT ATT TAG GTG ACA CTA TAG) were used dependent on the vector map.

2.2.2.6 Phenol:chloroform extraction of digested DNA

After confirming that the DNA digest has been successful (see 2.2.2.3) the linearized DNA was extracted from the reaction mix, as this contains reagents that are inhibitory to the RNA synthesis reaction. To the linearized plasmid 1ml of phenol:chloroform (25:24:1, volume, Sigma P3802), was added, vortexed and centrifuged at 4^oC for 30 minutes to extract the DNA. Subsequently, the aqueous phase (approximately 20µl) containing high molecular weight DNA was transferred into a new eppendorf. The remaining liquid from the phenol:chloroform incubation, containing extracellular membranes and polysaccharides, were discarded. DNA precipitation was achieved by incubating the aqueous phase DNA with 3M sodium acetate, NaOAc, (1/10 the volume of aqueous phase DNA) and 100% ethanol (3x the volume of aqueous phase DNA) for

10 minutes at RT^{o}C. The DNA was vortexed and incubated in the 100% ethanol:NaOAc mix at -20^{o}C for 30 minutes to maximise the yield of DNA precipitated from the solution. Subsequently, the mix was centrifuged for 30 minutes at 4^{o}C to form a DNA pellet. The 100% ethanol was discarded and a further 1ml of 70% ethanol added to wash the salt from the pellet. After vortexing, the DNA pellet in 70% ethanol was centrifuging for a final 15 minutes at 4^{o}C. All 70% ethanol was carefully removed with a pipette tip, taking care not to disrupt the pellet. The DNA pellet was incubated in a heat block set at 42^{o}C to evaporate the residual ethanol. Once dry the DNA pellet was dissolved in 20µl of RNase free (not DepC) TE buffer (10mM Tris-HCl [pH 7.4], 1mM EDTA) or molecular biology grade H_2O and stored at -20^{o}C.

2.2.2.7 Digoxigenin (DIG) labelled RNA probe synthesis

NB: This is an RNase sensitive protocol.

To synthesise RNA complementary to that of the linear, genomic DNA extracted by phenol:choloroform the following reaction was set up. To an eppendorf the following reagents were added in this order: Molecular biology, RNase free H_2O (DepC free), to give a final reaction volume of 20µl; 4µl of 5x transcription buffer (Promega) containing salts and spermidine required by the polymerase enzyme; 2µl of 0.1M Dithiothreitol (DTT, Promega) to stabilise the RNA polymerase, 2µl of DIG nucleotide mix (pH8.0) containing DIG-11-UTPs that are incorporated into the synthesised single-stranded RNA product by *in vitro* RNA polymerase mediated transcription, 1µl of linearized plasmid (approximately 1µg/µl) to generate 10µg/µl of full length DIG-labelled RNA, 0.5µl of RNase inhibitor (RNasin, Roche, 100U/ml) to prevent RNase mediated degradation of RNA, 1µl of RNA polymerase

(10U/µl) specific to the promoter site engineered into the vector/PCR template, e.g. SP6, T7, T3 (see Appendix D).

The *in vitro* RNA transcription reaction was left to proceed for either 12 hours at RT^{o}C or 2 hours at 37^{o}C. Subsequently 1µl of the transcription mix was removed for gel electrophoresis to visualize the RNA synthesized and approximate its yield, (see 2.2.1.4). After confirmation that RNA synthesis was successful, 2µl of RNase-free DNase1 (Roche) was added to the transcription reaction for 15 minutes, at 37^{o}C, to degrade the DNA template. Finally, the RNA probe was purified from the transcription reaction mix using 'SigmaSpin' post reaction clean-up columns (S0185). Briefly, the columns were inverted to dissipate the beads in the column. The caps of the columns were loosened, the bottom closure removed and the column centrifuged in an eppendorf for 2 minutes at 750 x *g*. The excess H_2O-preservative solution from the column is discarded. Probe was added to the column in a new eppendorf and centrifuged for 4 minutes at 750 x *g*. The eluted DNA is contained in H_2O with ~25ppm of Kathon, a preservative. The probe must be stored at -80^{o}C and defrosted on ice to prevent degradation of the RNA probe. See Appendix D for a list of probe used in this thesis.

2.3 Generation of mouse embryos

2.3.1 Mouse breeding strategies

Mice were bred and housed in accordance with home office regulations.

Conditional mouse lines are used throughout this project to recombine and thus delete floxed alleles. To achieve tissue specific deletion in endodermal and endothelial cells the Sox17-2Ai-Cre mouse line was utilised. $WNT1^{Cre}$ and $MESP1^{Cre}$ were used, respectively, to achieve tissue specific deletions of genes in the cranial neural crest cells and in the mesoderm. See Appendix E for mouse line references and information on the MGI ID number. Mouse breeding strategies are illustrated as schematics in Figures 6 to 11, below.

2.3.1.1 Generation of *Tbx1$^{flox/+}$*, *Sox17$^{icre/+}$;Tbx1$^{flox/+}$*, *Sox17$^{icre/+}$;Tbx1$^{flox/-}$*, *Sox17$^{icre/+}$;Sprouty1$^{flox/+}$;Sprouty2$^{flox/+}$;Tbx1$^{flox/-}$* and *Sox17$^{icre/+}$;Fgf8 $^{flox/+}$;Tbx1$^{flox/+}$* mice and embryos.

Fig 5

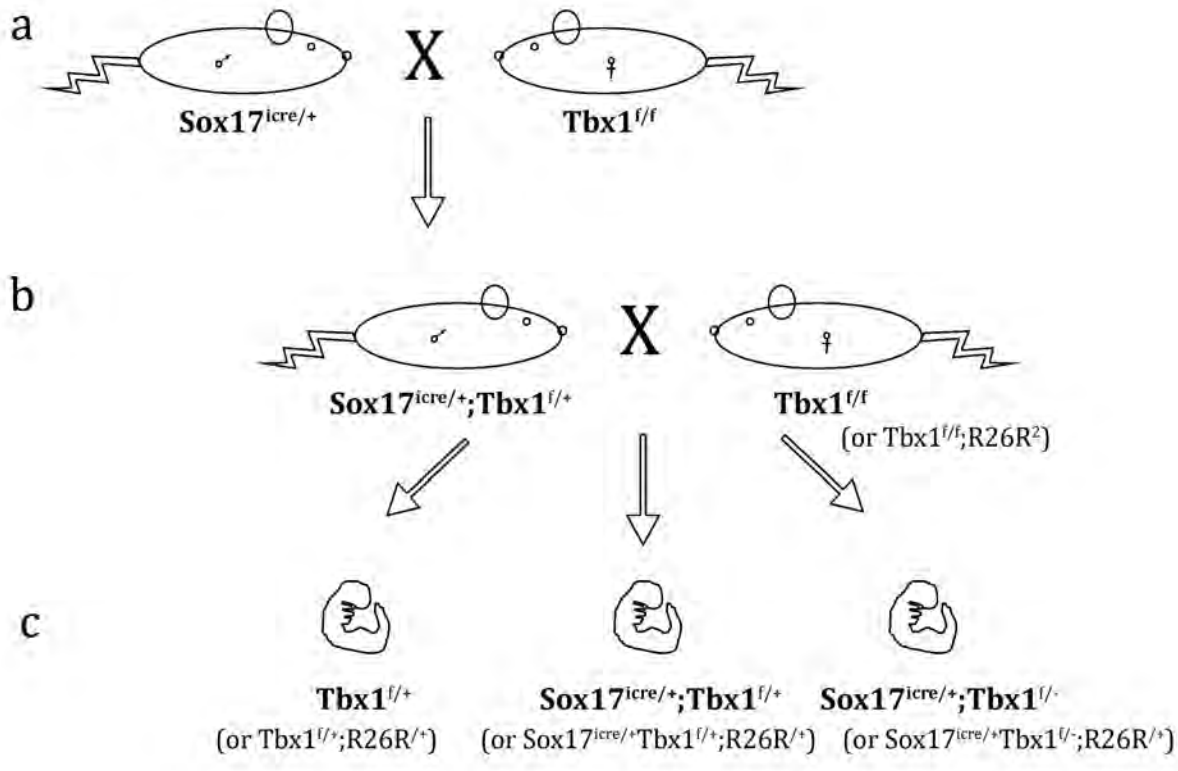

Fig 5 Illustrates the breeding strategy followed to generate *Tbx1$^{flox/+}$*, *Sox17$^{icre/+}$;Tbx1$^{flox/+}$* and *Sox17$^{icre/+}$;Tbx1$^{flox/-}$* embryos. a. A transgenic stud male heterozygous for the *Sox17$^{tm2.1(icre)Heli}$* allele (Sox17^{iCre}), that drives expression of *Cre* from the *Sox17* promoter, was crossed to female transgenic mice homozygous for the *Tbx1$^{tm1.1Bem}$* allele, (exon 5 of the gene *T-box 1* flanked by lox-P sites, i.e. *Tbx1^{flox}*). b. Male progeny heterozygous for *Sox17^{iCre}* and the *Tbx1^{flox}* allele (*Sox17$^{icre/+}$Tbx1$^{flox/+}$*) were kept from this cross and used to impregnate *Tbx1$^{flox/flox}$* females, or female mice homozygous for *Tbx1^{flox}* and for the gene trap *Rosa-26* allele, *Gt(ROSA)26Sor^{tm1Shoe}* (*Tbx1$^{flox/flox}$;R262^{2}*). c. The mating illustrated in (b) generated *Tbx1$^{flox/+}$* (Cre negative*), Sox17$^{icre/+}$Tbx1$^{flox/+}$* (*Tbx1cHetSox17*) and *Sox17$^{icre/+}$;Tbx1$^{flox/-}$* (*Tbx1cKOSox17*) embryos that are utilised within this thesis, all of which would also be heterozygous for *R26R* if derived from a *Tbx1$^{flox/flox}$R262^{2}* female in (b). NB: names in parentheses (documented in C), from here on, identify the genotype of embryos used throughout the thesis.

Fig 6

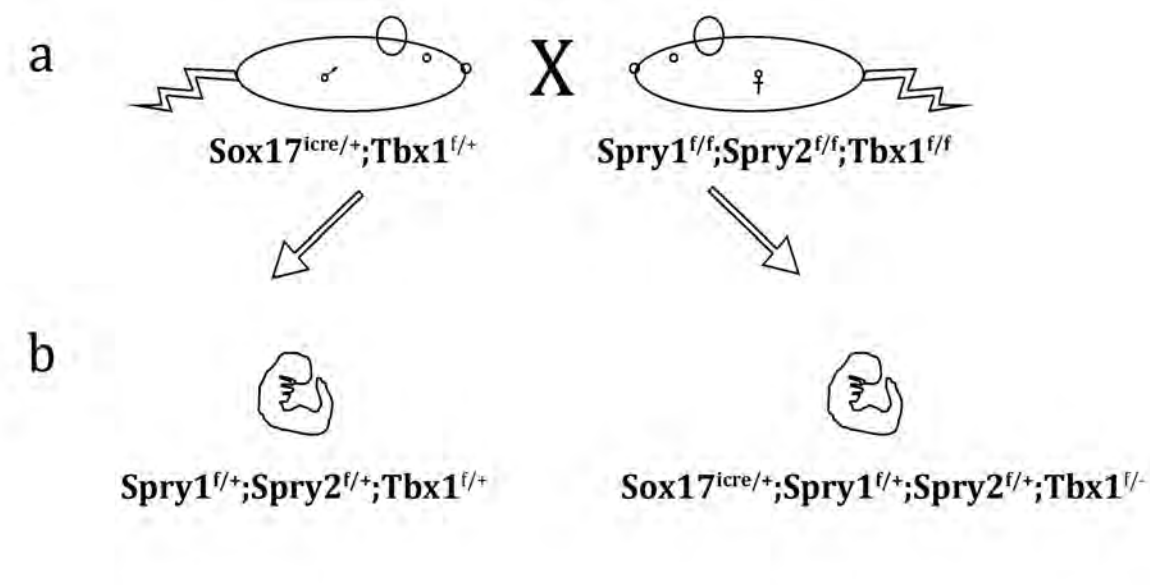

Fig 6 Illustrates the breeding strategy followed to generate *Spry1$^{flox/+}$;Spry2$^{flox/+}$,Tbx1$^{flox/+}$* and *Sox17$^{icre/+}$;Spry1$^{flox/+}$;Spry2$^{flox/+}$;Tbx1$^{flox/-}$* embryos. a. Male *Sox17$^{icre/+}$Tbx1$^{flox/+}$* mice were used to impregnate female mice homozygous for the alleles, *Spry1^{tm1Jdli}* (exon … of the gene Sprouty homolog 1 is flanked by lox-P sites, i.e. Spry1^{flox}), *Spry2 $^{tm1.1Mrt}$* (exon … of the gene *Sprouty homolog 2* is flanked by lox-P sites, i.e. *Spry2^{flox}*,) and *Tbx1^{flox}*. b. The mating generated *Spry1$^{flox/+}$;Spry2$^{flox/+}$,Tbx1$^{flox/+}$* (Cre negative), *Sox17$^{icre/+}$;Spry1$^{flox/+}$;Spry2$^{flox/+}$,Tbx1$^{flox/+}$* (*Spry1;Spry2;Tbx1cHet^{Sox17}*) and *Sox17$^{icre/+}$;Spry1$^{flox/+}$;Spry2$^{flox/+}$,Tbx1$^{flox/-}$* (*Spry1;Spry2cHet;Tbx1cKO^{Sox17}*) embryos that are utilised within this thesis. NB: names in parentheses (documented in b), from here on, identify the genotype of embryos used throughout the thesis.

Fig 7

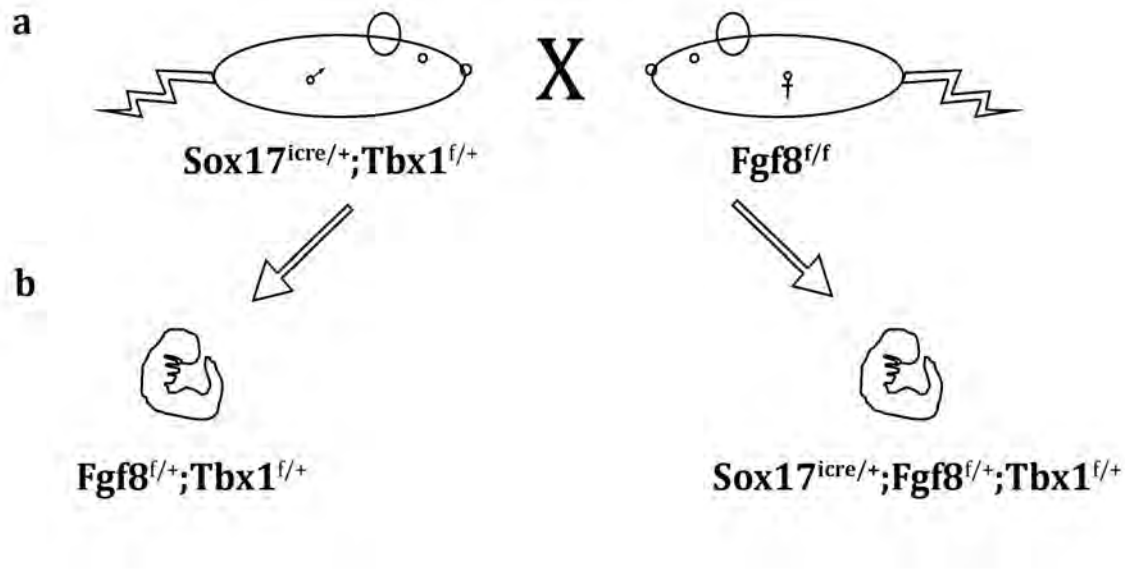

Fig 7 Illustrates the breeding strategy followed to generate *Fgf8$^{flox/+}$,Tbx1$^{flox/+}$* and *Sox17$^{icre/+}$;Fgf8$^{flox/+}$;Tbx1$^{flox/-}$* embryos. a. Male *Sox17$^{icre/+}$Tbx1$^{flox/+}$* mice were used to impregnate female mice homozygous for the alleles, *Fgf8$^{tm1.3Mrt}$* (exon … of the gene ***Fibroblast growth factor 8*** is flanked by lox-P sites, i.e. *Fgf8^{flox}*). b. The mating generated *Fgf8$^{flox/+}$;Tbx1$^{flox/+}$* (Cre negative) and ***Sox17$^{icre/+}$;Fgf8$^{flox/+}$;Tbx1$^{flox/+}$*** (*Fgf8cHet;Tbx1cHet^{Sox17}*) embryos that are utilised within this thesis. NB: names in parentheses (documented in b), from here on, identify the genotype of embryos used throughout the thesis.

2.3.1.2 Generation of *Fgf8*$^{flox/+}$, *Sox17*$^{icre/+}$;*Fgf8*$^{flox/+}$ and *Sox17*$^{icre/+}$;*Fgf8*$^{flox/-}$ embryos

Fig 8

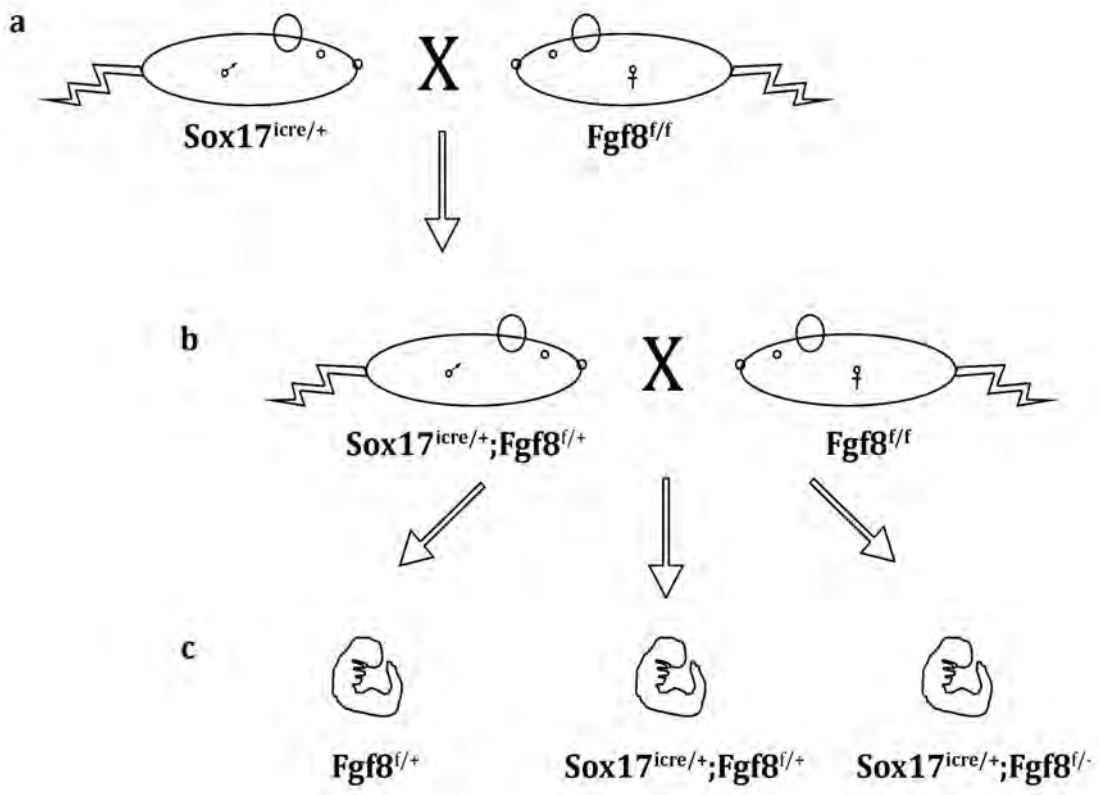

Fig 8 Illustrates the breeding strategy followed to generate *Fgf8*$^{flox/+}$, *Sox17*$^{icre/+}$;*Fgf8*$^{flox/+}$, *Sox17*$^{icre/+}$;*Fgf8*$^{flox/-}$ embryos. a. *Sox17*$^{iCre/+}$ males were crossed to *Fgf8*$^{flox/flox}$ females. b. Male progeny heterozygous for *Sox17*^{iCre} and the *Fgf8*^{flox} allele (*Sox17*$^{icre/+}$;*Fgf8*$^{flox/+}$) were kept from this cross and used to impregnate *Fgf8*$^{flox/flox}$ female's c. The mating illustrated in (b) generates *Fgf8*$^{flox/+}$ (Cre negative), *Sox17*$^{icre/+}$;*Fgf8*$^{flox/+}$ (*Fgf8cHet*^{Sox17}) and *Sox17*$^{icre/+}$;*Fgf8*$^{flox/-}$ (*Fgf8cKO*^{Sox17}) embryos that are utilised within this thesis. NB, names in parentheses (documented in C), from here on, identify the genotype of embryos used throughout the thesis.

2.3.1.3 Generation of *Fgfr1;Fgfr2$^{flox/+}$*, *Sox17$^{icre/+}$;Fgfr1;Fgfr2$^{flox/+}$*, *Sox17$^{icre/+}$;Fgfr1$^{flox/-}$;Fgfr2$^{flox/+}$*, *Sox17$^{icre/+}$;Fgfr1$^{flox/+}$;Fgfr2$^{flox/-}$* and *Sox17$^{icre/+}$;Fgfr1;Fgfr2$^{flox/-}$* embryos

Fig 9 (see below) Illustrates the breeding strategy followed to generate *Fgfr1$^{flox/+}$;Fgfr2$^{flox/+}$*, *Sox17$^{icre/+}$;Fgfr1$^{flox/+}$;Fgfr2$^{flox/+}$*, *Sox17$^{icre/+}$;Fgfr1$^{flox/+}$;Fgfr2$^{flox/-}$*, *Sox17$^{icre/+}$;Fgfr1$^{flox/-}$;Fgfr2$^{flox/+}$* and *Sox17$^{icre/+}$;Fgfr1$^{flox/-}$;Fgfr2$^{flox/-}$* embryos. a. *Sox17$^{iCre/+}$* males were crossed to female mice homozygous for the alleles, *Fgfr1^{tm3Cxd}*, (exon … of the gene *Fibroblast growth factor receptor 1* is flanked by lox-P sites, i.e. *Fgfr1^{flox}*) and *Fgfr2$^{tm1.1Dor}$*, (exon … of the gene *Fibroblast growth factor receptor 2* is flanked by lox-P sites, i.e. *Fgfr2^{flox}*). b. Male progeny heterozygous for *Sox17^{iCre}*, *Fgfr1^{flox}* and the *Fgfr2^{flox}* allele (*Sox17$^{icre/+}$;Fgfr1$^{flox/+}$;Fgfr2$^{flox/+}$*) were kept from this cross and used to impregnate *Fgfr1;Fgfr2$^{flox/flox}$* females or *Fgfr1;Fgfr2$^{flox/flox}$* female mice also homozygous for the allele *Gt(ROSA)26Sor$^{tm1.1(EYFP)Cos}$*, (*Rosa26 eYFP Cre* reporter allele, i.e. females are *Fgfr1;Fgfr2$^{flox/flox}$;RYFP^{2}*). c. The mating illustrated in (b) generates *Fgfr1$^{flox/+}$;Fgfr2$^{flox/+}$* (Cre negative), *Sox17$^{icre/+}$;Fgfr1$^{flox/+}$;Fgfr2$^{flox/+}$* (*R1;R2cHet^{Sox17}*), *Sox17$^{icre/+}$;Fgfr1$^{flox/+}$;Fgfr2$^{flox/-}$* (*R1cHet;R2cKO^{Sox17}*), *Sox17$^{icre/+}$;Fgfr1$^{flox/-}$;Fgfr2$^{flox/+}$* (*R1cKO;R2cHet^{Sox17}*) and *Sox17$^{icre/+}$;Fgfr1$^{flox/-}$;Fgfr2$^{flox/-}$* (*R1;R2cKO^{Sox17}*) embryos that are utilised within this thesis, which would also be heterozygous for *RYFP* if derived from a *Fgfr1;Fgfr2$^{flox/flox}$;RYFP^{2}* female in (b). NB: names in parentheses (documented in C), from here on, identify the genotype of embryos used throughout the thesis.

Fig 9

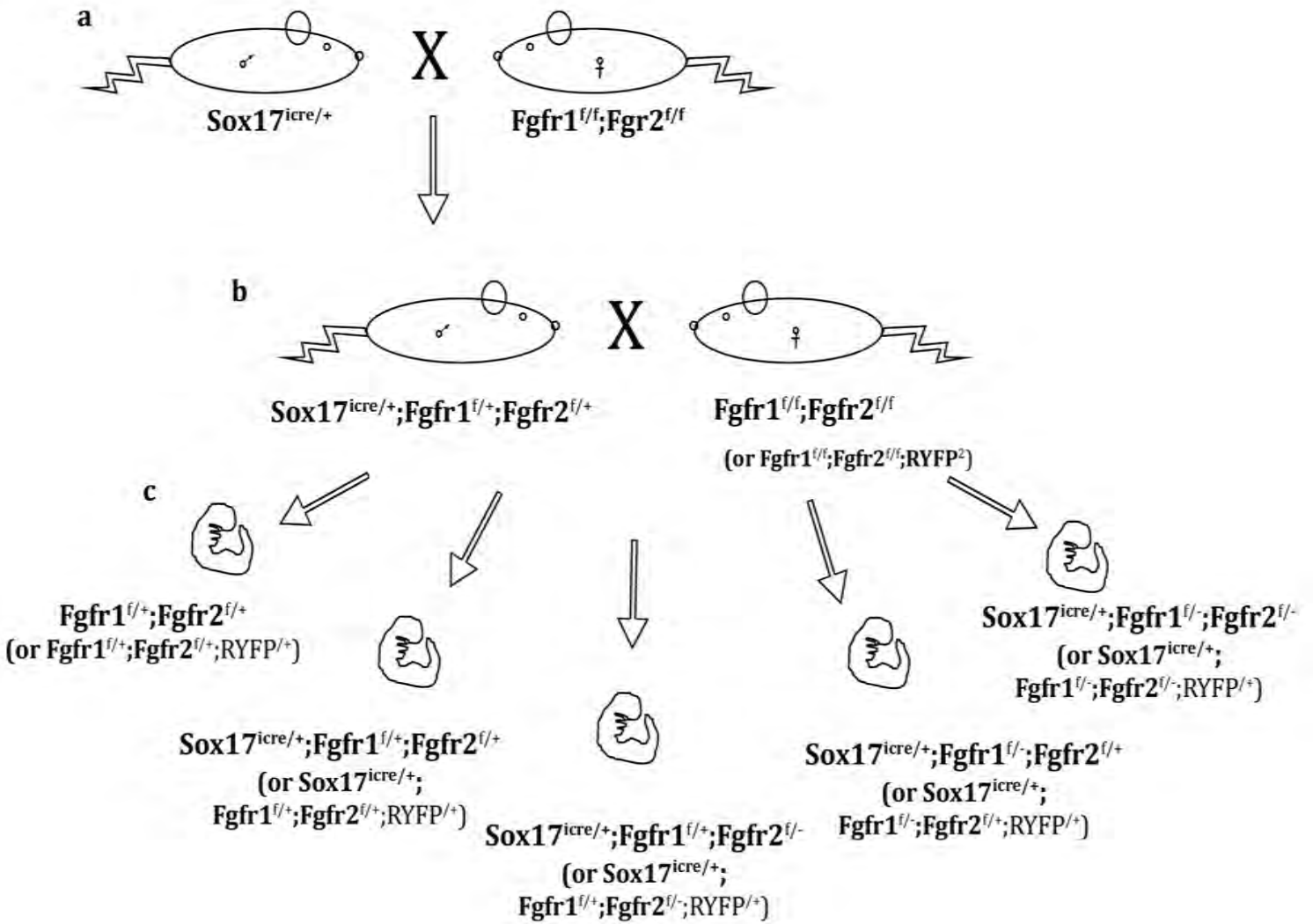
a
X
Sox17icre/+
Fgfr1f/f;Fgr2f/f
b
X
Sox17icre/+;Fgfr1f/+;Fgfr2f/+
Fgfr1f/f;Fgfr2f/f
(or Fgfr1f/f;Fgfr2f/f;RYFP2)
c
Fgfr1f/+;Fgfr2f/+
(or Fgfr1f/+;Fgfr2f/+;RYFP/+)
Sox17icre/+;Fgfr1f/+;Fgfr2f/+
(or Sox17icre/+;
Fgfr1f/+;Fgfr2f/+;RYFP/+)
Sox17icre/+;Fgfr1f/+;Fgfr2f/-
(or Sox17icre/+;
Fgfr1f/+;Fgfr2f/-;RYFP/+)
Sox17icre/+;Fgfr1f/-;Fgfr2f/+
(or Sox17icre/+;
Fgfr1f/-;Fgfr2f/+;RYFP/+)
Sox17icre/+;Fgfr1f/-;Fgfr2f/-
(or Sox17icre/+;
Fgfr1f/-;Fgfr2f/-;RYFP/+)

2.3.1.4 Generation of *Fgfr1;Fgfr2$^{flox/+}$*, *Mesp1$^{cre/+}$;Fgfr1;Fgfr2$^{flox/+}$*, *Mesp1$^{cre/+}$;Fgfr1$^{flox/+}$;Fgfr2$^{flox/-}$* and *Mesp1$^{cre/+}$;Fgfr1;Fgfr2$^{flox/-}$* embryos

Fig 10 (see below) Illustrates the breeding strategy followed to generate *Fgfr1$^{flox/+}$;Fgfr2$^{flox/+}$*, *Mesp1$^{Cre/+}$;Fgfr1$^{flox/+}$;Fgfr2$^{flox/+}$*, *Mesp1$^{Cre/+}$;Fgfr1$^{flox/+}$;Fgfr2$^{flox/-}$*, *Mesp1$^{Cre/+}$;Fgfr1$^{flox/-}$;Fgfr2$^{flox/+}$* and *Mesp1$^{Cre/+}$;Fgfr1$^{flox/-}$;Fgfr2$^{flox/-}$* embryos.

a. A transgenic stud male heterozygous for the ***Mesp1***$^{tm2(cre)Ysa}$ allele (*Mesp1^{Cre}*), that drives expression of *Cre* from the ***Mesoderm posterior 1*** (*Mesp1*) promoter, was crossed to a *Fgfr1;Fgfr2$^{flox/flox}$* female. b. Male progeny heterozygous for *Mesp1^{Cre}, Fgfr1^{flox}* and the *Fgfr2^{flox}* allele (*Mesp1$^{Cre/+}$;Fgfr1$^{flox/+}$;Fgfr2$^{flox/+}$*) were kept from this cross and used to impregnate *Fgfr1;Fgfr2$^{flox/flox}$* females or *Fgfr1;Fgfr2$^{flox/flox}$;RYFP^{2}* females. c. The mating illustrated in (b) generates *Fgfr1$^{flox/+}$;Fgfr2$^{flox/+}$* (Cre negative), *Mesp1$^{Cre/+}$;Fgfr1$^{flox/+}$;Fgfr2$^{flox/+}$* (*R1;R2cHet^{Mesp1}*), *Mesp1$^{Cre/+}$;Fgfr1$^{flox/+}$;Fgfr2$^{flox/-}$* (*R1cHet;R2cKO^{Mesp1}*) and *Mesp1$^{Cre/+}$;Fgfr1$^{flox/-}$;Fgfr2$^{flox/+}$* (*R1cKO;R2cHet^{Mesp1}*) embryos that were utilised in this thesis, which would also be heterozygous for RYFP if derived from a *Fgfr1;Fgfr2$^{flox/flox}$;RYFP^{2}* female in (b). *Mesp1$^{Cre/+}$;Fgfr1$^{flox/-}$;Fgfr2$^{flox/-}$* (*R1;R2cKO^{Mesp1}*) embryos that should have been recovered from this cross were never found in genotyped embryos of any stage. NB: names in parentheses (documented in C), from here on, identify the genotype of embryos used throughout the thesis.

Fig 10

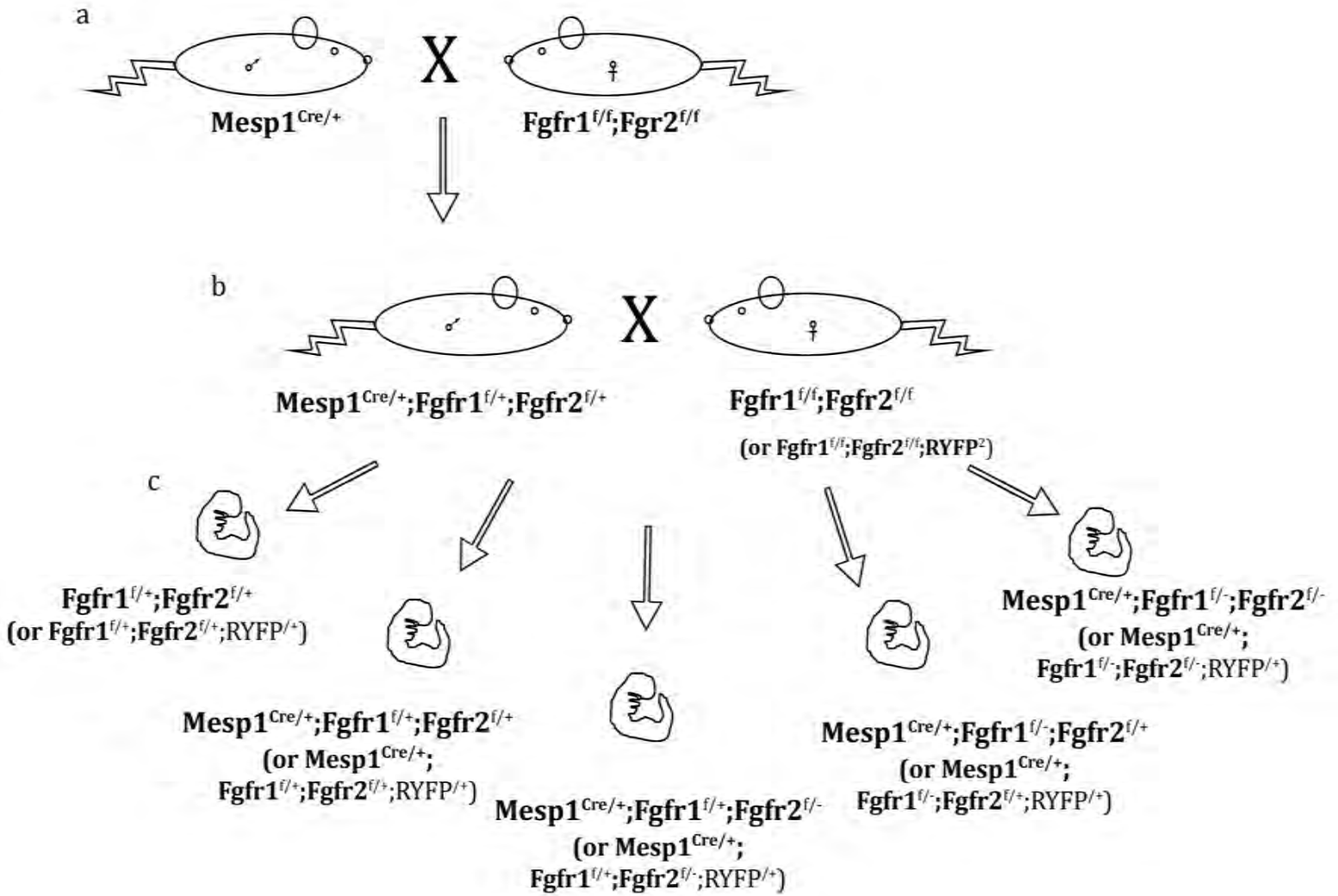
a
X
Mesp1Cre/+
Fgfr1f/f;Fgr2f/f
b
X
Mesp1Cre/+;Fgfr1f/+;Fgfr2f/+
Fgfr1f/f;Fgfr2f/f
(or Fgfr1f/f;Fgfr2f/f;RYFP2)
c
Fgfr1f/+;Fgfr2f/+
(or Fgfr1f/+;Fgfr2f/+;RYFP/+)
Mesp1Cre/+;Fgfr1f/+;Fgfr2f/+
(or Mesp1Cre/+;
Fgfr1f/+;Fgfr2f/+;RYFP/+)
Mesp1Cre/+;Fgfr1f/+;Fgfr2f/-
(or Mesp1Cre/+;
Fgfr1f/+;Fgfr2f/-;RYFP/+)
Mesp1Cre/+;Fgfr1f/-;Fgfr2f/+
(or Mesp1Cre/+;
Fgfr1f/-;Fgfr2f/+;RYFP/+)
Mesp1Cre/+;Fgfr1f/-;Fgfr2f/-
(or Mesp1Cre/+;
Fgfr1f/-;Fgfr2f/-;RYFP/+)

2.3.1.5 Generation of *Fgfr1;Fgfr2$^{flox/+}$*, *Wnt1$^{cre/+}$;Fgfr1;Fgfr2$^{flox/+}$* and *Wnt 1$^{cre/+}$;Fgfr1;Fgfr2$^{flox/-}$* embryos

Fig 11 Illustrates the breeding strategy followed to generate *Fgfr1$^{flox/+}$; Fgfr2$^{flox/+}$*, *Wnt1$^{Cre/+}$;Fgfr1$^{flox/+}$;Fgfr2$^{flox/+}$* and *Wnt1$^{Cre/+}$;Fgfr1$^{flox/-}$;Fgfr2$^{flox/-}$* embryos.

a. A transgenic stud male heterozygous for the *Tg(Wnt1-cre/Esr1*)10Rth* allele (Wnt1^{Cre}), that drives expression of Cre from the *Wingless-type MMTV integration site family, member 1* (*Wnt1*) promoter, was crossed to a *Fgfr1;Fgfr2$^{flox/flox}$* female. b. Male progeny heterozygous for *Mesp1^{Cre}*, *Fgfr1^{flox}* and the *Fgfr2^{flox}* allele (*Mesp1$^{Cre/+}$;Fgfr1$^{flox/+}$;Fgfr2$^{flox/+}$*) were kept from this cross and used to impregnate *Fgfr1;Fgfr2$^{flox/flox}$* or *Fgfr1;Fgfr2$^{flox/flox}$;RYFP^{2}* female's c. The mating illustrated in (b) generates *Fgfr1$^{flox/+}$;Fgfr2$^{flox/+}$* (Cre negative), *Wnt1$^{Cre/+}$;Fgfr1$^{flox/+}$;Fgfr2$^{flox/+}$* (*R1;R2cHet^{Wnt1}*) and *Wnt1$^{Cre/+}$;Fgfr1$^{flox/-}$;Fgfr2$^{flox/-}$* (*R1;R2cKO^{Wnt1}*) embryos that were utilised in this thesis, which would also be heterozygous for RYFP if derived from a *Fgfr1;Fgfr2$^{flox/flox}$;RYFP^{2}* female in (b). NB: names in parentheses (documented in C), from here on, identify the genotype of embryos used throughout the thesis.

Fig 11

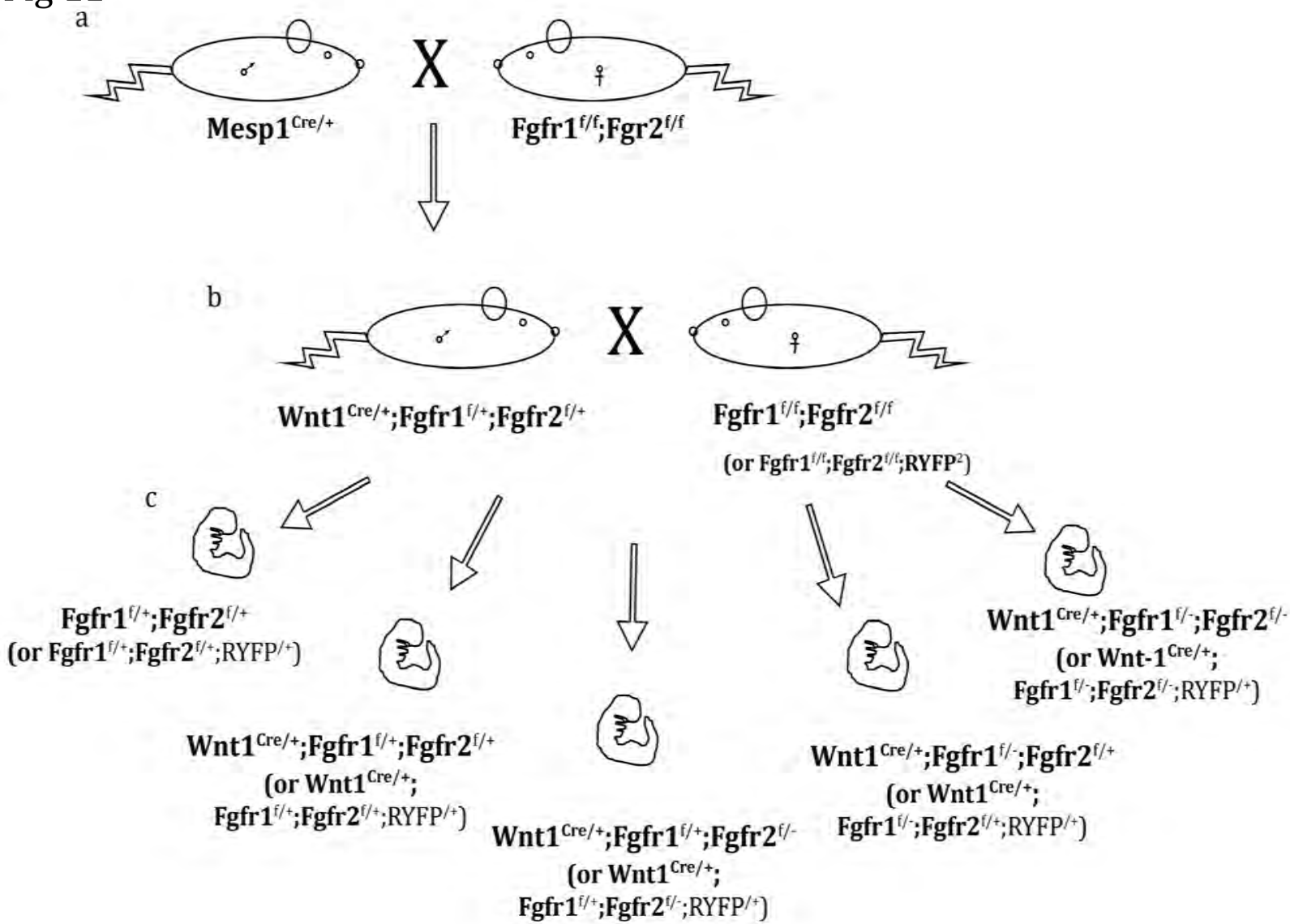
a
X
Mesp1Cre/+
Fgfr1f/f;Fgr2f/f
b
X
Wnt1Cre/+;Fgfr1f/+;Fgfr2f/+
Fgfr1f/f;Fgfr2f/f
(or Fgfr1f/f;Fgfr2f/f;RYFP2)
c
Fgfr1f/+;Fgfr2f/+
(or Fgfr1f/+;Fgfr2f/+;RYFP/+)
Wnt1Cre/+;Fgfr1f/+;Fgfr2f/+
(or Wnt1Cre/+;
Fgfr1f/+;Fgfr2f/+;RYFP/+)
Wnt1Cre/+;Fgfr1f/+;Fgfr2f/-
(or Wnt1Cre/+;
Fgfr1f/+;Fgfr2f/-;RYFP/+)
Wnt1Cre/+;Fgfr1f/-;Fgfr2f/+
(or Wnt1Cre/+;
Fgfr1f/-;Fgfr2f/+;RYFP/+)
Wnt1Cre/+;Fgfr1f/-;Fgfr2f/-
(or Wnt-1Cre/+;
Fgfr1f/-;Fgfr2f/-;RYFP/+)

2.3.2 Embryo preparation and staging

Embryonic day of development (E) E0.5, was determined as noon on the day a vaginal plug of the mated female was detected. Embryos of stages E8.5 through to E11.5 and E17.5 were dissected from the dams of pregnant females into DepC PBS (or Hanks solution if performing Lysotracker staining). The yolk sac was retained for genotyping (see 2.2.1.2) and the remaining uterine tissues and embryonic membranes were discarded. E8.5 to E11.5 embryos were staged with more accuracy by counting the number somites that had developed. E17.5 embryos were staged further by a comparison of their morphology with the atlas of mouse development (Kaufman, 1992). All embryos were fixed for a minimum of 2 hours at RT^{o}C or overnight 4^{o}C in 4%PFA (unless the protocol states otherwise. Post-fixation embryos were washed at least twice for a minimum of 5 minutes with DepC PBS to remove any PFA. Embryos were stored short term in 4^{o}C DepC PBS and long term in either 70% ethanol at 4^{o}C, or, in 100% methanol at -20^{o}C after a series of Methanol:PBT dehydration steps (see 2.4.4.1.a).

2.3.3 Embedding of embryos

2.3.3.1 Embedding embryos for paraffin wax sectioning

Dissected embryos were dehydrated from DepC PBS, to 30% and then 70% ethanol:DepC PBS (5min washes or until embryo equilibrates) and placed in embedding cassettes. The Leica series-300 was used to process embryos for wax embedding. The machine automatically fills and drains a retort (holding the embryos within their embedding cassettes) with a series of ethanol solutions (70%, 80%, 95% and 100% each applied twice) followed by three xylene changes

and a final incubation in paraffin. Embryos up to stage E11.5 were subjected to 1-hour incubation periods in the each solution. Subsequently the cassettes were transferred to fresh paraffin for embedding either frontally or sagittally.

A Leica microtome was used to cut 7um thick sections of paraffin wax embedded mouse tissue. Typically alternate sections were cut and floated onto a water bath set at 40^{o}C (RNase free H_2O). Tissue sections were mounted onto Superfrost plus slides, (Thermo scientific), dried briefly on a heat block and incubated in a 42^{o}C oven overnight so the sections bond to the slides.

2.3.3.1 Embedding embryos for cryosectioning

Dissected embryos were dehydrated into 30% sucrose/PBS typically for an hour and then into fresh 30% sucrose/PBS overnight. Embryos were then transferred from 30% sucrose/PBS into a 1:1 solution of 30% sucrose/PBS:OCT freezing media (Fisher, SD Lamb/OCT). After an hour incubation the embryos were transferred to 100% OCT and frozen over liquid nitrogen or dry ice. Samples were stored at -20^{o}C prior to cryosectioning. Frozen sections of embryonic tissue were cut to a thickness of 12µm in a cryostat set to between -20^{o}C and -24^{o}C. Typically alternate sections were cut and mounted onto Superfrost plus slides. Mounted slides can be kept up to 1 month if stored at -20^{o}C.

2.4 Staining of embryonic tissues

2.4.1 Staining solutions

See Appendix B for a list of specific solutions used in each staining protocol.

2.4.2 Whole mount X-gal staining to detect the Rosa26 Reporter

NB: all reagents are light sensitive and should be kept in foil.

X-gal (5-Bromo-4-chloro-3-indolyl-β-D-galactopyranoside) staining is a colorimetric reaction used to detect the activity of B-galactosidase expressed from the *R26R* allele.

Pre-prepared X-gal base solution was warmed to 37^{o}C. Embryos dissected from the uterus at stage E9.5 were fixed for 10 minutes on ice and immediately washed into PBS (2 x 5 minute washes). Fixed embryos were equilibrated in X-gal base solution for 30 minutes at 37^{o}C. Subsequently, X-gal enzyme (stock 40mg/ml, Fermentas R0941), was diluted 1:40 into the pre-warmed base solution and a minimum of 250µl was added to each embryo in a 24 well plate. The embryos were incubated in foil at either RT^{o}C (or 37^{o}C), typically for an hour, or until blue stain was evident in the embryos. Alternatively the colour reaction was left to proceed slowly overnight at 4^{o}C. Once appropriate staining had developed the reaction was stopped by washing the embryos in PBS and post fixing with 4% PFA overnight at 4^{o}C before imaging.

2.4.3. Whole mount LysoTracker staining

LysoTracker red (Invitrogen,L7528) probes (a fluorophore linked to a weak base), were used to stain acidic organelles, such as lysosomes, as an indicator of cell death. The probe will only accumulate in the acidic organelles of live cells, thus, embryos must be kept alive on removal from their mother's dam. Uteri containing embryos to be Lysotracker stained are collected and dissected in Hanks buffered saline solution (Hanks, Sigma H6684-1L), pre-warmed to 37^{o}C. Once all embryos have been collected they were incubated in Lysotracker red probe diluted 1/50 in Hanks for 15 minutes in the dark at 37^{o}C. After the incubation period embryos were fixed in 4% PFA for 30 minutes and dehydrated into 100% methanol to reduce background staining before being imaged.

2.4.5 Non-radioactive *in situ* hybridisation

Gene expression in fixed tissue can be qualitatively assessed by a technique called *in situ* hybridisation (ISH). The principle of ISH is to label endogenous mRNA, at a cellular level, with complementary antisense mRNA probes (see 2.2.2). The antisense mRNA probe contains labelled nucleic acids, (in this thesis all probes are labelled with DIG, see 2.2.28), which, after being bound by a specific antibody, can be visualised with specific chromogenic substrates. Thus, the greater the gene expression, the more endogenous mRNA:antisense mRNA probe complexes that will form, enabling greater antibody binding to the mRNA probe, thus increasing the signal from the chromogenic substrate.

2.4.5.1 Whole mount *in situ* hybridisation

To prevent trapping of staining substrates, embryos of a developmental stage E10.0 or older were perforated in the otic vesicle, hindbrain and nasal pit. All high temperature incubations were performed in a water bath.

2.4.5.1.a. WMISH, hybridisation steps

N.B. These steps are RNase sensitive.

Embryos were dehydrated by a series of methanol:PBT (25%, 50%, 75% and 100%) washes until equilibrated. Blood was bleached from the embryos by a 15 minute minimum incubation (embryo stage dependent) in 6% H_2O_2:methanol (stock H_2O_2 30% v/v solution, Sigma) at RT^{o}C. Embryos were rehydrated into a final solution of PBT through a series of methanol:PBT washes, (reverse of dehydration). Subsequently embryos were incubated in detergent mix for a minimum of two 20 minute periods and re-fixed by a 20 minute incubation in 4% PFA (all incubations at RT^{o}C). These steps ensure that the embryonic tissue is permeable to the uptake of mRNA probes and anti-DIG. After removing the PFA and washing the embryos in PBT, embryos were rinsed in 1:1 PBT:Hybridisation mix for 10 minutes at 65^{o}C. A 1hour incubation period at 65^{o}C in Hybridisation mix equilibrated the embryos for a subsequent incubation of 16hours minimum at 65^{o}C in the mRNA probe (typically 2µl/ml of mRNA probe was added to hybridisation mix), see 2.2.2 for probe synthesis details.

2.4.5.1.b. WMISH, Immunohistochemistry steps

The probe-hybridisation mix was removed and stored at -20^{o}C for re-use. Residual mRNA probe was removed by rinsing embryos in pre-warmed Solution X followed

by a series of four, 30-minute incubations in Solution X at 65°C. Subsequently embryos were rinsed in MABT and incubated in MABT for two 30-minute periods at RT°C. The MABT incubations ensure that the embryonic tissue is at pH optimal for the binding of the anti-DIG antibody to the endogenously bound DIG labelled RNA probe. Prior to the application of the antibody, non-specific binding was minimised by incubating the embryos in block 1 for 1 hour and then in block 2 for 1-3 hours (both incubation periods at RT°C). Post-blocking the anti-DIG-antibody, coupled to alkaline phosphatase (Roche), was diluted 1:2000 into block buffer 2 and applied to the embryos for a minimum of 16 hours at 4°C. To remove excess anti-DIG, after the incubation period, embryos were rinsed in MABT and washed hourly into fresh MABT for a further 8 hours before a final overnight incubation in fresh MABT.

2.4.5.1.c. WMISH signal detection steps

Alkaline phosphatase (AP) coupled to the endogenously bound anti-DIG antibody is detected by the addition of a chromogen substrate that reacts with AP will produce a visible colour precipitate. Subsequent to an overnight incubation in MABT the embryos are incubated in NTMT for four 10-minute periods, this buffer is optimal for the enzymatic activity of the alkaline phosphatase on the chromogen substrate. The enzymatic colour reaction was typically carried out using BM purple (Roche #11442074001) as the chromogen substrate. Embryos incubated with BM purple were kept in the dark at RT°C, or, at 4°C to slow the reaction. The progress of the colour reaction was checked every 30 minutes until the desired stain intensity was achieved. The colour reaction was stopped by washing the embryos out of BM purple and through a series of NTMT, PBT washes before fixing in 4% PFA and imaging the samples.

2.4.5.2 Section *in situ* hybridisation (ISH)

NB: All steps are carried out in autoclaved coplin jars at RT°C unless stated otherwise. The overnight incubation in RNA probe is carried out in a humid (H_2O:Formamide), floating chamber in a 65°C water bath.

2.4.5.2.a. ISH, hybridisation steps

N.B. These steps are RNase sensitive.

Wax was removed from tissue sections by incubating the slides in xylene, three times for 3minutes, before re-hydrating the tissue through a series ethanol:DepC H_2O, (100%, 95%, 70%) for two 2minute incubations. A subsequent 10minute incubation in 4%PFA ensured the tissue was bonded to the slides. After washing the slides twice in DepC PBS to remove the fixative the tissue was permeabilized by incubating it for 8minutes in 8µg/ml Proteinase K (PK, Dako S3020). After a 5minute incubation in DepC PBS the tissue was cross-linked in its 'permeable' state by a further 5 minute incubation in 4% PFA. Residual fix was washed away by another 5-minute incubation in DepC PBS. As the mRNA probe is negatively charged it may bind non-specifically to positively charged amino groups in the tissue, resulting in background staining. To reduce background staining, positively charged amino groups in the tissue are acetylated by incubation for 10minutes in the acetylation mix. The sections were washed a further three times in DepC PBS whilst diluting the mRNA probes to 2µl/ml of hybridization mix. The tissue was dehydrated from 70% to 95% ethanol ready for incubation with the probe-hybridisation mix. Probes were incubated at 80°C for 2 minutes to prevent non-specific binding before applying 300µl to each slide, covering with parafilm (Alcan PARAPM996) and incubating at 65°C for at least 16 hours.

2.4.5.2.b. ISH, immunohistochemistry steps

Coverslips were gently floated off from the slides in pre-warmed 5xSSC before being incubated in HIS for 20 minutes at 65°C. After equilibrating the tissue in RNase buffer for three 10 minutes washes at 37°C, unbound mRNA probe was removed from the sections by incubation with 100µg/ml of RNaseA (diluted in RNase buffer). A wash for 15 minutes at 37°C in RNase buffer followed by two 20minute washes in HIS were carried out to remove residual RNase enzyme. High stringency washes (15 minutes each at 37°C) in 2xSSC, and 0.1xSSC ensure removal of any mRNA probe not tightly bound to the endogenous mRNA sequence. After a final wash in PBT the slides are blocked in 10% HI GS in PBT for 1hour to prevent non-specific binding of the anti-DIG antibody. Subsequently the sections are incubated with anti-DIG-antibody diluted 1:5000 in 0.1% HI GS:PBT for a minimum of 16 hours at 4°C. Alternatively, the binding of the anti-DIG antibody to the endogenously bound DIG labelled RNA probe can be left to proceed for 3hours at RT°C before proceeding straight onto the signal detection steps.

2.4.5.2.c. ISH, signal detection steps

Residual, unbound anti-DIG antibody is removed by four 15-minute washes in PBT. Subsequently the tissue was incubated in NTMT for two 10-minute periods, this buffer is optimal for the enzymatic activity of alkaline phosphatase on the chromogen substrate. The enzymatic colour reaction was typically carried out using BM purple (*Roche* #11442074001) as the chromogen substrate. Embryos incubated with BM purple were kept in the dark at RT°C, or, at 4°C to slow the reaction. The progress of the colour reaction was checked at regular intervals until the desired stain intensity was achieved.

2.4.5.2d ISH, counterstaining and mounting

When the desired staining of the tissues was achieved the BM purple was removed and residual chromogen substrate removed by two 5minutes PBS washes. Tissue was counterstained with nuclear fast red (N3020) and diluted 1/50 in PBS for between 2-5 minutes. After dehydrating the tissue through a series ethanol:PBS (70%, 95%, 100%) washes, residual H_2O was removed by incubation in xylene before applying DPX mounting medium (a mix of distyrene, a plasticizer, and xylene, VWR) to the slides and mounting them with glass coverslips (VWR).

2.4.6 Immunohistochemistry (IHC)

This technique is used to detect the abundance of proteins by the detection of antigens unique to specific proteins. All steps are carried out at RT^{o}C in slide holders (Tissue-Tek 62540-01), unless otherwise stated. In all IHC protocols, after the blocking step excess solution was removed from the edges of the slides and a hydrophobic barrier was applied around the tissue sections with a PAP pen (Abcam ab2601). Subsequent solutions were drained from the slide onto paper towels and pipetting the next solution inside the hydrophobic barrier, onto the tissue. Antibodies used in the thesis are detailed in Appendix C.

2.4.6.1 HRP/Fluorescently conjugated immunohistochemistry on wax paraffin sections

2.4.6.1a Antigen blocking and primary antibody binding

Tissue sections were cleared of wax by two 10minute incubations in Xylene and rehydrated through a series of ethanol:PBS (100%, 95%, 90%, 70%) washes into

PBS, each gradient is performed twice for 5 minutes. Endogenous hydrogen peroxidase activity in the tissue will non-specifically oxidise the chromogen 3,3'-Diaminobenzidine tetra-hydrochloride (DAB Sigma, D5905), resulting in background staining. To minimise non-specific background staining, endogenous hydrogen peroxidase was blocked with 3% H_2O_2:PBS for 15 minutes. After washing in PBS, antigen retrieval was achieved by heating the slides in 10mM sodium citrate solution in the microwave on full power for four, 4minute intervals (topping up with H_2O after each heating period). Once the sections had cooled to RT^oC they were washed in with PBT_2 (0.2% Tween-20 in PBS) to permeabilize the tissue. Binding of the primary antibody to non-specific antigens in the tissue was minimised by applying wax-blocking solution (see Appendix B) to the sections for a minimum of 1 hour in a humid chamber. Subsequently, 100µl of primary antibody diluted in wax primary/secondary diluent (see Appendix B) was pipetted onto sections and incubated at 4^oC overnight in a humid chamber.

2.4.6.1b Secondary antibody binding, signal amplification and chromogen substrate detection

After an overnight incubation, the primary antibody was removed and the slides washed in PBT three times, each for 10 minutes. Subsequently 250µl of horseradish-peroxidase (HRP) conjugated secondary antibody, diluted 1:250 in wax primary/secondary diluent, was pipetted onto the sections that were incubated in a humid chamber for 1 hour. The secondary antibody solution was removed and the slides washed in PBT three times, each for 10 minutes. To amplify the amount of chromogen substrate signal A and B reagents (diluted 1:200 in wax primary/secondary diluent) were mixed and 250µl was applied to the sections for an hour in a humid chamber. The A and B reagents were removed by

three PBT washes, each for 10 minutes, followed by a further incubation of 5 minutes in PBS (in a coplin jar used only for DAB incubations). The chromogen substrate DAB (500µl) was added to 50mls of PBS, mixed carefully in a falcon and transferred to the coplin jar. To activate the reaction, 5µl of hydrogen peroxide (H_2O_2) was pipetted into the coplin jar and the colorimetric reaction was left to proceed for a minimum of 5 minutes in the dark. H_2O_2 is catalysed to H_2O and O_2 by the peroxidase activity of HRP (conjugated secondary antibody). DAB reacts with the O_2 produced to form a black/brown insoluble precipitate, marking the site of secondary antibody binding. If staining was optimal the DAB was removed and the slides washed in PBS for 5 minutes. Subsequently the tissue was counterstained with methyl green for 5 minutes, dipped in water one at a time to remove excess colour and left to dry. Sections were mounted with DPX and glass coverslips.

NB: If fluorescently labelled secondary antibodies are used instead of HRP-conjugated secondary antibodies the following steps are omitted; blocking of the endogenous peroxidase activity, addition of solutions 'A and B' and no chromogenic substrate reaction is required as the binding of the secondary antibody is directly visualised by detection of its conjugated fluorophore under a specific wave length of light. The slides are mounted as described in 2.4.5.2b.

2.4.6.2 Fluorescently labelled immunohistochemistry on cryosections.

2.4.6.2a Antigen blocking and primary antibody binding

OCT was removed by two 5 minute incubations in PBS and the tissue was permeabilized by a subsequent incubation in 0.5% Tween-20 in PBS before a final wash in PBS. Tissues were blocked for 1 hour with 'cryosection blocking solution' to minimise binding of the primary antibody to non-specific antigens. Finally 100µl of primary antibody diluted in 'cryosection primary/secondary diluent' was pipetted onto the sections and incubated at 4^{o}C overnight in a humid chamber.

2.4.6.2b Binding of fluorescently tagged secondary antibodies

After the overnight incubation, primary antibody was removed and the slides were washed in PBT three times, each for 10 minutes. Subsequently, 250µl of fluorescently labelled secondary antibody, diluted 1:250 in 'cryosection primary/secondary diluent', was pipetted onto the cryosections and incubated for 1 hour in a dark, humid chamber. After the hour-long incubation, the secondary antibody was removed and the slides were washed, in the dark, in PBT three times, each for 10 minutes. In the last minute of a final 5-minute PBS wash, Hoechst diluted 1:50,000 was added to mark the minor groove of AT-rich regions of DNA in the nucleus. Excess PBS was drained from the slides and the tissues were mounted in AF1 mountant solution (a glycerol:PBS based anti-fadent, Citifluor) and covered with glass coverslips.

2.7 Photo-microscopy

All photo microscopy images were processed and compiled in Photoshop CS2.

2.7.1 Whole mount fluorescent images

Embryos in PBS, detecting fluorescence from an RYFP reporter or from a Lysotracker probe, were captured as Z-stacks with a Zeiss Axioscope2. Fluorescence was detected under filtered UV light that masks all wavelengths of light but that emitted from the fluorophore of interest. Z-stacks were flattened into a compressed image using and the accompanying Axiovision software.

2.7.2 Whole mount images captured using white light

WMISH stained embryos were imaged using a Nikon Axiovision microscope with the accompanying Zeiss software.

2.7.3 White light and fluorescent images of sectioned tissue (not requiring Z-stacks)

White light was used to visualize BM purple or DAB precipitates in sectioned tissue on a Nikon SMZ1500 camera, attached to a Nikon driver, with the accompanying NIS Elements software. Fluorescently labelled tissue sections were visualized on a Nikon camera, attached to a Hamamatsu driver, with the accompanying NIS Elements software. UV light, with filters to mask all but the required wavelength of light, was used to excite emissions from the fluorophore conjugated to the secondary antibody.

2.7.4 Fluorescent images of sectioned tissue (requiring Z-stacks) processed on the confocal

Fluorescent images of cryosectioned tissue stained by IHC were captured as Z-stacks on a confocal microscope. Confocal microscopy uses lasers that emit and excite fluorophores with a specific wavelength of light. The Z-stack images were compressed in image J.

2.7.5 Quantitative analysis and Statistics

2.7.5.1 Proliferation assay

To determine the level of proliferation in the pharyngeal epithelia, fluorescently labelled tissue sections were visualized on a Nikon camera, attached to a Hamamatsu driver (see section 2.7.3) to visualise PH3 (identifies cells in S-phase i.e. proliferating) and E-cad (identifies epithelial cells) labelled cells. More than 2000 E-cad labelled cells were counted in both the endoderm and the ectoderm using Image J software, (ectoderm is used as a control because there should be no difference in proliferation between control and *Tbx1cKOSox17* ectoderm, as both are *Tbx1* positive). From the 2000 E-cad positive cells, the number of E-cad;PH3 positive (doubly labelled), cells were counted using Image J and a mitotic index (MI) was calculated as described Xu.et.al.,2005):

$$MI = \frac{\text{Number of proliferating cells (PH3 positive)}}{\text{Total cell number (E-cad;PH3 positive)}}$$

2.7.5.2 Calculating thymi circumference

E17.5 embryos were dissected from the uterus (see section 2.3.2), the chest cavity of each embryo was opened up and the overlying tissue e.g. skin, rib cartilage was carefully removed to reveal the position in which the thymus glands should lie. After imaging any thymi present, *in situ*, the glands were carefully removed to reveal and image the underlying thoracic vessels of the heart, (see section 2.7.3). Subsequently, the circumference of each thymi lobe was outlined and measured in Image J using the 'measure and label' tool. Arbitrary values corresponding to the circumference of each thymi, generated by the 'measure and label' tool in Image J, were converted to mm using the scale bar imaged at the same magnification as the thymi lobes.

2.7.5.3 Statistical analyses

Bar graphs, scatter plots and p-values (calculated using the Student's t-test) were produced with Graph Pad software.

Chapter 3

Results Part I

3.1 *Tbx1* is required in the endoderm for the formation of the pharyngeal pouches

T-box transcription factor 1 (*Tbx1*) is required for the outgrowth of the caudal pharyngeal pouches (pp 2-4) (Lindsay et al., 2001). The absence of caudal pouches and arches in *Tbx1*$^{-/-}$ embryos results in an un-segmented pharyngeal apparatus (PA) (Jerome and Papaioannou, 2001). Structures derived from every pharyngeal cell type are affected by the aberrant formation of the PA of *Tbx1*$^{-/-}$ embryos, (see sections 1.1.1-1.1.4). For instance, the pinna of the external ear is aplastic in *Tbx1*$^{-/-}$ embryos (Jerome and Papaioannou, 2001). The pharyngeal arch arteries (PAA) 3-6 do not form if *Tbx1* is absent during PA development and so the thoracic vessels of the heart are absent, or, re-arranged (Lindsay et al., 2001; Zhang et al., 2005; Calmont et al., 2009). The loss of *Tbx1* from the mesoderm also affects outflow tract (OFT) development and so the formation of the aorta (Lindsay et al., 2001; Kirby et al., 2008; Theveniau-Ruissy et al., 2008). The 3rd pouch is unable to form in the absence of *Tbx1* and so its derivatives, such as the thymi lobes, are aplastic (Jerome and Papaioannou., 2001; Liao et al., 2004).

The role of TBX1 in the development of specific PA structures is defined by the time, level and place of *Tbx1* expression. Over-expression of *Tbx1* recapitulates many of the PA defects observed in *Tbx1*$^{-/-}$ embryos, including thymus aplasia and ventricular septal defect, (Liao et al., 2004). However, the 'gain of function' *Tbx1*-mutants do not appear to display defects in pharyngeal pouch evagination. Caudal pouch aplasia manifests when the level of *Tbx1* mRNA in development is less than 25% the level synthesised in wild type embryos (Hu et al., 2004). In contrast, the deletion of one allele of *Tbx1* does not appear to affect caudal pouch evagination (Vitelli et al., 2002). By carrying out a timed deletion of *Tbx1* with a tamoxifen

inducible CRE mouse line, Xu et al. have identified a temporal requirement for *Tbx1* expression in pouch morphogenesis to be between E8.5 and E10.5 (Xu et al., 2005). As such, analyses of the role endodermal *Tbx1* plays in pharyngeal pouch morphogenesis in this have been conducted within this developmental period.

The deletion of *Tbx1* from specific cell types during development has begun to address the tissue specific requirements for *Tbx1* during pouch morphogenesis. Cranial neural crest cells (CNCCs) do not express *Tbx1* thus, accordingly, NCC specific deletions of *Tbx1* are not sufficient to cause pharyngeal pouch defects (Garg et al., 2001; Kochilas et al., 2002; Aggarwal et al., 2010). Embryos deficient in ectodermal *Tbx1* display hypoplastic thymi, however, no pharyngeal pouch defects have been reported in these mutants (Randall et al., 2009). In contrast, surprisingly, the expression of *Tbx1* from the mesoderm has been shown to be required for and is partially sufficient to drive pouch evagination, predominantly that of the 2nd pouch (Zhang et al., 2006).

Despite the wealth of tissue-specific CRE drivers available, a requirement for *Tbx1* in the endoderm during pouch morphogenesis has not been definitively proven. The NKX2.5^{Cre} driven deletion of *Tbx1* from domains within the 3rd and 4th pharyngeal pouches has been reported to cause a reduction in the size of the 4th arch and thymus hypoplasia, (Xu et al., 2004). Severe endodermal defects were not observed in these mutants because the endodermal domains of *Nkx2.5* and *Tbx1* only partially overlap in the caudal pouches, (Xu et al., 2004). Caudal pouch formation is absent in *Foxg1$^{Cre/+}$;Tbx1$^{flox/-}$* embryos (*PE-KO* embryos) bred on a Swiss-Webster (S-W) background, (Arnold et al., 2006). This is likely because *Foxg1* is expressed extensively throughout the pharyngeal endoderm. However, on

genetic backgrounds other than S-W, FOXG1^{Cre} is active in non-endodermal PA tissue (Zhang et al., 2005). Thus, taken together with the finding that mesodermal *Tbx1* is necessary and partially sufficient for pouch formation, the requirement and role of endodermal *Tbx1* expression alone during pouch morphogenesis is unclear.

The aim of the experiments presented in Chapter 3 were to determine a) whether endodermal *Tbx1* is required for caudal pouch formation; b) to what extent PA-derived organs and structures are affected by the loss of *Tbx1;* and c) whether the endodermal expression of genes in the FGF signalling cascade are affected by the loss of *Tbx1* from this tissue.

3.1.1 SOX17^{icre} deletes *Tbx1* specifically within the pharyngeal endoderm

Tbx1 is expressed in the ectoderm, mesoderm and endoderm of the PA between E8.5 and E11.5 when the pharyngeal pouches are evaginating (Vitelli et al., 2002). It is hypothesized that *Tbx1* is required specifically in the endoderm for pharyngeal pouch morphogenesis to occur (Arnold et al., 2006). Until recently this hypothesis was unable to be tested directly because the *Cre* lines available were expressed in non-endodermal tissues that have been shown to affect pouch or endocrine organ development. Recently a new mouse line that expresses *Cre recombinase* under the *Sox17* promoter has been generated (Engert et al., 2009; Liao et al., 2009). The activity of SOX17^{iCre} determined by *LacZ* expression from *ROSA26* conditional reporter (*R26R*), recapitulates the endogenous expression pattern of *Sox17* in endodermal and endothelial cells (Engert et al., 2009). To determine the requirement for *Tbx1* in the endoderm during pouch morphogenesis the *Sox17-2Ai-Cre* mouse line was used to generate *Tbx1$^{flox/+}$* and *Tbx1$^{flox/-}$* (Cre negative), *Sox17$^{icre/+}$Tbx1$^{flox/+}$* (*Tbx1cHet^{Sox17}*) and *Sox17$^{icre/+}$Tbx1$^{flox/-}$* (*Tbx1cKO^{Sox17}*) embryos, see 2.3.1 for details of breeding strategies. The deletion of *Tbx1* from endothelial cells using TIE2^{Cre} (the activity of this CRE protein is specific to endothelial tissue expressing *Tie2*), has not been reported to cause pouch defects (Xu et al., 2004; Chen et al., 2010). Thus, any perturbations in the pouch morphogenesis of *Tbx1cHet^{Sox17}* and *Tbx1cKO^{Sox17}* embryos will be a direct consequence of *Tbx1* being deleted from the pharyngeal endoderm.

The tissue-specific activity of SOX17^{iCre} in endoderm and endothelial cells, on a C57BL/6 genetic background, has been documented previously by Engert et al,

(Engert et al., 2009). To confirm that SOX17^{iCre} has the same specificity in a mixed genetic background, embryos were collected from crosses between *Sox17$^{icre/+}$Tbx1$^{flox/+}$* males and *Tbx1$^{f/f;}$R26R^{2}* females (see 2.3.1) and processed for X-gal staining. By E9.5 Cre negative embryos have formed their 1st and 2nd pouches and the 3rd pouch is just beginning to evaginate. No X-gal staining is evident in Cre negative embryos, (Fig 12a). Despite the X-gal marked SOX17^{iCre} activity present in the pharyngeal endoderm of *Tbx1cHet^{Sox17}* embryos, pharyngeal morphogenesis appears equivalent to that of Cre negative embryos (Fig 12: compare pouches indicated by arrows in panels a and b). In contrast, the endoderm of the *Tbx1cKO^{Sox17}* embryo is clearly un-segmented at E9.5 and only the 1st pouch can be detected (Fig 12 panel c, solid arrow). X-gal staining is only evident in the un-segmented endoderm and in the endothelial cells of the *Tbx1cKO^{Sox17}* embryos (Fig 12c). Some variation in the pattern of X-gal staining is evident between the *Tbx1cKO^{Sox17}* and *Tbx1cHet^{Sox17}* embryos (Fig 12 b vs c). The difference in stain appears specific to X-gal staining of endothelial cells. This inconsistency is not present when the Rosa26-eYFP (RYFP) reporter line is used to identify SOX17iCre activity, as fluorescence is always detected in endothelial and endodermal cells (see Fig 30).

The efficiency and specificity of the deletion of *Tbx1* by SOX17icre, within the PA, was assessed by immunohistochemistry using an anti-TBX1 antibody. TBX1 protein was detected in the caudal pharyngeal endoderm and in the core mesoderm of Cre negative and *Tbx1cHet^{Sox17}* embryos at E9.5 (Fig 12 g, h and e). These TBX1 positive domains in the PA corroborate with the domains of *Tbx1* expression in the PA (Fig 12 d). In contrast, TBX1 was absent from the pharyngeal endoderm of *Tbx1cKO^{Sox17}* embryos but was detected in the core mesoderm of the

pharyngeal arches, (Fig 12 f and i). The lack of TBX1 protein in the endoderm of *Tbx1cKO*^{Sox17} embryos confirms the efficient and specific deletion of *Tbx1* from the endoderm.

Fig 12: Caudal pouches do not form when SOX17-2A-icre ablates *Tbx1* from endoderm and endothelial cells. Whole mount images of E9.5 X-Gal stained embryos identify SOX17-2A-icre activity in the endoderm (black arrows mark endodermal pouches) and endothelial cells (white arrows in c) of the *Tbx1cHet*^{Sox17} (b) and *Tbx1cKO*^{Sox17} (c) embryos. X-gal staining is absent from Cre negative embryos (a), confirming that recombination of the *Rosa26 reporter* only occurs in the presence of SOX17^{iCre}. Anti-TBX1 immunohistochemistry identifies TBX1 in the endodermal and mesodermal tissues of the PA at E9.5 of Cre negative (g), *Tbx1cHet*^{Sox17} (e and h). TBX1 is maintained in the endoderm of *Tbx1cKO*^{Sox17} but its absent from the endoderm (f and i) n=2. When TBX1 is absent from the endoderm the caudal pouches do not form (denoted by a single arrow in (c) and * in (i). The grey line in panel a represents the level at which the sections in panels d – i were cut.

Annotations: Mesoderm (Meso), Endoderm (Endo), pp = pharyngeal pouch, ? = presumptive pouch, bv = blood vessels, yellow arrows = mesodermal staining, white arrows = endothelial cell staining, unfilled arrow = absence of endodermal staining, black arrows = endodermal staining. *Tbx1* expression domains shown by *in situ* hybridization are included for reference (d, low power image; red arrows indicate endoderm, black arrows indicate mesoderm).

Fig 12

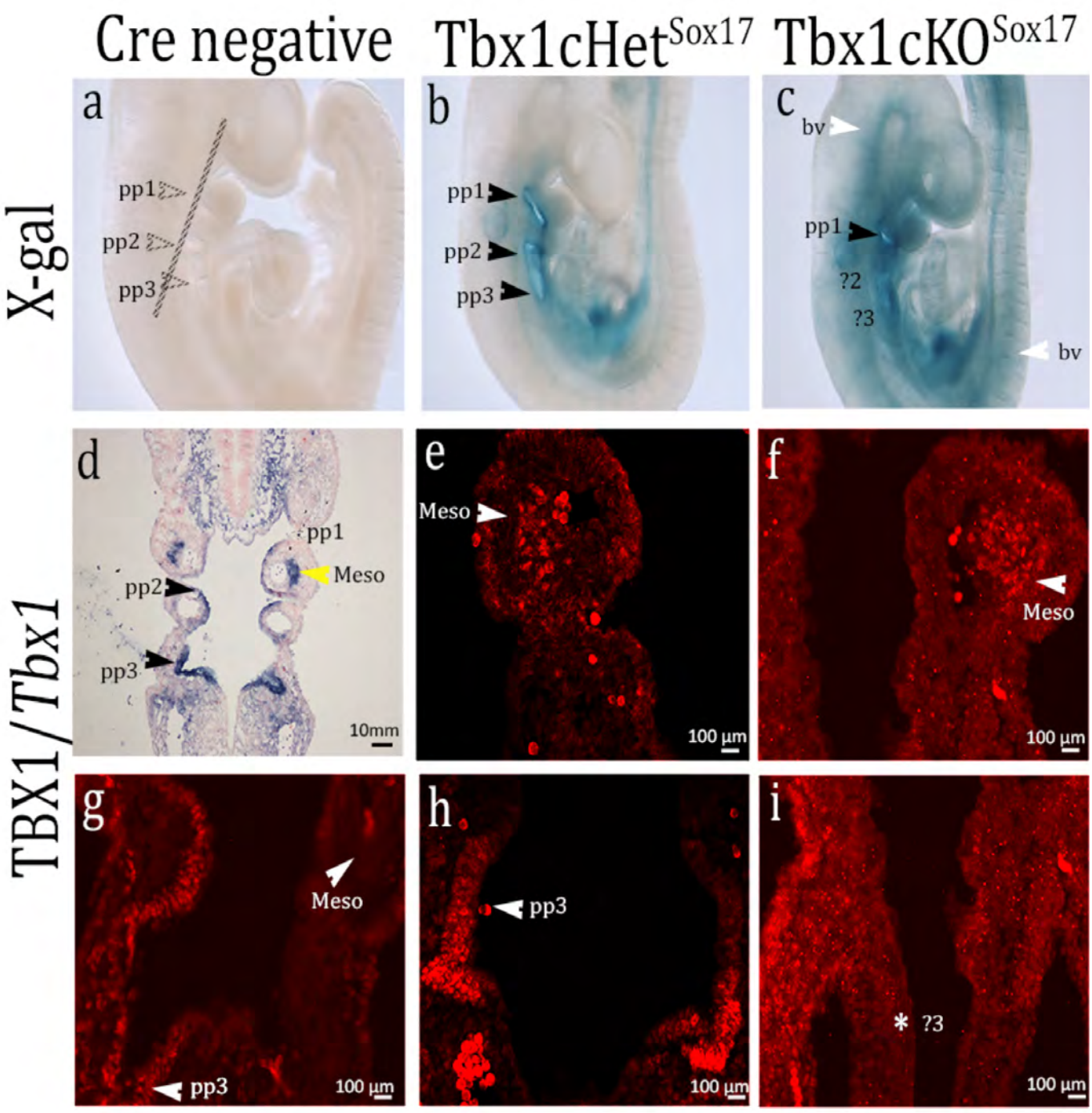
Cre negative
Tbx1cHetSox17
Tbx1cKOSox17
X-gal
TBX1/Tbx1
a
b
c
d
e
f
g
h
i
pp1
pp2
pp3
bv
?2
?3
Meso
10mm
100 µm
* ?3

3.1.2 *Tbx1cKO^{Sox17}* embryos are unable to form caudal pharyngeal pouches or endodermally derived thymi glands.

From Figure 12 it is evident that the pharyngeal endoderm of E9.5 *Tbx1cKO^{Sox17}* embryos is un-segmented. It is possible that the absence of endodermal *Tbx1* delays pouch formation, rather than preventing it. The *Paired box protein 1* (*Pax1*) is expressed in the pharyngeal pouches from E8.5, as such it is a good maker of pouch morphology (Wallin et al., 1996). To assess whether caudal pouch formation is delayed in *Tbx1cKO^{Sox17}* embryos, mutant and control embryos were collected at E10.5 and *Pax1* expression was analysed.

At E10.5 *Pax1* expression is visible in pharyngeal pouches 1 to 3 of Cre negative embryos, all of which have a slit-like morphology, (Fig 13, panel a: solid arrowheads mark *Pax1* expression in the pouches). The pattern of *Pax1* expression within the pouches of *Tbx1cHet^{Sox17}* embryos remained unchanged, however, the level of *Pax1* expression appears reduced (Fig 13b). In contrast, the absence of *Pax1* expression observed in *Tbx1cKO^{Sox17}* embryos caudal endoderm indicates that, caudal to the 1st pouch, no endodermal evagination has occurred between E9.5 and E10.5, (Fig 13, panel c). Overall these observations indicate that *Tbx1* is essential within the endoderm for caudal pharyngeal pouch formation.

The absence of 3rd pouch in *Tbx1$^{-/-}$* embryos prevents the development of the thymi in these mutant embryos (Jerome and Papaioannou, 2001). As the 3rd pouch is unable to form in *Tbx1cKO^{Sox17}* embryos it was predicted that the thymus would be unable to develop. To investigate the latter hypothesis, E17.5 *Tbx1cKO^{Sox17}*

embryos were examined. By E17.5 the thymus lobes should have migrated caudally from the PA to their final position above the heart (Blackburn and Manley, 2004). The two thymi of Cre negative and *Tbx1cHet*^{Sox17} embryos are visible in their appropriate location above the heart at E17.5 (Fig 14, panels a and b). In addition the circumference of *Tbx1cHet*^{Sox17} thymi were not significantly different in size from the Cre negative thymi (mean difference in circumference of thymi $p>0.5$, see Fig 14 panel d for details). The formation of 'normal' sized thymus lobes in *Tbx1cHet*^{Sox17} embryos further indicates that 3rd pouch morphogenesis occurs appropriately when one allele of *Tbx1* is deleted from the pharyngeal endoderm (see Fig 13 panel b). In contrast, thymus aplasia manifests in all *Tbx1cKO*^{Sox17} embryos at E17.5, (Fig 14 panel c, an asterix marks the location where thymi should have formed). The thymus aplasia evident in *Tbx1cKO*^{Sox17} embryos at E17.5 corresponds to the lack of 3rd pouch formation evident in *Tbx1cKO*^{Sox17} embryos at E10.5 (see Fig 13 panel c). This data demonstrates that *Tbx1* is required in the endoderm for the organogenesis of the thymus gland from the 3rd pharyngeal pouch.

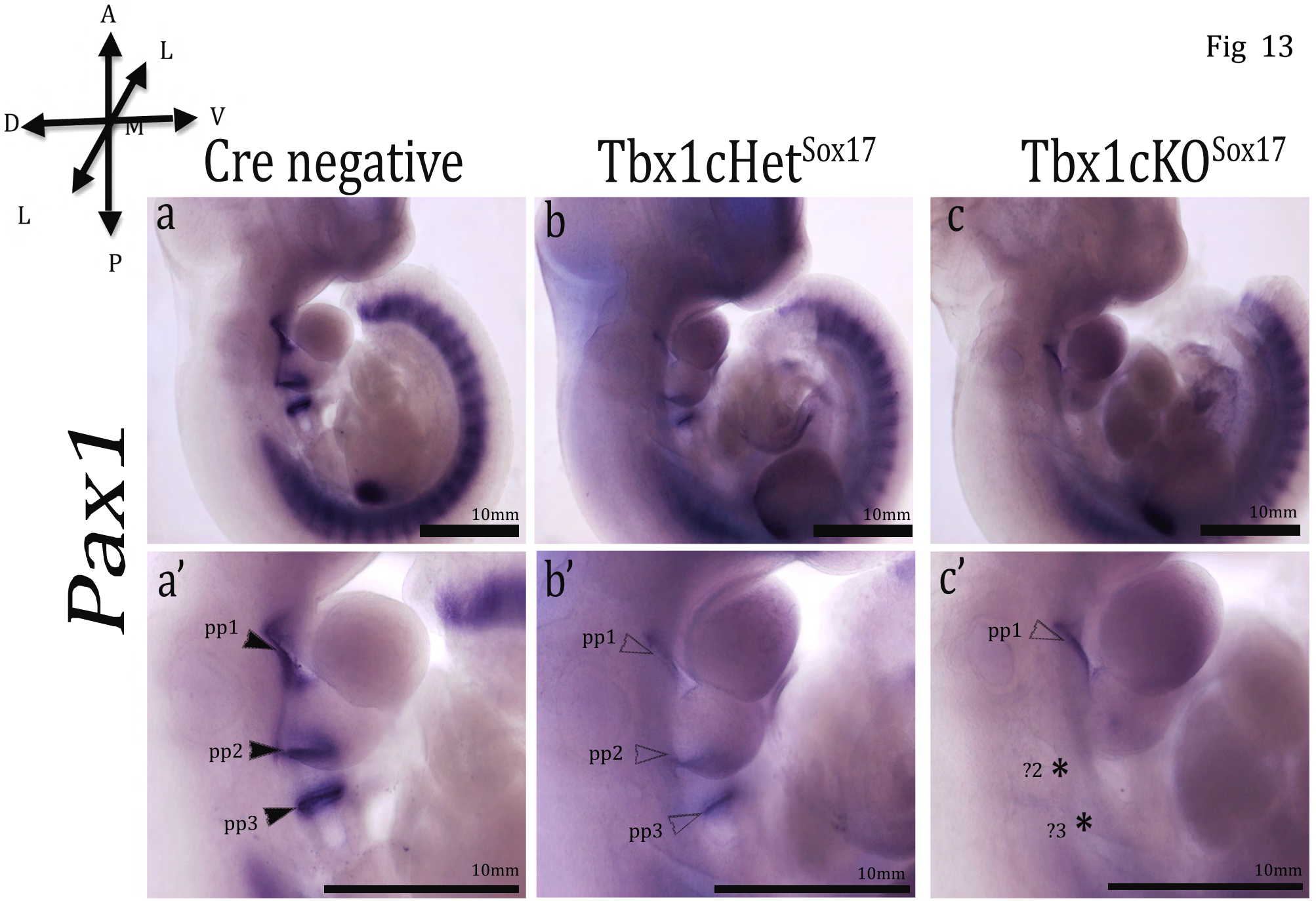
A
L
D
V
M
L
P
Cre negative
Tbx1cHet Sox17
Tbx1cKO Sox17
Pax1
a
b
c
10mm
10mm
10mm
a'
b'
c'
pp1
pp2
pp3
pp1
pp2
pp3
pp1
?2 *
?3 *
10mm
10mm
10mm

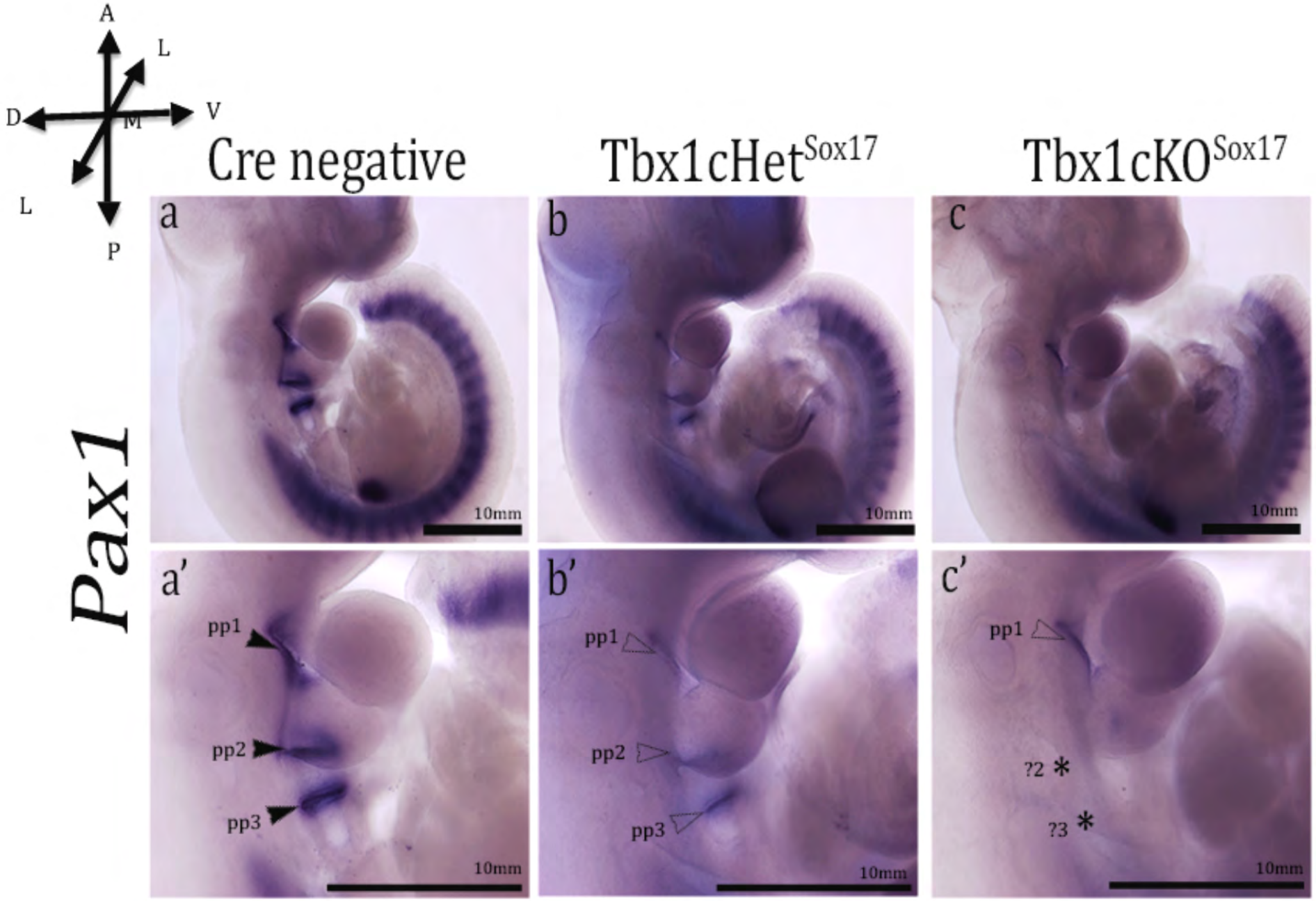
A
L
D
M
V
L
P
Cre negative
Tbx1cHet Sox17
Tbx1cKO Sox17
Pax1
a
b
c
10mm
a'
b'
c'
pp1
pp2
pp3
?2 *
?3 *

Fig 13: *Pax1*, which demarcates the endoderm of the pharyngeal pouches, identifies a lack of caudal pouches in *Tbx1cKO*^{Sox17} embryos.

a-c: low magnification (4x) side views of *Pax1* expression in E10.5 embryos. a'-c'; the pharyngeal apparatus of embryos a-c viewed at high (8x) magnification. Note that in *Tbx1cKO*^{Sox17} embryos (c and c' n=6) *Pax1* expression is reduced in the 1st pharyngeal pouch (pp), as indicated by the unfilled arrowhead, but is completely absent from the endoderm where pp 2 and 3 should have formed (* indicate absence of caudal pouches and a lack of *Pax1* expression). N=6

Annotations: Arrows to the left of the figure identify the orientation of the embryos: A = anterior, P = posterior, L = lateral, M = medial, V= ventral, D = dorsal. Outlined area in panel's a-c indicate the area magnified in panels a'-b'. L=Limb bud, S = somite, pp = pharyngeal pouch, ? = presumptive pouch, solid arrowheads identify areas of *Pax1* expression in each pouch, unfilled arrowheads identify areas of reduced *Pax1* expression in each pouch.

Fig 14: Thymus aplasia manifests in *Tbx1cKO*^{Sox17} embryos.

a-c: Open chest cavities of E17.5 embryos photographed frontally to display the two lobes of the thymus in Cre negative and *Tbx1cHet*^{Sox17} embryos (a and b, respectively), * denotes the absence of thymus glands in *Tbx1cKO*^{Sox17} embryos (c) (n=7). d: The circumference measurements were plotted in graph (d) using Graphpad software, (each symbol corresponds to an individual gland). Note there is no statistically significant size difference between the mean circumference between the circumference of Cre negative (n=7) and *Tbx1cHet*^{Sox17} (n=3) thymi glands (n=7), (p=0.565.and. p=0.742).respectively, by students T-test. Error bars display standard error of the mean. The mean thymi circumference for each genotype of embryo with the corresponding standard error of the mean and P-value (generated using the Student's T-test in GraphPad) are listed below.

Genotype	Right lobe Mean ± SEM (replicates)	Difference between means of mutants and Cre negatuve (P-value)	Left lobe Mean ± SEM (replicates)	Difference between means of mutants and Cre negative (P-value)
Cre negative	4.958 ± 0.2954 (N=8)		5.029 ± 0.1944 (N=8)	
Tbx1cHet^{Sox17}	5.274 ± 0.3147 (N=3)	-0.3160 ± 0.5283	4.907 ± 0.2708 (N=3)	0.1223 ± 0.3608
Tbx1cKO^{Sox17}	0.0 ± 0.0 (N=7)	-4.958 ± 0.317	0.0 ± 0.0 (N=7)	-5.029 ± 0.2088

Fig 14

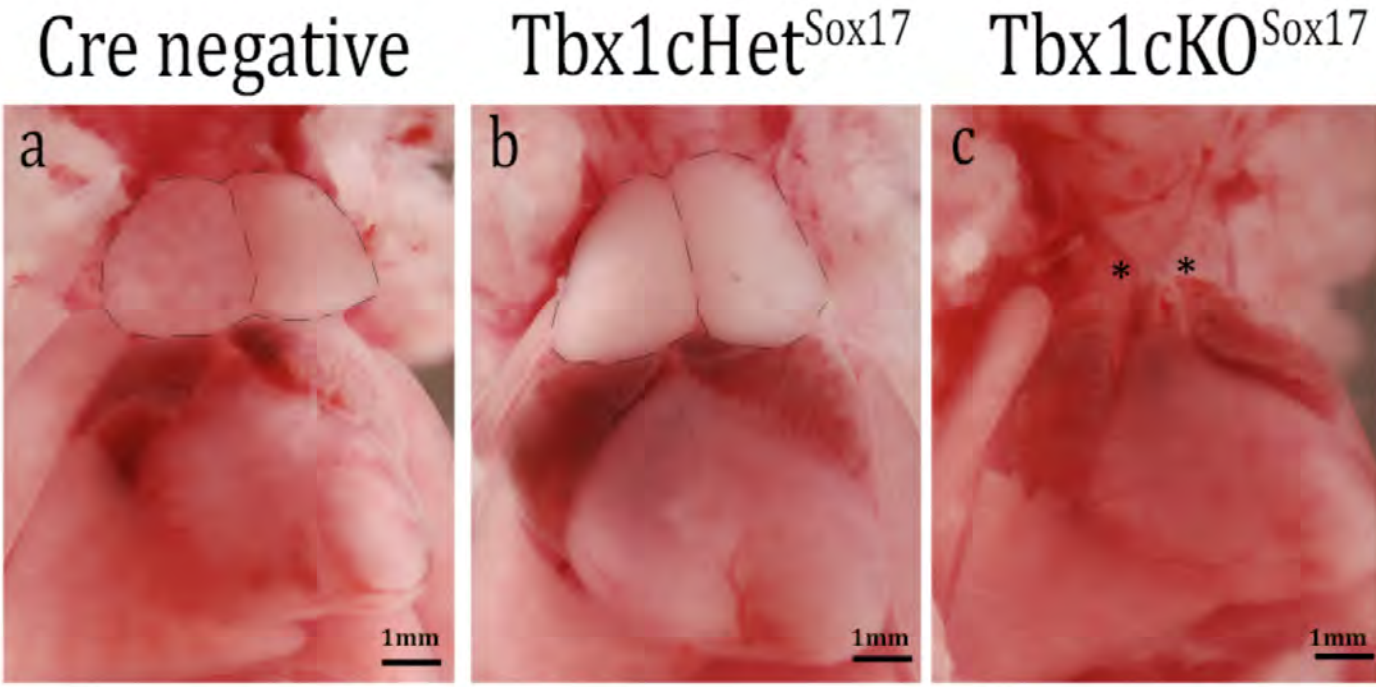
Cre negative
Tbx1cHetSox17
Tbx1cKOSox17
a
b
c
1mm
1mm
1mm

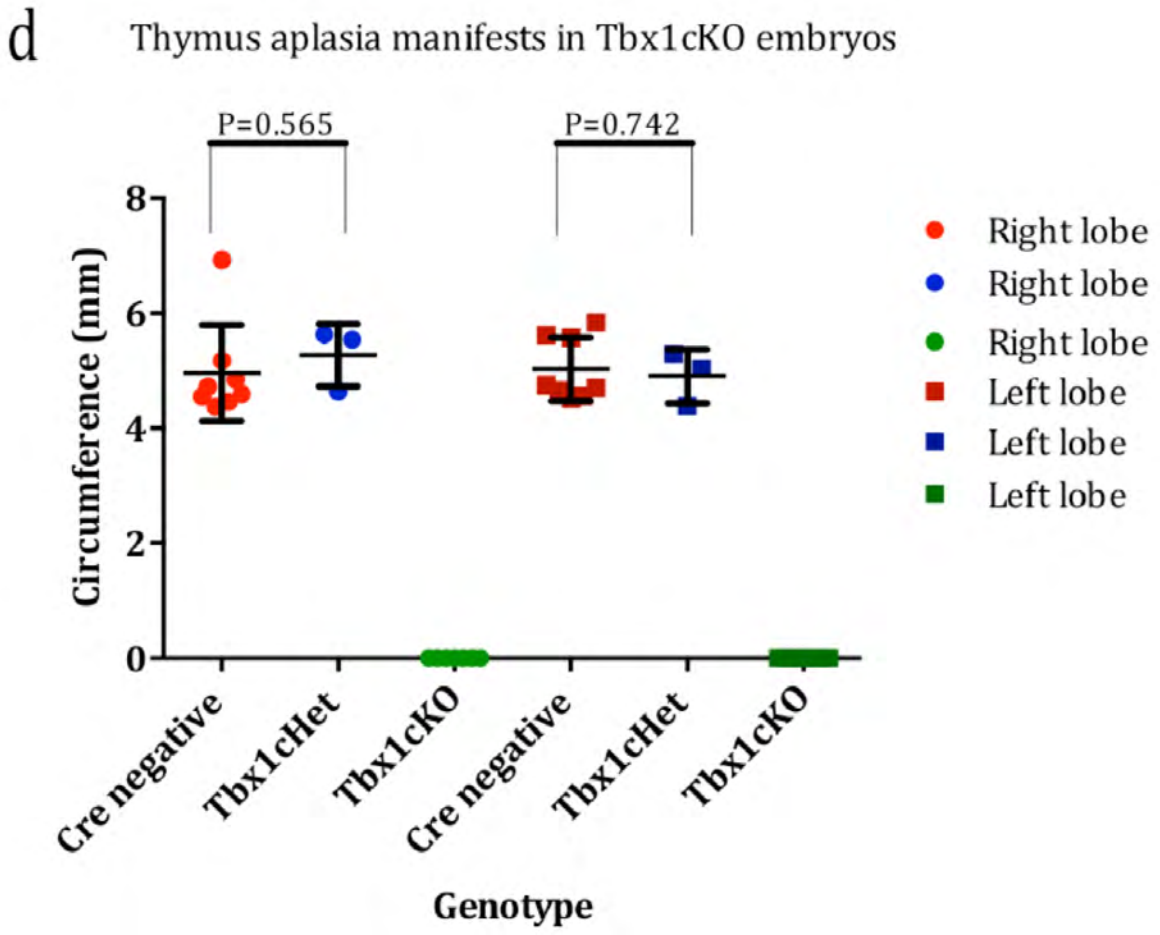
d
Thymus aplasia manifests in Tbx1cKO embryos
P=0.565
P=0.742
Circumference (mm)
0
2
4
6
8
Cre negative
Tbx1cHet
Tbx1cKO
Cre negative
Tbx1cHet
Tbx1cKO
Genotype
Right lobe
Right lobe
Right lobe
Left lobe
Left lobe
Left lobe

3.2 The loss of *Tbx1* from the endoderm affects the development of PA structures derived from tissues other than the pharyngeal endoderm

In addition to a lack of segmented pharyngeal endoderm, the caudal pharyngeal arches (2-6) do not form in *Tbx1cKO*^{Sox17} embryos. Thus, the PA of *Tbx1cKO*^{Sox17} embryos, as a whole, appears as an un-segmented structure (Fig 13 panel c), a morphology that is reminiscent of the PA of *Tbx1*$^{-/-}$ embryos. It is possible that the perturbed morphology of the *Tbx1cKO*^{Sox17} embryos pharyngeal endoderm, and/or, a loss of Tbx1-dependent signals from the endoderm will affect the development of adjacent PA tissues and their derivatives.

3.2.1 Cranial neural crest migration is reduced in *Tbx1cKO*^{Sox17} embryos

The pharyngeal arches are populated by mesenchyme that is, in part, derived from CNCC that migrate into the PA from the hindbrain (Graham et al., 2004) Reduced and/or ectopic CNCC migration into the PA can negatively impact upon arch formation. The latter is observed in *Tbx1*$^{-/-}$ embryos that do not form caudal arches (Vitelli et al., 2002). CNCC do not express *Tbx1*, hence, their migratory trajectories are disrupted in *Tbx1*$^{-/-}$ embryos because of the loss of *Tbx1* from the CNCC niche (Vitelli et al., 2002). As evaginating pharyngeal pouches normally segregate each arch it is possible that *Tbx1* dependent signals from the endoderm may act as CNCC guidance factors. To investigate this hypothesis *Tbx1cKO*^{Sox17} and Cre negative embryos were examined for *Dlx2* expression by whole mount *in situ*

hybridization. *Dlx2* is a gene normally expressed by migratory and post-migratory CNCC (Qiu et al., 1997). At E9.5 *Dlx2* expressing CNCC are visible in the proximal and distal halves of Cre negative embryos 1st and 2nd arches. The pharyngeal pouches segregate each domain of *Dlx2* positive CNNC in the PA (Fig 15, panel a: three arrowheads demarcate the segregation). Even in the caudal PA, that is yet to form a defined arch, the just forming 3rd pouch can be seen to divide the bulk of CNCC migrating into this region (Fig 15 panel a, area indicated by the posterior arrow). In the *Tbx1cKO*^{Sox17} embryos a reduction in *Dlx2* expression can be seen throughout the PA but in particular caudal in the 1st arch. The reduction in *Dlx2* expression is indicative of reduced CNCC migration into the PA (compare solid arrowheads in Fig 15 a to the unfilled arrowheads in 15 b and c). In addition, patches of ectopic migrating CNCC were observed rostral to the 1st arch in one *Tbx1cKO*^{Sox17} embryo (Fig 15 panel c, observe areas highlighted by solid arrows). The reduced and disorganized pattern of *Dlx2* expression observed in the *Tbx1cKO*^{Sox17} embryos indicates that *Tbx1* dependent signalling from the endoderm is necessary to guide the CNCC into the pharyngeal arches. To identify specific defects in the trajectories of CNCC migrating into the PA of *Tbx1cKO*^{Sox17} embryos it would be beneficial to analyse the expression pattern of CNCC markers that identify discreet populations of migratory crest, such as *Crabp1*. As an indication of whether the CNCC defects observed in *Tbx1cKO*^{Sox17} embryos would perturb the formation of structures derived from the rostral and caudal pharyngeal arches, the formation of the thoracic vessels and the external ear were thus analysed in *Tbx1cKO*^{Sox17} embryos.

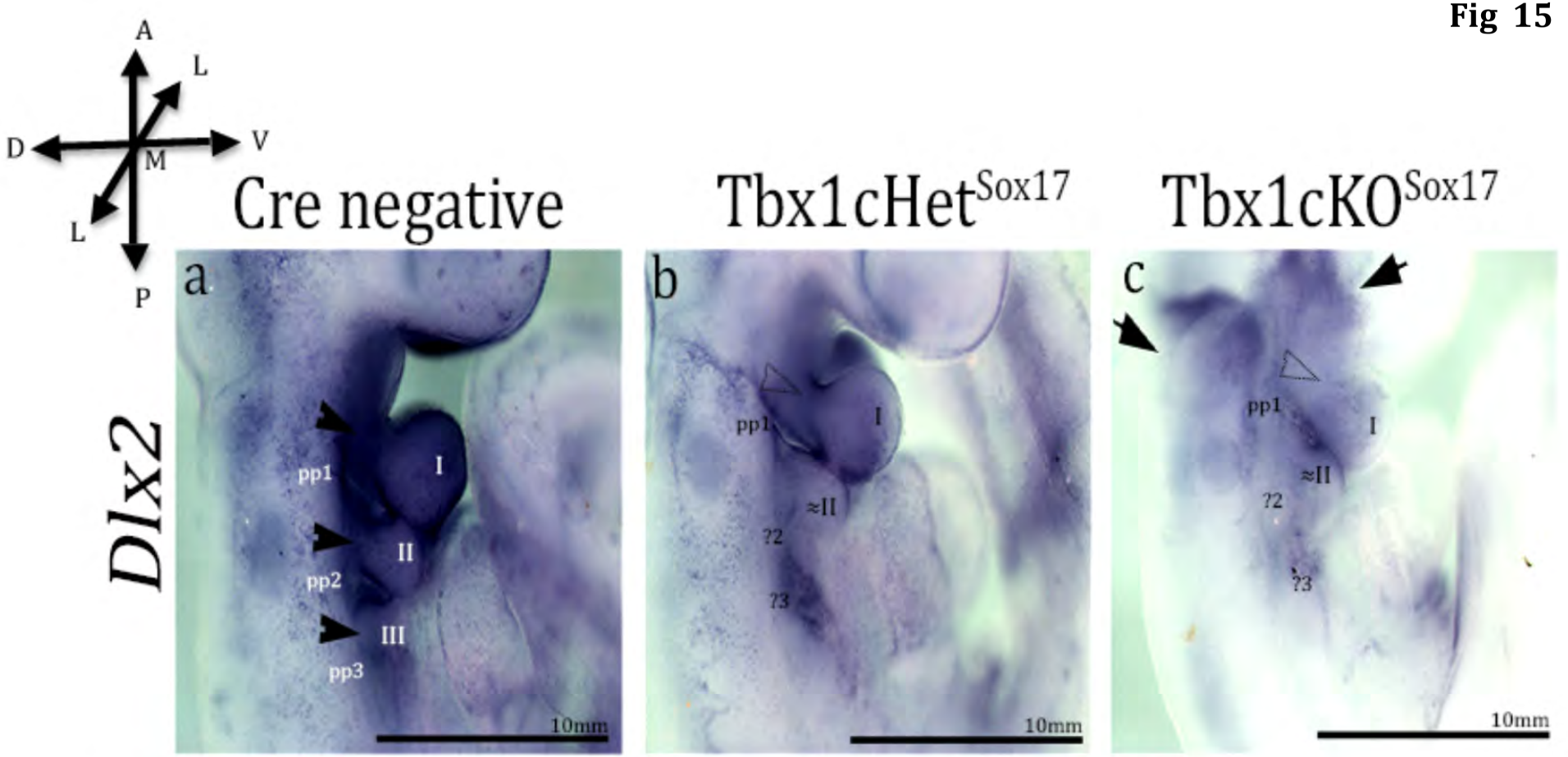

Fig 15: Loss of Tbx1 and/or endodermal tissue morphology disrupts the streams of CNCC populating the pharyngeal arches. a-c: side views of *Dlx2* expressing CNCC in E10.0 embryos. Note the reduced (open arrow heads in b and c) and ectopic (solid arrows in c) *Dlx2* staining in the Tbx1cKO^{Sox17} embryos (panels b and c), relative to the discreet *Dlx2* staining observed in the Cre negative embryo (solid arrowheads in panel a). Cre negative embryo n=1, Tbx1cKO^{Sox17} embryos n=2. Arrows to the left of the figure identify the orientation of the embryos: A = anterior, P = posterior, L = lateral, M = medial, V= ventral, D = dorsal. pp = pharyngeal pouch, ? = presumptive pouch, I-III = arches 1-3, ≈ = presumptive arches, solid arrowheads identify areas of *Dlx2* expression in each arch, unfilled arrowheads identify areas of reduced *Dlx2* expression in each arch, arrows identify ectopic *Dlx2* staining.

3.2.2 Hypoplasia of the external ear manifests in *Tbx1cKO^{Sox17}* embryos

The three structures that define the external ear, the pinna (external flap), the external acoustic meatus (EAM, the ear canal) and the tympanic membrane (ear drum), are derived from the rostral PA (Mallo and Gridley, 1996). The EAM is derived from the ectodermal cleft of the first arch and the endodermal epithelium of the tubotympanic recess, which contributes to the tympanic membrane, is formed from the first pouch (Mallo and Gridley, 1996). Furthermore the pinna are derived from six hillocks, mesenchymal/ectodermal thickenings, on the surface of the 1st arch (Alasti and Van Camp, 2009). External ear defects are exhibited in most DiGeorge syndrome patients, indicating that the loss of *Tbx1* may be required for the formation of this structure (Greenberg, 1989). Absence of the hyoid crest from the 2nd arch and its misrouting into the 1st arch were the defects proposed to cause absence of the external ear in *Tbx1$^{-/-}$* embryos (Moraes et al., 2005). However, as already noted above, CNCC do not express *Tbx1*. Thus, any CNCC migration defects that result in pinna aplasia occur because *Tbx1* is absent from adjacent tissues in the PA. *Tbx1cKO^{Sox17}* embryo's pinna were analysed at E17.5 to assess whether the observed defects in *Dlx2* marked CNCC perturb the formation of this external ear structure. All *Tbx1cKO^{Sox17}* mutants (Fig 16 b) (n=3/3) have slightly hypoplastic pinna (relative to Cre negative embryos, Fig 16 a) that are otherwise normal in morphology and position on the embryo's head (compare T-bars in Fig 16 a-c, the arrow in panels a-c indicates the position of the ear relative to the eye). The subtle hypoplasia observed in the pinna of *Tbx1cKO^{Sox17}* embryos is a major contrast to the aplasia presenting in *PE-KO* pinna (Arnold et al., 2006).

Fig 16

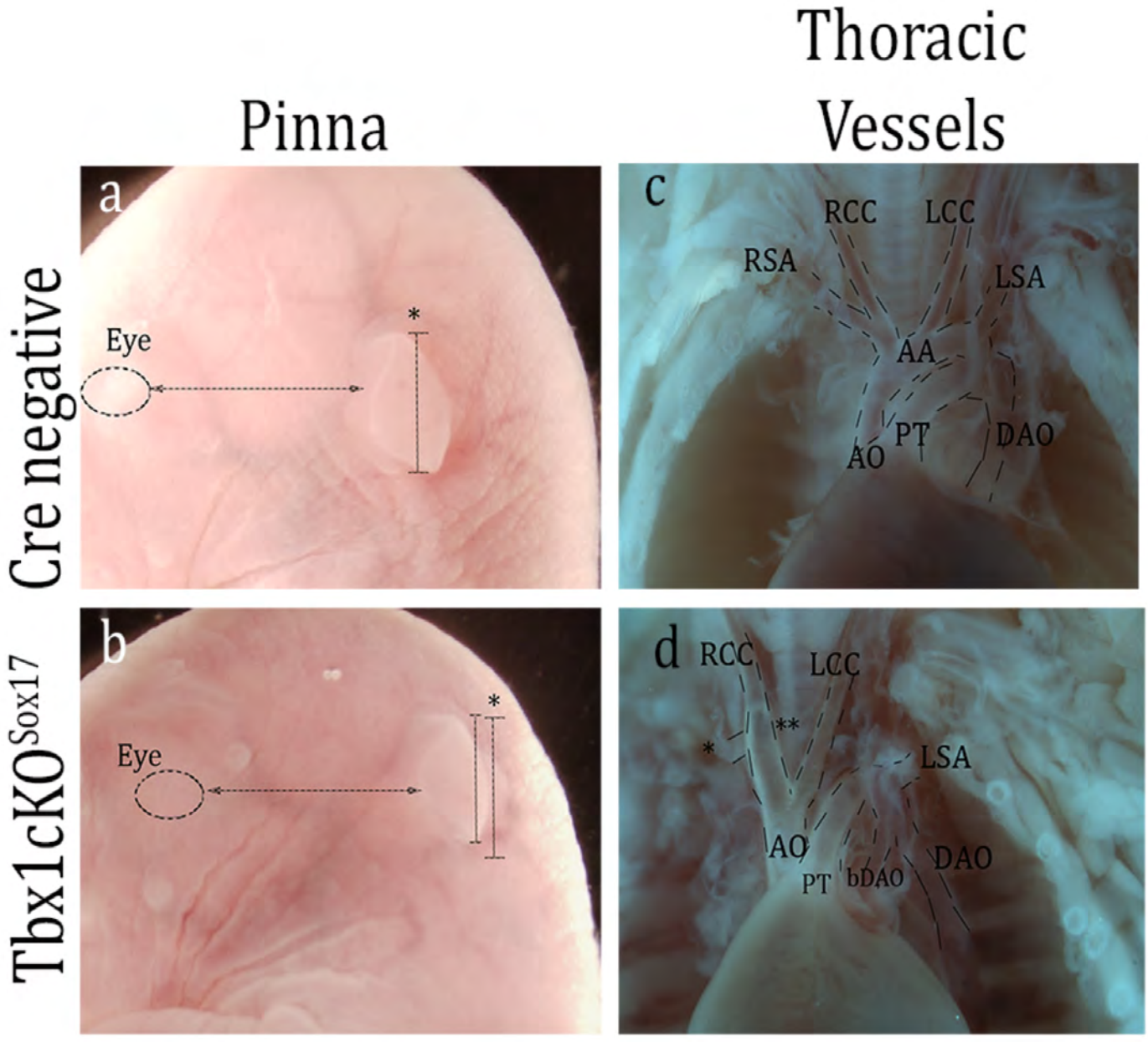
Pinna
Thoracic Vessels
Cre negative
Tbx1cKO Sox17
a
b
c
d
Eye
Eye
*
*
RCC
LCC
RSA
LSA
AA
AO
PT
DAO
RCC
LCC
*
**
LSA
AO
PT
bDAO
DAO

Fig 16: The formation of the pinna and the thoracic vessels, derived from the PA, are affected by the loss of endodermal *Tbx1*. a-b: The pinna of E17.5 *Tbx1cKO*^{Sox17} embryo's (panel b) do not appear to be 'low set' (*PE-KO* embryos are described as having low set ears), as indicated by the arrows that show the external ears of all embryos are in line with the eye (outlined structure). T-bars indicate the length of the pinna. By superimposing the Cre negative T-bar (denoted by the *) onto images of the mutant pinna it is evident that *Tbx1cKO*^{Sox17} embryo's pinna (b, n=3) are smaller than Cre negative embryo's pinna (a, n=3).

c-d: The heart and its associated vessels were imaged *in situ* within the chest cavity of E17.5 embryos. IIA-B and A-RSA were identified respectively in 1/3 and 2/3 *Tbx1cKO*^{Sox17} embryos analysed for thoracic vessel formation. PTA (scored as a single vessel arising from the heart) was not evident in any *Tbx1cKO*^{Sox17} embryos n=7/7. MPA = Main Pulmonary Artery, R/LCC = Right/Left common carotid, R/LSA = Right/Left Subclavian Artery, A0 = Aorta, AA = Aortic arch, DAO = Descending aorta, bDAO = branch of the descending aorta. * identifies the sight of absent/aberrant branching of the RSA in the *Tbx1cKO*^{Sox17} embryo, ** marks the site of the interrupted aortic arch type B (IAA-B) displayed in the *Tbx1cKO*^{Sox17} embryo.

3.2.3 Thoracic vessel formation may require *Tbx1* in the pharyngeal endoderm

The thoracic vessels of the heart and the aorta are, respectively, contributed to by the pharyngeal arch arteries (PAAs) and the OFT of the heart. Five bilateral PAAs (1-4 and 6) develop in the centre of each pharyngeal arch (Moffat, 1959; Hiruma et al., 2002). CNCC migrate to the PAAs where they differentiate into smooth muscle cells that 'reinforce' the vessels (Ryckebusch et al., 2010). If the PAAs do not form or remodel appropriately then thoracic vessel defects such as interrupted aortic arch type (IAA, discontinuity between the ascending and descending portions of the aorta) and aberrant branching of the right subclavian artery (A-RSA) occur; these defects manifest in DGS and *Tbx1* mutant mouse embryos (Mulay and Watterson, 1997; Scambler, 2010). The OFT is contributed to by the splanchic mesoderm, located caudal to the pharynx, and by CNCC migrating through the PA (Xu et al., 2004). The formation of this primitive vessel is required to connect the right ventricle to the PAAs (and thus the dorsal aorta) via the aortic sac. Division of the OFT later in gestation separates the pulmonary from the aortic (systemic) circulatory system (Xu et al., 2004). Cardiac defects incompatible with postnatal life, such as persistent truncus aterious (PTA), manifest when the OFT does not grow or divide properly (Finley et al., 1977; Xu et al., 2004). PTA can be identified as a single vessel arising from both ventricles of the heart, rather than the aorta and pulmonary trunk (Kirby et al., 2008). Again, these defects are present in *Tbx1*$^{-/-}$ embryos and contribute to the postnatal morbidity of these mutants (Theveniau-Ruissy et al., 2008).

The structure of the heart and its associated vessels were examined, *in situ* after removal of the thymi, to determine whether pharyngeal arch artery and cardiac defects arise in these mutants, (Fig 16 c and 16 d). No evidence of cardiac defects such as PTA were detected in the *Tbx1cKO*^{Sox17} or Cre negative embryos analysed (n=7). At E17.5 one *Tbx1cKO*^{Sox17} embryo presented with interrupted aortic arch type (IAA-B) (Fig 16 d) and two *Tbx1cKO*^{Sox17} embryos presented with aberrant branching of the right subclavian artery (Fig 16 d). An analysis of the heart's septum, (by haematoxylin and eosin staining, for example), would be required to confirm that ventral septal defects (that often occur in tandem with IAA-B) do not manifest in the conditional *Tbx1* mutants. The thoracic vessel defects are indicative of the PAA being unable to form or align properly during PA development. To verify the manifestation of IIA-B in *Tbx1cKO*^{Sox17} embryos an analysis of a larger sample of mutants at E17.5 is required, in combination with an analysis of PAA development in *Tbx1cKO*^{Sox17} embryos at E10.5. Time constrains and mutant numbers prevented such an extensive analysis of thoracic vessel formation in *Tbx1*-deficient embryos.

In summary, the data presented demonstrates that *Tbx1* is required in the endoderm for the formation of a segmented PA and the development of a number of its derivatives. The deletion of *Tbx1* from the pharyngeal endoderm perturbs CNCC migration, which may be responsible for the observed defects in the development of *Tbx1cKO*^{Sox17} embryos pinna and thoracic vessels later in gestation. The data has proven *Tbx1* is required within the endoderm for caudal pouch formation and the development of the endodermally derived thymus gland. The next question to address was which factors act downstream of *Tbx1*, within the endoderm, to enable pharyngeal pouch morphogenesis.

3.3 Expression of *Fgf8* within the pharyngeal endoderm is dependent on endodermal *Tbx1*

Fgf8 and *Tbx1* interact epistatically during the development of cardiac elements and endocrine glands derived from the PA (Vitelli et al., 2002b; Lania et al., 2009). *In vitro* data has shown that TBX1 is able to induce luciferase expression, driven from an *Fgf8* promoter (Hu et al., 2004). *In vivo* data has suggested that this positive regulation of *Fgf8* by TBX1 may be relevant to pouch development because *Fgf8* expression is absent from the pharyngeal endoderm of *Tbx1*$^{-/-}$ embryos (Vitelli et al., 2002b). To test whether *Tbx1* in the endoderm is required for the expression of *Fgf8* in the pharyngeal, the expression of this FGF ligand was assessed in *Tbx1cKO*^{Sox17} embryos by *in situ* hybridization.

At E9.5 *Fgf8* expression is detected robustly in the caudal pharyngeal endoderm with expression visible in the majority of the evaginating 3rd pouch. Rostral to the 3rd pouch the expression of *Fgf8* in the endoderm is restricted to the distal aspects of the 1st and 2nd pouch (Fig 17 panel a, black solid arrowhead show *Fgf8* expression in each pouch). In contrast *Fgf8* expression extends throughout the pharyngeal ectoderm (Fig 17 panel a, blue solid arrowhead). *Fgf8* expression in the endoderm of *Tbx1cHet*^{Sox17} embryos appears indistinguishable in pattern and level from that observed in Cre negative embryos. Unsurprisingly, the expression of ectodermal *Fgf8* is also unchanged in the *Tbx1*-positive endoderm of *Tbx1cHet*^{Sox17} embryos (Fig 17: compare endodermal *Fgf8* [black arrowheads] and ectodermal *Fgf8* [blue arrowhead] in panels a and b). In contrast, in the majority of *Tbx1cKO*^{Sox17} embryos analysed (n=2/3) *Fgf8* was absent from all but a small area of caudal endoderm where expression was extremely diminished, (Fig 17, panel c:

unfilled arrowhead identifies residual *Fgf8* expression). In the third *Tbx1cKO*^{Sox17} embryo analysed, *Fgf8* expression was absent from the entire pharyngeal endoderm. In all *Tbx1cKO*^{Sox17} embryos *Fgf8* expression was maintained in the un-segmented pharyngeal ectoderm (Fig 17, panel c: blue solid arrowhead). The loss of *Fgf8* specifically from the endoderm of *Tbx1cKO*^{Sox17} embryo's was also evident at E8.5 (compare Fig 17, solid black arrowheads in panels d and e). This data confirms that *Tbx1* is required in the endoderm for the endodermal expression of *Fgf8*.

Fig 17

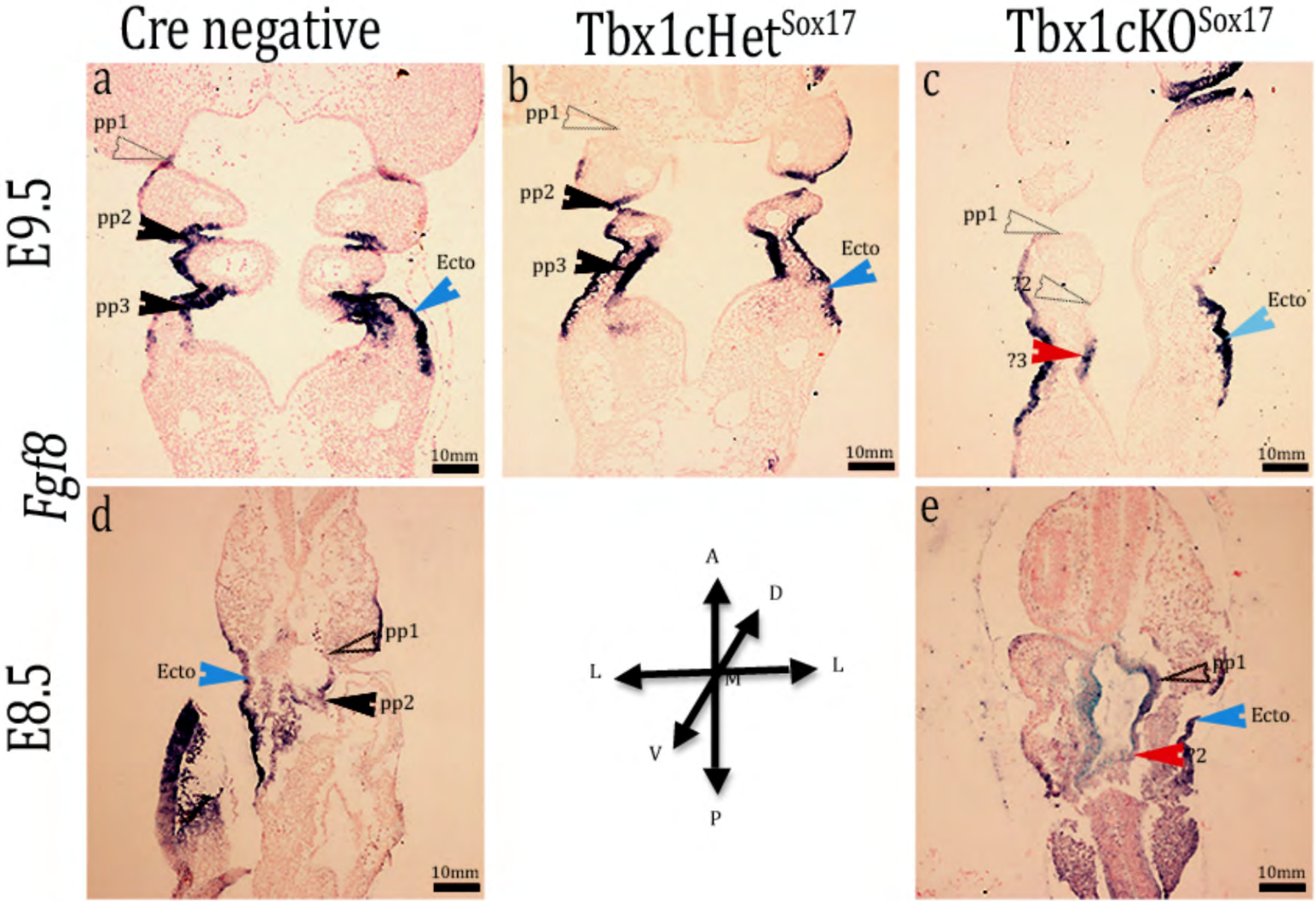
Cre negative
Tbx1cHet Sox17
Tbx1cKO Sox17
E9.5
Fgf8
E8.5
a
b
c
d
e
pp1
pp2
pp3
Ecto
?2
?3
10mm
A
D
L
L
M
V
P

Fig 17: *Fgf8* expression is greatly diminished in, or absent from, the pharyngeal endoderm of *Tbx1cK0*^{Sox17} embryos. *Fgf8* expression was assessed by *in situ* hybridisation on frontal sections of E9.5 embryo's pharyngeal apparatus. (a, b and e) Cre negative and *Tbx1cHet*^{Sox17} embryos show robust expression in the ectoderm (blue arrowhead) and endoderm (black arrowheads) at E8.5 and E9.5. In contrast, *Fgf8* is only weakly expressed in a small area of *Tbx1cKO*^{Sox17} embryos endoderm (panel c, red arrowhead) where the 3rd pp should have formed, (in one *Tbx1cKO*^{Sox17} no endodermal *Fgf8* expression was detected). However, ectodermal expression is maintained in the pharyngeal ectoderm of *Tbx1cKO*^{Sox17} embryos (panel c, blue arrowhead). Similarly, *Fgf8* expression is absent from the endoderm of *Tbx1cKO*^{Sox17} embryos at E8.5 (panel d, red, unfilled, arrowhead), but is present in the ectoderm, (blue arrowhead). NB: the light blue endodermal stain in (e) is X-gal staining detecting SOX17^{icre} activity. **. Èσǐ%ω8υǐ . È ç8%ψ8υ**

Annotations: Black arrowhead = endodermal pouch expression, blue arrowhead = ectodermal expression, unfilled arrowhead = endodermal pouch (no/little expression visible), red arrowhead = loss of endodermal pouch expression in the *Tbx1cKO*^{Sox17} embryos, pp = pharyngeal pouch, ? = presumptive pouch regions in *Tbx1*-deficient endoderm, ecto = ectoderm of the first pharyngeal arch. Arrows to the left of Fig illustrate the orientation of the pharyngeal apparatus sections; A = anterior, P = posterior, L = lateral, M = medial, V= ventral, D = dorsal.

3.4 The expression of genes in the FGF signalling cascade are maintained independently of *Tbx1* in the pharyngeal endoderm.

A number of FGF ligands are expressed in the pharyngeal endoderm at E9.5, in addition to *Fgf8*, including *Fgf3*, *Fgf10* and *Fgf15* (Kelly et al., 2001; Vincentz et al., 2005; Aggarwal et al., 2006). *In vitro,* TBX1 is sufficient to activate a luciferase expression construct driven by the *Fgf10* promoter, indicating that TBX1 may positively regulate the expression of multiple FGF ligands (Xu et al., 2004). The loss of *Fgf3* and *Fgf10* expression in *Tbx1*$^{-/-}$ embryos suggests that TBX1 is also required for the transcription of these ligands, *in vivo*, within the PA (Vitelli et al., 2002b; Aggarwal et al., 2006). To address whether TBX1 is required in the endoderm for the expression of *Fgf3*, *Fgf10* and *Fgf15*, these FGF ligands were analysed by *in situ* hybridisation in frontal sections of *Tbx1cKO*^{Sox17} embryos PA.

In Cre negative embryos the expression of *Fgf3* is confined to the posterior half of each pouch. Moreover, the domain of *Fgf3* expression in the 3rd pouch appears to be complimentary to the more anterior domain of *Fgf8* expression (compare the expression domain of *Fgf8* in the 3rd pouch [Fig 17, panel a] with the expression domain of *Fgf3* in the 3rd pouch [Fig 18, panel a]). The absence of endodermal TBX1 correlates with an extension of *Fgf3* expression. In *Tbx1cKO*^{Sox17} embryos *Fgf3* is expressed throughout the pharyngeal endoderm, in a largely un-segmented pattern, consistent with the morphology of this epithelium (Fig 18, panel a versus panel b). A similar change in the expression pattern of *Fgf15* is observed in *Tbx1cKO*^{Sox17} embryos when compared to controls (Fig 18, panel c versus panel d). *Fgf15* is expanded through rostral areas of pharyngeal endoderm in the absence of

endodermal TBX1. However, the extent of *Fgf15* expansion in *Tbx1cKO*^{Sox17} endoderm is less severe than that observed with *Fgf3*. There was no loss or change to the expression pattern of *Fgf10* in *Tbx1cKO*^{Sox17} embryos at E9.5 (Figure 18e and f).

In summary, it appears that within the endoderm only *Fgf8* expression is dependent on TBX1 as all the mRNA of all other FGF ligands analysed was maintained within TBX1-deficient endoderm. Thus, it was questioned whether the loss of *Fgf8* expression in *Tbx1cKO*^{Sox17} embryos would alter the level of FGF signalling within the pharyngeal endoderm. To address this, *Etv4* (*Pea3)* and *Etv5 (Erm*), *Sprouty 1* and *Sprouty 2* were utilised as 'readouts' of FGF signalling and their expression was analysed in *Tbx1cKO*^{Sox17} and control embryos at E9.5.

Pea3 and *Fgf8* appear to have similar patterns of expression within the pharyngeal endoderm at E9.5, (compare Fig 17 panel a and Fig 19 panel a). *Pea3* transcripts are present in the very distal tips of pharyngeal pouches 1 and 2, where the evaginating endoderm and invaginating ectoderm meet. In the 3rd pouch *Pea3* has a wide expression domain, (in comparison to the more rostral pouches), corresponding to the morphology of the outgrowing pouch. However, in contrast to *Fgf8,* the expression of *Pea3* was maintained in the pharyngeal endoderm of *Tbx1cKO*^{Sox17} embryos, significantly so within the presumptive 3rd pouch regions of the caudal endoderm, (compare magnified areas of caudal endoderm, Fig 19 panels a and b). Similarly, *Erm* expression is maintained in *Tbx1cKO*^{Sox17} embryos, indicating that the loss of *Fgf8* does not cause a loss of FGF signalling in the pharyngeal endoderm (Fig 19 panel d). *Erm* is expressed diffusely through most of the pharyngeal endoderm, except in the most medial areas of inter-pouch

endoderm (Fig 19, panel c solid arrowheads indicate *Erm* expression in the pharyngeal pouches). Robust *Erm* expression overlaps with the domains of *Fgf3* and *Fgf15* expression in the posterior halves of the rostral pouches and throughout the evaginating 3rd pouch (compare Fig 18, panels a and c with Fig 19, panel c). Akin to *Fgf3* and *Fgf15*, the expression domain of *Erm* expands along the A-P axis of *Tbx1cKO*^{Sox17} embryos pharyngeal endoderm, in contrast to the more dynamic expression pattern visible in Cre negative embryos (compare Fig 19 panels c and d).

Similarly, there was a loss of the segmented pattern of *Sprouty 1* (Fig 20, panels a and b) and *Sprouty 2* (Fig 20, panels c and d) expression observed in Cre negative embryos pharyngeal endoderm in *Tbx1cKO*^{Sox17} embryos. *Sprouty* genes are expressed in a continuous manner throughout TBX1-deficient endoderm, whereas, in TBX1-positive endoderm a segmented expression pattern is observed, with expression appearing more robust in the posterior half of the pharyngeal pouches than in the anterior (Fig 20, panels a and c vs d and e).

Overall, the analysis of FGF signalling readouts by *in situ* hybridisation indicates that FGF signalling is maintained in TBX1 deficient endoderm, despite the loss of *Fgf8* expression from this epithelium.

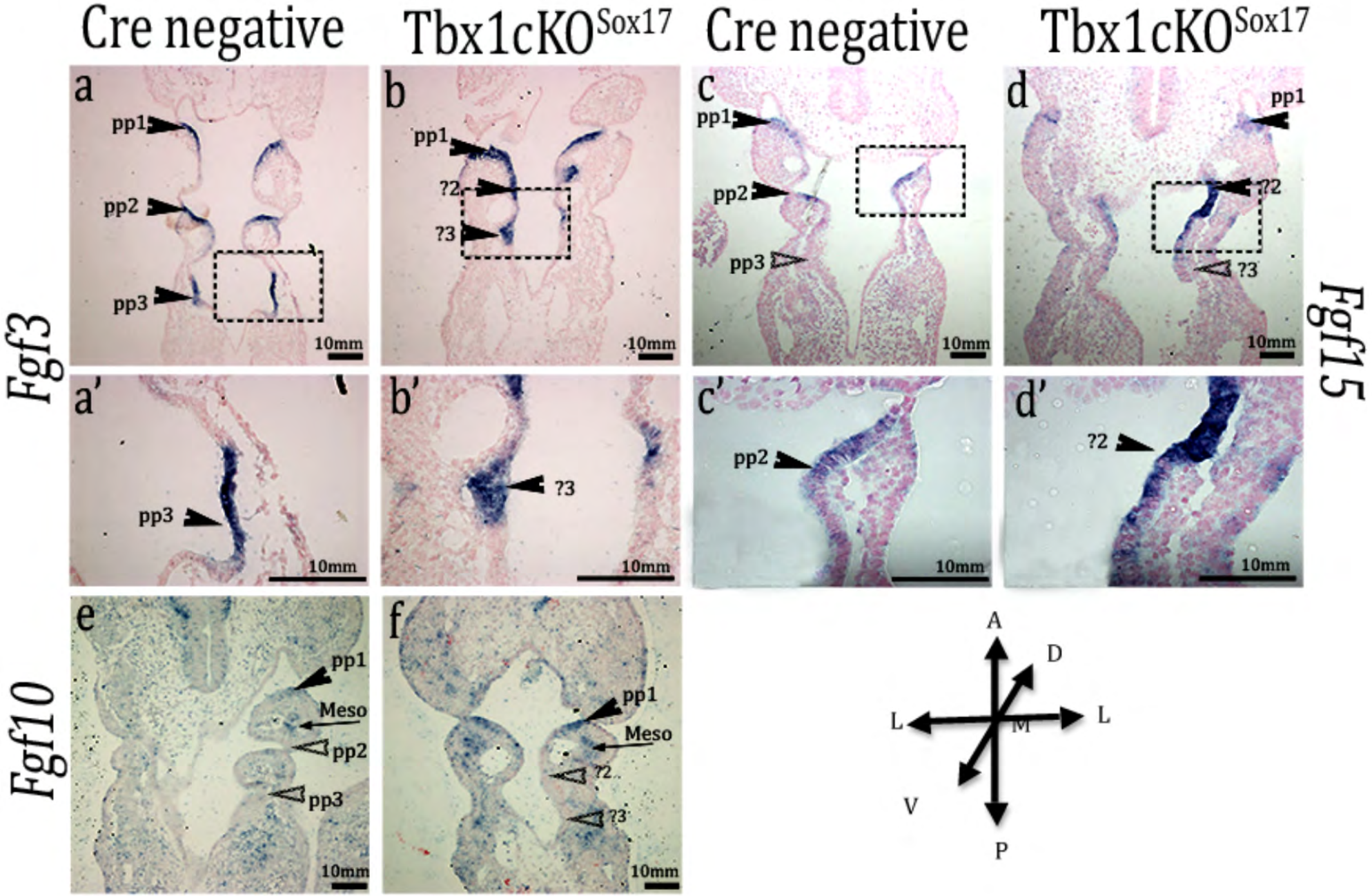
Cre negative
Tbx1cKO Sox17
Cre negative
Tbx1cKO Sox17
Fgf3
Fgf15
Fgf10
a
b
c
d
a'
b'
c'
d'
e
f
pp1
pp2
pp3
?2
?3
Meso
10mm
A
D
L
M
L
V
P

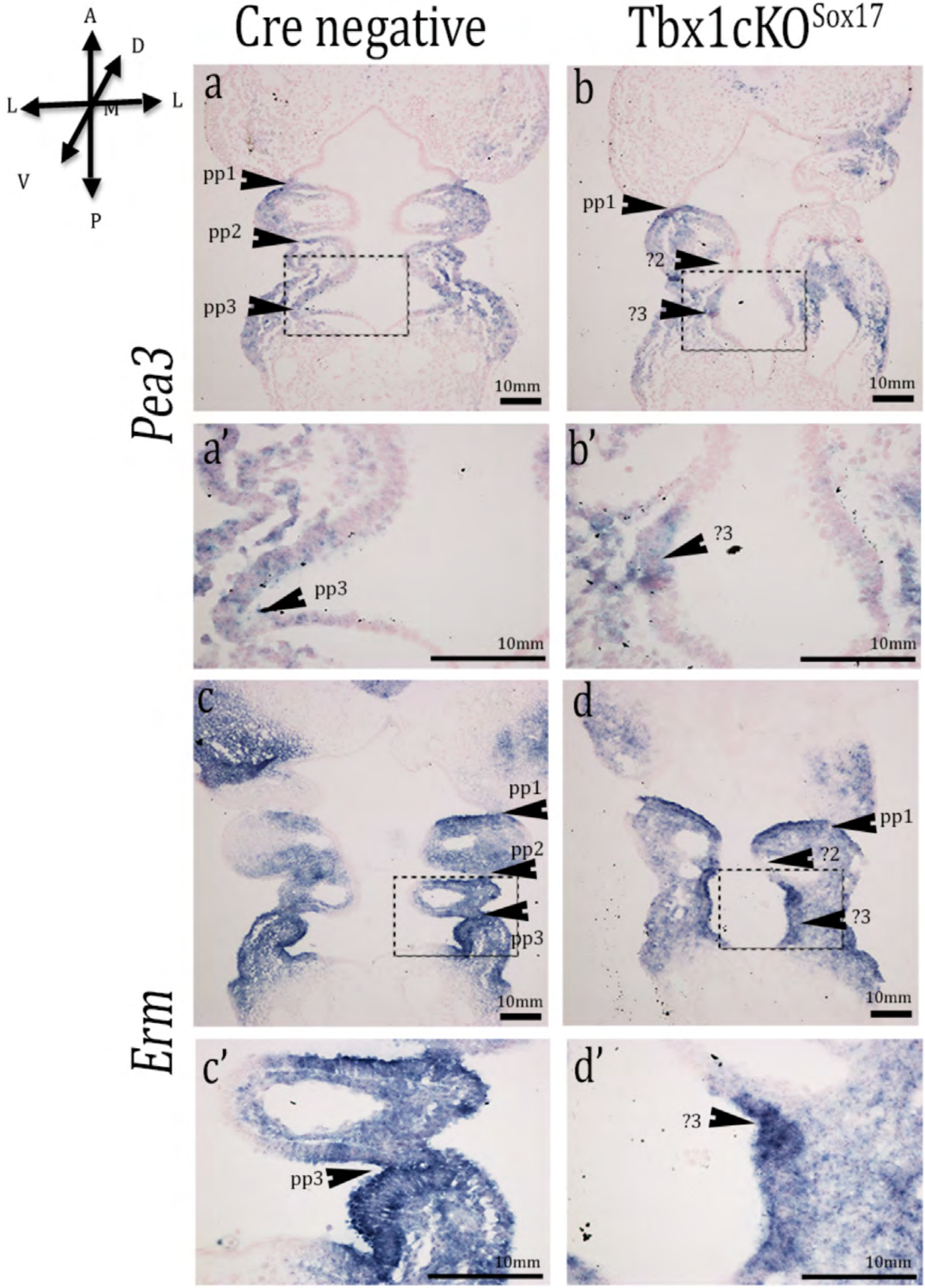
A
D
L
M
L
V
P
Cre negative
Tbx1cKO Sox17
Pea3
Erm
a
pp1
pp2
pp3
10mm
b
pp1
?2
?3
10mm
a'
pp3
10mm
b'
?3
10mm
c
pp1
pp2
pp3
10mm
d
pp1
?2
?3
10mm
c'
pp3
10mm
d'
?3
10mm

Fig 18: TBX1 is not required for the expression of *Fgf3, Fgf10* or *Fgf15* in the pharyngeal endoderm. Frontal sections of E9.*5* Cre negative (a, a', c, c' and e), and *Tbx1cKO*^{Sox17} (b, b', d, d' and f) embryo's PA reveal that the expression of *Fgf3* (a – b', n=2), *Fgf15* (c – d', n=1), and *Fgf10* (e and f n=1), is maintained in the endoderm independently of TBX1. Note the 'unsegmented' expression pattern of *Fgf3* and *Fgf15* in the pharyngeal endoderm of *Tbx1cKO*^{Sox17} embryos. a'- d' are high magnification images of panels a-d.

Annotations: Black arrowhead = endodermal pouch expression, unfilled arrowhead = endodermal pouch (no/little expression visible), pp = pharyngeal pouch, ? = presumptive pouch regions in TBX1-deficient endoderm, outlined areas in panels a-d indicate the area magnified in panels a'-d'. Meso labelled arrow = Mesodermal expression of *Fgf10*. Arrows to the right of figure illustrate the orientation of the pharyngeal apparatus sections; A = anterior, P = posterior, L = lateral, M = medial, V= ventral, D = dorsal.

Fig 19: Expression of *Fgf* signalling 'readouts' is maintained in the endoderm independently of cell-autonomous *Tbx1* expression.

In situ hybridization on frontal sections of E9.5 Cre negative (a,c) and *Tbx1cKO*^{Sox17} (b,d) pharyngeal pouches with an antisense *Pea3* (a-b and high power a'-b') or *Erm* (c-d and high power c'-d') mRNA probe. The *in situ* hybridisation reveals that FGF signalling is maintained in *Tbx1*-deficicent endoderm. In addition, *Erm* is expressed in an un-segmented pattern in the endoderm of *Tbx1cKO*^{Sox17}embryos. a'-d' are high power images of the corresponding outlined areas in a-d. Annotations: Black arrowhead = endodermal pouch expression, blue arrowhead = ectodermal expression, unfilled arrowhead = endodermal pouch (no/little expression visible), pp = pharyngeal pouch, ? = presumptive pouch regions in *Tbx1*-deficient endoderm, corresponding, outlined, areas in images a-d. Black arrows = Fgf ligand expression in the endoderm, Meso = Mesodermal expression of *Fgf10*. Arrows to the left of Fig 19 illustrate the orientation of the pharyngeal apparatus sections; A = anterior, P = posterior, L = lateral, M = medial, V≠= ventral, D = dorsal. N=2,for all.genes.

Fig 20

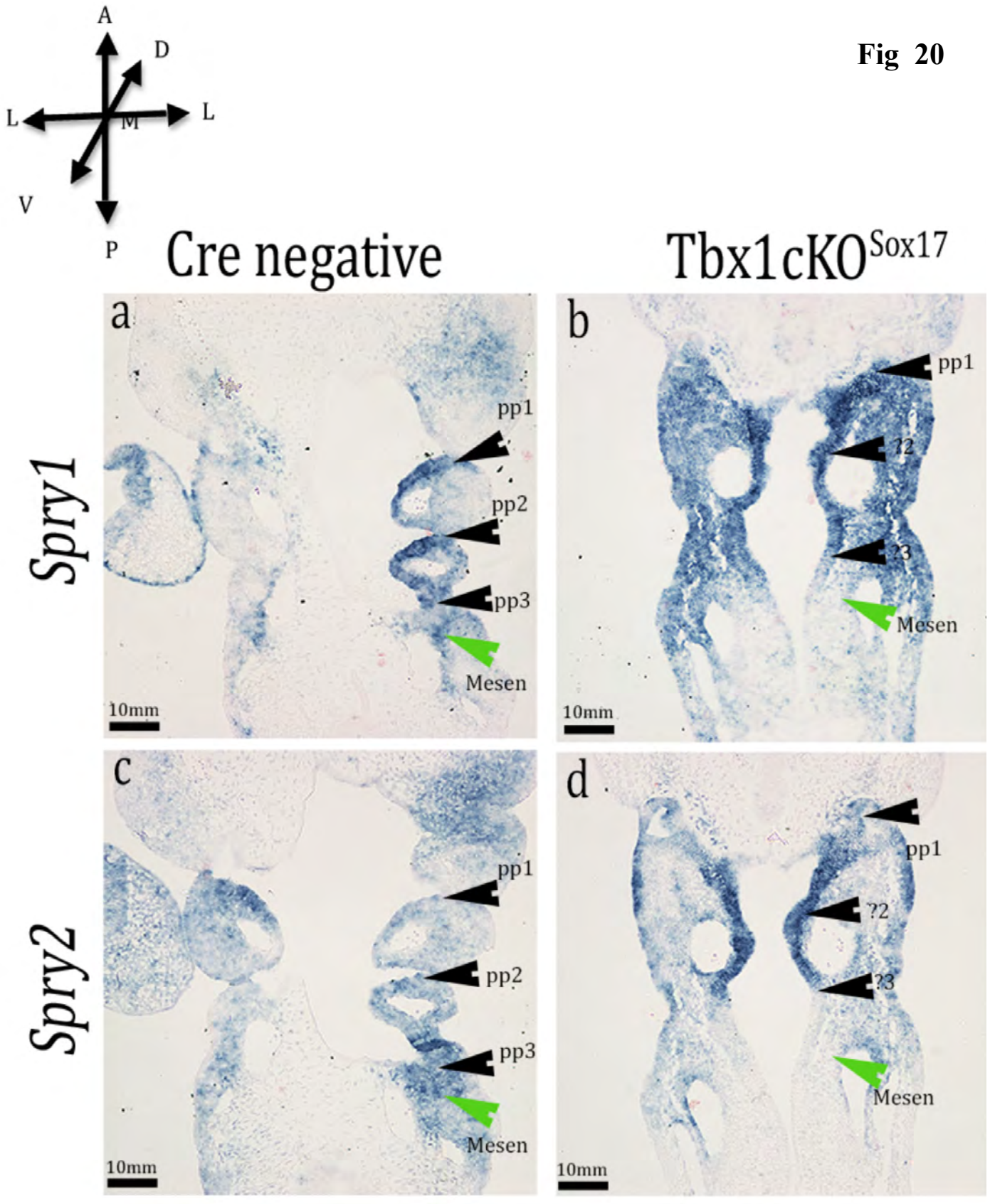
A
D
L
M
L
V
P
Cre negative
Tbx1cKO Sox17
Spry1
Spry2
a
b
c
d
pp1
pp2
pp3
?2
?3
Mesen
10mm

Fig 20: *Sprouty* genes are expressed in a de-regulated manner throughout the pharyngeal endoderm and mesenchyme when *Tbx1* is deleted from the endoderm. *In situ* hybridization for *Sprouty 1* (a and b) and *Sprouty 2* (c and d) showed that the segmented pattern of expression in Cre negative embryos (a and c) is absent from *Tbx1cKO*^{Sox17} embryos (b and d). *Sprouty 1* expression is expressed throughout the pharyngeal endoderm (black arrowheads) and mesenchyme (green arrowheads). An *in situ* hybridization for *Sprouty 2* also showed de-regulated expression in mutant's rostral, unsegmented endoderm (panel d, black arrowheads), but unlike *Sprouty 1*, the expression of *Sprouty* 2 in the mesenchyme appears to be similar to that of the mesenchyme of the Cre negative embryos (green arrows in panels c and d). N = 3 for each gene. Annotations: Black arrowhead = endodermal pouch expression, pp = pharyngeal pouch, ? = presumptive pouch regions in TBX1-deficient endoderm, Green arrowhead = pharyngeal mesenchyme. Arrows to the right of Fig 20 illustrate the orientation of the pharyngeal apparatus sections; A = anterior, P = posterior, L = lateral, M = medial, V= ventral, D = dorsal.

3.5 Discussion

A new transgenic mouse line with Cre activity specifically in the endoderm was required to determine whether *Tbx1* is required in the endoderm during pouch formation. Foxg1^{Cre} on a S-W genetic background was found to recombine *Tbx1* specifically in the endoderm (Arnold et al., 2006). However, this mouse line is not an ideal tool to study the role of specific genes within the endoderm because on genetic backgrounds other than S-W, Foxg1^{Cre} expression is not specific to the endoderm (Zhang et al., 2005). Conditional Cre lines that are expressed in multiple tissues, including the endoderm, (e.g. Hoxa2^{Cre} and Nkx2.5^{Cre}) may be utilised if recombination in the non-endodermal tissue alone does not cause pharyngeal pouch defects (Xu et al., 2004; Zhang et al., 2005). For instance, *Hoxa2* is expressed in the endoderm and ectoderm caudal to the 2nd pharyngeal pouch. Yet, thymus hypoplasia generated by the recombination of *Fgf8* by Hoxa2^{Cre} has been attributed to loss of *Fgf8* form the endoderm (Zhang et al., 2005). The latter was inferred because deletion of *Fgf8* by the Ap2alpha^{Cre} (expressed in ectoderm and CNCC) does not generate the same thymus defect (Zhang et al., 2005). However, the restricted temporal-spatial expression of the Hoxa2^{Cre} and Nkx2.5^{Cre} in the pharyngeal endoderm limits their use in studying pharyngeal pouch morphogenesis. For example, Hoxa2^{Cre} expression is only initiated after E9.0 in the PA where its expression is restricted to the caudal endoderm (Zhang et al., 2005).

In this thesis a new Cre line, Sox17-2Ai-Cre, has been utilised to delete *Tbx1* within the endoderm. *Sox17* (which drives the transcription of the *Cre*) is active before the pharyngeal endoderm forms (E7.0) and is expressed within all the cells of the pharyngeal endoderm. Thus, *Sox17-2Ai-Cre* is as ideal tool to study the role of genes expressed in the endoderm during pouch morphogenesis.

3.5.1 Variable X-gal staining in endothelial cells is a reporter specific discrepancy

There is some discrepancy between SOX17^{iCre} positive embryos in the level and pattern of *R26R* expression detected by X-gal staining. The difference in stain appears specific to the X-gal staining of endothelial cells, where *Sox17* is also expressed. Differences in reporter expression pattern, identifying Cre activity, have been documented for other tissue specific Cre lines (Hébert et al., 2000). For instance, the pattern of human-placental-alkaline-phosphatase staining (detecting *Z/AP* recombination) varied from the pattern of X-gal staining (detecting *R26R* recombination) when both were mediated by FOXG1^{Cre} (Hébert et al., 2000). One theory is that the *Z/AP* allele is more susceptible to recombination and occurs in the presence of very low levels of FOXG1^{Cre}. If this hypothesis is applicable to all conditional *Cre* lines it is possible that the *R26R* allele is less susceptible to recombination than the *RYFP* allele and so endothelial cell recombination is not always apparent. However, this also implies that endothelial cells have a lower level of *Sox17* expression than endodermal cells, which was not reported in the original report paper (Engert et al., 2009).

Although differences in SOX17^{icre} mediated endothelial cell recombination are important to document, the functional consequences of this discrepancy are not relevant for pharyngeal pouch morphogenesis, (i.e. the loss of *Tbx1* expression in endothelial cells). *Tie2* is expressed specifically within endothelial cells. Embryos deficient in endothelial *Tbx1* (*Tie2$^{Cre/+}$;Tbx1$^{flox/-}$*) do not display any cardiovascular defects and no pouch or endocrine defects were documented either (Xu et al., 2004; Chen et al., 2010). Furthermore the activity of SOX17^{iCre} at E9.5 is sufficient

to delete *Tbx1* and thus prevent the translation of TBX1 protein in the pharyngeal endoderm, the focus of this thesis analysis of pharyngeal pouch morphogenesis.

3.5.2 Caudal pouch formation is prevented by the efficient, SOX17^{icre}-mediated, deletion of *Tbx1* from the endoderm

The deletion of *Tbx1* in the endoderm by SOX17^{icre} is efficient and specific, as PA tissue, other than the pharyngeal endoderm, is positive for TBX1 protein when *Sox17^{iCre}* is expressed. This indicates that the pharyngeal defects of the *Tbx1*-deficient embryos are a direct result of the loss of *Tbx1* from the pharyngeal endoderm. *Tbx1$^{+/-}$* embryos do not have any documented defects in pharyngeal pouch evagination (Vitelli et al., 2002b; Liao et al., 2004). In agreement, pharyngeal pouch outgrowth was not affected by the deletion of one *Tbx1* allele from the endoderm. Thymus development also appears unaffected in the *Tbx1cHet^{Sox17}* embryos, with no apparent size or migration defects observed in these mutants. This data complements the findings of Arnold et al. who used the *Foxg1^{Cre}* mouse line on a S-W background to delete *Tbx1* from the endoderm (Arnold et al., 2006). It also suggests that thymus organogenesis is affected by the loss of *Tbx1* from multiple tissues as *Tbx1$^{+/-}$* embryos display a low incidence of thymus hypoplasia (Vitelli et al., 2002b). The thymus develops from *Foxn1* positive cells of the 3rd pouch, however CNCC also contribute to thymus organogenesis (Gordon et al., 2001; Blackburn and Manley, 2004). It is possible that loss of one allele of *Tbx1* from the ectoderm causes the perturbed migration of CNCC into the caudal PA of *Tbx1$^{+/-}$* embryos that subsequently perturbs thymi development (Calmont et al.,

2009). Certainly *PSE-KO* embryos display defects in CNCC migration and thymus hypoplasia (Randall et al., 2009). The cumulative affect of reduced *Tbx1* expression in the endoderm and mild CNCC defects may cause thymus hypoplasia in $Tbx1^{+/-}$ embryos. To validate this hypothesis a simultaneous analysis of CNCC migration and thymus defects in Cre negative embryos, $Tbx1^{+/-}$ embryos, $Tbx1cHet^{Sox17}$ embryos and embryos lacking one allele of *Tbx1* in ectodermal cells is required. $Tbx1cKO^{Sox17}$ embryos recapitulate the caudal pouch and thymus aplasia observed when *Tbx1* is deleted from all tissues ($Tbx1^{-/-}$ embryos). The lack of caudal pouch evagination in $Tbx1cKO^{Sox17}$ embryos proves that *Tbx1* is required within the endoderm for caudal pharyngeal pouch morphogenesis, corroborating the findings of Arnold et al., (Arnold et al., 2006). It is becoming apparent that the 1st pouch has an autonomous developmental programme. The major distinction between the 1st pouch and the caudal endoderm of $Tbx1cKO^{Sox17}$, $Tbx1^{-/-}$ and *Tbx1* hypomorphic embryos is that the 1st pouch is able to evaginate, enabling the 1st arch to form (Hu et al., 2004).

Caudal pouch evagination is unable to proceed in $Tbx1cKO^{Sox17}$ embryos despite the presence of a source of mesodermal *Tbx1*. Zhang et al., propose that *Tbx1* in the pharyngeal mesoderm was sufficient to partially drive pharyngeal pouch morphogenesis (Zhang et al., 2006). Re-activation of mesodermal *Tbx1* expression in *Tbx1* hypomorphic embryos normalized the 2nd pouch and partially normalized 4th pouch outgrowth. Residual *Tbx1* expression from the hypomorphic allele was deemed insufficient to support pouch outgrowth (Zhang et al., 2006). However, the residual amount of *Tbx1* may have enabled the endoderm to 'respond' to evagination signals from the mesoderm. Vitelli et al., propose that a minimal amount of *Tbx1* is required for cells to be able to respond to adjacent signalling

molecules, such as FGF8 (Vitelli et al., 2010). Mesenchymal embryonic fibroblast cells (MEFs) were harvested from *Tbx1*$^{neo/-}$ embryos (which express residual *Tbx1*) and from *Tbx1*$^{-/-}$ embryos. Only the *Tbx1*$^{neo/-}$ MEFs were able to respond to exogenous FGF8 as assayed by amount of phospho-RSK produced by the hypomorphic cells, relative to *Tbx1*$^{+/+}$ MEFs (Vitelli et al., 2010). Thus, *Tbx1* expression in the mesoderm of *Tbx1cKO*^{Sox17} embryos may be unable to support caudal pouch morphogenesis because the pharyngeal endoderm of these mutants is completely devoid of *Tbx1*.

3.5.3 Loss of *Tbx1* from the endoderm affects CNCC migration and the formation of the thoracic vessels and pinna

The amount of CNNC, indicated by the level of *Dlx2* expression, in the caudal PA of *Tbx1*$^{-/-}$ embryos is severely reduced (Vitelli et al., 2002). CNCC do not express *Tbx1* thus the defects observed in *Tbx1*$^{-/-}$ embryos are consequence of the loss of *Tbx1* in the pharyngeal epithelia and/or mesoderm (Garg et al., 2001; Vitelli et al., 2002). However, by collating data from embryos harbouring tissue-specific deletions of *Tbx1* it is becoming apparent that CNCC migration toward and infiltration of the PA requires *Tbx1* expression in every tissue of the PA. Deleting *Tbx1* in the pharyngeal ectoderm (*PSE-KO* embryos) causes migratory defects in *Sox10*-expressing CNCC (Calmont et al., 2009). The circumpharyngeal crest of the *PSE-KO* embryos were absent distally and often merged with the post otic crest proximally (Calmont et al., 2009). The tissue-specific deletion of *Tbx1* from mesodermal cells (*M-KO* embryos) also perturbs *Crabp1* marked CNCC migration into the caudal PA (Zhang et al., 2006). Finally, a reduction in *Dlx2* expressing CNCC was also observed in the

caudal PA of *Tbx1cKO*^{Sox17} embryos suggesting that the TBX1 dependent signals from, and/or the morphology of, the pharyngeal endoderm also influence CNCC development. A detailed analysis of CNCC markers such a *Sox10* and *Crabp1* in *Tbx1cKO*^{Sox17} embryos is required to determine 'stream'-specific migratory defects caused by the loss of *Tbx1* in the endoderm.

Tbx1$^{-/-}$ embryos display defects in multiple PA derivatives that are contributed to by CNCC, including, the external ear, OFT and thoracic vessels of the heart (Scambler, 2010). The pinna, one of the structures of the external ear, are derived from six hillocks, (mesenchymal/ectodermal thickenings), on the surface of the 1st arch (Alasti and Van Camp, 2009). Despite the mesenchymal/ectodermal origin of this structure, the deletion of *Tbx1* from the endoderm (by the FOXG1^{Cre} on a S-W background) recapitulates the pinna aplasia observed in *Tbx1*$^{-/-}$ embryos (Jerome and Papaioannou, 2001; Arnold et al., 2006). A mesodermal source of *Tbx1* has also been shown to be both necessary for the formation of the pinna. Hypoplastic pinna form when *Tbx1* is absent from the mesoderm (Zhang et al., 2006). Conversely reactivation of *Tbx1* in mesodermal cells (in a *Tbx1* hypomorphic background) rescues the external ear hypoplasia displayed in *Tbx1* hypomorphs (Zhang et al., 2006). Surprisingly, it was noticed that pinna are able to form, albeit hypoplastically, in *Tbx1cKO*^{Sox17} embryos. The pinna defects of *Tbx1cKO*^{Sox17} mutants appear akin to those of *M-KO* mutants, rather than the *PE-KO* mutants. The discrepancy between the *Tbx1cKO*^{Sox17} and *PE-KO* mutants is unusual considering the 1st arch forms in both mutants and the only loss of *Tbx1* is from the endoderm (Arnold et al., 2006). It is possible that the deletion of *Tbx1* from the endoderm on different genetic backgrounds affects pinna development to different extents. Alternatively, it may be that the contribution of CNCC to the 1st arch is

more severely disrupted in *PE-KO* mutants. But as CNCC migration was not analysed in *PE-KO* embryos a comparison cannot be made with the migration of CNCC in *Tbx1cKO*^{Sox17} and *M-KO* embryos, both of which retain some CNCC migration into their 1st arch (Zhang et al., 2006). Alternatively, the discrepancy in the expression of *Fgf3* between *PE-KO* and *Tbx1cKO*^{Sox17} embryos may explain the different severities of pinna defects observed in these endodermally deficient mutants (Arnold et al., 2006). For, pinna defects are associated with *Fgf3* homozygous loss of function mutations in human patients with syndromic deafness (Tekin et al., 2008).

The lack of caudal pouch outgrowth in *Tbx1cKO*^{Sox17} embryos corroborates the data of Arnold et al. demonstrating that *Tbx1* is required within the endoderm for pharyngeal pouch morphogenesis. However, the *Tbx1cKO*^{Sox17} phenotype does not support the authors conclusions that; 'complete inactivation of *Tbx1* in the endoderm results in a phenotype identical to the *Tbx1* homozygous null mutants' (Arnold et al., 2006). In addition to the pinna, another example provided by this thesis to suggest that the endoderm deletion of *Tbx1* is not sufficient to recapitulate the *Tbx1*$^{-/-}$ phenotype is that *Tbx1cKO*^{Sox17} do not present with any outflow tract (OFT) defects that manifest in *PE-KO* and *Tbx1*$^{-/-}$ embryos.

The division of the pulmonary and aortic (systemic) circulation is enabled by the division of the OFT into two channels which are separated by the formation of an aorto-pulmonary septum (Xu et al., 2004). Current literature proposes that *Tbx1* within the mesoderm is critical for OFT development whereas the role of expression from the endoderm is marginal (Zhang et al., 2006). However, OFT septation and alignment defects such as ventral septal defects (VSD) and persistent

truncus arteriosus (PTA) were detected in *PE-KO* embryos indicating that *Tbx1* in the endoderm is also required for the OFT to develop (Arnold et al., 2006). The deletion of *Tbx1* from mesodermal OFT precursor cells with the *Nkx2.5Cre* line also caused OFT septation defects but *Nkx2.5* is expressed within the endoderm of the 3rd and 4th pouch (Xu et al., 2004). OFT defects were present in all *M-KO* mutants and this defect was fully rescued by the reactivation of *Tbx1* in a *Tbx1* hypomorphic background (Zhang et al., 2006). This indicated that *Tbx1* in the mesoderm was crucial to the septation of the OFT but did not disprove any marginal role a basal level of endoderm expression may be playing. Even a low level of *Tbx1* in *Tbx1* hypomorphs can ameliorate the severity of OFT septation defects seen in $Tbx1^{-/-}$ embryos (Vitelli et al., 2010). The lack of OFT defects in $Tbx1cKO^{Sox17}$ supports the current view of Zhang et al., that *Tbx1* in the endoderm is not required for OFT development.

In contrast, the presence of aortic arch defects in $Tbx1cKO^{Sox17}$ embryos supports the hypothesis that *Tbx1* is required in the pharyngeal epithelia for 4th PAA development. The deletion of one allele of *Tbx1* in the pharyngeal epithelia, mediated by $FGF15^{Cre}$ (which has endoderm and ectoderm activity), $HOXA3^{Cre}$ (which has endoderm, ectoderm and mesoderm activity) and $Ap2alpha^{Cre}$ (which has ectoderm activity) all generate 4th PAA aplasia that leads to defects such as IAA-B (Zhang et al., 2005). Whilst the data presented here establishes that *Tbx1* is required for aortic arch development it is unclear whether this is due to a loss of arch formation, or, because TBX1-dependent signals from the endoderm are directly required for PAA formation. To determine the latter requires an analysis of thoracic vessel development in $Tbx1cHet^{Sox17}$ embryos. If IAA-B and a-RSA manifest in $Tbx1cHet^{Sox17}$ embryos this would confirm that TBX1-dependent

signals from the endoderm are directly required for PAA formation because the formation of the pharyngeal pouches and thus arches are not perturbed in these mutants.

3.5.4 *Fgf8* expression but not FGF signalling within the endoderm is dependent on *Tbx1*

After establishing that *Tbx1* is required in the endoderm for pharyngeal pouch formation, it was necessary to identify candidates that may act downstream of *Tbx1* to control pouch formation. Expression of *Fgf3* and *Fgf8* are both absent from the pharyngeal endoderm of *Tbx1*$^{-/-}$ and *PE-KO* embryos, mesodermal *Fgf10* expression domains are also absent from the PA of *Tbx1*$^{-/-}$ embryos (Vitelli et al., 2002b; Aggarwal et al., 2006; Arnold et al., 2006). TBX1 has been shown to directly activate *Fgf8* and *Fgf10*-luciferase constructs *in vitro* via *T-box* consensus sites within the promoters of these genes (Hu et al., 2004; Xu et al., 2004). The loss of *Fgf8* specifically from the endoderm of *Tbx1cKO*^{Sox17} embryos at E8.5 and E9.5 corroborates that TBX1 is required for the expression of this ligand in the pharyngeal endoderm. The loss of *Fgf8* from the un-segmented endoderm is unlikely to be caused by the change in tissue morphology as *Fgf8* is maintained in the ectoderm despite the loss of segmentation in this tissue.

In contrast, however, the expression of *Fgf3*, *Fgf10* and *Fgf15* are maintained in the endoderm of *Tbx1cKO*^{Sox17} embryos, indicating that expression of *Tbx1* in the endoderm is not required for the expression of these ligands. The change in the expression patterns of *Fgf3* and *Fgf15* in *Tbx1cKO*^{Sox17} embryos could be an indication of FGF ligand redundancy, particularly with regards to *Fgf3*. Normally

Fgf3 is restricted to the posterior portion of the forming 3rd pouch, complimentary to the anterior expression domain of *Fgf8*. In *Tbx1cKO*^{Sox17} embryos, however, the expression of *Fgf3* in the caudal endoderm extends into the *Fgf8* expression domain. Alternatively, the change in the expression pattern of these ligands may be secondary to the change in *Tbx1cKO*^{Sox17} embryos endodermal tissue morphology.

The ETS transcription factors *Pea3* and *Erm* have been shown to be expressed downstream of *Fgf8* (Roehl and Nusslein-Volhard, 2001). For instance, the ISLET1^{Cre} mediated deletion of *Fgf8* from the pharyngeal endoderm and anterior heart field severely reduces the expression of *Erm* in these cells (Park et al., 2006). *Sprouty* genes are also expressed in response to FGF8 signalling and are lost in the absence of *Fgf8*, indicating they mediate the regulation of an FGF8 induced signalling cascade (Minowada et al., 1999). However, despite the severely diminished expression of *Fgf8* in the pharyngeal endoderm of *Tbx1cKO*^{Sox17} embryos, the endodermal expression of *Erm, Pea3, Sprouty 1* and *Sprouty 2* is maintained. This expression data contrasts with the loss of expression of *Fgf* signalling readouts in the PA of *Tbx1*$^{-/-}$ and *Tbx1*$^{+/-}$ mutants. The expression of *Erm*, *Sprouty1* and *Sprouty2* appear reduced in the PA of *Tbx1*$^{+/-}$ embryos and the expression of *Sprouty1* and *Sprouty2* are severely diminished in *Tbx1*$^{-/-}$ embryos (Simrick et al., 2012). This same trend is observed in the expression of *Fgf receptor 1* (*Fgfr1*) in the PA of *Tbx1*$^{+/-}$ and *Tbx1*$^{-/-}$ embryos (Park et al., 2006).

It is likely that the maintained expression of FGF signalling readouts in *Tbx1cKO*^{Sox17} embryos is due to the maintenance of *Fgf3*, *Fgf10* and *Fgf15* expression in the pharyngeal endoderm of these mutants. However, *Fgf* expression in adjacent pharyngeal tissues, such as *Fgf10* in the mesoderm and *Fgf8* in the

ectoderm, may also be capable of eliciting FGF signalling in the pharyngeal endoderm of *Tbx1cKO*^{Sox17} embryos. Despite the maintenance of the FGF signalling cascade within the *Tbx1*-deficient endoderm, pharyngeal pouch evagination is not supported in *Tbx1cKO*^{Sox17} embryos. It is possible that although the endoderm is able to express FGF signalling factors it is unable to respond to these signals appropriately in the absence of *Tbx1*. A similar prediction has been made with respect to MEFs and a need to express at least 20% the normal level of *Tbx1* otherwise they are unable to elicit FGF signalling in response to FGF8 exposure (Vitelli et al., 2010). Alternatively, pharyngeal pouch morphogenesis may specifically require the TBX1 dependent expression of *Fgf8* in the pharyngeal endoderm, this hypothesis was tested in Chapter 4.

Chapter 4

Results part II

4.1 The expression of *Fgf8* within the endoderm is not essential for pharyngeal pouch formation

The requirement for *Fgf8* during the development of the pharyngeal pouches has been demonstrated in mouse lines that have a reduced level of transcription from the *Fgf8* allele (hypomorphs). Severe *Fgf8* hypomorphs have disorganised pouch formation; the two rostral pouches are present but fused and the two caudal pouches are hypoplastic or absent (Abu-Issa et al., 2002). *Fgf8* mild hypomorphs are unable to form their 3rd pouch, resulting in a fusion of the 3rd and 4th arches (Frank et al., 2002). The less extensive pouch defect of *Fgf8* mild hypomorphs indicates that caudal pouches are more sensitive to the loss of *Fgf8* than rostral pouches. The caudal pouch defects of both *Fgf8* mutant's correlates with the thymus hypoplasia and aplasia that manifests later in gestation (Abu-Issa et al., 2002; Frank et al., 2002)

Fgf8 is expressed in multiple tissues within the PA, thus the loss of *Fgf8* from each tissue could affect pharyngeal pouch morphogenesis (Crossley and Martin, 1995). Tissue specific deletions of *Fgf8* have not yet revealed a requirement for *Fgf8* in a defined population of cells during pouch formation. CNCC do not express *Fgf8*, accordingly, recombination of *Fgf8* by a Cre line only expressed in CNCC does not cause pharyngeal pouch defects (Frank et al., 2002). *Fgf8* is expressed widely throughout the pharyngeal ectoderm during PA development. Although the deletion of *Fgf8* from the ectoderm, (Ap2alpha$^{IRESCre/+}$;Fgf8$^{flox/-}$ embryos), generates 'fused' pharyngeal arches, no pouch phenotypes have been described in these mutants. Moreover, endocrine organs derived from the caudal pharyngeal pouches form normally (Macatee et al., 2003). Loss of *Fgf8* from the mesoderm

prevents 4th PAA formation but consequences for pouch formation were not assessed (Park et al., 2006).

In summary, this data indicates that pharyngeal pouch development may require expression of *Fgf8* specifically within the endoderm. The deletion of *Fgf8* with the Hoxa2^{Cre} supports the latter hypothesis as the incidence of thymus and parathyroid defects are comparable to that of severe *Fgf8* hypomorphs (Macatee et al., 2003). *Hoxa2* is expressed in the pharyngeal epithelia and mesenchyme caudal to the 2nd arch (Macatee et al., 2003). As neither ectodermal, mesodermal or CNCC deletions of *Fgf8* are reported to cause thymus or parathyroid defects, it is likely that a loss of *Fgf8* from the endoderm disrupts organogenesis of these endocrine glands. The conditional Cre lines available, until now, have not been suitable to directly test the role of *Fgf8* in the endoderm during pouch formation. The aim of the experiments presented in Chapter 3 was to determine whether the expression of *Fgf8* in the endoderm is required for the formation of the pharyngeal pouches and the thymus gland.

4.1.1 SOX17^{icre} deletes *Fgf8* specifically within the pharyngeal endoderm

Conditional Cre lines that have been used to delete *Fgf8* in the endoderm are not suitable to analyse the role of endodermal *Fgf8* in pouch morphogenesis because often the promoter driving the expression of Cre may be temporally-spatially restricted in the pharyngeal endoderm (these Cre lines were outlined in Chapter 3 with reference to the recombination of *Tbx1*). Alternatively, endoderm specific Cre lines may have weak activity within the pharyngeal endoderm as has been

observed with *Foxa3-Cre* line (Dominguez-Frutos et al., 2009). To address the requirement for *Fgf8* in the endoderm during pouch formation the SOX17^{iCre} mouse line was utilised (Engert et al., 2009). In Chapter 3 the efficiency and specificity of SOX17^{iCre} activity was demonstrated in *Tbx1cKO^{Sox17}* embryos. It was hoped that the same qualities would be observed when SOX17^{iCre} was used to drive recombination of the floxed exons (2 and 3) of the *Fgf8* allele (Meyers et al., 1998).

To determine the requirement for *Fgf8* in the endoderm during pouch morphogenesis the SOX17^{iCre} mouse line was used to generate and *Fgf8$^{flox/flox}$* (Cre negative), *Sox17$^{iCre/+}$;Fgf8$^{flox/+}$* (*Fgf8cHet^{Sox17}*) and *Sox17$^{iCre/+}$;Fgf8$^{flox/-}$* (*Fgf8cKO^{Sox17}*) embryos (see 2.3.1 for details of breeding strategies). *In situ* hybridisation with an *Fgf8-exon$^{2/3}$* antisense probe was used to test the efficiency and specificity of the SOX17^{iCre} recombination in *Fgf8cKO^{Sox17}* embryos. *Fgf8* exons 2 and 3 are flanked by loxP sites (floxed) and so should be excised in tissue with SOX17^{iCre} activity, to produce an *Fgf8* null allele (Meyers et al., 1998). In frontal sections of Cre negative embryos the expression of *Fgf8$^{ex2/3}$* is identical to the expression pattern of the full-length probe (compare black arrowheads marking *Fgf8* positive domains in the pharyngeal pouches in panels a of Fig 17 and 21). Of significance is the robust endodermal expression of *Fgf8$^{ex2/3}$* visible in the distal domains of the 1st and 2nd pouch and throughout the entire evaginating 3rd pouch. Whilst the expression of *Fgf8$^{ex2/3}$* in the ectoderm is maintained in *Fgf8cKOSox17* embryos, (light-blue arrowhead Fig 21, panel b), the endodermal expression domain of *Fgf8$^{ex2/3}$* is completely ablated (unfilled arrowheads in Fig 21 panel b). In summary, the data shows that SOX17^{iCre} mediated deletion of *Fgf8* is specific to the endoderm.

Fig 21

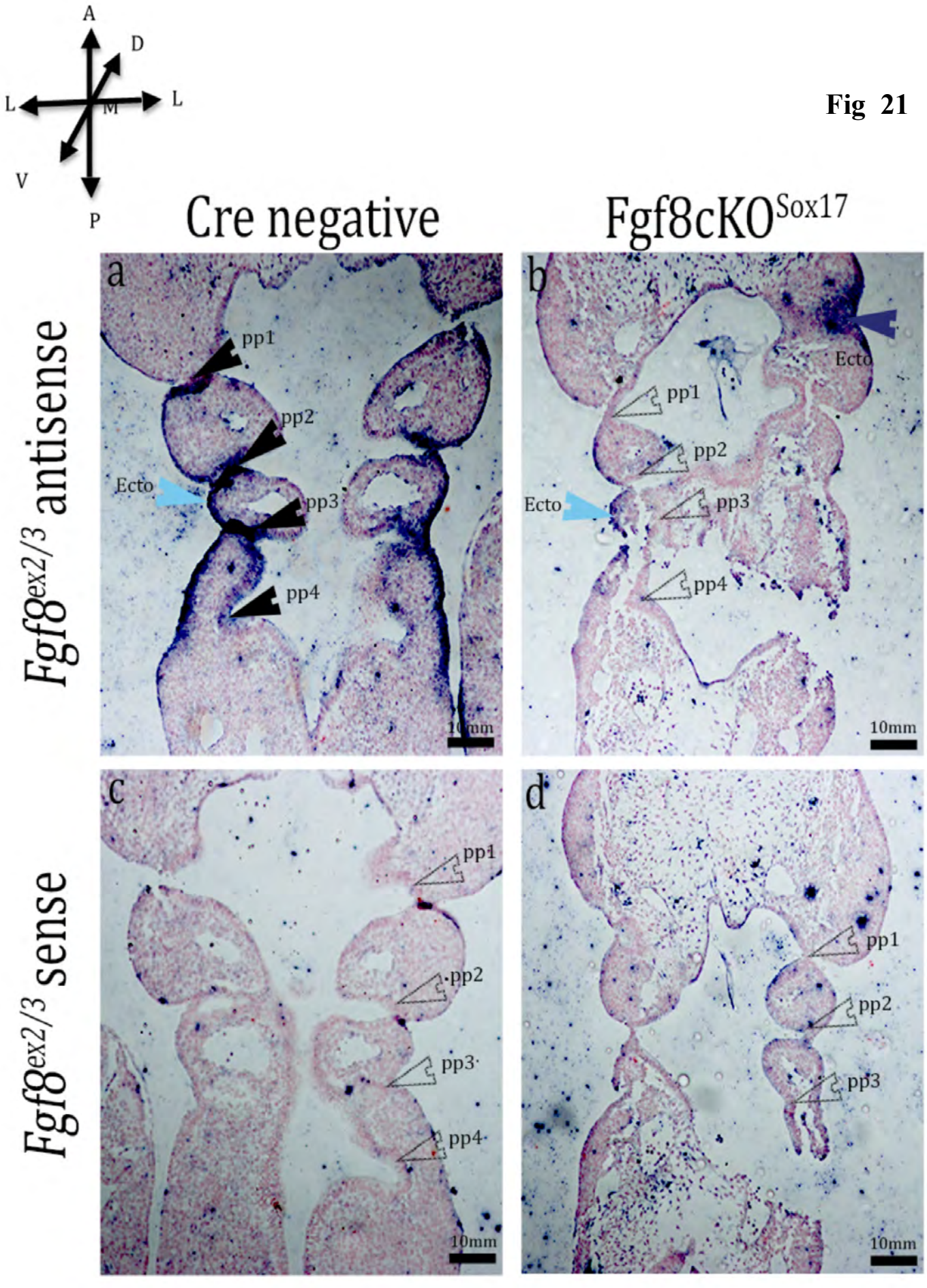
A
D
L
M
L
V
P
Cre negative
Fgf8cKO Sox17
Fgf8ex2/3 antisense
Fgf8ex2/3 sense
a
b
c
d
pp1
pp2
pp3
pp4
Ecto
10mm

Fig 21: *Fgf8* expression is absent in the endoderm of *Fgf8cKOSox17* embryos

In situ hybridization for *Fgf8* expression on frontal sections of Cre negative (a), and *Fgf8cKO*^{Sox17} (b) embryos PA using an antisense mRNA probe designed to hybridise to nascent sense transcripts of *Fgf8 exon 2* and *exon 3* (these exons are flanked by the loxP sites). Note *Fgf8* expression is absent from the endoderm (unfilled arrowheads) but is still detected in the ectoderm of the PA (light blue arrowhead in panel b) of *Fgf8cKO*^{Sox17} embryos. In situ hybridization using a sense mRNA probe designed to copy the nascent sense transcripts of *Fgf8 exon 2* and *exon 3* does not show any staining in the PA of Cre negative (c) or *Fgf8cKO*^{Sox17} (d) embryos. N = 2.

Annotations: Black arrowhead = endodermal pouch expression, light blue arrowhead = ectodermal PA expression, unfilled arrowhead = endodermal pouch (no expression visible), dark blue arrowhead (b) = ectoderm of the 1st pharyngeal arch, pp = pharyngeal pouch, ecto = ectoderm. Arrows to the left of Fig 21 illustrate the orientation of the pharyngeal apparatus sections; A = anterior, P = posterior, L = lateral, M = medial, V= ventral, D = dorsal.

4.1.2 *Fgf8cKO*^{Sox17} embryos do not display defects in pouch morphogenesis or patterning at stage E9.5 of development

Surprisingly, no overt defects in the formation or morphology of the pharyngeal pouches or arches are visible in the frontal sections of *Fgf8cKO*^{Sox17} presented in Fig 21, panel c. One way to assess the normality and extent of pharyngeal pouch and arch formation within the PA is to use genetic markers to identify specific regions within these structures. *Homeobox* (*Hox*) genes have specific expression domains within the PA and as such are good markers of arch and pouch identity (Hunt et al., 1991; Hunt et al., 1991b; Wendling et al., 2000). To determine whether the PA is regionalised in the absence of endodermal *Fgf8 t*he expression of *Hoxa2, Hoxa3* and *Hoxb1* were analysed in controls and embryos deficient in endodermal *Fgf8* by *in situ* hybridisation.

In frontal sections through the PA of Cre negative embryo's *Hoxa2* is expressed throughout the pharyngeal mesenchyme and is most robustly expressed in the 2nd pharyngeal arch, (green arrowhead, Fig 22, panel a). Endodermal expression of *Hoxa2* is present in a very small area of 'inter-pouch' endoderm that lines the third arch, (grey arrowhead, Fig 22, panel a). All the *Hoxa2* expression domains visible in Cre negative embryos are present in *Fgf8cHe*^{tSox17} and *Fgf8cKO*^{Sox17} at the same level and pattern of expression, (compare green and grey arrows in Fig 22 a, b and c). Similarly, no variation in *Hoxa3* expression is visible between Cre negative, *Fgf8cHet*^{Sox17} and *Fgf8cKO*^{Sox17} embryos, (compare Fig 22 c to e). Irrespective of genotype *Hoxa3* expression is maintained in the PA rostral to the 3rd arch. In particular, note the presence of *Hoxa3* expression in the caudal *Fgf8*-deficient

endoderm, posterior to the 3rd arch, (compare the two most posterior black arrowhead in Fig 22 d to e). *Hoxb1* expression is robust in the caudal pharyngeal epithelia, in the caudal endoderm *Hoxb1* appears to mark the out-pocketing 3rd pouch at E9.5 (black arrowhead Fig 22, panels g-i). In RA-deficient embryos that display caudal pouch aplasia, *Hoxb1* expression is absent from the caudal pharyngeal endoderm (Wendling et al., 2000). However, as with all the *Hox* genes analysed in the *Fgf8* conditional mutants there is no apparent change to the level or pattern of *Hoxb1* expression in any expression domain.

It is possible that pharyngeal pouch outgrowth and patterning at E9.5 is able to occur in *Fgf8cKO^{Sox17}* embryos because other *Fgf* ligands expressed in the endoderm can compensate for the loss of *Fgf8*. For instance, FGF3 has been shown to act redundantly with FGF8 in many developmental contexts (Maroon et al., 2002; Walshe et al., 2002). *Fgf3* is expressed within the endoderm at E9.5 in domains that overlap with the expression domain of *Fgf8*, (Vincentz et al., 2005; Aggarwal et al., 2006). However, at E9.5 *Fgf3* is not up-regulated or expanded in the pharyngeal endoderm of *Fgf8cKO^{Sox17}* embryos relative to controls (Fig 23, panels i and j respectively), (Vitelli et al., 2002b; Vincentz et al., 2005; Aggarwal et al., 2006). *Fgf3* expression does not extend into the 3rd pouch domain that normally expresses *Fgf8*, as was observed in *Tbx1cKO^{Sox17}* embryos (Fig 23 j vs Fig 17 c). The maintenance of FGF signalling effectors in *Fgf8*-deficient pharyngeal endoderm (Fig 23 b, d, f, and h) shows that FGF signalling is maintained despite the loss of this ligand. The diffuse expression of *Erm*, *Pea3*, *Sprouty 1* and Sprouty *2* in the mesenchyme and ectoderm is maintained in the PA of Cre negative and *Fgf8cKO^{Sox17}* embryos. In the rostral pouches the FGF readouts are expressed robustly in the posterior half of each pouch, generating a segmented expression

pattern that is evident in all embryos irrespective of genotype (black arrowheads in Fig 23 mark the robust expression in the pharyngeal pouches). Most significantly all the FGF readouts analysed are present and expressed robustly in the caudal evaginating endoderm (most posterior arrowhead in all panels of Fig 23). The maintenance of a segmented expression pattern of *Erm* (Fig 23, panels a and b), *Pea3* (Fig 23, panels c and d), *Sprouty 2* (Fig 23 e and f) and *Sprouty 1* (Fig 16 g and h) in the endoderm of *Fgf8cKO*^{Sox17} embryo's contrasts with the un-segmented expression pattern observed in the *Fgf8*-deficient endoderm of *Tbx1cKO*^{Sox17} embryos (Fig 19 and 20).

In summary, the expression data suggests that pharyngeal pouch formation in *Fgf8*-deficient endoderm, at E9.5, appears indistinguishable from that of Cre negative embryos in morphology and expression. To assess whether caudal pouch formation is maintained in the absence of endodermal *Fgf8* expression, pouch morphology was assessed a day later in embryonic development.

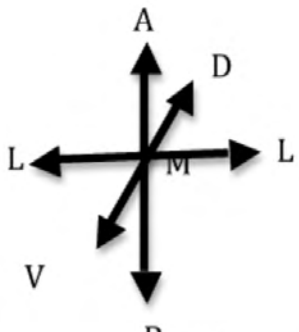
A
D
L
M
L
V
P

Fig 22

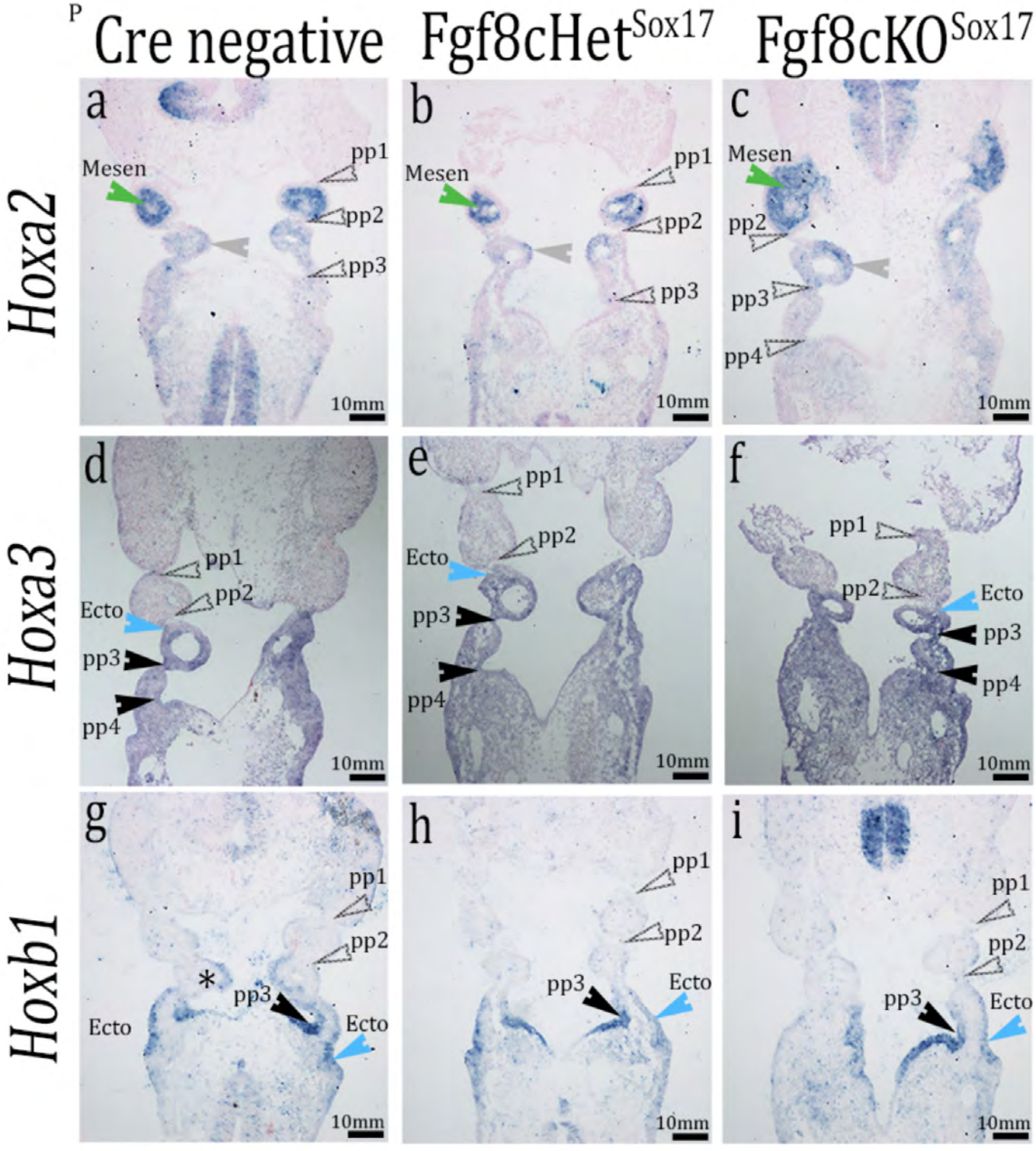
Cre negative
Fgf8cHetSox17
Fgf8cKOSox17
Hoxa2
Hoxa3
Hoxb1
a
b
c
d
e
f
g
h
i
Mesen
pp1
pp2
pp3
pp4
Ecto
*
10mm

Fig 22: Pharyngeal pouches form and *Hox* gene expression domains are maintained in endoderm that does not express *Fgf8*. Frontal sections of E9.5 embryo's pharyngeal apparatus show *Hoxa2* (a-c), *Hoxa3* (d-f) and *Hoxb1* (h-j) expression detected by *in situ* hybridisation is not changed in *Fgf8cKO*^{Sox17} embryos. Note the endodermal expression of *Hoxa2* detected in the Cre negative embryo (marked by an asterix) was also detected in ventral sections of *Fgf8* conditional mutants. N= 2 for *Hoxb1* and *Hoxa2,* N = 3 for *Hoxa3*.

Annotations: Black arrowhead = endodermal pouch expression, light blue arrowhead = ectodermal PA expression, unfilled arrowhead = endodermal pouch with no/little expression, green arrowhead = mesenchyme, pp = pharyngeal pouch, ecto = ectoderm, mesen = mesenchyme. Arrows to the left of Fig 22 illustrate the orientation of the pharyngeal apparatus sections; A = anterior, P = posterior, L = lateral, M = medial, V= ventral, D = dorsal.

Fig 23: Expression of genes in the FGF signalling pathway are not altered in the pharyngeal endoderm of *Fgf8cKO*^{Sox17} embryos. In situ hybridization on frontal sections of E9.5 Cre negative (a, c, e, g, i), and *Fgf8cKO*^{Sox17} (b, d, f, h, j) pharyngeal pouches with antisense RNA probes for; *Erm* (a,b), *Pea3* (c, d), *Sprouty 2* (e, f) and *Sprouty 1*(g, h) and *Fgf3* (a,b) reveal there is no change in FGF signalling in the endoderm (or any adjacent PA tissue) when *Fgf8* is deleted from the endoderm. Black arrowheads indicate the maintenance of strong FGF signalling within the rostral halves of the endodermal pouches that is maintained in both Cre negative and *Fgf8cKO*^{Sox17} embryos. N = 2 for each gene analysed by *in situ* hybridisation in Fig 23.

Annotations: Black arrowhead = endodermal pouch expression pp = pharyngeal pouch. Arrows in the bottom right hand corner of Fig 22 illustrate the orientation of the pharyngeal apparatus sections; A = anterior, P = posterior, L = lateral, M = medial, V= ventral, D = dorsal.

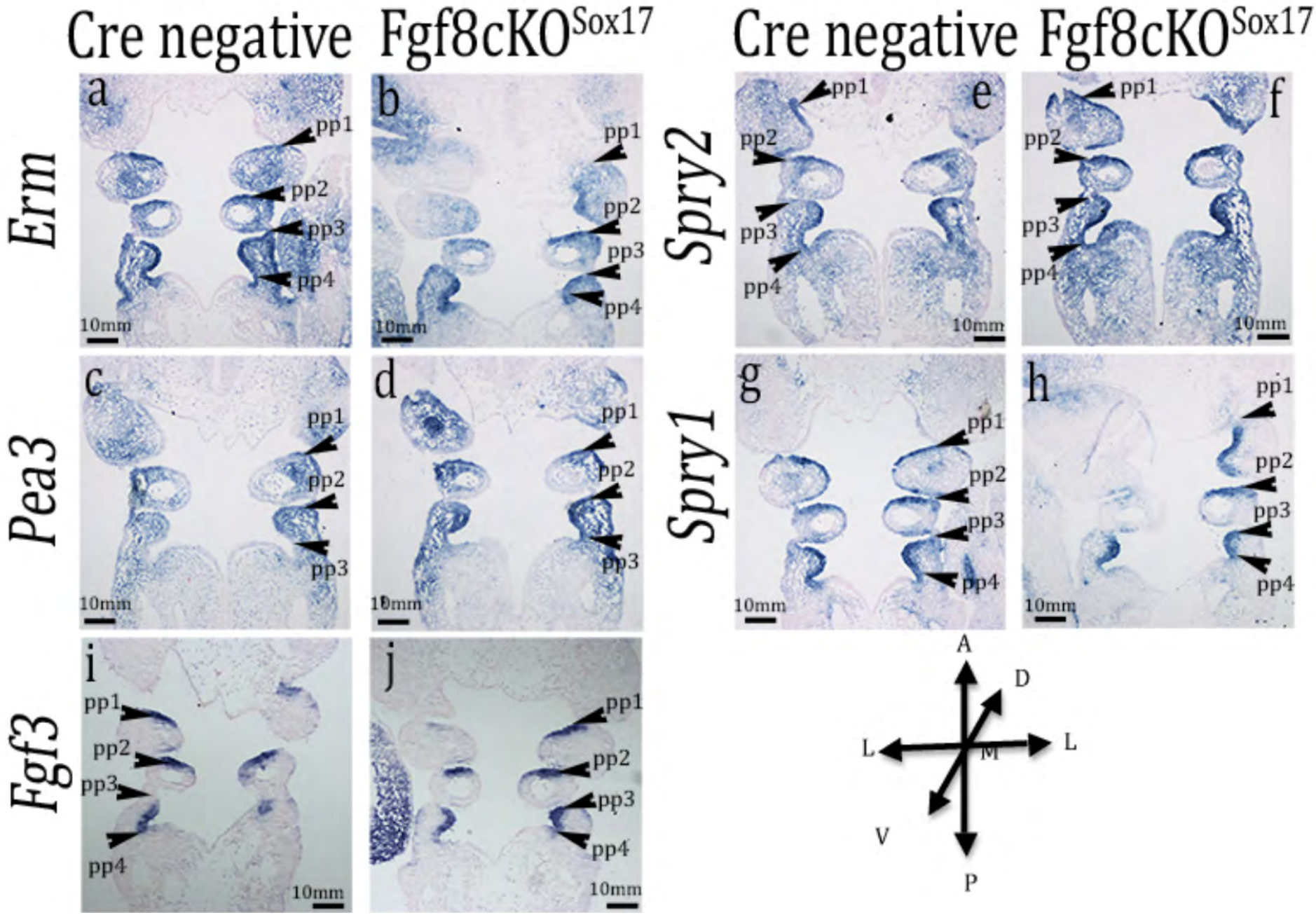
Cre negative
Fgf8cKO Sox17
Cre negative
Fgf8cKO Sox17
Erm
Pea3
Fgf3
Spry2
Spry1
a
b
c
d
e
f
g
h
i
j
pp1
pp2
pp3
pp4
10mm
A
D
L
L
M
V
P

4.1.3 *Fgf8cKO^{Sox17}* embryos display a slight hypoplasia of the 3rd pharyngeal pouch at stage E10.5

The initiation of caudal pouch outgrowth at E9.5 does not guarantee that caudal pouch morphogenesis will proceed normally throughout PA development. In *Shh* null embryos, for instance, pharyngeal pouches form at E9.5 but by E10.5 the pouches have atrophied, particularly the 1st pouch (Moore-Scott and Manley, 2005). The caudal pouches are most severely perturbed by the loss of *Fgf8* (Abu-Issa et al., 2002; Frank et al., 2002). Thus, it was necessary to determine whether caudal pouches continue to develop successfully in the absence of endodermal *Fgf8*. To address the latter pharyngeal pouch morphology of *Fgf8cKO^{Sox17}* embryo's was assessed at E10.5. The pharyngeal pouches of Cre negative and *Fgf8cKO^{Sox17}* embryos were delineated by whole mount *in situ* hybridisation for *Pax1* expression. Pharyngeal pouches 1 to 3 are visible in all embryos, having developed serially along the anterior-posterior axis of the PA (compare arrowheads in Fig 24, panels a'-d'). Although the slit-like pouch morphology of *Fgf8cKO^{Sox17}* embryos is indistinguishable from Cre negative embryos, the size of the mutants' third pouch appears to be reduced Interestingly, the level of *Pax1* expression is also appears to be reduced in the 3rd pouch of mutants both relative to control embryos (Fig 24, panels b' and d' most posterior unfilled arrowhead compared to most posterior solid arrowhead in panels a' and c').

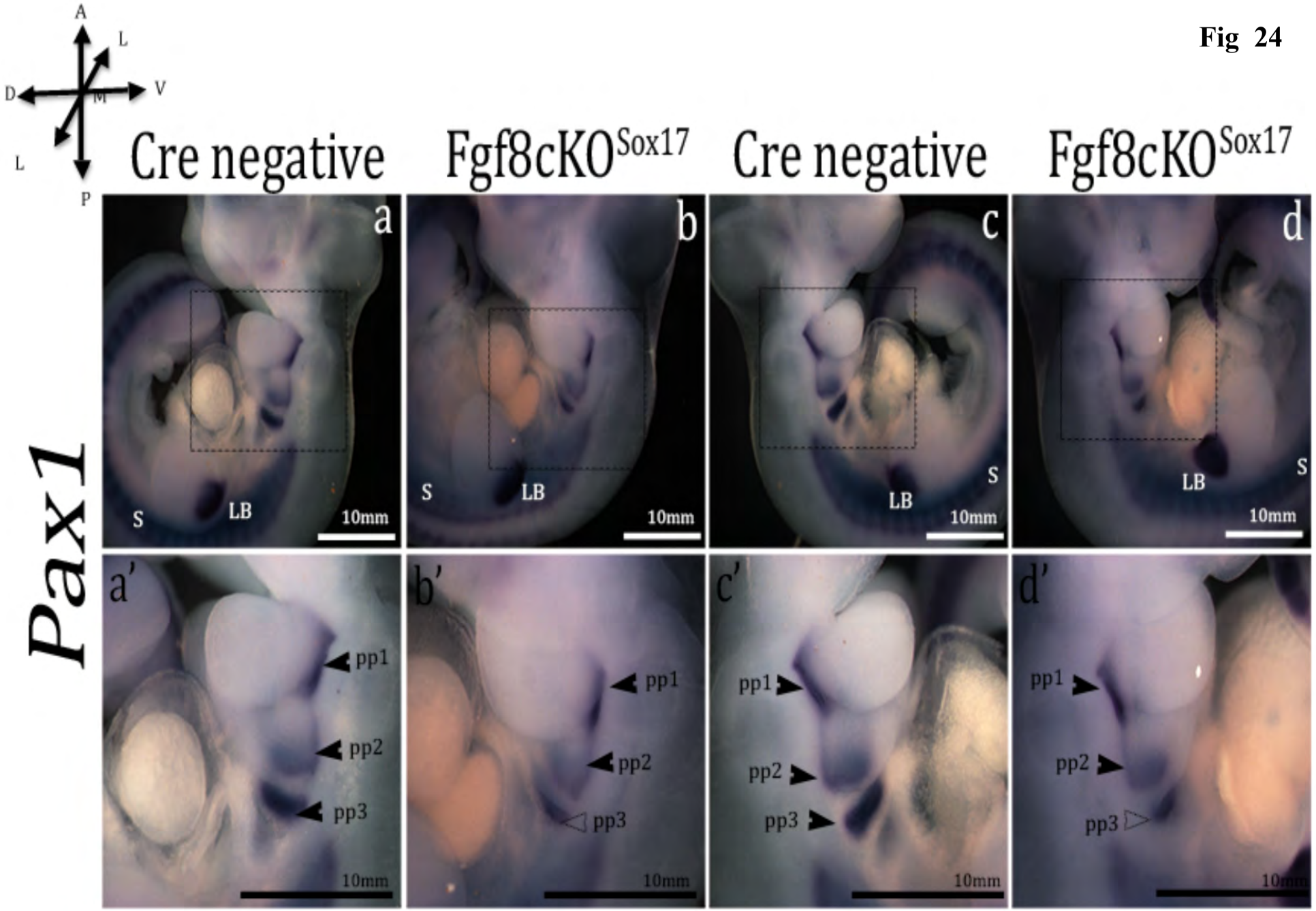
A
L
D
M
V
L
P
Cre negative
Fgf8cKO Sox17
Cre negative
Fgf8cKO Sox17
Pax1
a
b
c
d
S
LB
10mm
a'
b'
c'
d'
pp1
pp2
pp3

Fig 24: The expression of *Pax1*, which demarcates pouch morphology, appears reduced in the hypoplastic 3rd pouch of *Fgf8cKO^{Sox17}* embryos. (a-c) *Pax1* expression, detected by whole mount *in situ* hybridization, in E10.5 embryos at low magnification (4x). (a'-c') The pharyngeal apparatus of embryos a-c viewed at high magnification (8x). Solid arrowheads identify normal pouch morphology as demarcated by *Pax1* expression. Unfilled arrowheads identify the hypoplastic 3rd pouch of *Fgf8cKO^{Sox17}* that have reduced *Pax1* expression. N=3.

Annotations: Outlined area in panels a-d indicate the area magnified in panels a'-d'. Black arrowhead = endodermal pouch expression, unfilled arrowhead = endodermal pouch with reduced *Pax1* expression, pp = pharyngeal pouch, Lb=Limb bud, S = somite. Arrows to the left of Fig 24 illustrate the orientation of the pharyngeal apparatus sections; A = anterior, P = posterior, L = lateral, M = medial, V= ventral, D = dorsal.

4.2 *Fgf8* is required in the endoderm during thymus organogenesis

Although the initial evagination of the 3rd pouch appears to be normal in *Fgf8*-deficient pharyngeal endoderm, the 3rd pouch at E10.5 appears slightly hypoplastic. This indicates that *Fgf8* in the endoderm may be required for the development of the thymus from the 3rd pouch, rather than for 3rd pouch formation itself. The thymus and parathyroid organs are derived, respectively, from *Foxn1* and *Gcm2* positive cells within the 3rd pharyngeal pouch (Gordon et al., 2001). If the 3rd pharyngeal pouch forms but the establishment of these presumptive organ domains are disrupted, thymus and parathyroid defects will manifest in the embryo, as observed in *Hoxa3*$^{-/-}$ embryos, Sprouty1;2$^{-/-}$ embryos and Pbx1$^{-/-}$ embryos (Manley and Capecchi, 1995; Manley et al., 2004; Gardiner et al., 2012). To assess the patterning of the 3rd pouch into presumptive thymus and parathyroid domains, in the absence of endodermal *Fgf8*, stage E11.5 *Fgf8cKO*^{Sox17} embryos were collected and evaluated for the expression of *Foxn1* and *Gcm2*.

Analysis of *Fgf8cKO*^{Sox17} embryos 3rd pouch at E11.5 demonstrated that the presumptive thymus and parathyroid domains are able to form despite the absence of endodermal *Fgf8* (Fig 25). In both Cre negative and *Fgf8cKO*^{Sox17} embryos, *Foxn1* expression at E11.5 is limited to the posterior ventral domain of the 3rd pouch, (Fig 25c and d) and *Gcm2* expression is present in a complimentary anterior dorsal domain (Fig 25 c and d). The *Foxn1* and *Gcm2* expression domains of *Fgf8cKO*^{Sox17} do not appear to be distinguishable in terms of size or position within the 3rd pouch from Cre negative embryos.

The absence of *Fgf8* from endodermal cells the 3rd pouch of Hoxa2$^{Cre/+}$Fgf8$^{flox/-}$ embryos and Nkx2.5$^{Cre/+}$Fgf8$^{flox/-}$ embryos was determined to be the cause of thymus hypoplasia detected in these mutants, despite the Cre lines also being active in non-endodermal tissues (Macatee et al., 2003; Ilagan et al., 2006). The observation that a *Foxn1* domain is maintained in *Fgf8cKO^{Sox17}* embryos suggest that thymus organogenesis may not be perturbed by the absence of *Fgf8* from the endoderm alone. To address the requirement for endodermal-*Fgf8* during thymus organogenesis the thymus glands of *Fgf8cKO^{Sox17}* embryos were scored (as present/absent) and the circumference of each lobe was measured as an indicator of lobe size. Two thymus lobes are detected at E17.5 in all control and mutant embryos (Fig 26, panels a and b), corresponding to the presence of the 3rd pouch at E9.5 and E10.5 (Fig 23 and Fig 24 respectively). In addition, there was no significant difference in the circumference of *Fgf8cKO^{Sox17}* and Cre negative embryo's left or right thymus lobes (p=0. 518 and p =0.592, respectively, see figure legend of Fig 26 and panel d) when measured from the 2D images of the lobes. The lack of overt 3rd pouch defects in *Fgf8cKO^{Sox17}* embryos indicated that thymus development may not be affected in these mutants, which is corroborated by the data analysing thymus organogenesis in *Fgf8cKO^{Sox17}* embryos.

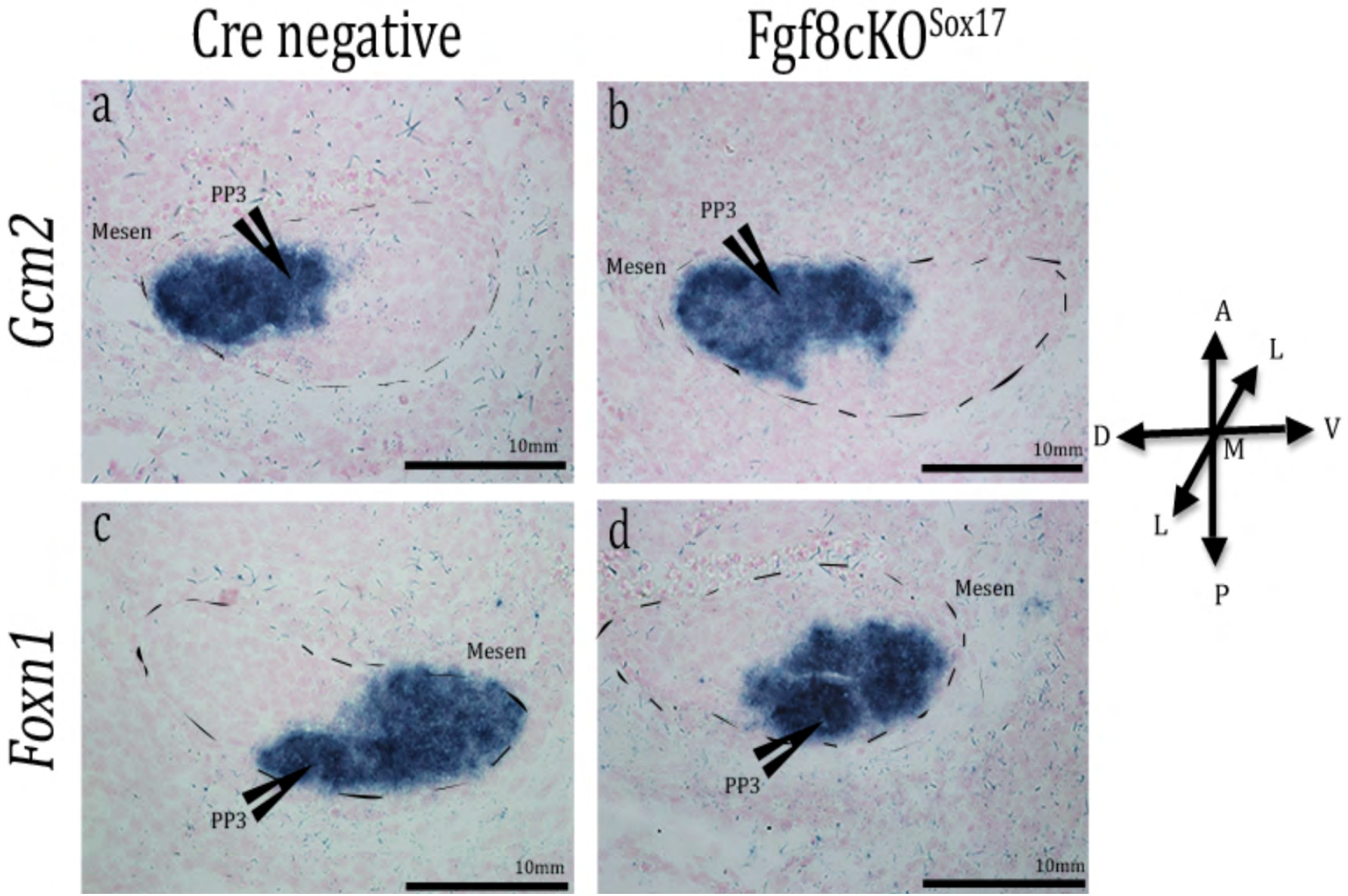
Cre negative
Fgf8cKO Sox17
Gcm2
Foxn1
a
b
c
d
PP3
Mesen
10mm
A
L
D
V
M
L
P

Fig 25: The 3rd pouch at E11.5 is patterned into *Foxn1* and *Gcm2* domains when *Fgf8* is absent from the endoderm. *In situ* hybridization on sagittal sections of E11.5 embryos identifies the expression of *Gcm2* in the correct anterior, dorsal domain of the 3rd pouch that should form the parathyroid later in gestation. The expression of *Foxn1* is also in the correct posterior, ventral domain of the 3rd pouch that should form the thymus later in gestation (c and d). (N=2).

Annotations: Dashes outline the 3rd pouch to aid visualization of the structure. Black arrowhead = endodermal pouch expression, pp = pharyngeal pouch, Mesen = Mesenchyme. Arrows to the right of Fig 25 illustrate the orientation of the pharyngeal apparatus sections; A = anterior, P = posterior, L = lateral, M = medial, V= ventral, D = dorsal.

Fig 26: Thymus hypoplasia manifests in the right thymus lobe of *Fgf8cKO^{Sox17}* embryos.

Open chest cavities of E17.5 embryos photographed to display the two thymus lobes present in Cre negative (a) and *Fgf8cKO^{Sox17}* (b) embryos. Circumference of individual thymus lobes were measured in image J and converted to micrometres using imaged scale bars. The circumference measurements were plotted in graph (c) using Graphpad software, (each symbol corresponds to an individual gland). Note there is no statistically significant size difference between the mean circumference of the left or right thymus lobe of Cre negative (n=7) and *Fgf8cKO^{Sox17}* (n=5) samples (p=0.520 and p=0.592 respectively, by students T-test). Error bars display standard error of the mean. The mean thymi circumference for each genotype of embryo with the corresponding standard error of the mean and P-value (generated using the Student's T-test in GraphPad) are listed below.

Lobe	Mean ± SEM of Cre negative	Mean ± SEM of Fgf8cKO^{Sox17}	Difference between means	P value
Left	5.111 ± 0.3448 N=7	4.799 ± 0.2637 N=5	-0.3121 ± 0.467	0.5197
Right	5.136 ± 0.2972 N=7	4.932 ± 0.1062 N=5	-0.2036 ± 0.3674	0.5916

Fig 26

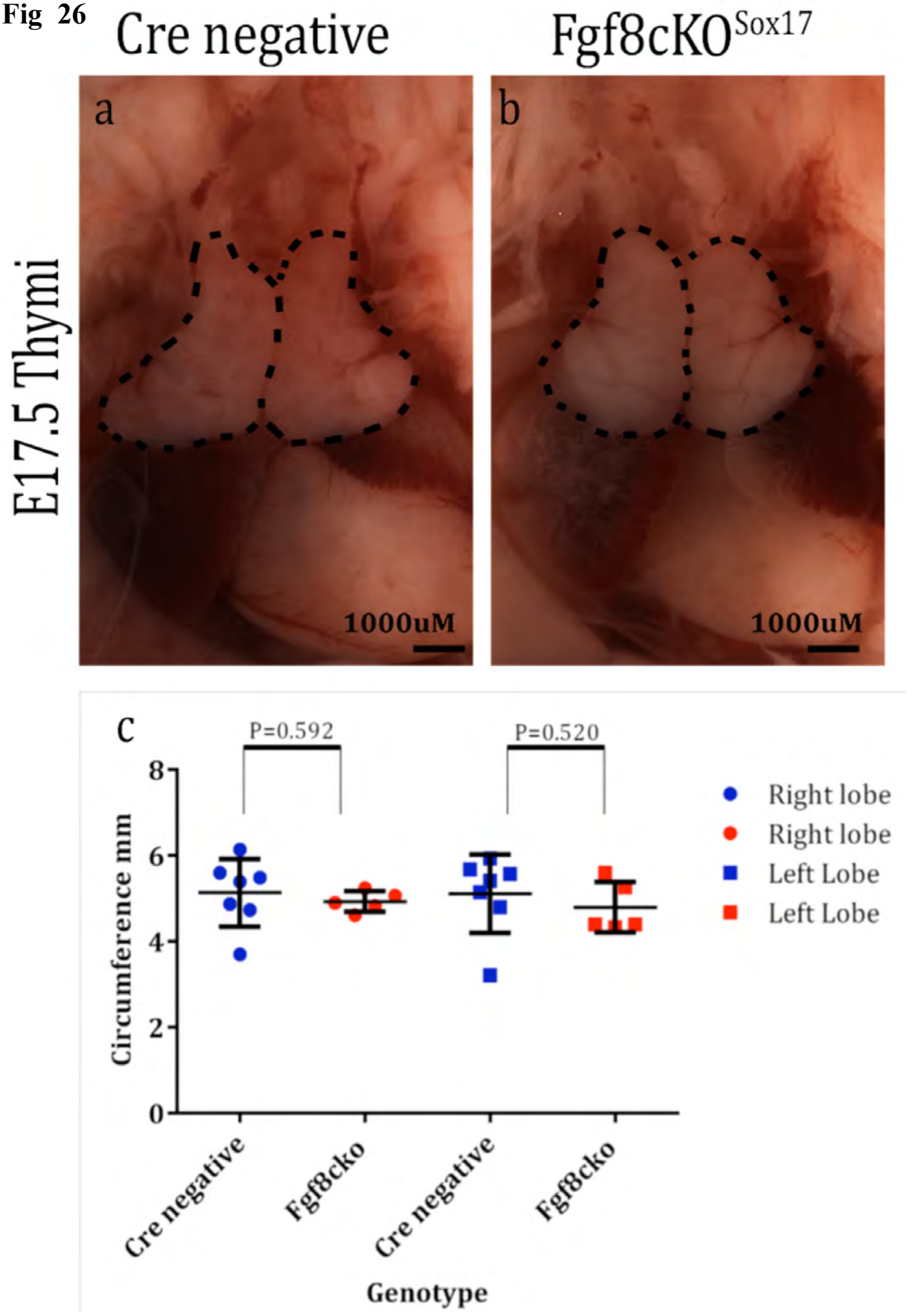
Cre negative
Fgf8cKO Sox17
E17.5 Thymi
a
b
1000uM
1000uM
C
P=0.592
P=0.520
Circumference mm
8
6
4
2
0
Right lobe
Right lobe
Left Lobe
Left Lobe
Cre negative
Fgf8cko
Cre negative
Fgf8cko
Genotype

4.3 *Fgf8* and *Tbx1* do not interact epistatically within the pharyngeal endoderm during pouch formation

The caudal pouch defects observed in *Fgf8*-hypomorphs, *Tbx1*-hypomorphs and *Tbx1*$^{-/-}$ embryos indicate that FGF8 and TBX1 may act in the same pathway during pouch morphogenesis (Abu-Issa et al., 2002; Frank et al., 2002). This was supported by data in Chapter 3 that showed *Fgf8* expression was tissue specifically diminished in the endoderm of *Tbx1cKO*^{Sox17} embryos. However, a comparison of pouch formation in *Fgf8KO*^{SOX17} and *Tbx1cKO*^{Sox17} embryos illustrates that whilst endodermal-*Tbx1* is essential for pouch formation, endodermal-*Fgf8* is dispensable. If FGF8 and TBX1 function in the same pathway during pharyngeal pouch morphogenesis this would be revealed by an experiment to test for genetic epistasis. The compound deletion of one allele of *Fgf8* and *Tbx1* from the endoderm during development should have an additive effect on pouch formation if both genes act in the same pathway during this process. To test this, *SOX17*$^{icre/+}$*;Tbx1*$^{flox/+}$*;Fgf8*$^{flox/+}$ (*Fgf8;Tbx1cHet*^{Sox17}) embryos were generated (see section 2.3.1 for details of the breeding strategy). Pouch formation and morphology (delineated by *Pax1* expression) of *Fgf8cHet*^{Sox17}, *Tbx1cHet*^{Sox17} and *Fgf8;Tbx1cHet*^{Sox17} embryos were assessed, relative to Cre negative embryos. Stage matched *Tbx1cHet*^{Sox17} embryos were generated from a separate *Sox17*$^{icre/+}$*;Tbx1*$^{flox/+}$ by *Tbx1*$^{flox/flox}$ cross.

In both single and compound heterozygotes, pouches 1 to 3 have formed in their correct location along the anterior to posterior axis of the PA and have a narrow, slit like morphology. Pouch morphogenesis and *Pax1* expression was indistinguishable between Cre negative and *Fgf8cHet*^{Sox17} embryos (compare black

arrowheads in panels a and b of Fig 27). As was observed in Chapter 1 (Fig 20, panel b), *Pax1* expression is reduced in the pharyngeal pouches of *Tbx1cHet*^{Sox17} embryos, relative to Cre negative embryos (compare solid arrowheads in panel a of Fig 27 to unfilled arrowheads in panel c of Fig 27). The morphology and level of *Pax1* expression in the pouches of *Fgf8;Tbx1cHet*^{Sox17} embryos is equivalent to that of *Tbx1cHet*^{Sox17} embryos (compare unfilled arrowheads in Fig 27, panels c and d). This data demonstrates that there is no epistatic interaction between *Fgf8* and *Tbx1* in the endoderm during pouch formation. Furthermore it suggests that *Fgf8* does not act downstream of *Tbx1* during pouch morphogenesis.

Fig 27

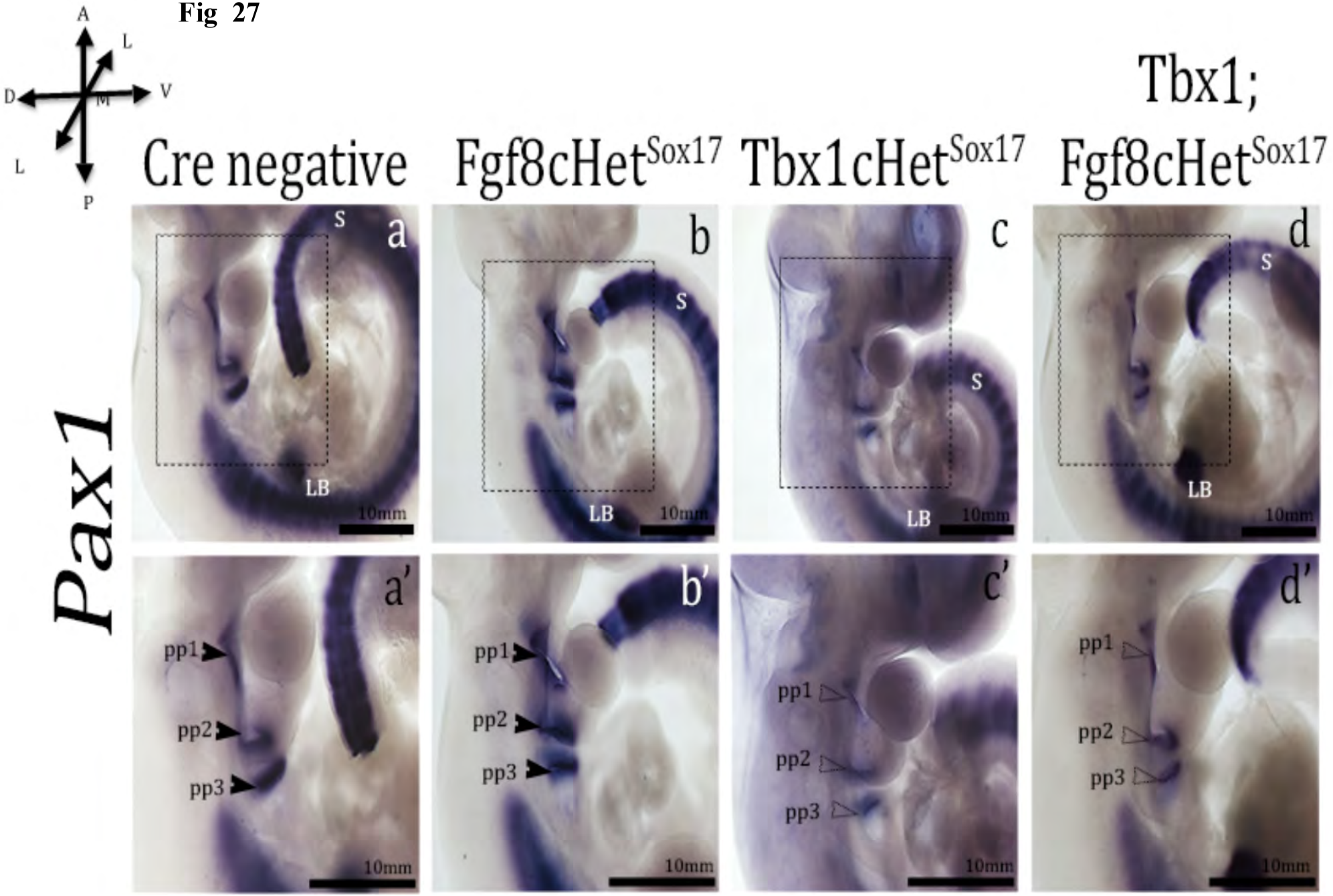
A
L
D
M
V
L
P
Cre negative
Fgf8cHetSox17
Tbx1cHetSox17
Tbx1;
Fgf8cHetSox17
Pax1
a
b
c
d
s
LB
10mm
a'
b'
c'
d'
pp1
pp2
pp3

Fig 27: *Tbx1* and *Fgf8* in the endoderm do not appear to act synergistically during pouch formation. (a-d) Side views of Pax1 expression in E10.5 embryos, 4x magnification. (a'-d') The pharyngeal apparatus of embryos a-d viewed at 6x magnification. Note that pouch morphology of *Fgf8*;*Tbx1cHet*^{Sox17} embryos (d and d') is no more perturbed than that of *Tbx1cHet*^{Sox17} embryos (c and c') indicating that *Fgf8* and *Tbx1* do no interact epistatically within the pharyngeal endoderm during pouch formation.N=4

Annotations: Arrows to the left of the figure identify the orientation of the embryos: A = anterior, P = posterior, L = lateral, M = medial, V= ventral, D = dorsal. Outlined area in panels a-d indicate the area magnified in panels a'-d'. L=Limb bud, S = somite, pp = pharyngeal pouch, solid arrowheads identify areas of *Pax1* expression in each pouch, unfilled arrowheads identify areas of reduced *Pax1* expression in each pouch.

4.4 DISCUSSION

4.4.1 Loss of *Fgf8* from the endoderm is not sufficient to disrupt pharyngeal pouch formation

To the best of my knowledge, this thesis presents the first study addressing the requirement for *Fgf8* expression within the endoderm, during mammalian pharyngeal pouch morphogenesis. The expression of *Fgf8* in the endoderm during pouch evagination and the pouch defect observed in *Fgf8* hypomorphs indicated that *Fgf8* may function in the endoderm during pouch morphogenesis (Crossley and Martin, 1995; Abu-Issa et al., 2002; Frank et al., 2002). Conditional mutant lines support the inference that *Fgf8* may be required in the endoderm for pouch morphogenesis. Tissue specific deletions of *Fgf8* from the ectoderm or mesoderm were not reported to produce pharyngeal arch or pouch defects (Macatee et al., 2003; Park et al., 2006). Moreover, the deletion of *Fgf8* with Cre lines expressed in restricted regions of the endoderm, (i.e. Hoxa2^{Cre} and Nxk2.5^{Cre}) generated embryos with hypoplastic thymi, however, pouch formation was not specifically analysed in these mutants (Macatee et al., 2003; Ilagan et al., 2006). Consequently *Fgf8cKO^{Sox17}* embryos provide the first evidence, in a mammalian model, to suggest that expression of *Fgf8* within the endoderm is not essential for pouch formation.

The formation of the pharyngeal pouches by the evagination of the pharyngeal endoderm is only the initial step of pouch morphogenesis. The out-pocketing of pharyngeal endoderm must also become constrained to form a narrow slit-like morphology (Quinlan et al., 2004). The morphology of the pharyngeal pouches can be affected by the loss of many genes. Interestingly the latter often correlates with changes in *Fgf8* expression within the pharyngeal endoderm, as is observed in

Shh$^{-/-}$ embryos and RA deficient embryos (Niederreither et al., 2003; Moore-Scott and Manley, 2005). This is also evident in the rostral pouches of the severe *Fgf8* hypomorphs that appear to be able to evaginate toward the ectoderm but maintain a splayed, diamond shaped morphology (Abu-Issa et al., 2002). However, the *Fgf8cKO^{Sox17}* data suggest that the formation of discreet pharyngeal pouches is not dependent on *Fgf8* expression within the endoderm. Furthermore the data in Chapter 4 suggests that endodermal-*Fgf8* is not required for the pattering of the 3rd pouch into prospective thymus and parathyroid domains.

There are two (not mutually exclusive) reasons why the deletion of *Fgf8* from the endoderm does not cause defects in pharyngeal pouch morphogenesis. *Fgf8* is a secreted ligand and thus has the ability to elicit FGF signalling in a paracrine manner (Itoh and Ornitz, 2011). The expression of *Fgf8* in adjacent pharyngeal tissues may be able to compensate for the loss of *Fgf8* from one tissue, such as the endoderm, during pouch formation. This is supported by the observation that the deletion of *Fgf8* from a single tissue type has not been reported to cause pouch/arch defects, (i.e. utilising the Mesp1$^{Cre/+}$Fgf8$^{flox/-}$ and Ap2alpha-IRES$^{Cre/+}$Fgf8$^{flox/-}$ embryos), (Macatee et al., 2003; Park et al., 2006). On the other hand, Nxk2.5$^{Cre/+}$Fgf8$^{f/-}$ embryos have hypoplastic arches at E9.5, which implies pouch development may also be disrupted in these mutants (Ilagan et al., 2006). Nxk2.5^{Cre} is expressed in the endoderm but it is also active in a number of other pharyngeal tissues including the pharyngeal ectoderm (Moses et al., 2001). It is possible that the PA defects in the Nxk2.5$^{Cre/+}$Fgf8$^{flox/-}$ embryos arise because of an additive effect of loosing *Fgf8* in multiple PA domains. The second possible explanation for why pouch morphogenesis is grossly unperturbed in *Fgf8cKO^{Sox17}* embryos is that multiple FGF ligands may act redundantly in the PA to regulate

pouch development, compensating for the loss of *Fgf8* in the endoderm. However, the expression of *Fgf3* and multiple FGF signalling readouts were not up-regulated or expanded in the pharyngeal endoderm of *Fgf8cKO*^{Sox17} embryos, as assessed by *in situ* hybridisation. The hypothesis that FGF ligands in the endoderm act redundantly to control pouch formation was tested in Chapter 5.

4.4.2 *Fgf8* in the endoderm is not required for thymus organogenesis

Macatee et al. describe a requirement for *Fgf8* in the endoderm during thymus formation (Macatee et al., 2003). However, unlike the *Hoxa2Cre*$^{/+}$*Fgf8*$^{flox/-}$ embryos, *Fgf8cKO*^{Sox17} thymi did not display unilateral or bilateral defects in thymus size. This suggests that there may be an additive affect of losing *Fgf8* from the caudal ectoderm and endoderm for thymus organogenesis. The thymus develops from the *Foxn1* positive domain of the 3rd pouch but it is also contributed to by CNCC (Blackburn and Manley, 2004). *Hoxa2*$^{Cre/+}$*Fgf8*$^{flox/-}$ embryos are not reported to have pouch defects, and the data in this study indicates that the loss of *Fgf8* alone from the endoderm does not affect pouch formation. Thus, it is possible that the loss of *Fgf8* from the pharyngeal epithelia affects the CNCC that migrate into the PA and contribute to the thymus.

Fgf8 has been shown to act as guidance factor for NCC entering the PA. When cardiac NCC were exposed to exogenous sources of *Fgf8 in vitro*, or, *in vivo* the cells migrated toward the source of this FGF ligand (Sato et al., 2011). Whether *Fgf8* is a general chemo-attractant for all CNCC entering the PA is questionable. The migration of *Crabp1* and *Ap2α* expressing CNCC were grossly unperturbed in Fgf8-

severe hypomorphs (Abu-Issa et al., 2002). Moreover, *Hox* gene expression is maintained in the pharyngeal mesenchyme of *Fgf8cKO*^{Sox17} embryos indicating that CNCC are able to populate the pharyngeal arches relatively normally.

Alternatively, *Fgf8* in the endoderm may act as a survival factor for CNCC entering the caudal PA. *Fgf8* in the 1st arch ectoderm is required for the survival of CNCC here (Trumpp et al., 1999). A reduced number CNCC also enter the caudal arches of Fgf8-severe hypomorphs, this correlates with an increase in apoptosis within the PA of these embryos (Abu-Issa et al., 2002). Presumably, if endodermal *Fgf8* is a survival cue for CNCC in the caudal PA, one would hypothesis that there would be more CNCC doubly labelled for a CNCC marker, such as *Crabp1*, and an apoptosis marker, such as CASPASE-3 in *Fgf8cKO*^{Sox17} embryos, relative to control embryos. Conversely, the re-activation of *Fgf8* expression in *Fgf8*-severe hypomorphs may also increase the number of CNCC in the caudal PA to that observed in control embryos.

4.4.3 *Fgf8* does not act downstream of *Tbx1* in the endoderm during pouch formation

The endoderm specific loss of *Fgf8* expression in *Tbx1cKO*^{Sox17} embryos corroborated with data in the literature that suggested *Tbx1* regulates the expression of *Fgf8* in the pharyngeal endoderm (see 1.3.2.4) (Vitelli et al., 2010, Vitelli et al., 2002, Lania et al., 2009). However, a comparison of *Fgf8cKO*^{Sox17} and *Tbx1cKO*^{Sox17} embryos revealed that whilst endodermal *Tbx1* is essential for pouch formation, endodermal *Fgf8* is dispensable. Thus indicating that the tissue-specific loss of *Fgf8* expression downstream of *Tbx1* in the endoderm may not be

functionally relevant to pouch morphogenesis. This inference was supported by the observation that the *Pax1* delineated morphology of *Fgf8;Tbx1cHet*^{Sox17} embryos pharyngeal pouches are indistinguishable from those of *Tbx1cHet*^{Sox17} embryos. The epistasis data indicates that *Fgf8* and *Tbx1* do not function in the same endodermal pathway during pouch morphogenesis. The data presented in Chapter 4 may explain why the forced expression of *Fgf8* from the *Tbx1* allele (*Tbx1*$^{fgf8/fgf8}$ embryos) does not rescue the majority of caudal endoderm defects associated with loss of *Tbx1*. For example, the caudal PA of *Tbx1*$^{fgf8/fgf8}$ embryo's is hypoplastic, like that of *Tbx1*$^{-/-}$ embryos (Vitelli et al., 2006).

There is evidence that *Fgf8* and *Tbx1* interact during the formation of the thyroid whose follicular cells are partially contributed to by the endoderm of the 2nd pouch. The deletion of Fgf8$^{flox/flox}$ alleles by Tbx1^{Cre}, (generating embryos that were *Fgf8* null in *Tbx1* expression domains), caused a reduction in the *Nkx2.1* positive thyroid precursor cells in the pharyngeal endoderm and a subsequent reduction in the size of the thyroid at E18.5 (Lania et al., 2009). Thyroid size was normalised by driving *Fgf8* expression from the *Tbx1* promoter. However, *Tbx1* is not expressed within the endodermal thyroid precursors per se. Thus it is predicted that *Tbx1* acts upstream of *Fgf8* in the mesoderm and that the loss of mesodermal *Fgf8* affects the proliferative capacity of the thyroid progenitor cells of the pharyngeal endoderm (Lania et al., 2009).

The additive affect of the loss of *Fgf8* and *Tbx1* from multiple PA tissues may explain the increased incidence of thymus defects in Fgf8;Tbx1$^{+/-}$ embryos, relative to single heterozygotes (Vitelli et al., 2002b). Certainly the loss of mesodermal *Tbx1* has been shown to cause thymus hypoplasia (Zhang et al., 2006). On the other

hand, *Tbx1* and *Fgf8* may act in the same endodermal pathway during the patterning of the 3rd pouch into presumptive thymus and parathyroid domains. Timed deletion of *Tbx1* has shown that *Tbx1* is also required after the 3rd pouch has formed, at the time of pouch patterning, for thymus growth to occur normally (Xu et al., 2005). The expression of *Foxn1* and *Gcm2* is initiated at E11.25 in the 3rd pouch of *Fgf8;Tbx1cHet*^{Sox17} embryos. However, this data was not included because an analysis of E11.5 embryos is required to determine whether *Foxn1* and *Gcm2* domains form normally in the 3rd pouch, something that time did not permit in this study. An analysis of thymus gland formation in *Fgf8;Tbx1cHet*^{Sox17} embryos would also be necessary to determine whether *Fgf8* and *Tbx1* function together in the endoderm to regulate pouch patterning and/or thymus development.

Chapter 5

Results part III

5.1 Functional redundancy exists between *Fgf3* and *Fgf8* in the pharyngeal endoderm during pouch formation

The process of pharyngeal pouch outgrowth was assumed to require a source of *Fgf8* in the endoderm because: a) *Fgf8* is robustly expressed in the endoderm, most significantly in the caudal-most forming pouch (Crossley and Martin, 1995), b) *Fgf8* hypomorphs have disorganised pouch development (Abu-Issa et al., 2002; Frank et al., 2002) c) *Fgf8* expression is absent in the endoderm of *Tbx1*$^{-/-}$ and indeed *Tbx1cKO*^{Sox17} embryos (Fig 17c) (Vitelli et al., 2002b). However, when this assumption was tested experimentally by the deletion of *Fgf8* from then endoderm it revealed that the deletion of *Fgf8* alleles from the endoderm does not perturb pharyngeal pouch morphogenesis.

Current literature suggests that *Fgf3* may act redundantly with *Fgf8* during pouch morphogenesis. *Fgf3* and *Fgf8* have overlapping expression domains in the endoderm during PA formation (Vitelli et al., 2002b; Vincentz et al., 2005). Although the deletion of *Fgf3* from mouse lines (Fgf3$^{-/-}$ embryos) has not implicated this ligand in pouch formation, Fgf3$^{-/-}$ mutants display thymus hypoplasia (Aggarwal et al., 2006). Moreover, changes in the level and pattern of *Fgf3* expression are associated with mouse mutants that have perturbed pouch outgrowth. For instance, mice exposed to exogenous RA display 1st pouch aplasia and fusion of the 1st and 2nd arches and within the fused rostral arches expression domain of *Fgf3* was expanded (Mahmood et al., 1996). *Tbx1*$^{-/-}$ embryos lose expression of *Fgf3* in their un-segmented caudal endoderm, (although this was not observed in *Tbx1cKO*^{Sox17} embryos), (Aggarwal et al., 2006). Finally, *Fgf3* expression is initiated but not maintained in the hypoplastic pharyngeal pouches

of the *foxi1* (*forkhead box I1*, A transcription factor) zebrafish mutant (Nissen et al., 2003).

Direct genetic evidence showing that FGF3 functions redundantly in pouch formation with FGF8 has been demonstrated in a non-mammalian model. Zebrafish with a strong loss of function *fgf8* mutation, (also defined as *Acerebellar* or *fgf8*$^{-}$ mutants) normally form misshapen, and/or, hypoplastic pouches (Crump et al., 2004). Exposing *fgf8*$^{-}$ mutants to an *fgf3* morpholino (*fgf8*$^{-}$*;fgf3*-MO) prevents all pouch formation, suggesting that *fgf3* can compensate for the loss of *fgf8* during pouch formation (Crump et al., 2004). To examine whether *Fgf3* and *Fgf8* function redundantly during mammalian pouch morphogenesis, *Sox17*$^{icre/+}$*Fgf3*$^{flox/-}$*;Fgf8*$^{flox/-}$ (*F3;F8cKO*^{Sox17}) embryos were generated. Sets of *F3;F8*^{Sox17} mutant embryos were bred and kindly provided by Professor Suzanne Mansour from Utah, Salt Lake City. The following experiments were conducted to analyse pouch morphogenesis in *F3;F8cKO*^{Sox17} embryos:

a) Pouch morphology of embryos deficient in the expression of endodermal *Fgf3* and *Fgf8* were analysed at E10.5 by *Pax1* expression.
b) *Erm* expression was evaluated by whole mount *in situ* hybridisation to assess the level of FGF signalling in conditional *F3:F8* mutant embryos.

5.1.1 Analysis of pharyngeal pouch formation in *F3;F8*^{Sox17} mutants

Pharyngeal pouch formation of embryos deficient in the endodermal expression of *Fgf3* and *Fgf8* was analysed between E10.0 and E10.5 days of development. The loss of one allele of *Fgf3* and one allele of *Fgf8* from the endoderm has little effect

on the formation of the pharyngeal pouches. Pouches 1 to 3 and the forming 4th pouch are evident in *Sox17$^{icre/+}$Fgf3$^{flox/+}$;Fgf8$^{flox/+}$*, (*F3;F8cHet^{Sox17}*) embryos. The level and pattern of *Pax1* expression in the pharyngeal pouches of *F3;F8cHet^{Sox17}* embryos and Cre negative embryos is indistinguishable (Fig 28, solid arrows panel a and a' vs b and b'). However, if three or more alleles of a combination of *Fgf3* and *Fgf8* are deleted from the endoderm, pouch morphogenesis no longer occurs normally. *Sox17$^{icre/+}$Fgf3$^{flox/-}$;Fgf8$^{flox/+}$*, (*F3cKO;F8cHet^{Sox17}*) and *Sox17$^{icre/+}$Fgf3$^{flox/+}$;Fgf8$^{flox/-}$*, (*F3cHet;F8cKO^{Sox17}*) embryos display a unilateral fusion of the first and second pouches, with variable penetrance (identified by brackets in panels c' and d of Fig 28, frequencies of pouch fusion are outline in Table 6). The incidence of pouch fusion is greater in *F3cHet;F8cKO^{Sox17}* than *F3cKO;F8cHet^{Sox17}*. Bilateral fusion of the rostral pouches, a more severe pouch phenotype than the unilateral fusion results when all alleles of *Fgf3* and *Fgf8* are deleted from the endoderm, (Fig 28, panels e and e', fusion in the F3;F8cKO^{SOX17} embryos is highlighted by the brackets). Surprisingly, however, the penetrance of pouch fusion in *F3;F8cKO^{Sox17}* embryos is not higher than that observed in *F3cHet;F8cKO^{Sox17}* embryos (Table 6). Another interesting observation is that the proximal portion of the 2nd arch appears hypoplastic wherever the 1st and 2nd pouch fusion is evident (compare outlined 2nd arch in panels a' and e' of Fig 28). For a summary of the incidence and type of rostral pouch fusion observed in each *F3;F8^{Sox17}* mutant, refer to Table 6 below.

Table 6: Incidence and type of rostral pouch fusion in E10.0/10.5 *F3;F8*^{Sox17} mutants.

	Counts of pouch fusion observed per embryo				Total pouch fusion observed per side of each embryo
Genotype	**None**	**Unilateral (L)**	**Unilateral (R)**	**Bilateral**	
Cre Negative	6/6	0/6	0/6	0/6	0/12
***F3;F8cHet*^{Sox17}**	2/2	0/2	0/2	0/2	0/4
***F3cKO;F8cHet*^{Sox17}**	3/4	1/4	0/4	0/4	1/8
***F3cHet;F8cKO*^{Sox17}**	0/2	0/2	2/2 (*)	0/2	2/4
***F3;F8cKO*^{Sox17}**	3/6	1/6	0/6	2/6	5/12
Totals	14/20	2/20	2/20	2/20	8/40

(*) Indicates significance value of $p<0.02$, when comparing incidence of pouch fusion incidence in Cre negative embryos. L=left side, R = right side.

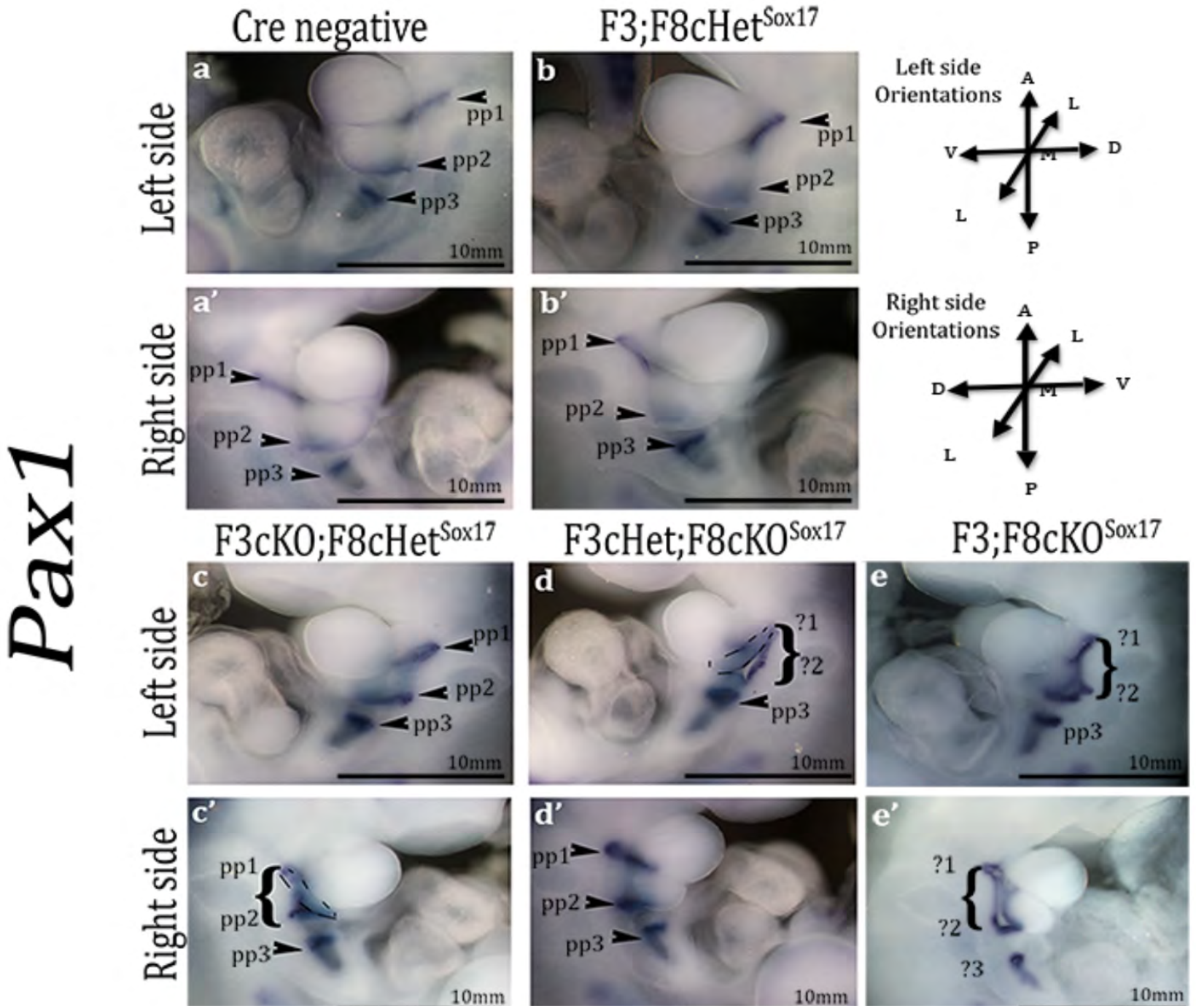
Pax1
Cre negative
F3;F8cHet^Sox17
Left side
Right side
a
b
a'
b'
pp1
pp2
pp3
10mm
Left side Orientations
Right side Orientations
A
L
V
D
M
P
F3cKO;F8cHet^Sox17
F3cHet;F8cKO^Sox17
F3;F8cKO^Sox17
c
d
e
c'
d'
e'
?1
?2
?3

Fig 28: Deletion of a combination of three or more alleles of *Fgf3* and *Fgf8* from the endoderm results in *Pax1* demarcated rostral pouch fusion. *Pax1* whole mount *in situ* hybridisation on the left side (a-e) and right side (a'-e') of E10.5 embryos. Fusion of the 1st and 2nd pouches is evident unilaterally in embryos with only one allele of *Fgf3* (d') or *Fgf8* (c) expressed in the endoderm. Bilateral (e and e') and unilateral fusion is evident in *F3;F8cKO^{Sox17}* embryos.

Annotations: Arrows to the right of the figure identify the orientation of the embryos: A = anterior, P = posterior, L = lateral, M = medial, V= ventral, D = dorsal. Brackets identify rostral pouch fusion. Dashed lines demarcate hypoplasia of the proximal aspect of the 2nd arch. L=Limb bud, S = somite, pp = pharyngeal pouch, ? = presumptive pouch, solid arrowheads identify areas of *Pax1* expression in each pouch.

5.1.2 Analysis of FGF signalling in the pharyngeal pouches of *F3;F8^{Sox17}* mutants

The level and pattern of FGF signalling within the PA of *Fgf8cKOSox17* embryos was not altered by the deletion of *Fgf8* from the endoderm (Fig 23). *Fgf3* and *Fgf8* have been demonstrated to regulate the expression of *Erm* (a readout of FGF signalling) (Raible and Brand, 2001). The presence of *Fgf3* in the endoderm of *Fgf8cKO^{Sox17}* embryos may have maintained FGF signalling here, enabling pouch morphogenesis to proceed. It is tempting to predict that the level of FGF signalling in the endoderm of *F3;F8^{Sox17}* mutants that display rostral pouch fusion would be reduced below a threshold that is required for normal pouch morphogenesis. A reduction in FGF signalling should be represented by a loss of *Erm* expression in the endoderm of the *F3;F8^{Sox17}* mutants with fused pouches.

To address the prediction that rostral pouch fusion in *F3;F8^{Sox17}* mutants is caused by a reduction in FGF signalling in the rostral endoderm, sets of E9.25 *F3;F8^{Sox17}* embryos were analysed for the expression of *Erm* by whole mount *in situ* hybridisation. At this developmental time point 2nd arch hypoplasia is identifiable and can be referenced as an indicator of rostral pouch fusion, at a time when the 2nd pouch is still forming. Of those E9.25 *F3;F8^{Sox17}* mutants analysed, pharyngeal pouch fusion was only evident in the *F3;F8cKO^{Sox17}* embryos, (1/3 displayed bilateral fusion [Fig 29, panels e and e'], 1/3 displayed unilateral fusion). *Erm* at E9.25 is expressed in a segmented pattern in the PA and is highly expressed in the posterior half of each pharyngeal pouch (high levels of *Erm* expression in pharyngeal pouches are indicated by labels pp1 and 2 in Fig 29). Surprisingly, the level of *Erm* does not appear to be reduced in the *F3;F8cKO^{Sox17}* embryos that

display rostral pouch fusion (Fig 29, panel e) when compare to any of the embryos that do not display rostral pouch fusion (Fig 29, panels a-d). It is possible that FGF signalling is reduced in the *F3;F8cKO*^{Sox17} embryos but that this reduction is undetectable by *in situ* hybridisation.

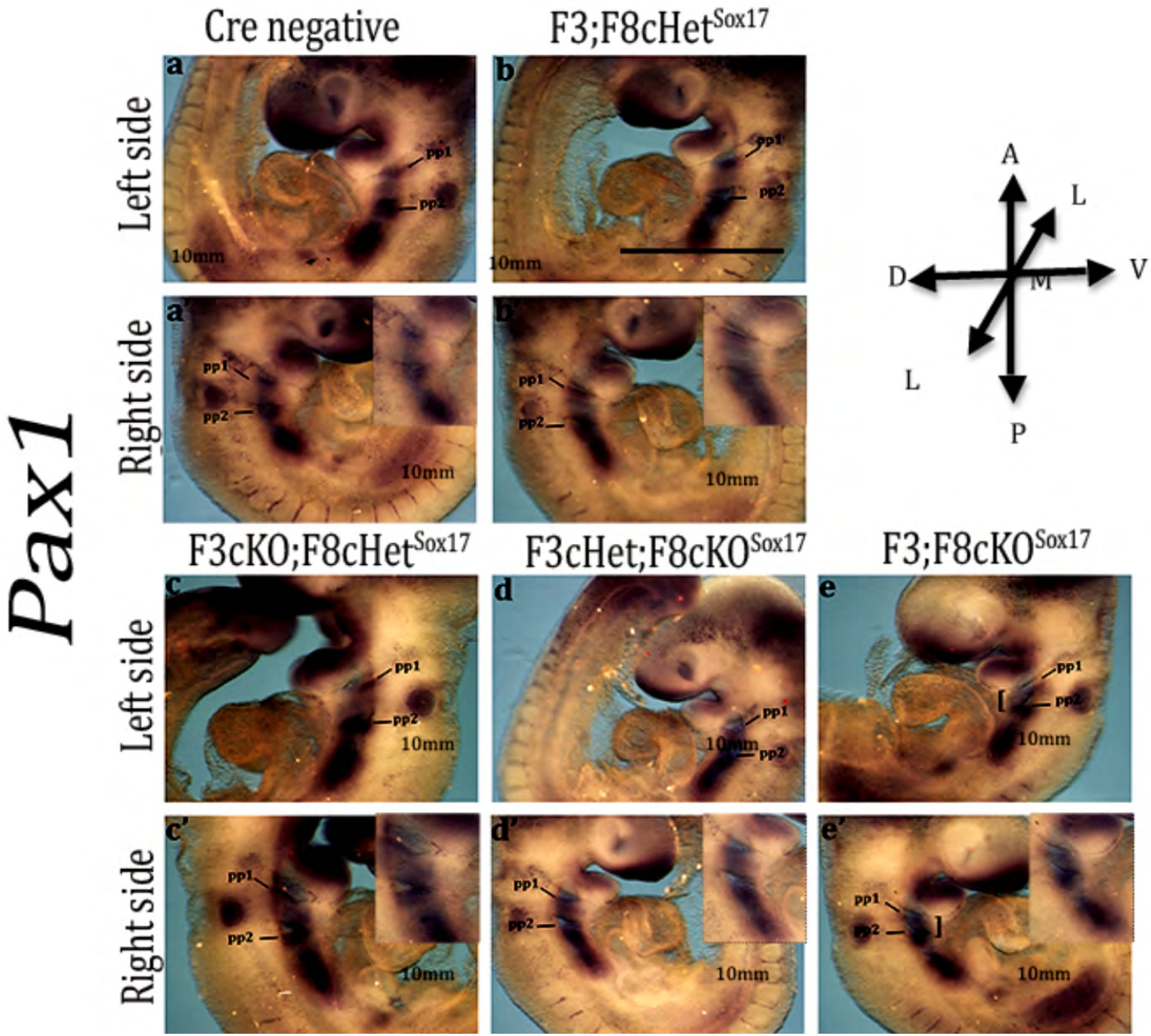
Pax1
Cre negative
F3;F8cHet Sox17
Left side
Right side
a
b
a'
b'
pp1
pp2
10mm
A
L
D
M
V
L
P
F3cKO;F8cHet Sox17
F3cHet;F8cKO Sox17
F3;F8cKO Sox17
c
d
e
c'
d'
e'

Fig 29: *Erm* expression does not appear to be reduced in the fused rostral pouches of *F3;8cKO^{Sox17}* embryos. Whole mount *in situ* hybridization on E9.25 Cre negative (a,a'), *F3;F8cHet^{Sox17}* (b,b') *F3cKO;F8cHet^{Sox17}* (c,c'), *F3cHet;F8cKO^{Sox17}* (d-d') and *F3;F8cKO^{Sox17}* (e,e') embryos with an antisense mRNA probe for *Erm*. Brackets highlight the hypoplastic arch of the *F3;F8cKO^{Sox17}* embryo, caused by the rostral pouch fusion. Lines denote the areas of high *Erm* expression within pharyngeal pouches (pp) 1 and 2. Inserts are high magnification images focusing on the 1st and 2nd pp of embryos shown in Fig s a'-e'. n=1 for each genotype.

Annotations: Arrows to the right of the figure identify the orientation of the embryos: A = anterior, P = posterior, L = lateral, M = medial, V= ventral, D = dorsal. Brackets identify rostral pouch fusion. pp = pharyngeal pouch.

5.2 A requirement for FGF signalling downstream of *Fgfr1* and *Fgfr2* in the pharyngeal endoderm during pouch formation

Rostral pouch fusion is not fully penetrant in *F3;F8cKO*^{Sox17} embryos and no reduction in FGF signalling was observed in the areas of fused rostral pharyngeal endoderm (as assessed by *in situ* hybridisation). This data suggests that FGF signalling elicited in the endoderm by FGF ligands other than *Fgf3* and *Fgf8* may enable some pouch morphogenesis to proceed. Pharyngeal pouch defects occur in *Fgfr1* hypomorphs and in embryos that are unable to initiate Map Kinase signalling, through Frs2alpha, downstream of *Fgfr1* (*Fgfr1*$^{\Delta Frs/\Delta Frs}$ embryos) (Trokovic et al., 2003; Trokovic et al., 2005; Hoch and Soriano, 2006). Bilateral rostral pouch fusion, identical to that observed in some *F3;F8cKO*^{Sox17} embryos, is 100% penetrant in both of these *Fgfr1* mutants. This data supports the hypothesis that multiple FGF ligands act redundantly to elicit FGF signalling downstream of FGFR1 binding, during pouch formation.

Whether pouch evagination requires tissue specific expression of *Fgfrs* has not yet been tested. *Fgfr1*, *Fgfr2* and *Fgfr3* are all expressed in the PA during pouch morphogenesis (Walshe and Mason, 2000). Thus, it was predicted that multiple FGFRs may function redundantly to regulate pharyngeal pouch out-pocketing. The expression of *Fgfr3* in the PA is weaker and more restricted than *Fgfr1* and *Fgfr2* (Walshe and Mason, 2000). Thus, it was predicted that little signalling would be elicited through this receptor during pouch morphogenesis. The deletion of *Fgfr1* or *Fgfr2* ubiquitously from all tissues arrests embryonic development during gastrulation (Deng et al., 1994; Yamaguchi et al., 1994; Arman et al., 1998). Thus,

tissue specific Cre lines must be used to analyse the role of FGF signalling during pouch formation. To maximise the efficiency of Cre mediated recombination, the number of *Fgfr* genes targeted for deletion was limited to two, *Fgfr1* and *Fgfr2*. Pouch morphology of embryos deficient in the expression of *Fgfr1* and *Fgfr2* in either; endodermal cells, mesodermal cells or NCCs, was analysed at E10.0/10.5 by *Pax1* whole mount *in situ* hybridisation.

5.2.1 Analysis of pharyngeal pouch morphology in embryos with tissue specific deletions of *Fgfr1* and *Fgfr2*

5.2.1a The recombination of *Fgfr1* and *Fgfr2* in the endoderm by SOX17^{iCre} results in rostral pouch fusion

In keeping with the previous analyses within this thesis, the SOX17^{iCre} line was used to delete floxed *Fgfr1* and *Fgfr2* alleles specifically from the endoderm (see 2.3.1 for details of breeding strategies). Recombination of the floxed Rosa-Fluorescent-Yellow-Protein (RYFP) by the activity of SOX17^{icre} only occurred in endothelial and endodermal cells. Fluorescence is detected diffusely throughout the embryo, highlighting the endothelial cells of the vascular network (Fig 30 panels b and b'). A strong signal is emitted from the endoderm, in particular from each of the slit like pharyngeal pouches (Fig 30, panels b', b'', strong RYFP in the pouches is indicated by the arrows). In the absence of SOX17^{iCre} no fluorescence is detected in the embryo (Fig 30, panel a). This data confirms that the activity of SOX17^{icre} in the *R1;R2^{Sox17}* line was specific to the tissues that *Sox17* is expressed in i.e. the endoderm and endothelial cells.

Whole mount *in situ* hybridisation for *Pax1* revealed that rostral and caudal pouch defects manifest in *Sox17$^{icre/+}$;Fgfr1$^{flox/-}$;Fgfr2$^{flox/-}$* **(*R1;R2cKO^{Sox17}*)** embryos. All *R1;R2cKO^{Sox17}* embryos display bilateral fusion of the 1st and 2nd pharyngeal pouches (brackets Fig 31 panels b, b', c and c') and thus bilateral hypoplasia of the 2nd pharyngeal arch. Some variation in the severity of the pouch fusion is evidenced by the size of the second arch; compare the almost non-existent 2nd pharyngeal arch in the 'severe' *R1;R2cKO^{Sox17}* embryo (Fig 31, panels c and c'– the 2nd arch is outlined to aid identification) to the mild *R1;R2cKO^{Sox17}* embryo that has a hypoplastic but still identifiable proximal 2nd arch (Fig 31, panels b and b' – the 2nd arch is outlined to aid identification). Rostral pouch development is perturbed in the same way by the deletion of *Fgf3* and *Fgf8* or *Fgfr1* and *Fgfr2* from the endoderm. However, the penetrance and severity of rostral pouch fusion is significantly increased in *R1;R2cKO^{Sox17}* compared to *F3;F8cKO^{Sox17}.* The incidence of rostral, bilateral pouch fusion detected in embryos from E9.0 to E10.5 was almost 50% more prevalent in *R1;R2cKO^{Sox17}* embryos than *F3;F8cKO^{Sox17}* embryos (respectively, n=12/12 vs n=4/9, p=0.0016). Finally, the 3rd pouch is also hypoplastic in the majority of *R1;R2cKO^{Sox17}* embryos, indicating that the loss of *Fgfr1* and *Fgfr2* affects both rostral and caudal pouch development (unfilled arrowheads Fig 31 panels b – c'). This data indicates that the expression of *Fgfr1* and *Fgfr2* in the endoderm is required for pouch morphogenesis. However, it is not known whether pouch formation would also be perturbed by the loss of signalling downstream of FGFR1 and FGFR2 signalling from adjacent PA tissues.

Fig 30

Fig 30. SOX17^{iCre} activity, identified by fluorescence from the RYFP reporter, is present only in the endoderm and endothelial cells of the *R1;R2^{Sox17}* line. Yellow fluorescence from the RYFP reporter, detected under UV light, is only present in embryos carrying the *Sox17^{iCre}* allele (b-b''), no fluorescence is detected in Cre negative embryos (a). A diffuse fluorescent signal is detected in the endothelial cells of the blood vessels and a strong fluorescent signal is emitted from the endodermal pouches (white arrows b and b'') of SOX17^{icre} positive embryos. b-b'' are the same embryo taken at low power (b), at high power (b') and high power with low exposure to dampen the endothelial cell fluorescence (b''). **. È σ**

Annotations: Arrows to the right of the figure identify the orientation of the embryos: A = anterior, P = posterior, L = lateral, M = medial, V= ventral, D = dorsal. Outlined area in panels b indicates the area magnified in panels b' and b''. White arrowheads = strong fluorescent signal emitted fro the endodermal pouches, pp = pharyngeal pouches.

Fig 31: *Pax1* expression identifies bilateral rostral pouch fusion and 3rd pouch hypoplasia present in all *R1;R2cKO^{Sox17}* embryos. *Pax1* whole mount *in situ* hybridisation on E10.5 embryos reveals a fusion of the 1st and 2nd pouches and hypoplasia of the 3rd pouch on the left side (a-c) and right side (a'-c') of *R1;R2cKO^{Sox17}* embryos. Pouch defects ranged in severity; the most severe case shown in panel c in which the proximal part of the *R1;R2cKO^{Sox17}* embryo's 2nd arch is barely identifiable. n=2

Annotations: Arrows to the left of the figure identify the orientation of the embryos: A = anterior, P = posterior, L = lateral, M = medial, V= ventral, D = dorsal. L=Limb bud, S = somite, pp = pharyngeal pouch, ? = presumptive pouch, solid arrowheads identify areas of *Pax1* expression in each pouch, unfilled arrowheads identify 3rd pouch hypoplasia and reduced *Pax1* expression. Brackets identify rostral pouch fusion. Dashed lines demarcate hypoplasia of the proximal aspect of the 2nd arch.

Fig 31

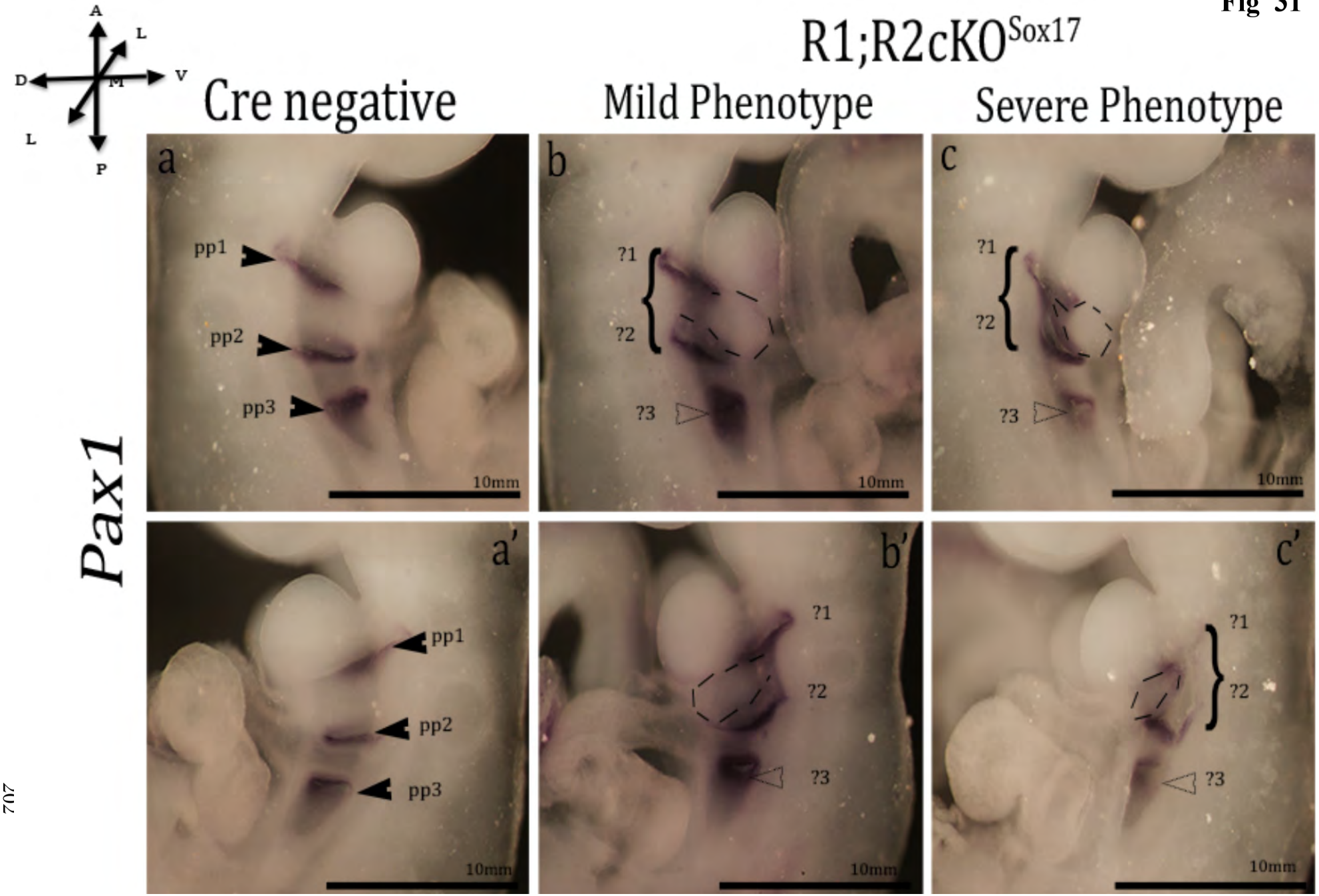
A
L
D
M
V
L
P
R1;R2cKO Sox17
Cre negative
Mild Phenotype
Severe Phenotype
Pax1
a
b
c
pp1
pp2
pp3
?1
?2
?3
10mm
a'
b'
c'

5.2.1.b The recombination of *Fgfr1* and *Fgfr2* in the mesoderm and CNCC does not cause defects in pouch formation

To verify that FGF signalling within the endoderm is of primary importance for pharyngeal pouch morphogenesis, the requirement for *Fgfr1* and *Fgfr2* expression in other pharyngeal tissues during pouch evagination was analysed.

To analyse the role of FGF signalling in the mesoderm during pouch morphogenesis, floxed *Fgfr1* and *Fgfr2* alleles were genetically recombined in the mesoderm using MESP1^{Cre} (see 2.3.1 for details) (Saga et al., 1999). The RYFP reporter illustrates that when *Mesp1^{Cre}* is expressed that it is active only in the mesodermal cells of embryo (Fig 32, panel b and b'). Of significance is the fluorescence detected in the mesodermal core that runs through each pharyngeal arch (arrows Fig 32, panel b'). Fluorescence is not detected in Cre negative embryos (Fig 32, panel a). Subsequently *Pax1* defined pouch morphology was analysed in mutants deficient of FGFRs in the mesoderm and in control embryos. *R1;R2cKO^{Mesp1}* embryos were not recovered from the cross. It is possible that *R1;R2cKO^{Mesp1}* embryos died before E9.5 because they were unable to develop mesodermal cells at gastrulation. This prediction is based on Xenopus data that has shown that FGF signalling is required to induce mesoderm during gastrulation, (Deng et al., 1994). For, Xenopus embryos injected with a construct containing dominant-negative FGFR1 were observed to display gastrulation defects attributed to a lack of mesoderm induction during early embryogenesis (Deng et al., 1994).

An analysis of *Pax1* expression in the pharyngeal endoderm revealed normal pouch morphology in all embryos deficient for mesodermal *Fgfr1* and *Fgfr2,* even when only one allele of *Fgfr1* or *Fgfr2* was retained in the mesoderm (Fig 33). The pharyngeal pouches of the mesodermal *Fgfr* mutants appear to be of the same size as Cre negative controls (Fig 33 a vs b). However, the 2nd pouch of *R1cKO;R2cHet*^{Mesp1} embryo, depicted in Fig 33, panel c, appears slightly more splayed than the controls embryos pouch (the splayed 2nd is denoted by the question mark in Fig 33, panel c). As this is not an overt pouch phenotype it is unlikely that this mild perturbation of pouch morphology deviates beyond 'normal variation' during development. However, to validate this a more extensive analysis of pouch morphogenesis and an analysis of thymus organogenesis in *R1cKO;R2cHet*^{Mesp1} mutants is required, something that time did not permit for this thesis.

The CNCC specific activity of the Wnt1^{cre} line was utilized to recombine and thus delete the floxed alleles of *Fgfr1* and *Fgfr2* from these cells (Danielian et al., 1998). The specificity of WNT1^{Cre} activity within CNCCs and structures contributed to by CNCCs, such as the PAAs, was visualized by the fluorescence from the RYFP reporter (Fig 34 b and b'). Comparing the *Pax1*-expressing pharyngeal pouches of Fgfr-deficient CNCC mutant embryos to Cre negative embryos reveals no difference in pouch morphology, (compare pouches indicated by solid arrowheads in all panels of Fig 35). Pharyngeal pouches 1 to 3 and the just forming 4th pouch at E10.5 have formed in the correct order, orientation and size irrespective of the genotype of the embryo. No evidence of rostral pouch fusion or caudal pouch hypoplasia was observed in the Fgfr-deficient CNCC mutants, accordingly the pharyngeal arches of these mutants appear to be of a normal proportion.

Fig 32

Fig 32. MESP1^{Cre} activity, identified by fluorescence from the RYFP reporter, is present only in the mesodermal cells of the *R1;R2^{Mesp1}* line. Yellow fluorescence from the RYFP reporter, detected under UV light, is only present in embryos carrying the *Mesp1^{Cre}* allele (b-b'), no RYFP is detected in Cre negative embryos (a). A fluorescent signal is detected in the mesodermal cells of the splanchic mesoderm and in the core mesoderm running through each pharyngeal arch (arrows b'). b-b' are the same embryo taken at low power (b), at high power (b'). N=2

Annotations: Arrows to the left of the figure identify the orientation of the embryos: A = anterior, P = posterior, L = lateral, M = medial, V= ventral, D = dorsal. pp = pharyngeal pouch, solid white arrowheads identify areas of fluorescence within the core mesoderm, sp.meso = splanchic mesoderm.

Fig 33: *Pax1* expression identifies normal pouch morphology in embryos that are deficient of *Fgf receptor 1* and *Fgf receptor 2* in their mesoderm. (a-c) *Pax1* whole mount *in situ* hybridisation on E10.5 embryos at low magnification (4x). (a'-c') The pharyngeal apparatus of embryos a-c viewed at high magnification shows normal pouch morphology in all embryos (8x). One mutant imaged in c' appears to have a slightly splayed 2nd pouch (question mark by the middle arrowhead in panel c').N=2

Annotations: Arrows to the left of the figure identify the orientation of the embryos: A = anterior, P = posterior, L = lateral, M = medial, V= ventral, D = dorsal. L=Limb bud, S = somite, pp = pharyngeal pouch, solid black arrowheads identify *Pax1* expression in the pharyngeal pouches.

Fig 33

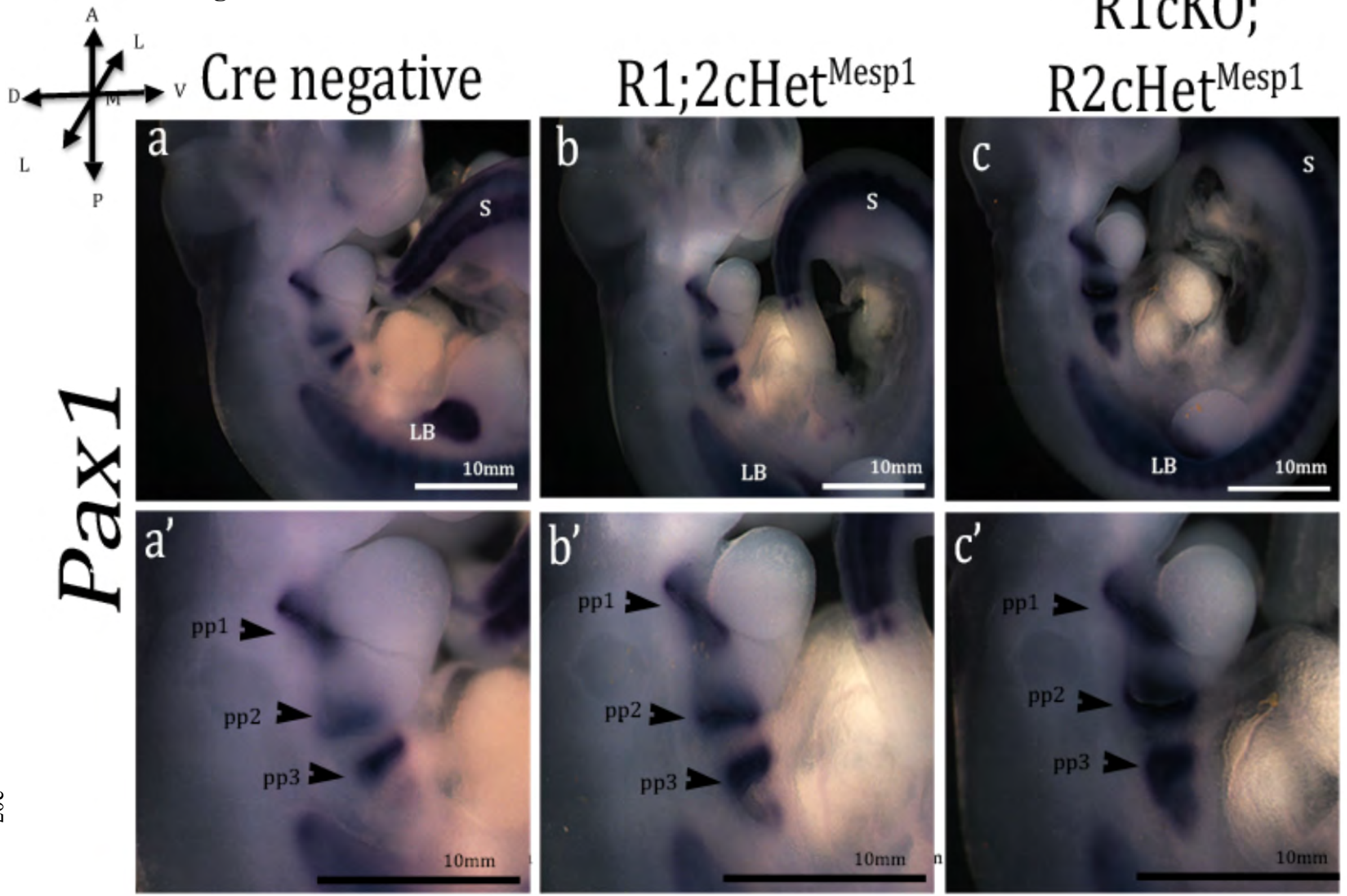
A
L
D
V
M
L
P
Cre negative
R1;2cHet^Mesp1
R1cKO;
R2cHet^Mesp1
Pax1
a
b
c
s
LB
10mm
a'
b'
c'
pp1
pp2
pp3

Fig 34

Fig 34: WNT1^{Cre} activity, identified by fluorescence from the RYFP reporter, is present only in the CNCC cells and their derivatives in the R1;R2^{Wnt1} line. Yellow fluorescence from the RYFP reporter, detected under UV light, is only present in embryos expressing the *Wnt1^{Cre}* allele (b-b'), no RYFP is detected in Cre negative embryos (a). A fluorescent signal is detected in the streams of CNCC migrating into the arches (arrowheads) and in the PAA running through each pharyngeal arch (PAA) (b'). The same embryo is images in b-b', taken at low power (b), at high power (b'). N=2
Annotations: Arrows to the left of the figure identify the orientation of the embryos: A = anterior, P = posterior, L = lateral, M = medial, V= ventral, D = dorsal. pp = pharyngeal pouch, solid white arrowheads identify streams of fluorescing CNCC, PAA labels fluorescing CNCC within the PAA.

Fig 35: Pouch morphology, as highlighted by *Pax1* expression, appears normal in R1;R2cKO^{Wnt1} embryos. (a-c) *Pax1* whole mount *in situ* hybridisation on E10.5 embryos at low magnification (4x). (a'-c') The pharyngeal apparatus of embryos a-c viewed at high magnification shows normal pouch morphology in all embryos (8x). N=2
Annotations: Arrows to the left of the figure identify the orientation of the embryos: A = anterior, P = posterior, L = lateral, M = medial, V= ventral, D = dorsal. L=Limb bud, S = somite, pp = pharyngeal pouch, solid black arrowheads identify *Pax1* expression in the pharyngeal pouches.

Fig 35

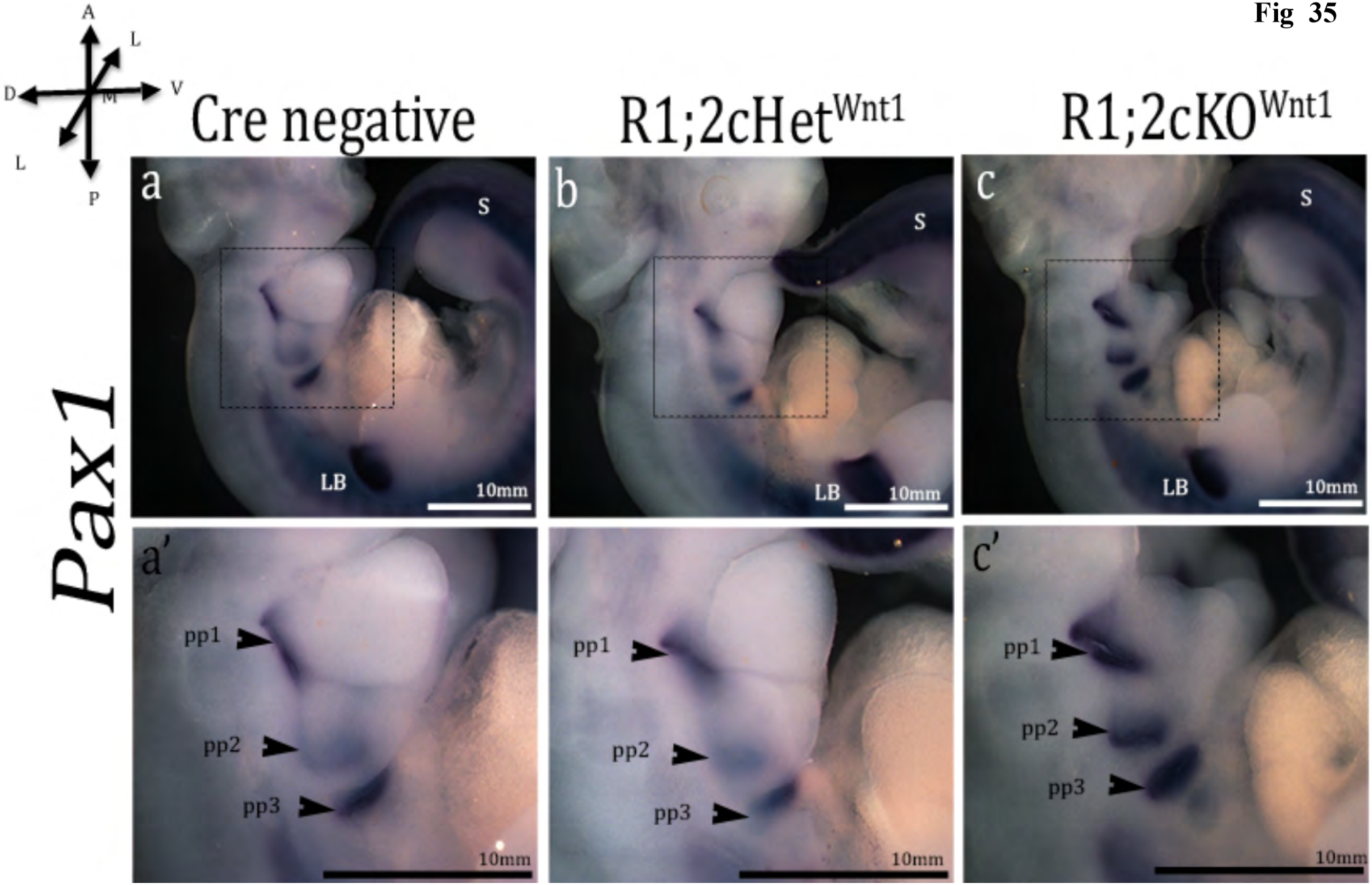
A
L
D
M
V
L
P
Cre negative
R1;2cHet Wnt1
R1;2cKO Wnt1
Pax1
a
s
LB
10mm
b
s
LB
10mm
c
s
LB
10mm
a'
pp1
pp2
pp3
10mm
pp1
pp2
pp3
10mm
c'
pp1
pp2
pp3
10mm

5.2.2 Assessment of 3rd pouch development in *R1;R2cKO^{Sox17}* embryos

The data presented thus far in Chapter 5 demonstrates that *Fgfr1* and *Fgfr2* are required in the endoderm (but not in the mesoderm or CNCC) for pouch morphogenesis to occur 'normally'; the rostral pouch defects in the *R1;R2cKO^{Sox17}* embryos recapitulate those observed in *Fgfr1* hypomorphs. In addition to displaying fused rostral pouches the *R1;R2cKO^{Sox17}* embryos also appear to form a hypoplastic 3rd pouch. The following experiments were conducted to analyse, in detail, the endoderm specific requirement for *Fgfr1* and *Fgfr2* during pouch morphogenesis:

a) 3rd pouch development was assessed in endodermal *Fgfr1;Fgfr2* mutants. At E11.5 the patterning of the 3rd pouch into presumptive thymus (*Foxn1* expressing and parathyroid (*Gcm2* expressing) domains was evaluated by *in situ* hybridisation. Thymus gland formation was assessed at E15.5.

b) CNCC presence/migration, (assessed by the pattern and level of *Dlx2* expression) and cell death (assessed by Lysotracker and Caspase 6 staining) was assessed in endodermal *Fgfr1;Fgfr2* mutants

c) FGF signalling readouts were analysed by *in situ* hybridisation to assess the level of FGF signalling in *Fgfr1* and 2 mutants.

5.2.2a A severely aplastic 3rd pouch, that is unable to pattern correctly into presumptive thymus and parathyroid domains, forms from *Fgfr1;Fgfr2* deficient endoderm at E11.5.

Caudal pouch defects have not previously been reported in embryos that are deficient of FGF signalling (*Fgfr1* hypomorphs and *Fgfr1*$^{\Delta Frs/\Delta Frs}$ embryos) (Trokovic et al., 2003; Trokovic et al., 2005; Hoch and Soriano, 2006). 3rd pouch hypoplasia and aplasia does, however, respectively manifest in *Fgf8*-mild and *Fgf8*-severe hypomorphs (Abu-Issa et al., 2002; Frank et al., 2002). Conversely, although the rostral pouches are described as 'disorganised' in severe *Fgf8* hypomorphs, their bilateral fusion is not documented (Abu-Issa et al., 2002). As such, the combination of both rostral pouch fusion and 3rd pouch hypoplasia observed in *R1;R2cKO*^{Sox17} embryos appears to be a unique pouch phenotype, or at the most resembles the pouch defects of *Fgf8*-severe hypomorphs. To further assess the development of the 3rd pouch in the absence of *Fgfr1* and *Fgfr2*, the patterning of this pouch and its morphogenesis into the thymus was analysed.

No *R1;R2cKO*^{Sox17} embryos were recovered at E11.5 (0/9 embryos) or E15.5 (0/14 embryos), however, defects in 3rd pouch development were observed in embryos with only one allele of *Fgfr1* or *Fgfr2*. At E11.5 the 3rd pouch should be patterned into presumptive thymus (*Foxn1* positive) and parathyroid (*Gcm2* positive) domains (see section 1.1.1). Only a remnant of the 3rd pouch can be detected in the *R1cHet;R2cKO*^{Sox17} embryo analysed at E11.5. The 3rd pouch remnant of the *Fgf receptor* mutant did not express *Gcm2* (Fig 36, panel c), and only contained a small patch of *Foxn1* positive cells that were still attached to the pharynx (Fig 36, panel

f). The 3rd pouch of *R1;R2cHet*^{Sox17} embryo appears to be smaller than the 3rd pouch of the Cre negative embryo (Fig 36 compare panels a and d to b and e). However, the compound heterozygote's pouch is patterned correctly into a *Foxn1* positive (ventral-posterior) domain (Fig 36, panel b) and a *Gcm2* positive (dorsal-anterior) domain (Fig 36, panel e). By E15.5 two thymus glands should be visible above the heart (Blackburn and Manley, 2004). This was observed in all Cre negative (n=8/8) and *R1;R2cHet*^{Sox17} (2/2) embryos (Fig 37 panels a and b, in each the thymus is outlined to aid visualisation). Thymus lobes were, as expected, absent in embryos with only one copy of either *Fgfr1* or *Fgfr2* (the latter genotype is displayed in Fig 37 panel c, asterix mark where the thymi lobes should have formed). Thymus aplasia at E15.5 correlates with the severely hypoplastic pouch observed at E11.5 in the *R1cHet;R2cKO*^{Sox17} mutant.

It is unclear whether the 3rd pouch defects observed in the *R1cHet;R2cKO*^{Sox17} mutant occurs because of early perturbations in pouch outgrowth or due to defects during pouch patterning. A retrospective analysis of embryos with only one copy of *Fgfr1* or *Fgfr2,* that had been processed for section *in situ* hybridisation at E9.5 revealed rostral pouch fusion and a hypoplastic 3rd pouch in a small proportion of embryos, (see Fig 38, rostral pouch fusion is evident in *R1cKO;R2cHet*^{Sox17}, displayed in panels g to i, as well as in *R1;R2cKO*^{Sox17} embryos, displayed in panels j to k). Thus, the thymus defects observed are likely to be a result of perturbations during pharyngeal pouch morphogenesis caused by a loss of FGF signalling from the endoderm. However, the PA defects observed in *R1;R2cKO*^{Sox17} embryos may also be contributed to by secondary defects in the colonisation of the arches by the CNCC; this is addressed in the following section 5.2.3.

Fig 36

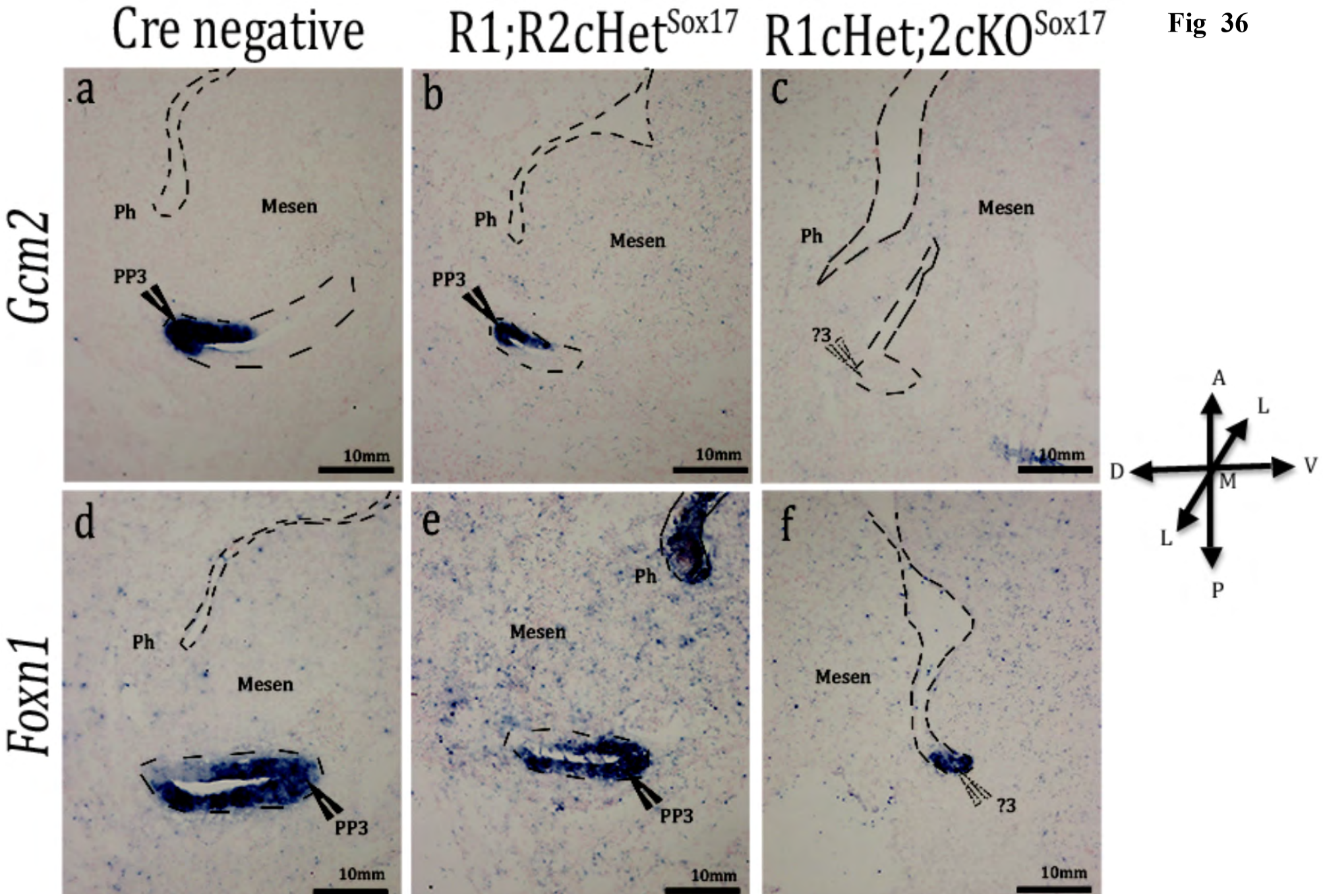
Cre negative
R1;R2cHet Sox17
R1cHet;2cKO Sox17
Gcm2
Foxn1
a
b
c
d
e
f
Ph
Mesen
PP3
?3
10mm
A
L
D
V
M
L
P

Fig 36: *Fgfr1* and *Fgfr2* are required in the endoderm for the patterning of the 3rd pouch into *Foxn1* and *Gcm2* positive domains at E11.5. *In situ* hybridization on sagittal sections of E11.5 embryos identifies the expression of *Gcm2* (a) in the anterior, dorsal domain of the 3rd pouch and *Foxn1* (d) in the posterior, ventral domain of the 3rd pouch of Cre negative embryos n=1. *Gcm2* and *Foxn1* domains are maintained in the smaller 3rd pouch of the *R1;R2cHet*^{Sox17} embryo (respectively, panels b and e), n=1. Only a rudiment of the 3rd pouch is identified in the *R1cKO;R2cHet*^{Sox17} embryo (panels c and f), correlating with thymus aplasia at E15.5 (see figure 37). No *Gcm2* expression is evident in the 3rd pouch rudiment of the *R1cKO;R2cHet*^{Sox17} embryo (panel c), and only a small area of cells appears to express *Foxn1* (panel f), n=1.

Annotations: Arrows to the right of the figure identify the orientation of the embryos: A = anterior, P = posterior, L = lateral, M = medial, V= ventral, D = dorsal. pp = pharyngeal pouch, solid black arrowheads identify areas of *Foxn1* or *Gcm2* expression in the pp, unfilled arrowheads identify areas of no, or reduced, *Foxn1* or *Gcm2* expression in the pp, ? = presumptive pouch, Mesen = mesenchyme, Ph = pharynx. Dashes outline the 3rd pouch to aid visualization of the structure.

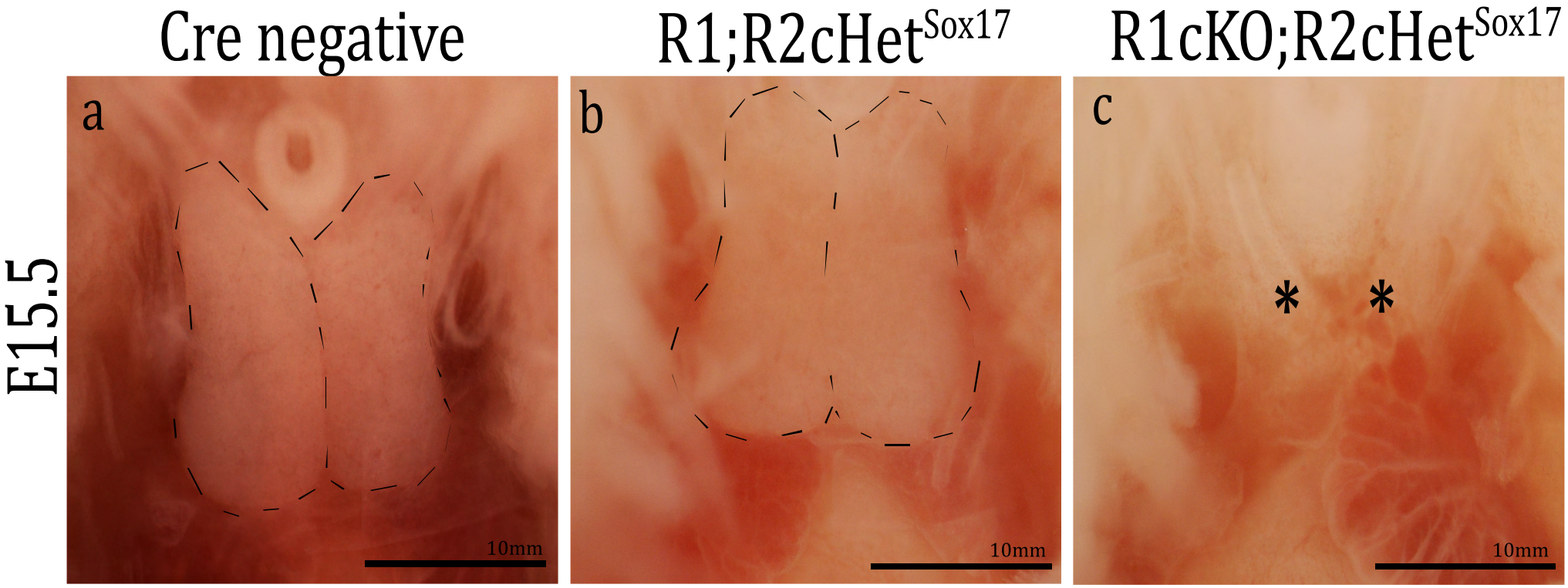

Fig 37: Thymus aplasia manifests in embryos when only one allele of either *Fgfr1* or *Fgfr2* is expressed in the endoderm during development. Open chest cavities of E15.5 embryos photographed to display the two thymus lobes (dashed outlines) present in Cre negative (panel a n=8/8) and *R1;R2cHet*^{Sox17} embryos (panel b, n=2/2) embryos. All embryos expressing only one allele of either *Fgfr1* or *Fgfr2* in their endoderm develop thymus aplasia (n=4/4, one *R1cKO;R2cHet*^{Sox17} embryo, three *R1cHet;R2cKO*^{Sox17} embryos) represented by the *R1cKO;R2cHet*^{Sox17} embryo in panel c. * denotes the absence of thymus glands in panel c, dashes outline the thymi lobes to aid visualization of these structures.

5.2.3 CNCC migration and mesenchyme patterning is perturbed in the absence of endodermal *Fgfr1* and *Fgfr2*

In *Fgfr1* hypomorphs migrating CNCC are only evident in the very proximal aspect of the hypoplastic 2nd arch (Trokovic et al., 2003). This defect was attributed to the loss of *Fgfr1* from the ectoderm, as arch development is not affected by a cell autonomous loss of *Fgfr1* expression from the CNNC (Trokovic et al., 2003). However, a loss of *Fgfr1* expression from the endoderm may also affect the migration and/or survival of CNCC migrating into the PA of *Fgfr1* hypomorphs. To assess the requirement for endoderm specific *Fgfr* expression during the colonisation of the PA by the CNCC, *Dlx2* expressing CNCC were analysed in the PA of embryos with *Fgfr*-deficient pharyngeal endoderm. At E9.25 *Dlx2* expression is evident in the 1st and 2nd arches of Cre negative, *R1cKO;R2cHet*^{Sox17} and *R1;R2cKO*^{Sox17} embryos. This data is indicative of the CNCC being able to populate the arches despite the lack of *Fgfrs* in the adjacent endodermal niche (compare robust distal *Dlx2* expression in the rostral 1st and 2nd arches of all embryos in Fig 38 panels d-e'). There is a slight reduction in the amount of *Dlx2* staining in the proximal aspect of the 2nd arch of the *R1;R2cKO*^{Sox17} mutant, (compare the arch regions indicated by solid arrowheads in Fig 38 panels a - b' to the regions indicated by unfilled arrowheads in panels c and c'). This suggests that their may be a reduction in the number of late migrating CNCC that are able to colonise the second arch of the *R1;R2cKO*^{Sox17} embryos.

In *Fgfr1* hypomorphs and *Fgfr1*$^{\Delta Frs/\Delta Frs}$ embryos a stalling of the CNCC is observed in an area proximal to the 2nd arch (Trokovic et al., 2003; Hoch and Soriano, 2006). Trockovic et al., correlated the accumulation of CNNCs just peripheral to the *Fgfr1*

hypomorph's 2nd arch to an increase in apoptosis in this area, (Trokovic et al., 2003). Cell death was analysed in embryos deficient of endodermal *Fgfr1* and *Fgfr2* using Lysotracker – a marker of acidic organelles that are abundant in apoptosing cells – to investigate whether the reduction in *Dlx2* correlated with a change in cell death (Birk et al., 2008). No increase in cell death was evident in the arches of Lysotracker stained control and conditional *Fgf receptor* mutants (Fig 38 panels a-c'). This data is consistent with the observation that the *Dlx2* expressing CNCC are able to enter the arches of the mutants. An ectopic region of fluorescence emitted from the Lysotracker probe is visible in and around the otic vesicle of the *R1;R2cKO*^{Sox17} embryo in panels c and c' of Fig 38, (identified by the question mark labelled arrowhead). It is unclear whether the dying cells in the otic region are the ectoderm and mesenchyme of the otic proper or of misrouted CNCC.

It has been hypothesised that the CNCC are multipotent when they enter the arches and that their fate is influenced by the adjacent pharyngeal tissues (Trainor and Krumlauf, 2001). FGF signalling within the branchial arches has been shown to affect the expression of *Hox* genes in the CNCC that colonise the PA (Trainor et al., 2002). *Hox* gene expression was analysed in the PA of conditional *Fgf receptor* mutants to investigate whether a loss of *Fgfr* expression specifically from the endoderm affects CNCC derived mesenchymal patterning. *Hoxa2* is strongly expressed in the CNCC derived mesenchyme of the 2nd pharyngeal arch (refer to Cre negative in Fig 39, panel a, anterior solid arrowhead indicates 2nd arch expression). There is also a small region of *Hoxa2* expressing endodermal cells in the inter-pouch region lining the medial aspect of the 3rd arch (solid grey arrowhead indicates endodermal expression). Fusion of the rostral pharyngeal endoderm is evident in the *R1cKO;R2cHet*^{Sox17} (Fig 39, panel c) and *R1;R2cKO*^{Sox17}

(Fig 39, panel d) mutants. Despite the hypoplasia of the 2nd arch in these *Fgf receptor* mutants and the loss of *Hoxa2* expression in the fused rostral endoderm (unfilled arrowhead, Fig 39, panels c and d), *Hoxa2* expression is maintained in the mesenchyme of the 2nd arch (yellow arrowheads, Fig 39, panels c and d). *Hoxb1* is expressed in the ectoderm, mesenchyme and most strongly in the endoderm of the PA caudal to the 3rd arch (Fig 39 panels e-h'). Third pouch hypoplasia is evident in the *R1;R2cKO^{Sox17}* embryo (Fig 39 panels h and h', this defect correlates with a severe reduction in *Hoxb1* expression in both the un-segmented caudal endoderm and, surprisingly, in the adjacent mesenchyme.

The CNCC data shows that this cell population is able to migrate toward and infiltrate (possibly in reduced number with regards to the distal aspect of the 2nd arch) the PA of the endodermal *Fgfr* mutants. However, in the absence of normal endodermal patterning and morphology, (significantly in the caudal PA), the expression of *Hox* genes is perturbed within the caudal CNCC derived mesenchyme.

Fig 38

Lysotracker
Left side
Right side
Dlx2
Left side
Right side
Cre negative
R1cKO; R2cHetSox17
R1; R2cKOSox17
a
a'
b
b'
c
c'
d
d'
e
e'
I
II
III
10mm

Fig 38: Deleting *Fgfr1* and *Fgfr2* from the endoderm perturbs migration of the CNCC into the proximal aspect of the 2nd arch and results in ectopic cell death proximal to the otic.

Embryos were processed for Lysotracker staining as an indication of cell death (a-c') and subsequently for whole mount *in situ* hybridization of *Dlx2* (d-f'), as an indicator of CNCC migration. No overt differences in cell death in the arches of *Fgf receptor* mutants is observed in the Lysotracker stained embryo. However, the *R1;R2cKO^{Sox17}* embryo (panel c and c') displays ectopic cell death in and around the otic, ('question mark' denotes the ambiguity concerning the identity of the tissue in which cell death is observed, i.e. is it the CNCC in the otic or the otic tissue itself). *Dlx2* expressing CNCCs were detected in the arches of all embryos. However there appears to be a reduction in staining in the proximal aspect of the 2nd arch of the *R1;R2cKO^{Sox17}* embryo (f and f' unfilled arrowhead). N=2

Annotations:, solid black arrowheads identify robust *Dlx2* expression in the arches, unfilled arrowheads identify reduced *Dlx2* expression in the proximal aspect of the 2nd arch, I-III = arches 1-3.

Fig 39: *Fgf receptor* mutants with perturbed pouch formation display a loss of *Hox* gene expression in the pharyngeal endoderm and arches.

Frontal sections of E9.5 embryo's pharyngeal apparatus show *Hoxa2* (a-d), and *Hoxb1* (e-h') expression, detected by *in situ* hybridization, is severely reduced in the endoderm of *R1;R2cKO^{Sox17}* embryos (unfilled arrowheads in panels d, h and h'). Some *Hox* gene expression is maintained in the *R1;R2cKO^{Sox17}* embryos mesenchyme and ectoderm, primarily *Hoxa2* expression in the mesenchyme of the 2nd arch (yellow arrow panel d). Note also the fused rostral pouch phenotype and loss of *Hoxa2* expression in the *R1cKO;R2cHet^{Sox17}* embryo (panels c, g, g'). *N=1*

Annotations: Black arrowhead = endodermal pouch expression, light blue arrowhead = ectodermal PA expression, unfilled arrowhead = endodermal pouch with no/little expression, green arrowhead = mesenchyme, grey arrowhead = inter pouch expression of *Hoxa2*, red arrowhead = absence of inter pouch expression of *Hoxa2*, pp = pharyngeal pouch, ? = presumptive pouch, ecto = ectoderm, mesen = mesenchyme. Arrows to the left of the figure illustrate the orientation of the pharyngeal apparatus sections; A = anterior, P = posterior, L = lateral, M = medial, V= ventral, D = dorsal.

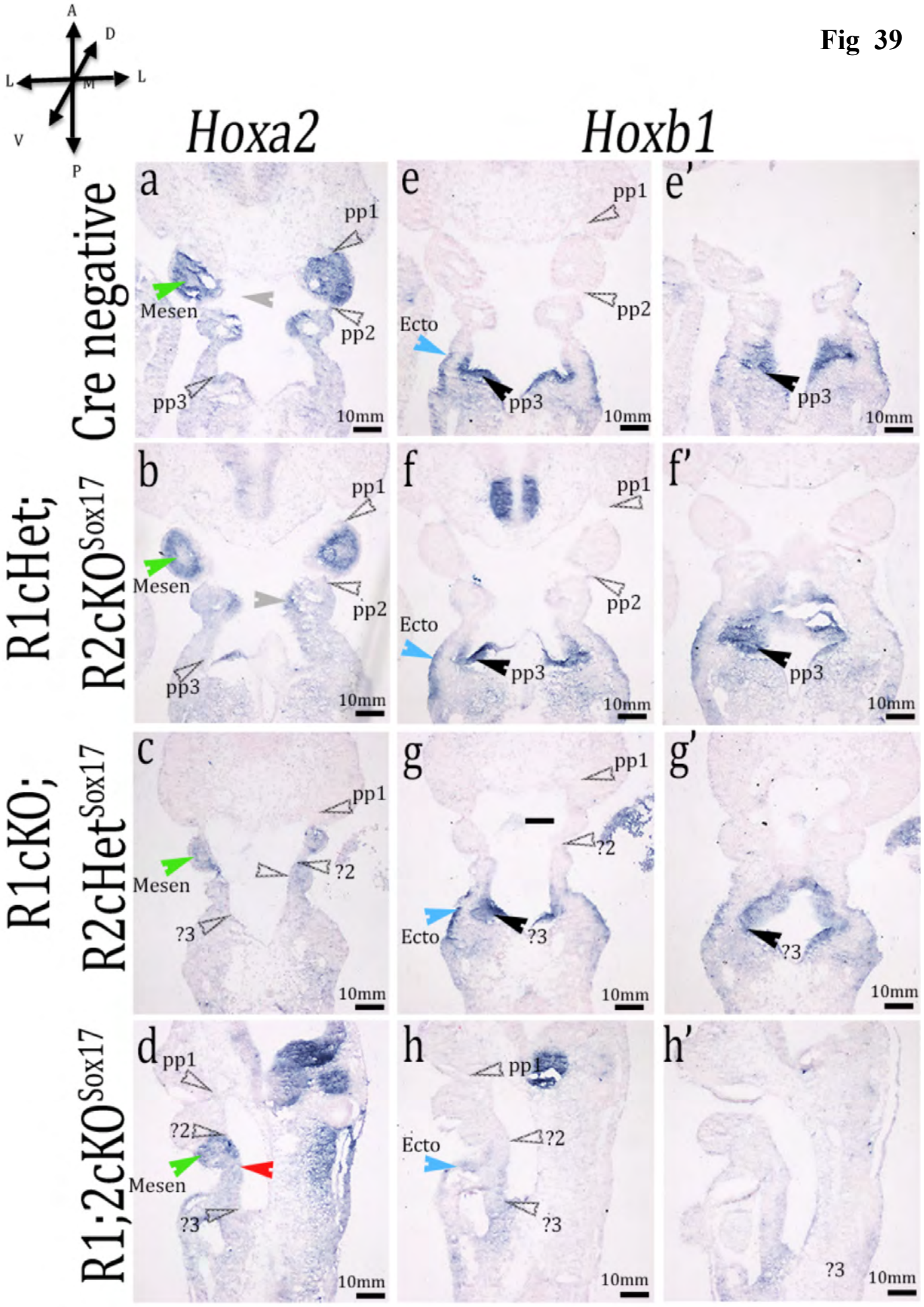
A
D
L
M
L
V
P
Hoxa2
Hoxb1
Cre negative
R1cHet;
R2cKOSox17
R1cKO;
R2cHetSox17
R1;2cKOSox17
a
b
c
d
e
e'
f
f'
g
g'
h
h'
pp1
pp2
pp3
Mesen
Ecto
?2
?3
10mm

5.2.4 Deletion of *Fgfr1* and *Fgfr2* from the endoderm results in a severe decrease in the level of FGF signalling within this pharyngeal epithelium

The data so far demonstrates that the deletion of *Fgfr1* and *Fgfr2* from the endoderm prevents the discreet evagination of the endoderm that in turn affects the formation of the thymus. The deletion of *Fgfr1* and *Fgfr2* from the endoderm was predicted to decrease the amount of FGF signalling specifically in this tissue. To test this hypothesis the expression of several FGF readouts were analysed by *in situ* hybridisation in frontal sections of E9.5 *R1;R2cKO*^{Sox17} embryo's PA.

An endoderm specific loss of, *Erm, Pea3, Sprouty 2* and *Sprouty 1* was observed in *R1;R2cKO*^{Sox17} embryos, indicative of a tissue specific loss of FGF signalling downstream of the SOX17^{iCre} mediated deletion of *Fgfr1* and *2*. FGF signalling is abundant throughout the endoderm of the PA but particularly in the evaginating 3rd pouch of Cre negative embryos, as evidenced by the strong expression of the *Sprouty* and *Ets* genes in the caudal endoderm, (Cre negative images in panels a' (or a'') in Figs). In clear contrast all FGF signalling readouts are markedly reduced in the endoderm of the *R1;R2cKO*^{Sox17} embryos, although the reduction in *Sprouty1* expression is less pronounced (*R1;R2cKO*^{Sox17} images in panels b' (or b'') in Figs). The sparse distribution of mesenchyme in the *R1;R2cKO*^{Sox17} embryos (for example in Fig b'), relative to Cre negative embryos, likely accounts for the slight reduction FGF signalling in this tissue.

Fig 40

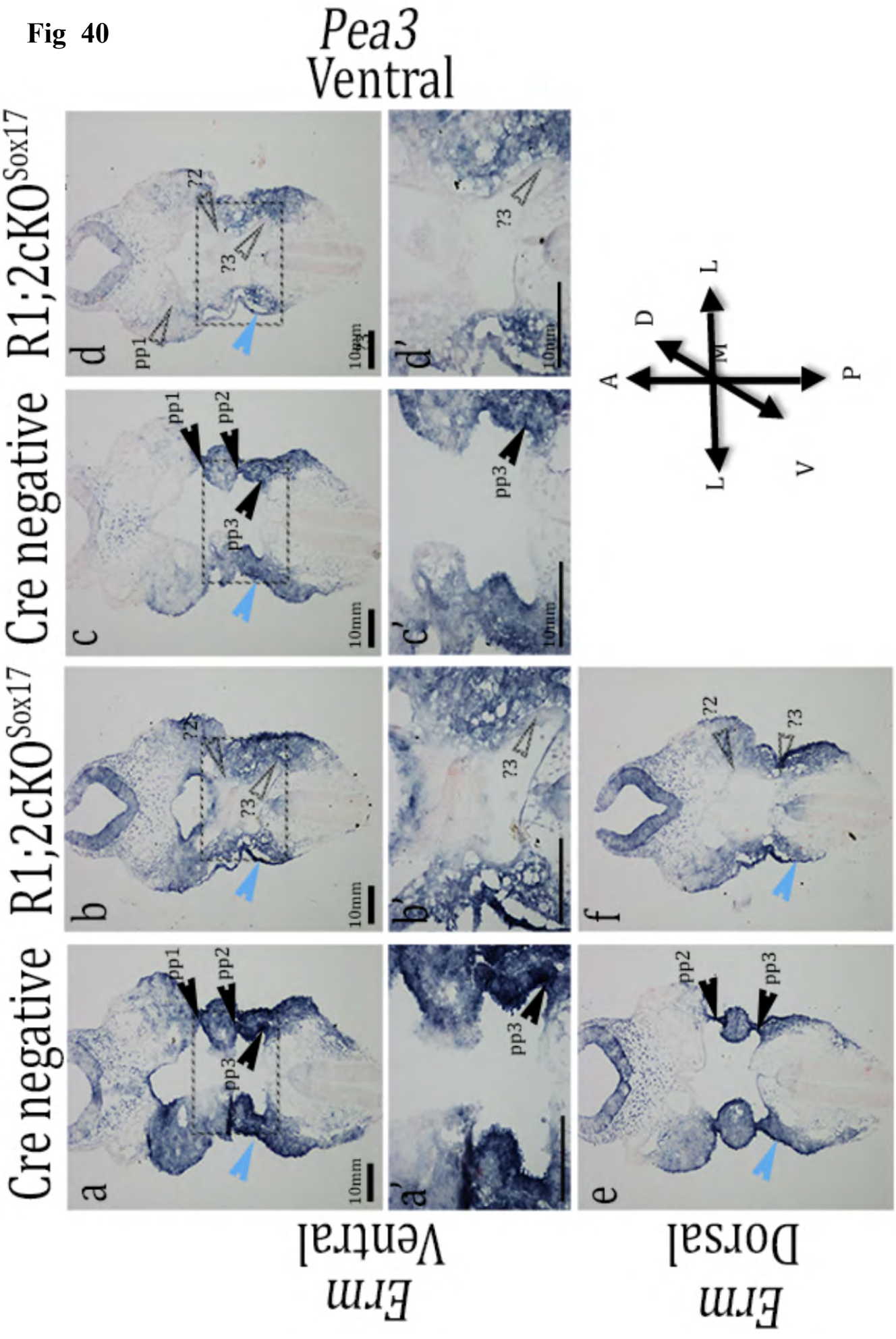
Pea3
Ventral
Cre negative
R1;2cKO Sox17
Cre negative
R1;2cKO Sox17
Erm
Ventral
Erm
Dorsal
a
b
c
d
a'
b'
c'
d'
e
f
pp1
pp2
pp3
?2
?3
10mm
A
D
L
M
L
V
P

Fig 40: Expression of the FGF signalling readouts, *Erm* and *Pea3*, are absent from the endoderm of *R1;R2cKO^{Sox17}* embryos.

In situ hybridization for *Erm* (a, a', b ,b', e and f) and *Pea3* (c, c', d and d') on frontal sections of E9.25 Cre negative (a, a', c, c' and e) and *R1;R2cKO^{Sox17}* (b, b', d, d' and f), embryo's pharyngeal apparatus shows there a is a tissue specific loss of FGF signalling in the endoderm of mutant embryos. Outlined area in panels a', b', c' and d' indicate the area magnified in panels a, b, c and d.

Annotations: Black arrowhead = endodermal pouch expression, light blue arrowhead = ectodermal PA expression, unfilled arrowhead = endodermal pouch with no expression, pp = pharyngeal pouch, ? = presumptive pouch. Arrows in the bottom right of Fig 40 illustrate the orientation of the pharyngeal apparatus sections; A = anterior, P = posterior, L = lateral, M = medial, V= ventral, D = dorsal. N=2

Fig 41: Expression of *Sprouty1* and *Sprouty2*, negative feedback regulators of FGF signalling, is absent from the endoderm of *R1;R2cKO^{Sox17}* embryos.

In situ hybridization for *Sprouty1* (a – b') and *Sprouty2* (c – d') on frontal sections of E9.25 Cre negative (a, a', c and c') and *R1;R2cKO^{Sox17}* (b, b', d and d'), embryos pharyngeal apparatus shows there is a tissue specific loss of FGF signalling in the endoderm of the mutant embryos. Outlined area in panels a a-d indicate the area magnified in panels a' - d'.

Annotations: Black arrowhead = endodermal pouch expression, light blue arrowhead = ectodermal PA expression, unfilled arrowhead = endodermal pouch with no expression, pp = pharyngeal pouch, ? = presumptive pouch. Arrows to the left of Fig 41 illustrate the orientation of the pharyngeal apparatus sections; A = anterior, P = posterior, L = lateral, M = medial, V= ventral, D = dorsal. N=2

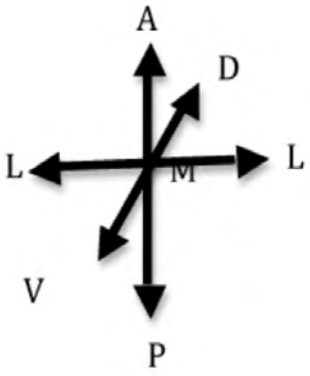
A
D
L
M
L
V
P

Fig 41

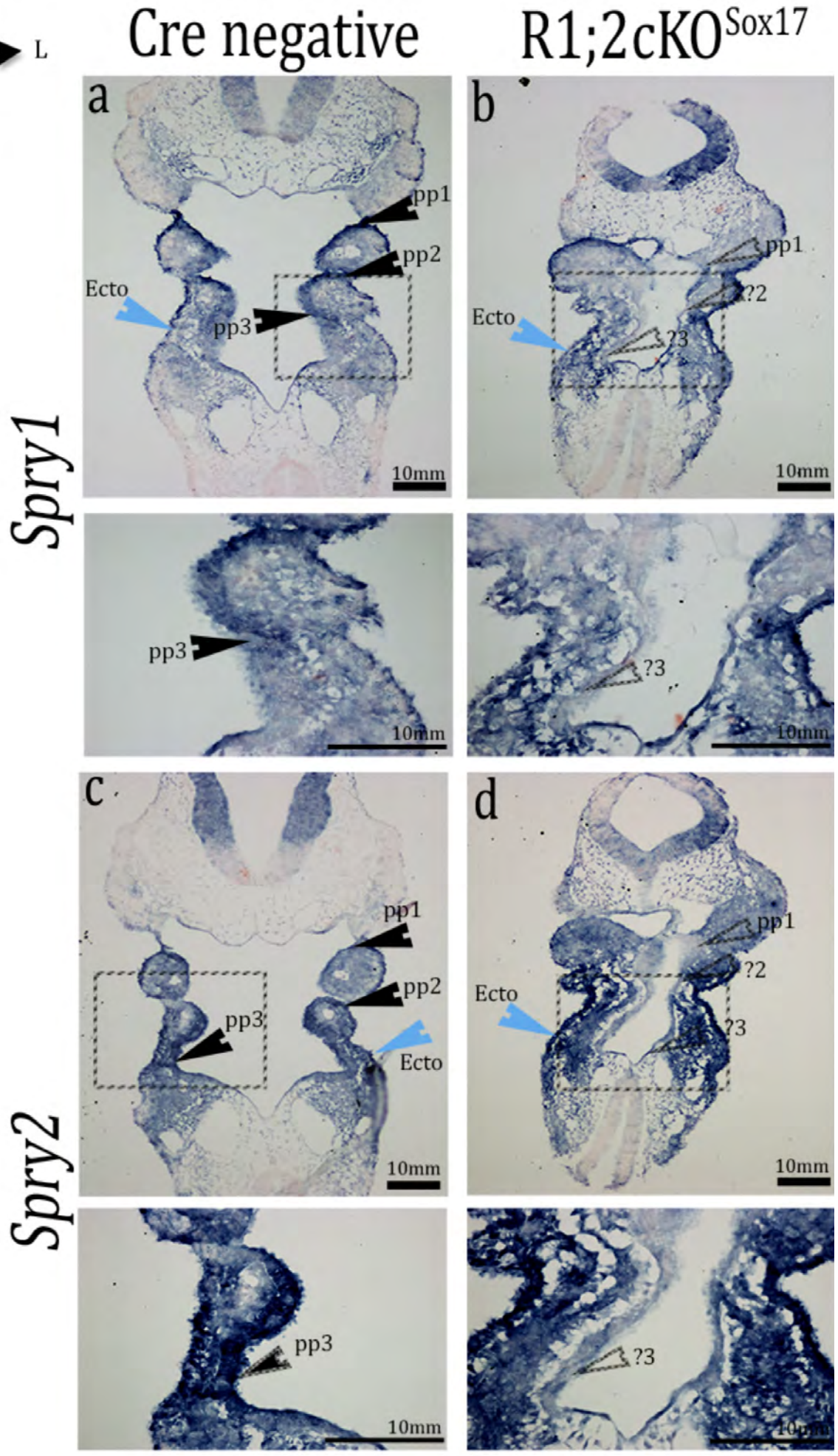
Cre negative
R1;2cKO Sox17
Spry1
Spry2
a
b
c
d
pp1
pp2
pp3
Ecto
?2
?3
10mm

5.3 Investigating the genetic interaction between TBX1 and FGF signalling in the pharyngeal endoderm during pouch morphogenesis

Park et al. have demonstrated a dosage sensitive reduction in the expression of *Fgfr1* in the PA of *Tbx1*$^{+/-}$ and *Tbx1*$^{-/-}$ embryos (Park et al., 2006). From this data the group inferred that TBX1 may regulate FGF signalling at multiple levels, i.e. not just at the level of *Fgf8* transcriptional control (Hu et al., 2004; Park et al., 2006). Alternatively, the loss of *Fgfr1* expression in *Tbx1*$^{-/-}$ embryos may be attributed to the TBX1 dependent loss of *Fgf8,* for Moon et al. have demonstrated that *Fgf8* activates FGR1 *in vivo* (Moon et al., 2006). The data presented in Chapter 3 and 5 is beginning to reveal that endodermal TBX1 may not be an effector of FGF signalling within this tissue, for, FGF signalling readouts are maintained in the pharyngeal endoderm of *Tbx1cKO*^{Sox17}. Moreover, TBX1 and FGF8 do not appear to function in the same endodermal pathway during pouch morphogenesis. This inference is supported by a comparison of PA sections from *R1;R2cKO*^{Sox17} and *Tbx1cKO*^{Sox17} embryos.

5.3.1 A comparison of pouch defects in *R1;R2cKO*^{Sox17} and *Tbx1cKO*^{Sox17} reveals that the two mutants have distinct phenotypes

The *in situ* data presented in Fig 40 and Fig 41 adds to the *Pax1* assessment of pouch morphology in *R1;R2cKO*^{Sox17} embryos, (see Fig 31). From PA sections one can identify for example that, in contrast to *Tbx1cKO*^{Sox17} embryos, the pharyngeal

endoderm of *R1;R2cKO*^{Sox17} embryos appears to evaginate toward the ectoderm but does so without any focal point. A number of other marked differences in the pharyngeal phenotype of *Tbx1cKO*^{Sox17} and *R1;R2cKO*^{Sox17} embryos have been summarised in Table 7. These discrepancies in pouch morphogenesis suggests that the FGF signalling cascade does not act downstream of *Tbx1* in the endoderm during pharyngeal pouch morphogenesis.

Table χ: A comparison of endodermal phenotypes in embryos lacking either *Tbx1* or *Fgfr1* and *Fgfr 2* expression in the endoderm

Phenotypes	***Tbx1cKO*^{Sox17}**	***R1;R2cKO*^{Sox17}**
1st pouch	Formed	Formed
2nd pouch	Aplastic	Fused to 1st pouch, 2nd arch is thus reduced
3rd pouch	Aplastic	Hypoplastic
Epithelial morphology	Thick, cells appear to be stacked and restricted to the midline.	Thin, epithelium is expanded and often appears to be one cell thick.
Endodermal evagination	None evident	The rostral endoderm appears to move toward the ectoderm without as one mass rather than foci of evaginations
FGF signalling	Maintained	Severely diminished/absent

5.3.2 Genetically increasing the level of endodermal FGF signalling does not rescue caudal pouch formation in endoderm devoid of *Tbx1* expression

The phenotypes of *R1;R2cKO*^{Sox17} and *Tbx1cKO*^{Sox17} embryos summarised in Table 7 suggest that *Tbx1* and FGF signalling do not function in the same endodermal pathway during pouch morphogenesis. To directly test the genetic interaction between FGF signalling and TBX1 in the endoderm *Sox17*$^{icre/+}$*Sprouty1*$^{flox/+}$*;Sprouty2*$^{flox/+}$*;Tbx1*$^{flox/+}$ (*Spry1;Spry2cHet;Tbx1cHet*^{Sox17}) and *Sox17*$^{icre/+}$*Sprouty1*$^{flox/+}$*;Sprouty2*$^{flox/+}$*;Tbx1*$^{flox/-}$ (*Spry1;Spry2;Tbx1cKO*^{Sox17}) embryos were generated (see 2.3.1 for details of breeding). The literature predicts that TBX1 functions upstream of FGF signalling because the expression of genes in the FGF pathway are reduced in *Tbx1*$^{-/-}$ embryos and because MEFs derived from *Tbx1*$^{-/-}$ embryos are unable elicit a response to FGF8 stimulation, (Vitelli et al., 2010). *Sprouty* family members are negative feedback regulators of FGF signalling and their genetic deletion has been demonstrated to de-regulate FGF signalling within the 3rd pouch, perturbing its development to endocrine glands (Gardiner et al., 2012). If endodermal TBX1 functions to positively regulate FGF signalling in the pharyngeal endoderm during pouch outgrowth, an increase in FGF signalling, (mediated by a loss of endodermal *Sprouty* expression) may compensate for the loss of *Tbx1* from this tissue, rescuing pouch outgrowth. This hypothesis was tested by:

a) Evaluating pouch formation at E10.5 in *Spry1;Spry2cHet;Tbx1cKO*^{Sox17} embryos by *Pax1 in situ* hybridisation.
b) Evaluating FGF signalling in the compound mutants by *Erm in situ hybridisation*.

Comparing the pouches of *Tbx1cKO*^{Sox17} and *Spry1;Spry2cHet;Tbx1cKO*^{Sox17} embryos to *Spry1;2;Tbx1cHet*^{Sox17} and Cre negative embryos it was evident that only the 1st pharyngeal pouch forms in mutants null for endodermal-*Tbx1* (Figure 42, panels c and d, asterix mark where caudal pouches were expected to form). This data indicates that reducing the level of *Sprouty* in the endoderm is not sufficient to rescue caudal pouch aplasia in *Tbx1*-deficient endoderm. However, surprisingly, the level of endodermal *Erm* and *Pea3* expression in *Spry1;Spry2cHet;Tbx1cKO*^{Sox17} does not appear to be increased compared to Cre negative embryos (Fig 43, compare panels a vs c and panels d vs f). Moreover, in contrast to the un-segmented endodermal expression pattern of *Erm* in *Tbx1cKO*^{Sox17} at E9.5 (Fig 19 panels d and d') the pattern of *Erm* and *Pea3* expression in *Spry1;Spry2cHet;Tbx1cKO*^{Sox17} mutants is somewhat segmented, despite the tissue morphology (Fig 43 arrows in panels c and f highlight discreet areas of FGF signalling).

Interestingly, *Fgf8* expression is also absent from the endoderm of *R1;R2cKO*^{Sox17} embryos (Figure 44 panels a and a' vs b and b'), as was observed in *Tbx1cKO*^{Sox17} embryos (Fig 17). It is tempting to speculate that FGF signalling may be linked indirectly to *Tbx1* expression or function in the endoderm via an intermediate pathway that in turn affects the expression of *Fgf8*.

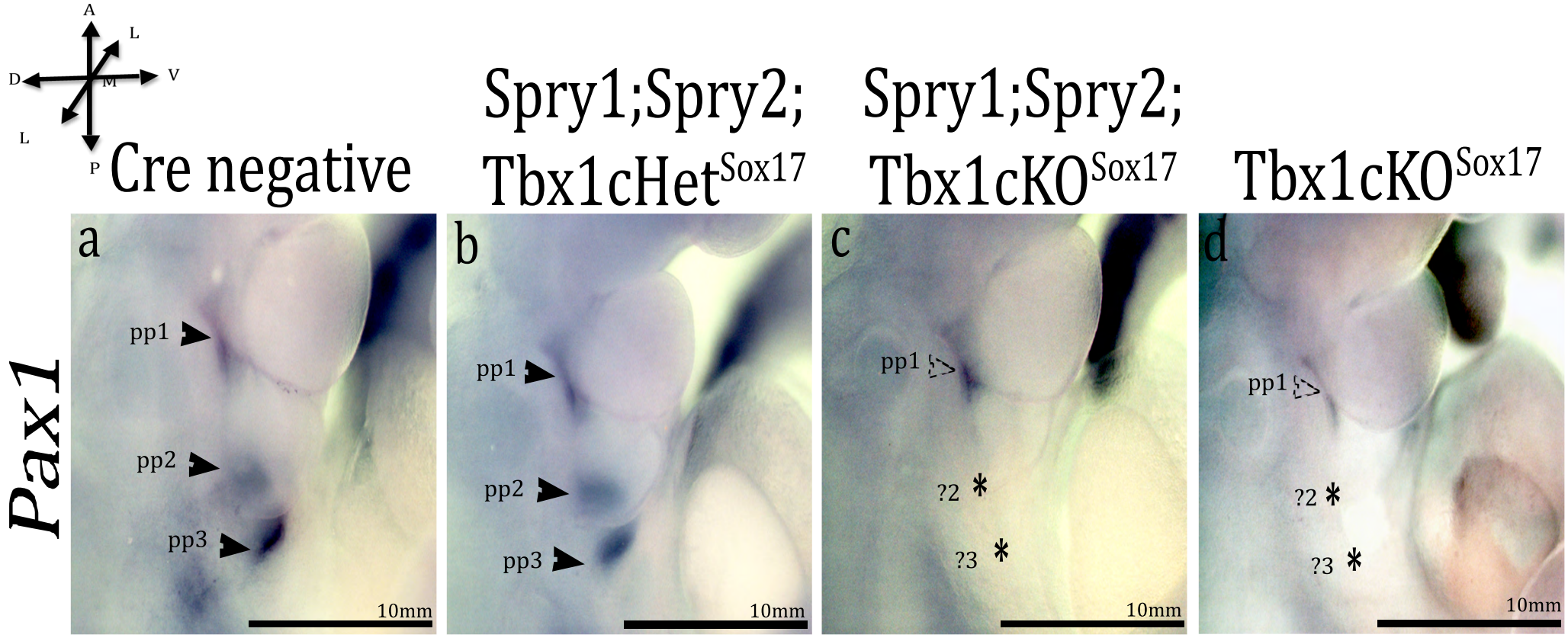

Fig 42: *Pax1* expression in the endoderm, which demarcates pouch morphology, identifies a lack of caudal pouches in *Tbx1cKO*^{Sox17} and *Spry1;Spry2cHet;Tbx1cKO*^{Sox17} embryos. a-d Side views of *Pax1* expression in E10.5 embryos pharyngeal apparatus. Note, that in *Tbx1cKO*^{Sox17} and *Spry1;Spry2cHet;Tbx1cKO*^{Sox17} embryos *Pax1* expression is maintained in the 1st pharyngeal pouch (pp), as indicated by the solid arrowhead, but is absent in the endoderm where pp 2, and 3 should form (* indicate absence of caudal pouches). N=3

Annotations: Black arrowhead = endodermal pouch expression, pp = pharyngeal pouch, ? = presumptive pouch. Arrows to the left of Fig 42 illustrate the orientation of the pharyngeal apparatus sections; A = anterior, P = posterior, L = lateral, M = medial, V= ventral, D = dorsal. N=3

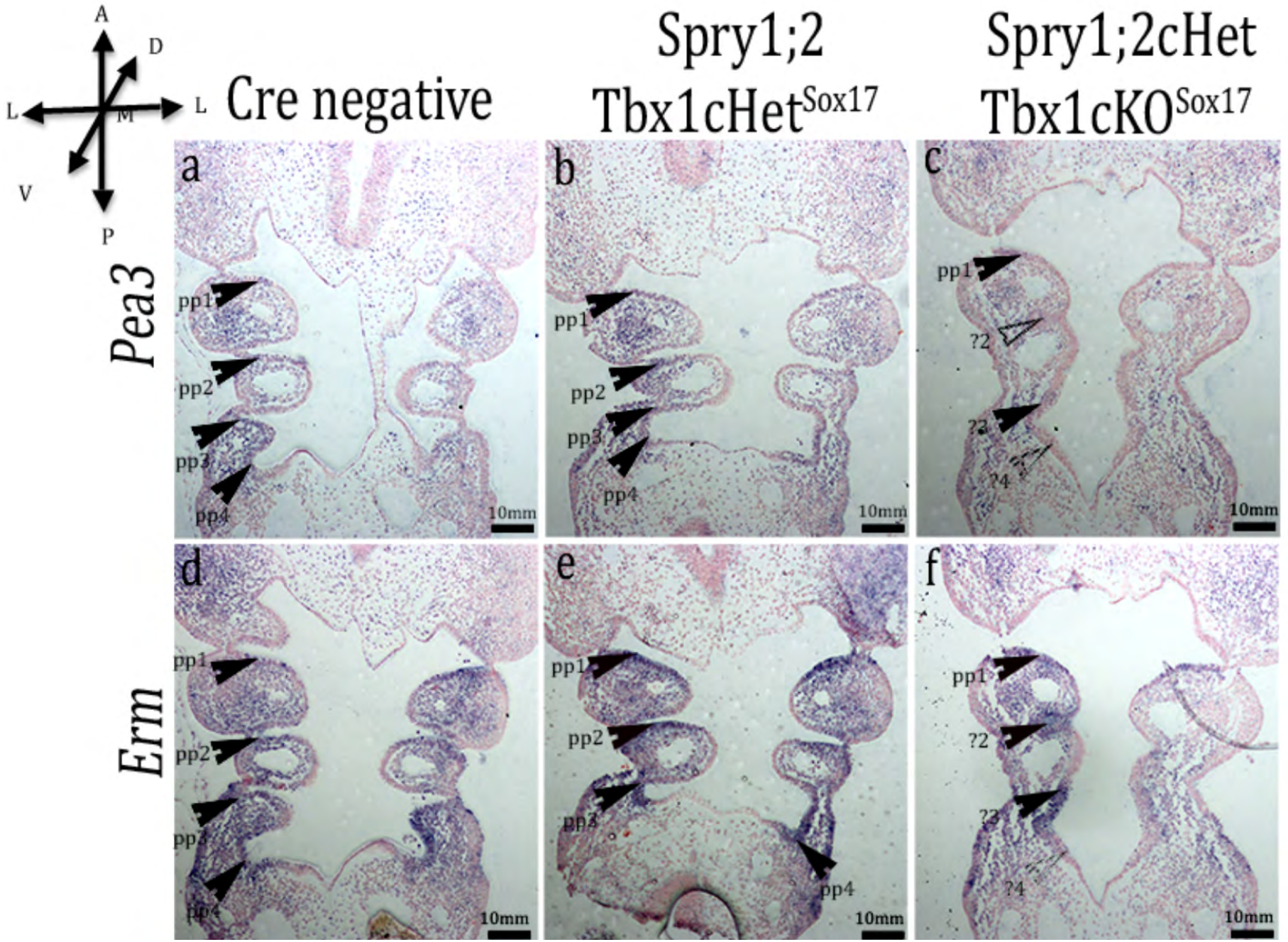
A
D
L
M
L
V
P
Cre negative
Spry1;2
Tbx1cHetSox17
Spry1;2cHet
Tbx1cKOSox17
Pea3
Erm
a
b
c
d
e
f
pp1
pp2
pp3
pp4
?2
?3
?4
10mm

Fig 43: The expression pattern of *Ets* genes *Pea3* and *Erm* is relatively segmented despite the un-segmented morphology of the endoderm of *Spry1;Spry2cHet;Tbx1cKO*^{Sox17} embryos. *In situ* hybridization for *Pea3* (a-c) and *Erm* (d-f) on frontal sections of E9.25 Cre negative (a and d) Spry1;2;*Tbx1cHet*^{Sox17} (b and e) and *Spry1;Spry2cHet;Tbx1cKO*^{Sox17} (c and f) embryos pharyngeal apparatus reveals that, surprisingly, FGF signalling is relatively segmented when endoderm that is devoid of *Tbx1* is also deficient in *Spry1* and *Spry2* expression. Arrowheads indicate the maintenance of FGF signalling within the endoderm. Annotations: Black arrowhead = endodermal pouch expression, unfilled arrowhead = reduced/no endodermal pouch expression, pp = pharyngeal pouch, ? = presumptive pouch. Arrows to the left of Fig 43 illustrate the orientation of the pharyngeal apparatus sections; A = anterior, P = posterior, L = lateral, M = medial, V= ventral, D = dorsal. N=1

Fig 44: *Fgf8* expression is absent from the endoderm of *R1;R2cKO*^{Sox17} embryos. *Fgf8* expression assessed by *in situ* hybridisation in frontal sections of E9.25 embryo's pharyngeal apparatus. (a and a') Cre negative embryos show robust *Fgf8* expression in both the pharyngeal ectoderm, mesenchyme and endoderm. In contrast *Fgf8* expression is absent from the endoderm of *R1;R2cKOSox17* embryos but is maintained in the ectoderm and mesenchyme. Annotations: Black arrowhead = endodermal pouch expression, unfilled arrowhead = no endodermal pouch expression, light blue arrowhead = ectodermal expression, green arrowhead = mesenchymal expression, pp = pharyngeal pouch,? = presumptive pouch, ecto = ectodermal, mesen = mesenchyme. Arrows to the left of Fig 43 illustrate the orientation of the pharyngeal apparatus sections; A = anterior, P = posterior, L = lateral, M = medial, V= ventral, D = dorsal. N=2

Fig 44

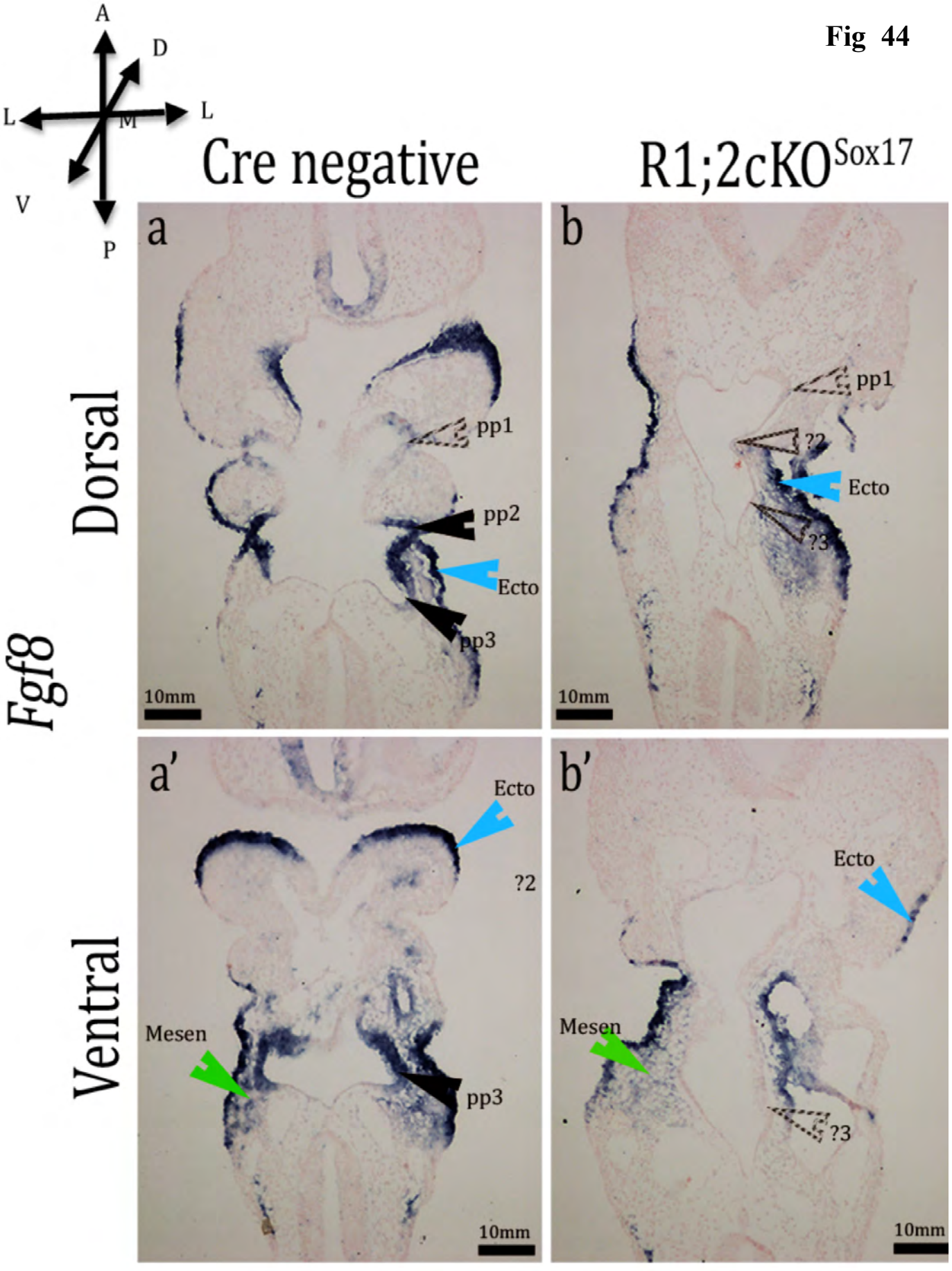
A
D
L
M
L
V
P
Cre negative
R1;2cKO Sox17
Fgf8
Dorsal
Ventral
a
b
a'
b'
pp1
pp2
Ecto
pp3
?2
?3
Mesen
10mm

5.4 DISCUSSION

A thorough analysis of pharyngeal pouch development in a range of conditional FGF mutants has revealed that FGF signalling is required in the endoderm for pharyngeal pouch morphogenesis to proceed normally. Functional redundancy amongst FGF ligands and FGF receptors appears to ensure that FGF signalling is maintained within the endoderm during pouch development.

5.4.1. Functional redundancy of FGF ligands and FGF receptors in the endoderm regulates pharyngeal pouch evagination

Pouch morphogenesis occurs normally in *Fgf8*-deficient endoderm, however, (unlike *Tbx1*-deficeint endoderm), rostral pouch fusion manifests in endoderm deficient of *Fgf8* and *Fgf3* expression. This data indicates that FGF3 and FGF8 function redundantly within the pharyngeal endoderm during rostral pouch morphogenesis. Functional redundancy between FGF3 and FGF8 ligands has been demonstrated in many developmental contexts, for instance: in the formation and patterning of the otic vesicle and hindbrain and during the induction of the three epibranchial placodes (Maroon et al., 2002; Walshe et al., 2002; Nechiporuk et al., 2005). Of most significance to this thesis is the observation that FGF3 and FGF8 act redundantly during zebrafish pouch morphogenesis. Variably penetrant and expressive pouch defects manifest in *fgf8*$^{-}$ zebrafish mutants (Crump et al., 2004). Inhibiting the expression of *fgf3* in *fgf8*$^{-}$ zebrafish (*fgf8*$^{-}$*;fgf3*-MO embryos) increases the severity of pharyngeal pouch defects, for, no pharyngeal pouches are able to form in the *fgf8*$^{-}$*;fgf3*-MO embryos (Crump et al., 2004).

However, in contrast to the zebrafish *fgf8*$^{-}$*;fgf3*-MO mutants, the penetrance of pouch defects in *F3;F8cKO*^{SOX17} embryos is variable. This data suggests that either;

a) *Multiple FGF ligands in the endoderm function to maintain pouch evagination*. Endodermal expression domains of *Fgf15* and *Fgf4* both overlap with *Fgf3* and *Fgf8,* highlighting these ligands as additional candidates that may function during pouch morphogenesis (Dracker and Goldfarb, 1993).

b) *FGF ligands in adjacent (non-endodermal) PA tissue may be able to maintain pouch evagination.*

This is thought to be the case in *fgf8*$^{-}$*;fgf3*-MO zebrafish mutants whose pouch outgrowth was surprisingly rescued by a combination of neural and mesodermal 'wild type' cells, rather than by transplantation of 'wild type' endodermal cells (Crump et al., 2004). To determine which tissue-specific source of *Fgf3* and *Fgf8* is **sufficient** to drive pouch morphogenesis requires an analysis of pouch formation in embryos null for *Fgf3* and hypomorphic for *Fgf8* that have had *Fgf3* and *Fgf8* expression re-activated in one tissue type, such as the endoderm. This type of experiment is required before it can be conclusively determined which tissue source of *Fgf3* and *Fgf8* is essential for pouch morphogenesis.

c) FGF signalling in adjacent (non-endodermal) tissues in the PA may be capable of maintaining pharyngeal pouch evagination.

The absence of pouch defects in embryos that lack *Fgfr1* and *Fgfr2* in CNCC or in mesodermal cells, (as determined by this thesis), suggests that this is not the case. The absence of pouch defects in the R1;R2cKO^{Wnt1} embryos is consistent with data

which demonstrated that CNCC specific deletions of *Fgfr1* do not cause pouch defects and that the reactivation of *Fgfr1* in the CNCC of *Fgfr1* hypomorphs is not sufficient to rescue the pouch fusion (Trokovic et al., 2003). Trokovic et al. proposed that the loss an ectodermal signalling centre was the cause of 2nd arch hypoplasia (and thus likely rostral pouch fusion) in *Fgfr1* hypomorphs (Trokovic et al., 2003; Trokovic et al., 2005). Regrettably an assessment of the requirement for *Fgfr1* and *Fgfr2* in the ectoderm during pouch and arch formation was not tested. This could have been achieved by the generation of Ap2alpha$^{Cre/+}$;Fgfr1$^{flox/-}$;Fgfr2$^{flox/-}$ embryos. Incidentally, however, the maintenance of FGF signalling within the ectoderm of *R1;R2cKO^{Sox17}* embryos is not sufficient to maintain pouch morphogenesis in *Fgfr1;Fgfr2*-deficient pharyngeal endoderm.

In contrast, the deletion of *Fgfr1* and *Fgfr2* from the endoderm during embryogenesis is sufficient to recapitulate the fully penetrant, bilateral rostral pouch fusion, observed in *Fgfr1* hypomorphs. The pouch defects of the *R1;R2cKO^{Sox17}* embryos are due to the loss of FGF signalling specifically from the endoderm, (as determined from the observed loss of FGF signalling effector expression in this tissue). This data suggests that FGF signalling is specifically required within the endoderm during pharyngeal pouch morphogenesis.

5.4.2 Rostral pouch evagination appears more sensitive to reductions in the level of endodermal FGF signalling than caudal pouch evagination

Bilateral fusion of the rostral pouches and 2nd arch hypoplasia are evident in *F3;8cKO^{Sox17}*, *R1cKO;R2cHet^{Sox17}* and *R1;R2cKO^{Sox17}* embryos and *Fgfr1* hypomorphs.

Interestingly, the compound deletion of *Fgfr1* and *Fgfr2* from the endoderm also results in 3rd pouch hypoplasia. This observation suggests that caudal pouch development is less susceptible to reductions in the level of FGF signalling than rostral pouch development. It is unclear why the rostral apparatus is highly sensitive to the loss of FGF signalling. The caudal PA gives rise to structures that are essential for postnatal viability including; the 3rd- 6th PAA that give rise to the thoracic vessels of the heart, CNCC that migrate through the caudal PA to form the cushions of the aortic sac and the 3rd pouch from which the thymus and parathyroid are derived (Hiruma et al., 2002; Blackburn and Manley, 2004; Vincentz et al., 2005). It is tempting to speculate that functional redundancy between *Fgfr1* and *Fgfr2* in the caudal endoderm exists to ensure the correct formation of these postnatal structures. Supporting this inference is the observation that thymus aplasia presents in *R1cKO;R2cHet*^{Sox17} and *R1cHet;R2cKO*^{Sox17} embryos but has not reported in *Fgfr1* hypomorphs (Trokovic et al., 2003; Trokovic et al., 2005). On the other hand, thymus aplasia may manifest in compound endodermal FGF receptor mutants because FGF signalling downstream of FGFR2 in the endoderm is required for the organogenesis of these organs. Supporting this view is the observation that *Fgfr2*$_{IIIb}$ null mice develop thymus and cardiac defects (Dooley et al., 2007).

5.4.3 CNCC migration and differentiation is perturbed by the loss of FGF signalling from the endoderm

The 2nd arch hypoplasia in *Fgfr1* hypomorphs and *Fgfr1*$^{\Delta Frs/\Delta Frs}$ embryos is attributed to a loss of CNCC migration and survival (Trokovic et al., 2003; Hoch and Soriano, 2006). For instance, the hypoplastic 2nd arch of *Fgfr1*$^{\Delta Frs/\Delta Frs}$ mutants is

completely devoid of *Sox10* expressing CNCC. This CNCC defect is correlated with an increase in cell death and a decrease in proliferation in the 2nd arch of the *Fgfr1*$^{\Delta Frs/\Delta Frs}$ embryos (Hoch and Soriano, 2006). Interestingly, although the 2nd arch is hypoplastic in the *R1;R2cKO*^{Sox17} embryos, similar CNCC defects were not observed in these mutants. For, *R1;R2cKO*^{Sox17} embryos appear to have a reduction in the amount of *Dlx2* expressing CNCC in the proximal aspect of their 2nd arch, rather than a complete loss of CNCC specific markers. Thus, the lack of CNCC infiltration into the 2nd arch of *Fgfr1* hypomorphs and *Fgfr1*$^{\Delta Frs/\Delta Frs}$ embryos may be due to the loss of ectodermal FGF signalling, (or indeed due to a loss of FGF signalling from both pharyngeal epithelia), rather than from the endoderm alone.

CNCC infiltration is also reduced in *Sox3* null embryos (*Sox3*$^{-/-}$) that also display 2nd arch hypoplasia (Rizzoti and Lovell-Badge, 2007). *Sox3*, like *Fgfr1* and *Fgfr*2, is expressed in both pharyngeal epithelia and the loss of *Sox3* perturbs the formation of the rostral pouches. Rizzoti et al. predict that it is the perturbed morphology of the *Sox3*$^{-/-}$ embryo's 2nd pouch that restricts the amount of CNCC migration into the 2nd arch (Rizzoti and Lovell-Badge, 2007). It is possible that the fused morphology of the *R1;R2cKO*^{Sox17} mutants rostral pouches may be restricting the amount of late-migrating CNCC that are able to enter the 2nd arch. The ectopic region of cell death visible in and around the otic vesicle of the *R1;R2cKO*^{Sox17} embryo may represent misrouted CNCC destined for the 2nd arch. Although *Dlx2* expressing CNCCs are not detected in/around the otic vesicle, double staining for alternative CNCC markers i.e. *Crabp1* and Caspase antigens, or, otic cell markers and Caspase antigens would be necessary to confirm the identity of these dying cells. FGF signalling from the endoderm also appears to be required for the maintenance of *Hox* gene expression in the caudal CNCC-derived mesenchyme. It is interesting to note that the loss of

Hoxb1 from the endoderm of *R1;R2cKO*^{Sox17} embryos correlates with a loss of *Hoxb1* expression in the mesenchyme, whereas the loss of *Hoxa2* from the inter-pouch endoderm covering the 2nd arch does not affect the maintenance *Hoxa2* expression in the adjacent mesenchyme. This data fits with the observation that regions of endoderm with distinct signalling profiles are able to direct and/or influence the development of the CNCC, for instance into visceral skeleton (Couly et al., 2002). It is possible that domains of FGF signalling within the pouch endoderm, rather than the inter-pouch endoderm, may be required to form a permissive environment for CNCC differentiation.

5.4.4 TBX1 and FGF signalling appear to function in parallel pathways within the endoderm during pharyngeal pouch morphogenesis

Literature suggests that TBX1 is able to positively regulate FGF signalling. However, in Chapter 3 it was observed that FGF signalling is maintained in the endoderm of *Tbx1cKO*^{Sox17} embryos. The following two hypotheses aim to resolve this dichotomy:

1) FGF signalling **is** reduced in *Tbx1cKO*^{Sox17} embryos but the reduction cannot be detected by *in situ* hybridisation
2) FGF signalling is not regulated in a TBX1 dependent manner within the endoderm during pouch morphogenesis

It was reasoned that increasing FGF signalling (by reducing *Sprouty* expression, a negative regulator of FGF signalling) in *Tbx1*-deficient endoderm would test these hypotheses. If caudal pouches formed in *Spry1;Spry2cHet;Tbx1cKO*^{Sox17} embryos it

would support hypothesis (1); that a specific level of FGF signalling maintained by TBX1 is required for caudal pouch formation. Alternatively, if the pouch phenotype of *Spry1;Spry2cHet;Tbx1cKO*^{Sox17} and *Tbx1cKO*^{Sox17} embryos was identical, this would support hypothesis (2). The caudal pouches of *Spry1;Spry2cHet;Tbx1cKO*^{Sox17} embryos are aplastic; however, the expression of *Erm* within the un-segmented endoderm appears patterned, unlike the expression of *Erm* in *Tbx1cKO*^{Sox17} embryos. The finding that caudal pouch formation does not manifest in *Spry1;Spry2cHet;Tbx1cKO*^{Sox17} embryos suggests that FGF signalling is unlikely to function downstream of TBX1 in the endoderm during pouch outgrowth. This inference is supported by the observation that *R1;R2cKO*^{Sox17} embryos and *Tbx1cKO*^{Sox17} embryos have distinct pouch phenotypes (see Table 7), indicative of TBX1 and FGF signalling having unique roles in the endoderm during caudal pouch formation. On the other hand, the partial rescue in the pattern of FGF signalling expression within the pharyngeal endoderm of *Spry1;Spry2cHet;Tbx1cKO*^{Sox17} embryos suggests that that TBX1 and FGF signalling may interact in parallel pathways to control pouch outgrowth.

A recent paper by Simrick et al. demonstrated that the interaction between TBX1 and FGF signalling may not be linear. When one allele of *Tbx1* is deleted from all tissues in a *Spry1;2*$^{+/-}$ or *Spry1;2*$^{-/-}$ embryo, *Erm* expression (normally decreased in *Tbx1*$^{+/-}$ embryos) is up-regulated (Simrick et al., 2012). Surprisingly, in an endoderm-specific context, the loss of one allele of both *Sprouty1* and *Sprouty2* in a *Tbx1* null background appears to normalise *Erm* expression in this tissue. This data supports the inference of Simrick et al., that the interaction between TBX1 and FGF signalling is not linear and adds an extra layer of complexity to the mechanism of this interaction.

If FGF signalling is not directly regulated by TBX1 during pouch formation, which signalling cascades or cellular mechanisms could TBX1 be affecting in the endoderm to drive pouch morphogenesis? This question was addressed in Chapter 6.

Chapter 6

Results Part IV

6.1 TBX1 may regulate pouch morphogenesis in the endoderm independently from its effects on FGF signalling

The data presented so far suggests that TBX1 and FGF signalling are both required in the endoderm for the process of pharyngeal pouch morphogenesis. However, the loss of TBX1 or FGF signalling from the endoderm has a different effect on the formation of the pharyngeal pouches. Deletion of *Tbx1* from the endoderm prevents the initiation of caudal pouch outgrowth, whereas the loss of FGF signalling from the endoderm results in rostral pouch fusion and caudal pouch hypoplasia. These data indicates that TBX1 in the endoderm may regulate pouch morphogenesis independently from its effects on FGF signalling. The next aim of this study was to identify a TBX1-dependent regulator of pouch morphogenesis. The first part of this chapter focuses on signalling cascades that may be transcriptional targets of TBX1, such as the RA signalling pathway. The second part of this chapter focuses on how deletion of *Tbx1* from the endoderm may affect the endoderm at the cellular level by altering its proliferation or proteins associated with the cells architecture.

6.2 Loss of endodermal *Tbx1* affects the expression of genes in signalling pathways predicted to act up and down stream of *Tbx1* expression

Retinoic acid (RA), the active form of Vitamin A, is a small lipophilic molecule that if absent, or present in excess, during embryogenesis can affect the formation of

the pharyngeal pouches. Caudal pouch aplasia similar to that exhibited in *Tbx1cKO*^{Sox17} embryos, manifests in embryos that lack, or have increased, RA signalling (Wendling et al., 2000; Niederreither et al., 2003; Roberts et al., 2005; Roberts et al., 2006). Data in the literature demonstrates that there is a reciprocal inhibition of *Tbx1* expression and RA signalling during development. Retinol-soaked beads grafted into the pharyngeal pouches of quail embryos results in a decrease in the level of *Tbx1* expression around the bead and Vitamin A Deficient (VAD) quails lack *Tbx1* expression (Quinlan et al., 2002). Conversely, the expression of *Raldh2* (an enzyme that synthesises RA) is extended anteriorly in the PA of *Tbx1*$^{-/-}$ embryos. The latter coincides with a loss in expression of the catabolic enzymes *Cyp26a1, Cyp26b1* and *Cyp26c1* which function to clear RA (Niederreither et al., 2003). However, Roberts et al. demonstrated that in cell culture the application of exogenous RA did not elicit an immediate inhibition of *Tbx1* expression (Roberts et al., 2005). Moreover, *Tbx1* expression was only partially repressed in embryos exposed to a drug that inhibits expression of the *Cyp26* genes (Roberts et al., 2006). These data indicate that the interaction between TBX1 and RA during pouch morphogenesis may be more complex than a direct reciprocal inhibition, which is further highlighted by the complex interaction between *Tbx1,* RA and *Hox* genes during PA development.

RA is able to regulate the expression of a number of *Hox* genes, including *Hoxb1* and *Hoxa2* (Guris et al., 2006; Diman et al., 2011). In the case of *Hoxb1* expression, regulation by RA is likely to be direct, by virtue of the *Hoxb1* retinoic acid responsive enhancer (Langston et al., 1997). Reducing the level of RA during embryonic development results in a loss or reduction in *Hoxb1* expression in the caudal PA (Wendling et al., 2000; Vermot et al., 2003) Conversely, embryos treated

with a specific *Cyp26* inhibitor (R115866) display expanded domains of *Raldh2* expression, indicative of increased RA levels, and a reciprocal expansion of *Hoxb1* (Roberts et al., 2006). Similarly, *Hoxa2* expression is induced in NCC cultures exposed to exogenous RA and in the pharyngeal endoderm of embryos implanted with RA-soaked beads (Bayha et al., 2009; Ishikawa and Ito, 2009).

The relationship between *Tbx1,* RA and *Hox* gene expression is complex and varies depending on the specific member of the *Hox* family and the tissue being analysed. Despite the elevated levels of RA in *Tbx1*$^{-/-}$ embryos and the sensitivity of the *Hoxa3* promoter to RA, *Hoxa3* expression is not altered in the PA of *Tbx1*$^{-/-}$ embryos (Ivins et al., 2005). Moreover, the expression of *Hoxa2* is reduced in the 2nd pharyngeal arch of *Tbx1*$^{-/-}$ embryos, despite the observation that RA signalling is expanded into the rostral PA of these mutants (Guris et al., 2006; Aggarwal et al., 2010). In contrast, the expansion of RA signalling results in a corresponding expansion of *Hoxb1* in the PA expression whether the former occurs as a result of *Tbx1* deletion, or, due to the application of exogenous RA (Guris et al., 2006; Bayha et al., 2009).

In contrast, SONIC HEDGEHOG (SHH) has been demonstrated to act upstream of *Tbx1*, regulating its expression via Forkhead transcription factor (*Foxa2*) (Garg et al., 2001; Yamagishi et al., 2003). However, whether this interaction is relevant to pouch morphogenesis is questionable. The deletion of either *Tbx1* or *Shh* during embryogenesis generates pouch defects, yet the defects are distinct, respectively having the most severe affects on either caudal or rostral pouch morphogenesis (see section 1.9.2 for a more detailed explanation) (Jerome and Papaioannou, 2001; Moore-Scott and Manley, 2005). The dorsal-ventral patterning of the 3rd

pouch is thought to be established, in part, by the opposing effects of *Shh* and *Bmp4* mediated signals (Moore-Scott and Manley, 2005). In E10.5 *Shh*$^{-/-}$ embryos the expression of *Bmp4* is expanded in the 3rd pouch. A consequence of the expanded *Bmp4* expression domain is that the 3rd pouch is no longer able to maintain expression of the presumptive parathyroid marker, *Gcm2* (Moore-Scott and Manley, 2005).

Bmp4 is expressed within the pharyngeal endoderm and mesenchyme during pouch morphogenesis (Patel et al., 2006). A tissue-specific requirement for *Bmp4* within the endoderm during pouch morphogenesis has not yet been reported (Liu et al., 2004; Gordon et al., 2010). However, *Bmp4* is required in the pharyngeal epithelia for the correct morphogenesis and migration of endocrine glands that are derived from the pharyngeal endoderm (Gordon et al., 2010). Loss of *Tbx1* from all pharyngeal tissues results in a proximal shift of the *Bmp4* expression domain in the 1st arch ectoderm, where it reciprocally restricts the domain of *Fgf8* expression (Aggarwal et al., 2010). Whether *Bmp4* expression domains in the caudal apparatus are shifted or lost in response to a loss of *Tbx1* expression has not been determined.

6.2.1 Deletion of *Tbx1* from the endoderm affects the endodermal expression of genes in the RA signalling pathway but not the RA targets *Hoxb1* and *Hoxa2*

To assess the interaction of *Tbx1* and RA signalling in the endoderm, expression of genes in the RA pathway and their targets were compared between *Tbx1cKO*^{Sox17} and control embryos.

6.2.1.1 *Rarb* expression is expanded anteriorly in the endoderm of *Tbx1cKO^{Sox17}* embryos, despite the maintained mesenchymal expression domain of *Raldh2*

The expansion and up-regulation of RA signalling in the PA of *Tbx1$^{-/-}$* embryos is proposed by Guris et al. to account for the un-segmented morphology of this structure (Guris et al., 2006). It was hypothesised that the deletion of *Tbx1* from the endoderm would result in a tissue-specific disruption of retinoid homeostasis, which may account for the loss of caudal pouch morphogenesis in *Tbx1cKO^{Sox17}* embryos. To investigate whether the synthesis of RA is altered in *Tbx1cKO^{Sox17}* embryos, the expression of *Raldh2* was analysed by *in situ* hybridization performed on mutant and control PA sections. RALDH2 catalyses synthesis of RA by the oxidation of retinaldehyde. As this oxidative step is irreversible any changes to the level of *Raldh2* expression will be reflected in the amount of RA produced (Kam et al., 2012). *Raldh2* expression is limited to the very caudal mesenchyme only, just caudal to the forming 3rd pouch (green arrowhead on Fig 45 panel a identifies the anterior limit of *Raldh2* in the mesenchyme in Cre negative embryos). The pharyngeal endoderm is absent of *Raldh2* expression. In *Tbx1cKO^{Sox17}* embryos the level and pattern of *Raldh2* expression in the mesenchyme is identical to that observed in Cre negative embryos (Figure 45 compare panel b to panel a, green arrows depict the anterior limit of *Raldh2* expression in the mesenchyme). It is significant to note that there is no extension to the anterior limit of *Raldh2* expression domain in the un-segmented mesenchyme of *Tbx1cKO^{Sox17}* embryos.

For active RA signalling to occur, retinol, synthesised by *Raldh2*, must bind to one of its receptor targets, such as *Rarb*. High levels of *Rarb* expression are detected in the caudal PA at E9.5. In particular, robust endodermal *Rarb* expression is detected in the evaginating 3rd pouch, proximal to the domain of mesenchymal *Raldh2* expression (Fig 45, compare endodermal expression of *Rarb* in panels c to mesenchymal *Raldh2* expression in panel a). Active RA signalling indicated by the expression of *Rarb* is extended throughout *Tbx1*-devoid endoderm (Fig 45, panel d). In addition the level of *Rarb* expression in the rostral endoderm is significantly increased, (Fig 45, compare the two posterior unfilled arrows in panel c with the 2 posterior black arrows in panel d). In keeping with the endoderm-specific deletion of *Tbx1*, there is no change to the mesenchymal domain of *Rarb* expression (Fig 45, compare the rostral limit of mesenchymal expression in panels c and d marked by green arrows).

Fig 45

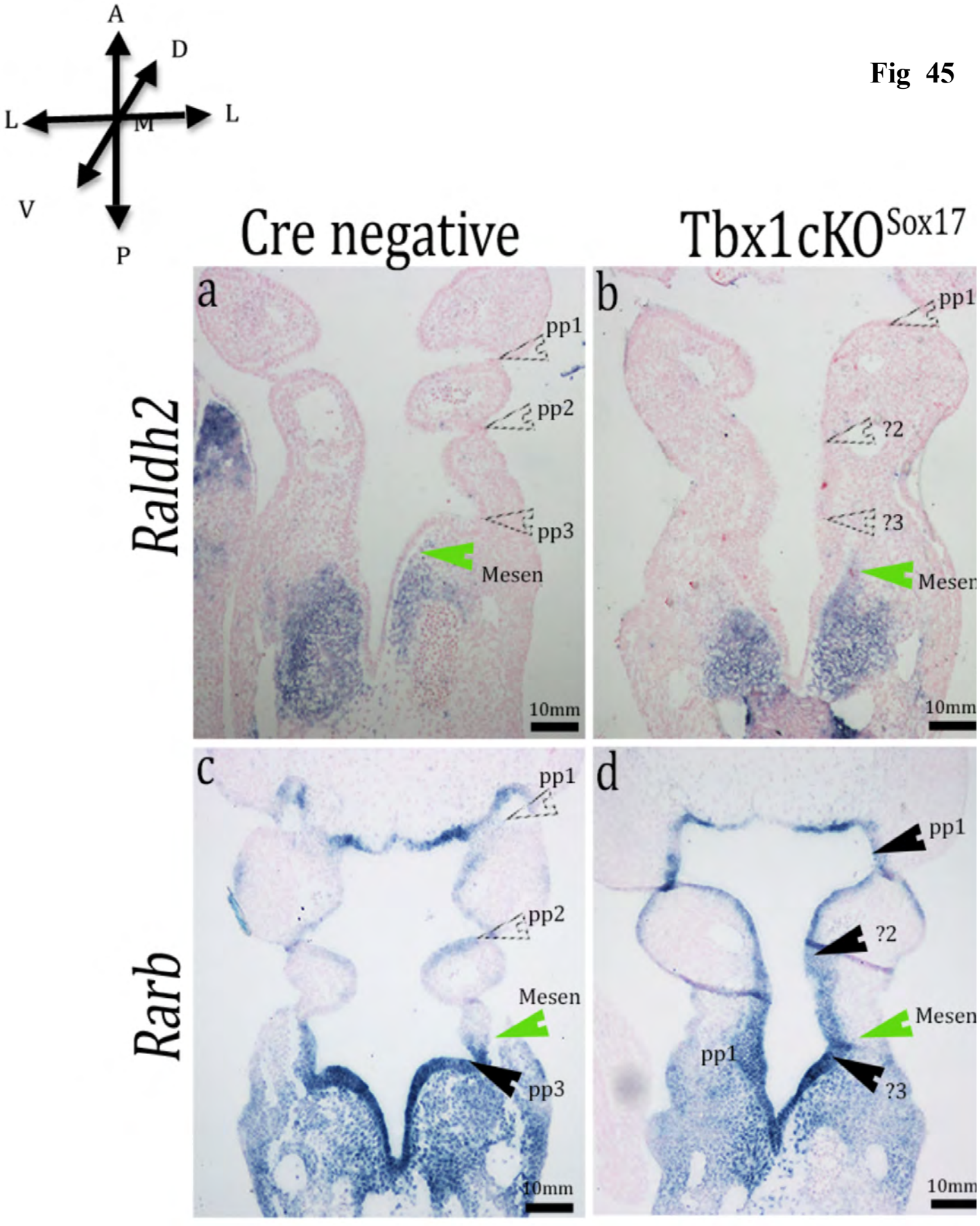
A
D
L
M
L
V
P
Cre negative
Tbx1cKOSox17
Raldh2
Rarb
a
b
c
d
pp1
pp2
pp3
?2
?3
Mesen
10mm

Fig 45: *Tbx1cKO*^{Sox17} embryos display an anterior expansion of active RA signalling in the pharyngeal endoderm. Frontal sections of E9.5 embryo's pharyngeal apparatus show *Raldh2* (a and b), and *Rarb* (c and d) expression, detected by *in situ* hybridization. The rostral limit of mesenchymal *Raldh2* and *Rarb* expression is unchanged in *Tbx1cKO*^{Sox17} embryos (compare expression limits marked by green arrowheads in panels a-d). In contrast, *Rarb* expression is expanded anteriorly throughout the entire pharyngeal endoderm of *Tbx1cKO*^{Sox17} embryos (panel c vs d). Note the level of rostral *Rarb* expression in the mutant is elevated (anterior black arrowheads in d vs unfilled arrowhead in c) but the extent of mesenchymal *Rarb* expression is unchanged (green arrowheads). N=2 for each gene analysed by *in situ* hybridisation.
Annotations: Black arrowhead = endodermal pouch expression, green arrowhead = mesenchymal PA expression, unfilled arrowhead = endodermal pouch with no expression, pp = pharyngeal pouch, ? = presumptive pouch. Arrows to the left of Fig 45 illustrate the orientation of the pharyngeal apparatus sections; A = anterior, P = posterior, L = lateral, M = medial, V= ventral, D = dorsal.

6.2.2.2 *Cyp26* genes are maintained in *Tbx1cKO^{Sox17}* embryos pharyngeal endoderm

The expansion of RA signalling throughout the endoderm of *Tbx1cKO^{Sox17}* embryos cannot be explained by changes in the extent of RALDH2 mediated RA synthesis. An alternative possibility is that the loss of *Tbx1* in the endoderm results in a reciprocal down-regulation, or loss, of RA catabolisers (mediated by the *Cyp26* genes), as is observed in *Tbx1$^{-/-}$* embryos (Guris et al., 2006; Roberts et al., 2006).

Cyp26c1 is restricted to the 1st pouch of the PA and diffusely within the mesenchyme rostral to the 1st arch. Considering the 1st pouch forms in *Tbx1cKO^{Sox17}* embryos, it is perhaps not surprising that *Cyp26c1* expression is maintained here, (Fig 41, compare black arrowheads which indicate endodermal expression of *Cyp26a1* in panels a and b). *Cyp26a1* is expressed diffusely throughout the pharyngeal endoderm and mesenchyme. There appears to be some evidence of *Cyp26a1* enrichment in the inter-pouch regions and in the third pouch and reduced expression in the lateral tip of the first and second pouches (indicated by unfilled arrowheads in panel c), however, this pattern is not clear. Guris et al. and Roberts et al. reported that *Cyp26a1* expression was down regulated in the PA of *Tbx1$^{-/-}$* embryos (Guris et al., 2006; Roberts et al., 2006). In contrast, the expression of *Cyp26a1* appears to be maintained in the endoderm of *Tbx1cKO^{Sox17}* embryos at a level comparable to that of Cre negative embryos, (Fig 46 panels c and d). However, small reductions in *Cyp26a1* expression may not be detected by *in situ* hybridisation. The diffuse pattern of endodermal *Cyp26a1* expression makes it difficult to determine whether the pattern of *Cyp26a1* expression is altered in *Tbx1cKO^{Sox17}* embryos, however this gene may be extended throughout the rostral apparatus (black arrowhead labelled as '?2' in panel d marks the possible

extension of *Cyp26a1* expression in the rostral endoderm of *Tbx1cKO*^{Sox17} embryos).

In contrast to the expression of *Cyp26a1* and *Cyp26c1* (that appear to show little change in the PA of *Tbx1cKO*^{Sox17} embryos), the expression of *Cyp26b1* in *Tbx1cKO*^{Sox17} embryos epithelia is striking (Fig 46, compare panels e and f). *Cyp26b1* expression is normally observed in endodermal domains complementary to the expression of *Rarb.* In contrast, *Cyp26b1* transcripts extended anteriorly in *Tbx1*-deficient endoderm to overlap the ectopic, rostral areas of *Rarb* expression (compare the extent of 'posteriorised' *Rarb* and *Cyp26b1* expression in, respectively, Fig 45 panel d and 46 panel f). Interestingly, the endodermal expansion of *Cyp26b1* is mirrored in the ectoderm of *Tbx1cKO*^{Sox17} embryos (compare the blue brackets marking the ectodermal *Cyp26b1* expression domains in Fig 46 e and f). In addition, the level of *Rarb* and *Cyp26b1* expression in the rostral endoderm appears equivalent to that normally observed in the evaginating 3rd pouch. This observation was surprising because *Cyp26b1* expression was strongly down regulated in the endoderm of *Tbx1*$^{-/-}$ embryos (Roberts et al., 2006).

The observation that genes encoding an enzyme that degrades retinol and a receptor that is responsive to retinol are both expanded anteriorly within the same ectopic expression domain suggests that overall there may be no change in the amount of RA signalling. If RA signalling is not altered in the endoderm of *Tbx1cKO*^{Sox17} embryos there should be no change to the level or pattern of expression of genes targeted by RA signalling, such as the *Hox* genes.

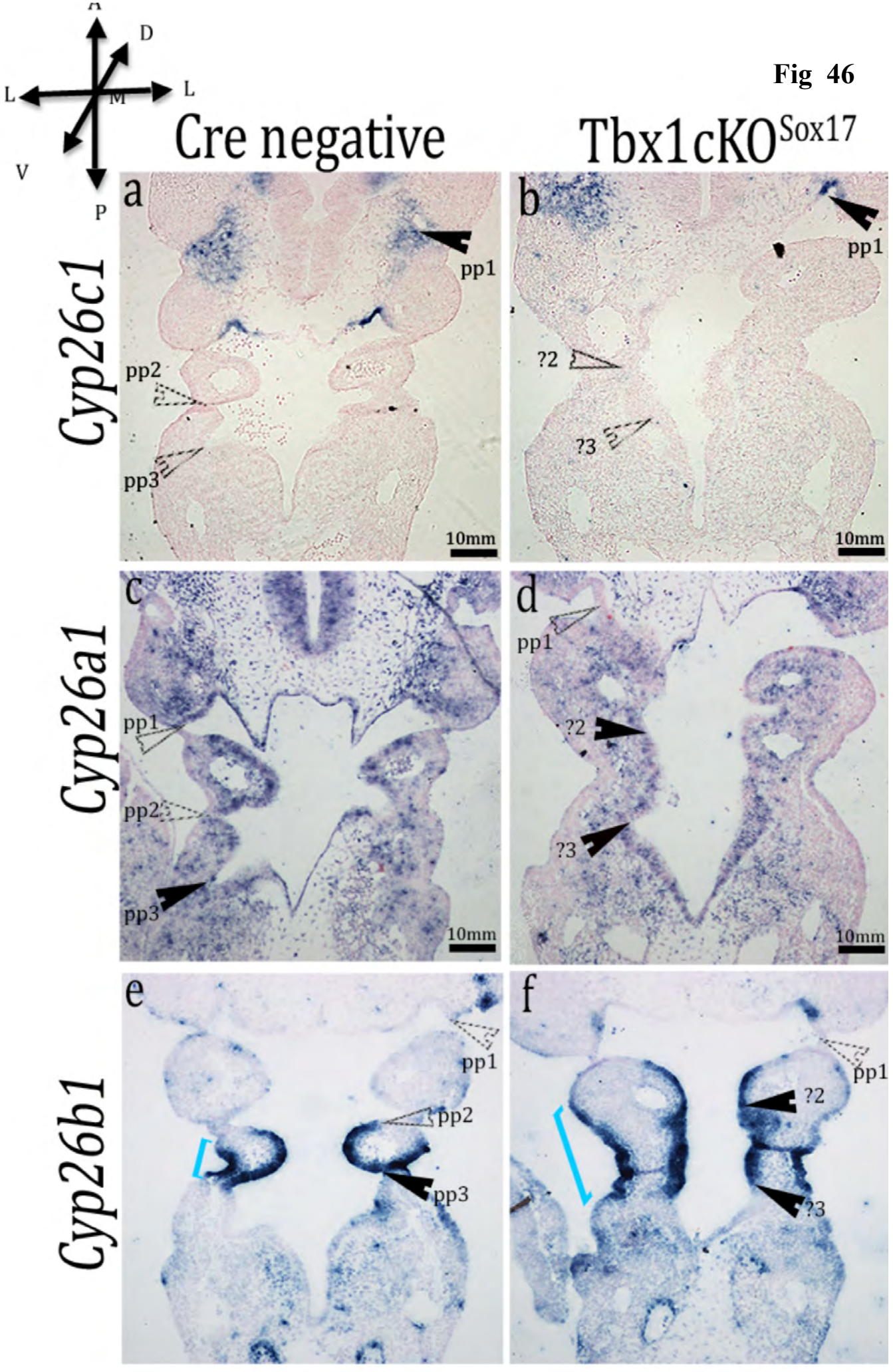
A
D
L
M
L
V
P
Cre negative
Tbx1cKO Sox17
Cyp26c1
Cyp26a1
Cyp26b1
a
b
c
d
e
f
pp1
pp2
pp3
?2
?3
10mm

Fig 46: *Tbx1cKO^{Sox17}* embryos display an anterior expansion of *Cyp26b1* expression that overlaps with the ectopic expression domain of *Rarb*. Frontal sections of E9.5 embryos pharyngeal apparatus show *Cyp26c1* (a-b), *Cyp26a1* (c-d) and *Cyp26b1* (e-f) expression, (as detected by *in situ* hybridization), is maintained in *Tbx1cKO^{Sox17}* embryos. The 1st pouch expression domain of *Cyp26c1* is unchanged in *Tbx1cKO^{Sox17}* embryos, (endodermal expression of *Cyp26c1* in the 1st pouch of Cre negative and *Tbx1cKO^{Sox17}* embryos is respectively indicated by black arrowheads in panels a and b, n = 1). There is no loss of diffuse endodermal *Cyp26a1* expression in the PA of *Tbx1cKO^{Sox17}* embryos, although the expression pattern appears to be partially unsegmented (panels c and d, n = 2). Note the anterior expansion of *Cyp26b1* expression in the pharyngeal epithelia of *Tbx1cKO^{Sox17}* embryos compared to Cre negative embryo (panels e and f, n=2). In panel e the endodermal *Cyp26b1* expression domain is delineated caudally by a black arrowhead and rostrally by an unfilled arrowhead at the level of the 2nd pouch. In panel f, at the level of the 2nd pouch a solid arrowhead highlights the ectopic expression of *Cyp26b1*. Interestingly the endodermal expansion of *Cyp26b1* is mirrored in the ectoderm (compare length of blue brackets marking the ectodermal expression domains of *Cyp26b1* in panels e and f).

Annotations: Black arrowhead = endodermal pouch expression, blue arrowhead = mesenchymal PA expression, unfilled arrowhead = endodermal pouch with no expression, pp = pharyngeal pouch, ? = presumptive pouch, blue brackets = ectodermal expression domain of *Cyp26b1*. Arrows to the left of Fig 46 illustrate the orientation of the pharyngeal apparatus sections; A = anterior, P = posterior, L = lateral, M = medial, V= ventral, D = dorsal.

6.2.2.3 *Hoxb1* and *Hoxa2* gene expression is not altered in the pharyngeal endoderm of *Tbx1cKO^{Sox17}* embryos, despite the observed expansion in RA signalling

At E9.5, *Hoxb1* is expressed in the 3rd pouch endoderm, in the adjacent caudal mesenchyme and caudal ectoderm covering the presumptive 4th arch. In *Tbx1$^{-/-}$* embryos the domain of *Hoxb1* expression is expanded anteriorly (Guris et al., 2006). In contrast, no change is distinguishable between the expression of *Hoxb1* in Cre negative and *Tbx1cKO^{Sox17}* embryos (Fig 47 compare panels a and b). As expected, mesenchymal *Hoxb1* transcripts were restricted to their normal caudal domain in *Tbx1cKO^{Sox17}* embryos, coinciding with the maintenance of RA signalling in this tissue. Surprisingly, no change to the rostral limit of *Hoxb1* expression was observed in the un-segmented endoderm and ectoderm of *Tbx1cKO^{Sox17}* embryos (endodermal expression is identified by black arrowheads and ectodermal expression by blue arrowheads Fig 47 a and b), despite the rostral expansion of *Rarb* expression in these pharyngeal epithelia.

Similarly, *Hoxa2* expression remains unchanged in *Tbx1cKO^{Sox17}* embryos, despite the loss of *Tbx1* and the presumed gain of RA signalling in the mutant's endoderm. In the un-segmented rostral PA of *Tbx1cKO^{Sox17}* embryos a mesenchymal domain of *Hoxa2* expression is maintained in an area equivalent to the 2nd arch of Cre negative embryos, (highlighted by green arrowheads in Fig 47 panels c and d). *Hoxa2* positive cells are also visible in the pharyngeal endoderm of *Tbx1cKO^{Sox17}* embryos at a level equivalent to the inter-pouch region covering the 2nd arch of Cre negative embryos (indicated by grey arrowheads in Fig 47 c' and d'). Again, there appears to be no change to the level of *Hoxa2* expression in this discreet population of *Hoxa2* expression endodermal cells in *Tbx1cKO^{Sox17}* embryos.

The maintenance of discrete domains of *Hox* gene expression in *Tbx1cKO*^{Sox17} embryos endoderm indicates that the level of RA in this epithelium may not be increased. It is possible that the expanded endodermal expression domains of *Rarb* and *Cyp26b1* occur as a secondary consequence of the perturbed endodermal morphology of *Tbx1cKO*^{Sox17} embryos, rather than a direct response to the loss of *Tbx1*. If the former is true then one would expect to detect similar changes to the endodermal expression domains of genes in signalling pathways thought to act upstream of *Tbx1,* in *Tbx1cKO*^{Sox17} embryos.

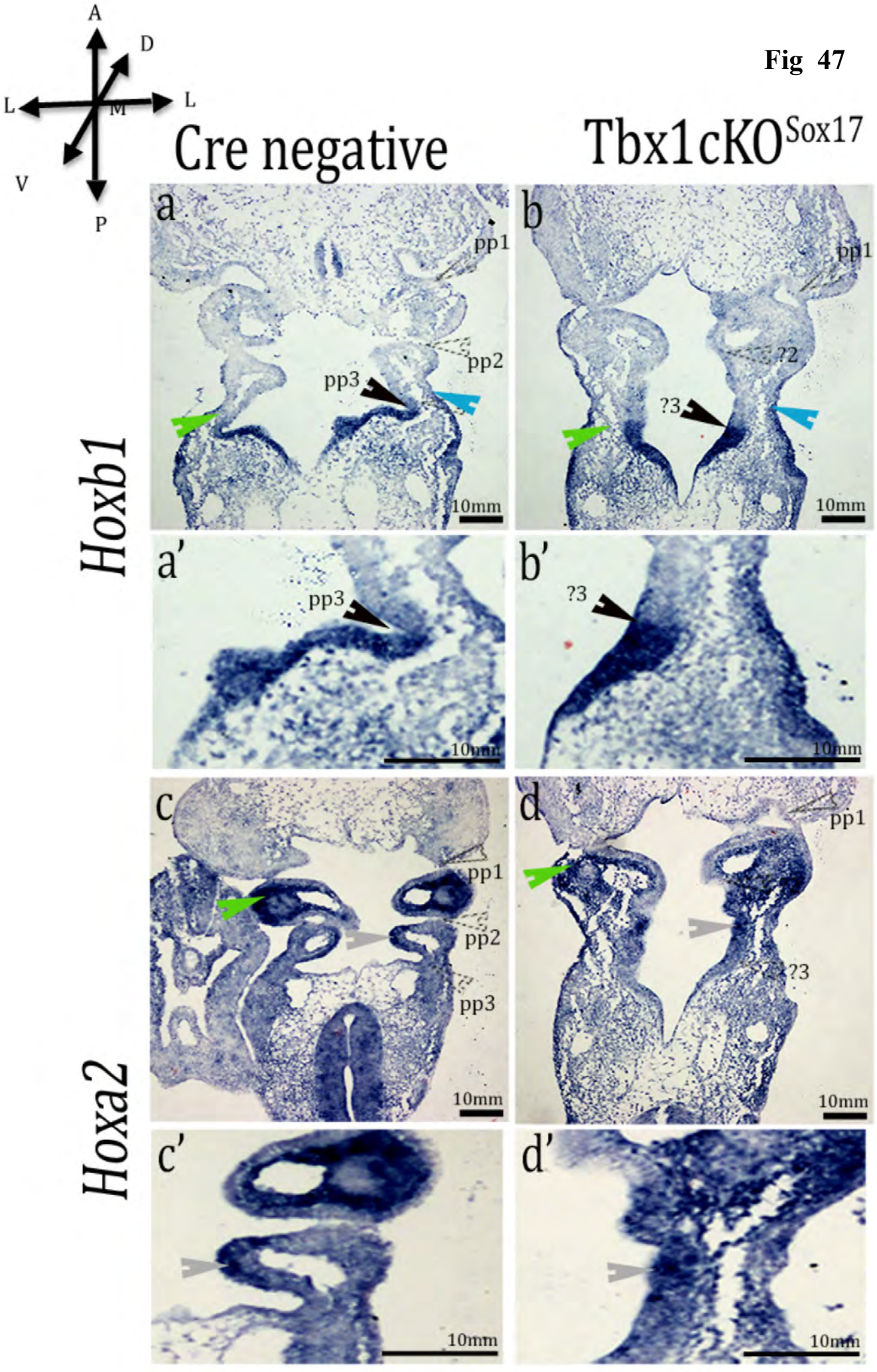
A
D
L
M
L
V
P
Cre negative
Tbx1cKOSox17
Hoxb1
Hoxa2
a
pp1
pp2
pp3
10mm
b
pp1
?2
?3
10mm
a'
pp3
10mm
b'
?3
10mm
c
pp1
pp2
pp3
10mm
d
pp1
?3
10mm
c'
10mm
d'
10mm

Fig 47: *Hox* gene expression domains are not expanded anteriorly in the pharyngeal endoderm of *Tbx1cKO^{Sox17}* embryos. Frontal sections of E9.5 embryos PA show that the RA responsive genes, *Hoxb1* (a-b'), and *Hoxa2* (c-d'), (detected by *in situ* hybridization) do not mimic the expression pattern of *Rarb* in *Tbx1cKO^{Sox17}* embryos. Surprisingly, the discrete endodermal expression domains of *Hoxb1* in the 3rd pouch and *Hoxa2* in the inter-pouch region covering the 3rd arch (marked by black and grey arrowheads in panel b' and panel d', respectively) are maintained in *Tbx1cKO^{Sox17}* embryos. Interestingly, the limits of ectodermal and mesenchymal *Hox* gene expression are also maintained, despite the perturbed morphology of the PA (indicated by green and blue arrowheads, respectively). a'-d' are magnified images of the corresponding embryos shown in a-d. N=2 for each *Hox* gene analysed.

Annotations: Black arrowhead = endodermal pouch expression, light blue arrowhead = ectodermal PA expression, unfilled arrowhead = endodermal pouch with no/little expression, green arrowhead = mesenchyme, pp = pharyngeal pouch, ? = presumptive pouch. Arrows to the left of Fig 47 illustrate the orientation of the pharyngeal apparatus sections; A = anterior, P = posterior, L = lateral, M = medial, V= ventral, D = dorsal.

6.3 Deletion of *Tbx1* from the endoderm affects the endodermal expression of genes in the SHH, but not the BMP pathway

To assess whether an interaction between *Tbx1* and SHH signalling is present in the pharyngeal endoderm during pouch formation, the expression of genes in the SHH cascade were analysed in *Tbx1cKO*^{Sox17} embryos. If SHH signalling acts upstream of *Tbx1* in the endoderm, as the literature suggests, there should be no change to the expression of genes in this cascade. If genes in the SHH signalling cascade are altered in the endoderm of *Tbx1cKO*^{Sox17} embryos this may be indicative of a feedback loop between *Tbx1* and SHH signalling in this tissue. The latter inference would be supported by data showing that genes that interact with SHH, such as *Bmp4*, also have altered expression in *Tbx1* deficient endoderm.

6.3.1 *Shh* expression is expanded in the pharyngeal endoderm of *Tbx1cKO*^{Sox17} embryos

The expression pattern of *Shh* in the pharyngeal endoderm at E9.5 is similar to the expression of *Cyp26b1* (compare Fig 48, panel a, with Fig 46, panel e). *Shh* transcripts in Cre negative embryos are detected in the inter-pouch regions of endoderm that line the medial aspects of the 2nd and 3rd pharyngeal arches (Fig 48 panel a, bracket identifies the *Shh* positive inter-pouch region in the endoderm lining the 2nd arch, unfilled arrowhead mark *Shh* devoid pouch endoderm). In contrast, the expression of *Shh* is expanded in the rostral endoderm of *Tbx1cKO*^{Sox17} particularly at the level of the presumptive 2nd arch. The expansion of the *Shh* expression domain is similar to the altered expression pattern of *Cyp26b1*

observed in the endoderm of *Tbx1cKO*^{Sox17} embryos. This data suggests that *Tbx1* may reciprocally regulate the expression of *Shh* and thus the amount of SHH signalling in the pharyngeal endoderm. Alternatively, the loss of *Shh* negative domains may reflects the loss of pharyngeal endoderm identity in *Tbx1cKO*^{Sox17} embryos.

6.3.2 A reciprocal expansion of the SHH signalling targets *Gli1* and *Ptch1* is observed in *Tbx1*-deficient pharyngeal endoderm

GLI1, a mediator of the SHH pathway, and PTCH1, a feedback inhibitor of the SHH pathway are both transcriptionally induced by SHH signalling. If the expanded *Shh* expression in the pharyngeal endoderm of *Tbx1cKO*^{Sox17} embryos results in an expansion of SHH signalling, this should be reflected in a corresponding expansion of endodermal *Gli1* and *Ptch1*. As predicted, *Gli1* and *Ptch1* transcripts were visible throughout the rostral and caudal aspects of *Tbx1cKO*^{Sox17} embryo's endoderm (Fig 48 panels d and f). Surprisingly *Gli1* and *Ptch1* expression is also slightly expanded in the mesenchyme of *Tbx1cKO*^{Sox17} embryos, suggesting that *Tbx1* in the endoderm may also regulate SHH signalling in adjacent PA tissue.

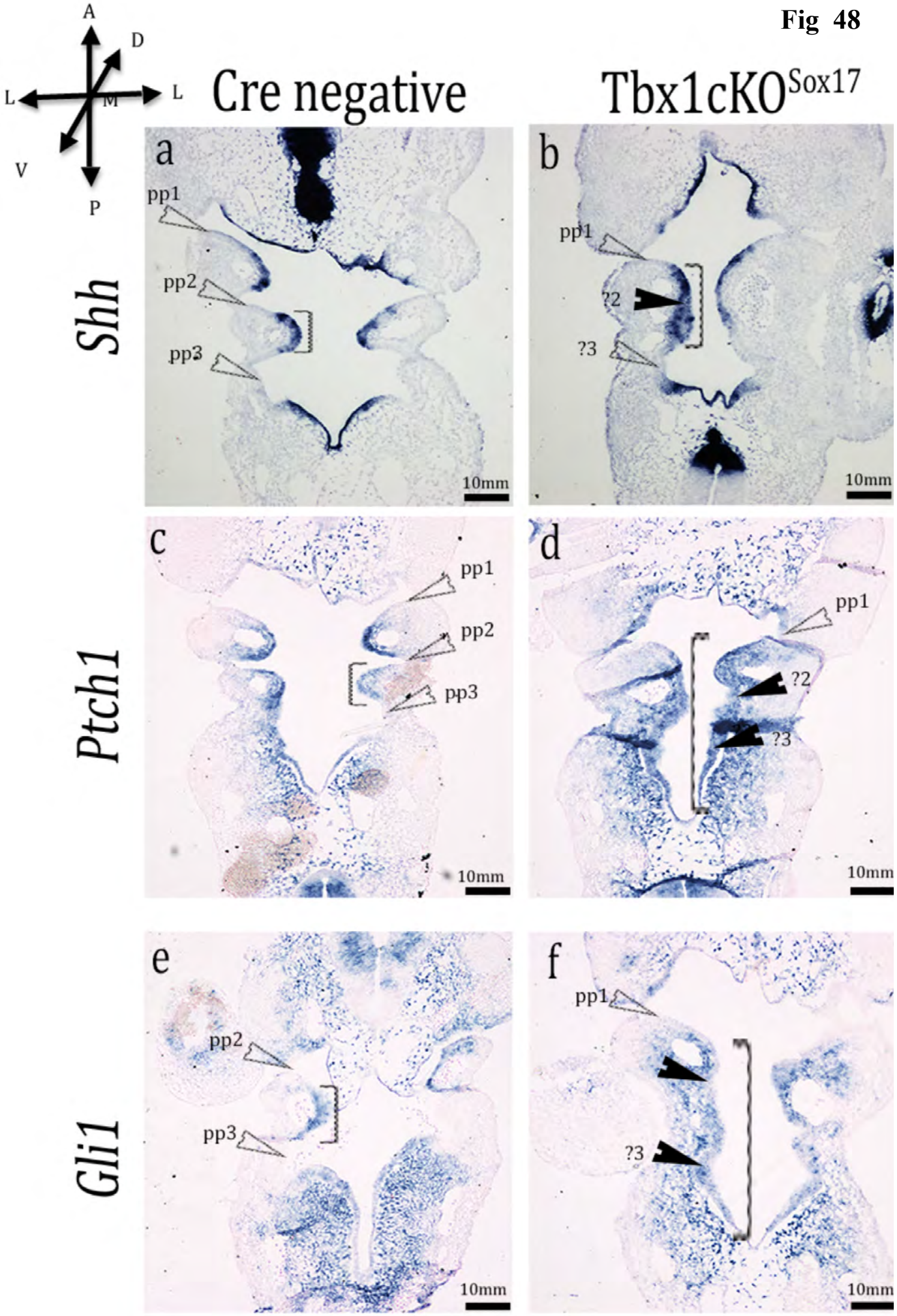
A
D
L
M
L
V
P
Cre negative
Tbx1cKO Sox17
Shh
Ptch1
Gli1
a
b
c
d
e
f
pp1
pp2
pp3
?2
?3
10mm

Fig 48: Expression of genes in the SHH signalling cascade are expanded in the pharyngeal endoderm of *Tbx1cKO^{Sox17}* embryos. Frontal sections of E9.5 embryo's PA show *Shh* (a-b), *Ptch1* (c-d) and *Gli1* (e-f) expression, detected by *in situ* hybridization, is maintained in a perturbed expression pattern in the endoderm of *Tbx1cKO^{Sox17}* embryos. Whilst the expression pattern of *Shh* in *Tbx1cKO^{Sox17}* embryos shows some segmentation (note *Shh* absence in the presumptive 3rd pouch and in the 1st pouch of *Tbx1cKO^{Sox17}* embryos indicated by unfilled arrowheads in panels b), *Gli1* and *Ptch1* are expressed throughout the entire pharyngeal endoderm. Brackets delineate the extent of un-segmented expression in the pharyngeal endoderm of each gene. N=2 for all genes.
Annotations: Black arrowhead = endodermal pouch expression, unfilled arrowhead = endodermal pouch with no expression, pp = pharyngeal pouch, ? = presumptive pouch, brackets identify the domain of endodermal expression of each gene. Arrows to the left of Fig 48 illustrate the orientation of the pharyngeal apparatus sections; A = anterior, P = posterior, L = lateral, M = medial, V= ventral, D = dorsal.

6.3.3 *Bmp4* expression in unchanged in the caudal pharyngeal endoderm of *Tbx1cKO^{Sox17}* embryos

Bmp4 is expanded in the caudal pharyngeal endoderm of *Shh$^{-/-}$* embryos (Moore-Scott and Manley, 2005). If the SHH pathway is expanded in the pharyngeal endoderm of *Tbx1cKO^{Sox17}* embryos it would be predicted that *Bmp4* would conversely be reduced. The relationship between *Tbx1* and *Bmp4* in the caudal pharyngeal endoderm has not previously been analysed. In contrast to the 1st arch ectoderm of the *Tbx1$^{-/-}$* embryos there does not appear to be any shift in the expression domain of *Bmp4* in the caudal PA of *Tbx1cKO^{Sox17}* embryos. The expression of *Bmp4* in the caudal PA appears to mimic that of control embryos. In both mutant and control embryos *Bmp4* is most robustly expressed in ventral endoderm, caudal to the 2nd arch (panels a'' and b'' of Fig 49, robust endodermal expression domains are highlighted by brackets). Medially, small areas of *Bmp4* positive inter-pouch regions covering the medial aspect of the pharyngeal arches are evident in Cre negative embryos. The medial areas of *Bmp4* expression are also identifiable in medial sections of the *Tbx1cKO^{Sox17}* embryos un-segmented endoderm (Fig 49 arrows in panels a' and b'). The deletion of *Shh* (and presumably its downstream transcriptional targets) results in an expansion of *Bmp4* in the caudal endoderm at E10.5 (Moore-Scott and Manley, 2005). Thus a decrease in *Bmp4* expression would be predicted in pharyngeal endoderm exposed to ectopic SHH signalling. The maintenance of the level and discreet pattern of endodermal *Bmp4* expression in *Tbx1cKO^{Sox17}* embryos suggests that the SHH pathway may not be expanded in these mutants. The expanded expression of *Shh* pathway genes, and similarly RA pathway genes, may not be a transcriptional response to the loss

of *Tbx1* from the endoderm but is instead a secondary consequence to the change in *Tbx1cKO*^{Sox17} endoderm morphology.

Fig 49: The level and pattern of *Bmp4* expression is unchanged in the pharyngeal endoderm of *Tbx1cKO*^{Sox17} embryos. Frontal sections of E9.5 embryo's PA reveal *Bmp4* expression, detected by *in situ* hybridization, in *Tbx1cKO*^{Sox17} embryos (b-b'') is indistinguishable from Cre negative embryos (a-a'') in level and pattern. The extent of endodermal *Bmp4* expression in both embryos increases from dorsal to ventral aspects of the PA. Brackets delineate the most robust domain of *Bmp4* expression in the ventral PA sections, (a'' and b''). Solid arrowheads identify more discreet areas of *Bmp4* expression in medial sections (a' and b'). N = 2.

Annotations: Grey arrowhead = endodermal inter-pouch expression, unfilled arrowhead = endodermal pouch with no expression, pp = pharyngeal pouch, ? = presumptive pouch, brackets identify the domain of endodermal expression of each gene. Arrows to the left of Fig 49 illustrate the orientation of the pharyngeal apparatus sections; A = anterior, P = posterior, L = lateral, M = medial, V= ventral, D = dorsal.

Fig 49

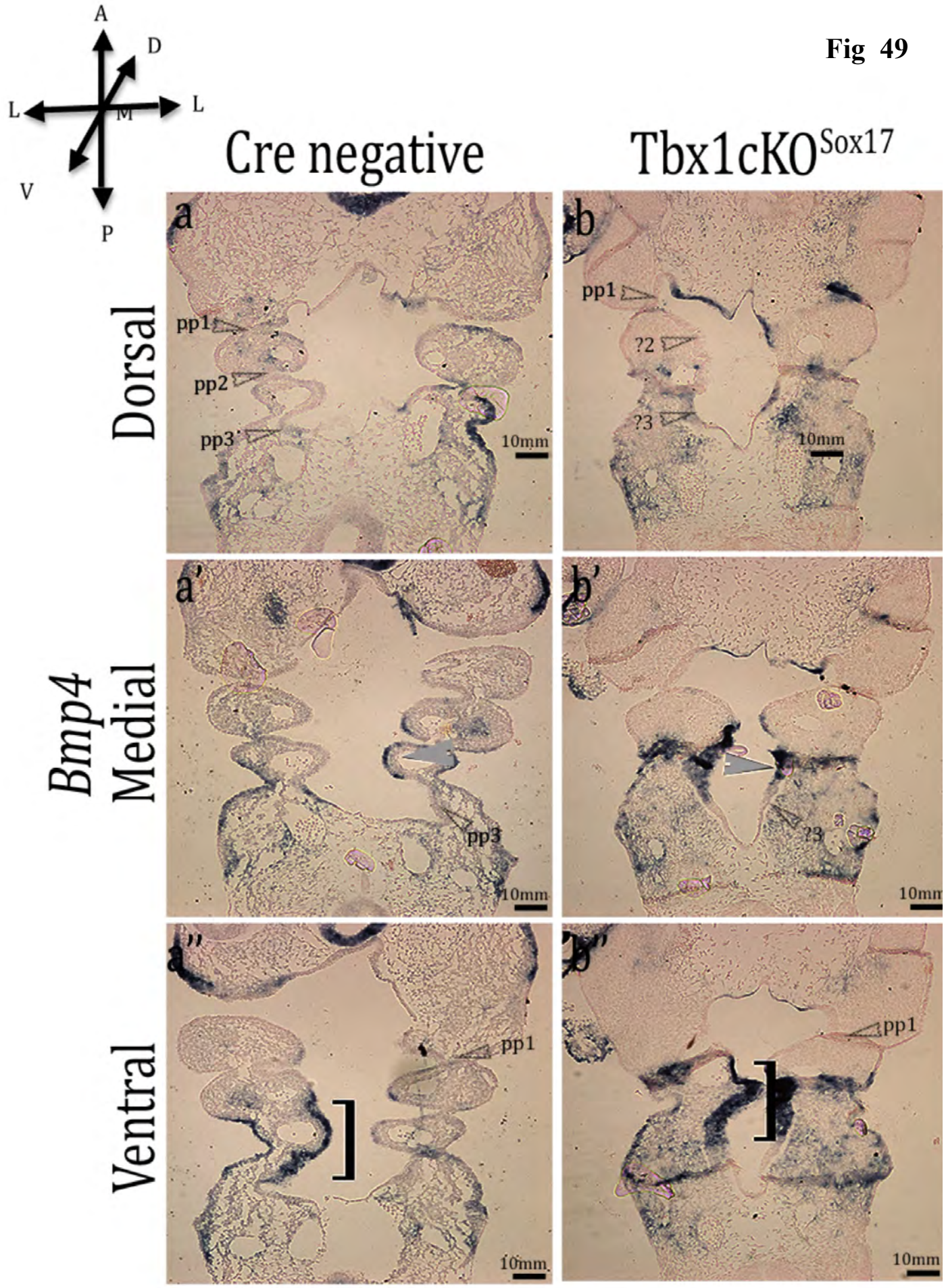
A
D
L
M
L
V
P
Cre negative
Tbx1cKO Sox17
Dorsal
Bmp4
Medial
Ventral
a
b
a'
b'
a''
b''
pp1
pp2
pp3
?2
?3
10mm

6.4 *Tbx1*-dependent changes to the cells of the pharyngeal endoderm

The formation of discreet, slit-like pouches in the chick embryo has been demonstrated to require a network of actin cables enriched along the apical side of the evaginating endoderm (Quinlan et al., 2004). The ectopic accumulation of actin has been found to prevent morphogenetic movements in an ectodermal epithelium (Sai and Ladher, 2008). A crucial step in the formation of the inner ear is the invagination of the otic placode, a thickening of ectoderm between the pharyngeal arches and the hindbrain, to form the otic cup (Sai and Ladher, 2008). Sai et al. have shown that actin must become polarized along the apical edge of the otic placode at the 13-somite stage of chick development for invagination to occur. Active myosin II (pMLC) is able to function in a 'non-canonical' capacity as an actin depolymerisation factor (ADF) (Haviv et al., 2008). The presence of pMLC prevents the formation of F-actin along the basal edge of the otic placode and the resulting polarity in the actin network enables the ectoderm to invaginate (Sai and Ladher, 2008). An FGF dependent depletion of pMLC in the otic placode results in the accumulation of F-actin along the apical and basal edges of the placode. The loss in actin polarity prevents the invagination of the ectodermal epithelium (Sai and Ladher, 2008).

The polarisation of the actin network, that constrains the formation of the otic placode, is thought to occur independently of ectodermal cell polarity. However, loss of endodermal cell polarity in the pharyngeal endoderm could also play a role in preventing pharyngeal pouch evagination. Laminins are integral components of the basal membrane as they act as anchors upon which cytoskeletal assembly can

occur (Li et al., 2003; Miner and Yurchenco, 2004). The loss of laminin in flies and worms has been found to disrupt cell polarity, perturbing the association between neighbouring cells (Li et al., 2003). The latter can affect the morphogenesis of structures during development. For instance, cleft formation in salivary glands is perturbed by the loss of laminin, as is observed from E13.0 in Laminin-α-5$^{-/-}$ mouse embryos (Rebustini et al., 2007). E-cadherin is also involved in the regulation of epithelial apico-basal polarity. For instance, when cells are cultured with a virus carrying dominant negative E-cadherin they orientate randomly i.e. unpolarised (Desai et al., 2009).

It is possible that the loss of *Tbx1* may affect the polarity of either the endodermal cells themselves, the actin cytoskeleton within the pharyngeal endoderm, or indeed both. However, the finding that a number of cytoskeletal effectors are down regulated in the endoderm of *Tbx1* null embryos indicates that *Tbx1* may influence the actin network. A microarray comparing gene expression in *Tbx1* null and control embryos at E9.5 revealed a number of LIM domain proteins were down regulated in the mutant's *Tbx1*-deficient PA (Ivins et al., 2005). The LIM domain consists of two cysteine and histidine rich zinc fingers motifs that are tandemly repeated throughout the protein (Bach et al., 2000; Kadrmas and Beckerle, 2004). One function of LIM proteins is to act as actin effectors, regulating the structure and dynamics of actin in a cell. For instance, the α-actinin-associated LIM protein (ALP) co-localises with the actin cross-linking protein, α-actinin, enhancing its ability to bundle actin fibres (Pomies et al., 1999).

6.4.1 Loss of actin polarity in *Tbx1cKO^{Sox17}* embryos endoderm may account for caudal pouch aplasia

The polarisation of actin within an epithelium has been suggested to underlie morphogenetic processes including otic placode invagination and pharyngeal pouch formation in avian embryos. The distribution of F-actin (detected using a phalloidin-conjugated fluorophore) was analysed in *Tbx1cKO^{Sox17}* embryos to determine if the deletion of *Tbx1* from the endoderm results in a loss of actin polarity within this tissue. In accordance with avian data, actin accumulates strongly in the pharyngeal pouches of murine embryos, particularly in the 3rd pouch (Quinlan et al., 2004). Phalloidin-marked actin accumulates primarily along the apical edge of the evaginating mammalian pouch (red arrows Fig 50 panels a and c). The phalloidin staining appears robust and continuous along the apical edge of pharyngeal endoderm. F-actin was also visible along the basal edge of the evaginating endoderm, primarily concentrated around the apex of the pouch (white arrows Fig 50 panels a and c). The phalloidin staining at the basal edge of the 3rd pouch endoderm is less intense and is punctate in nature (highlighted by short dashed lines in Fig 50 panel c'). The differences in phalloidin staining along the apical and basal edge of the 3rd pouch demonstrates that actin is polarised in the evaginating endoderm, akin to the invaginating ectoderm of the otic vesicle (Sai and Ladher, 2008).

The absence of *Tbx1* from endodermal cells perturbs the distribution of actin in the caudal pharyngeal endoderm. The accumulation of actin along the apical edge of *Tbx1cKO^{Sox17}* embryos endoderm is relative to that observed in the 3rd pouch of controls (Fig 50, compare apical actin identified by red arrows in panels b and d

[*Tbx1cKO*^{Sox17}] to panels a and c [Cre negative]). In contrast, actin accumulation along the basal edge of the mutant's endoderm is markedly increased (Fig 50, compare basal actin identified by white arrows in panels b and d to panels a and c). The normally punctate, weak staining along the basal edge of the endoderm is stronger and more continuous in appearance, reflecting the type of staining normally observed at the apical edge (highlighted by longer dashed lines in Fig 45 panel d'). The observations suggest that TBX1 in the endoderm functions in the endoderm to regulate the polarity of the actin network.

It is possible that the loss of actin polarity observed in the *Tbx1cKO*^{Sox17} embryos reflects a loss in polarity of the endodermal cells, thus other cytoskeletal proteins known to influence cell polarity were analysed in the *Tbx1*-deficient endoderm. However, in contrast to the actin network, the endodermal cells of *Tbx1cKO*^{Sox17} embryos PA appear to be polarised, indicated by the maintenance of laminin, E-cadherin and polarised cell proliferation in this epithelium.

Although the basal lamina of *Tbx1cKO*^{Sox17} embryos appears thicker, perhaps indicative of cell stacking, there is no loss or change to the location of laminin protein (Fig 51, compare panels a and a' to panels b and b', arrows indicate equivalent areas of basement membrane in control and mutant's endoderm). This indicates that the laminin is not dependent on TBX1 for its accumulation in the basal lamina of the pharyngeal endoderm. The observation that E-cadherin appears unchanged in the endoderm of *Tbx1cKO*^{Sox17} embryos further indicates that the pharyngeal endoderm is polarised in the absence of TBX1. (Fig 51 compare overall E-cadherin staining in panels c and d). Small areas of enriched E-cadherin staining are visible in the unsegmented endoderm of *Tbx1cKO*^{Sox17}

embryos, akin to the enriched E-cadherin staining visible in the pouches of control embryos (Fig 51 arrows in panels c and d indicate areas of increased E-cadherin, more clearly visible at high magnification in panels c' and d').

Consistent with the hypothesis that the pharyngeal endoderm of *Tbx1cKO*^{Sox17} embryos is polarised, the orientation of cell proliferation in the mutants pharyngeal endoderm is also unchanged (Fig 52). The position of the nuclei in S-phase is indicative of the polarity of the cell that can be inferred by analysing the division of cells in prophase (i.e. cells labelled by an anti-Phospho-Histone H3, PH3 antibody). The mean number of proliferating cells in the entire pharyngeal endoderm of *Tbx1cKO*^{Sox17} embryos was not significantly different to that of Cre negative embryos. More significantly, there was no change to the number of apical versus basal PH3 marked cells in the TBX1-deficient the endoderm of the conditional mutants (see graph c in Fig 52).

The data so far suggests that the deletion of *Tbx1* from the pharyngeal endoderm specifically perturbs the polarity of the actin network, rather than the polarity of the endodermal cells *per se*.

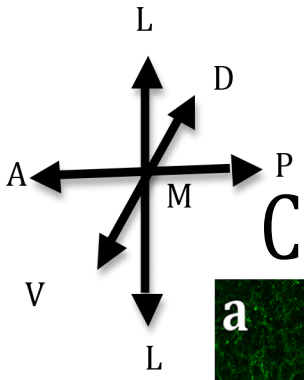

Cre negative

Tbx1cKO^{Sox17}

Cre negative

Tbx1cKO^{Sox17}

Phalloidin

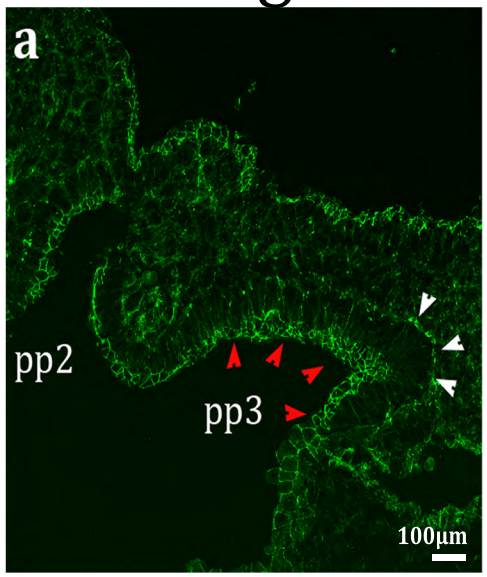

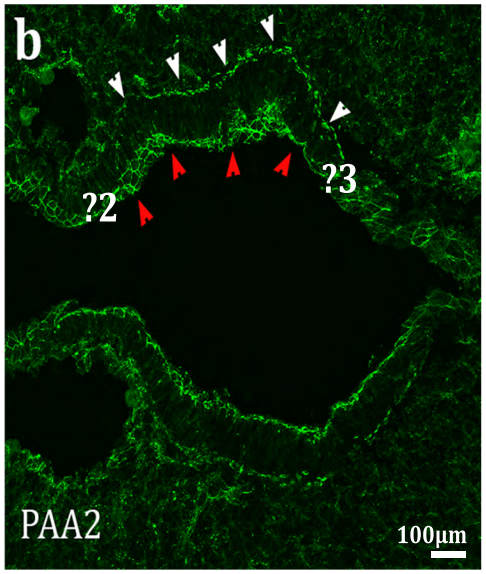

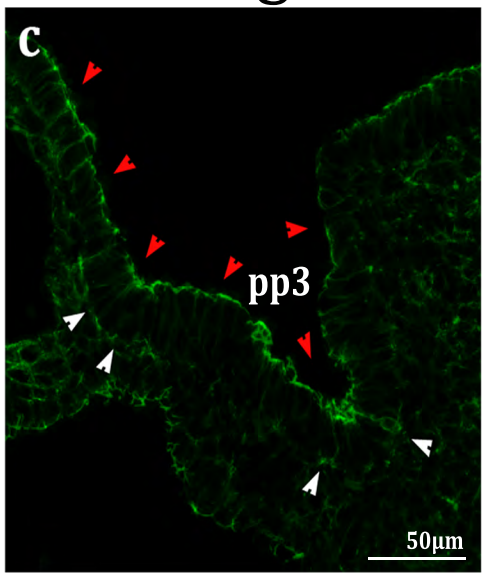

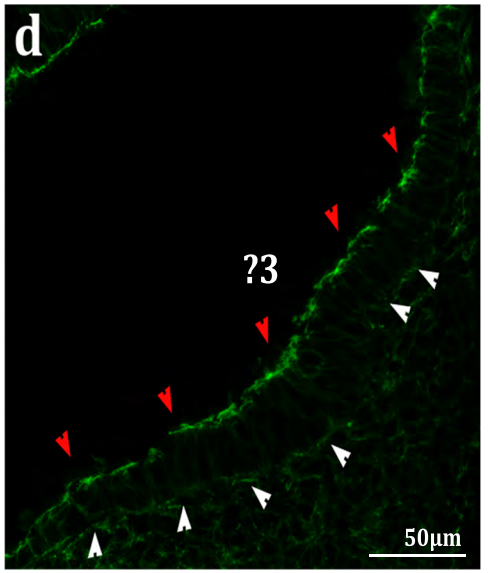

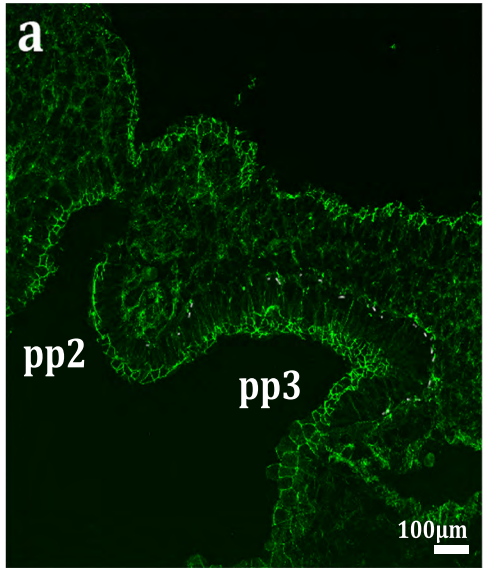

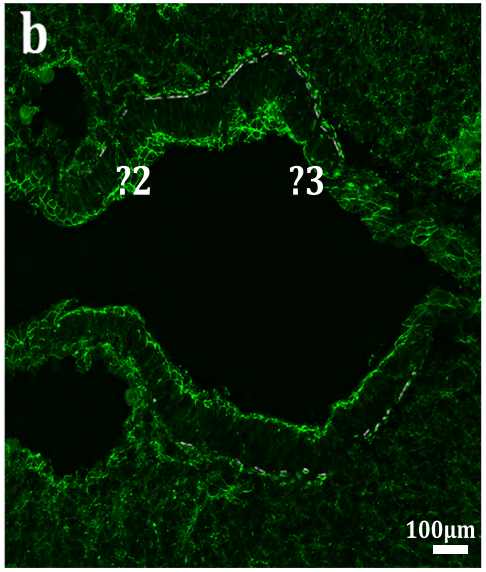

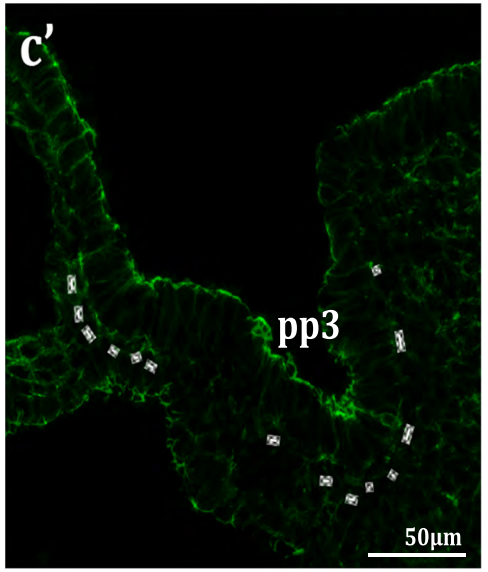

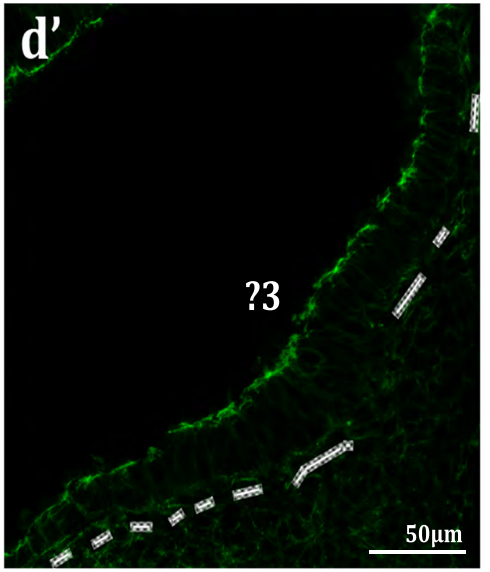

Fig 50: Actin accumulates at the basal edge of *Tbx1cKO^{Sox17}* embryo's pharyngeal endoderm.

Phalloidin marked F-actin is enriched along the apical edge of Cre negative embryos pharyngeal endoderm, (red arrows panels a and c), at the basal edge actin staining is limited. Basal phalloidin staining is punctate in appearance (highlighted by dashes in panel c') and concentrated around the apex of the evaginating pouch (white arrows panels a and c). In contrast, phalloidin marked, F-actin is enriched along the **apical and basal** edges of *Tbx1cKO^{Sox17}* embryos pharyngeal endoderm (highlighted, respectively, by red and white arrows in panels b and d that mirror each other in distribution). Areas of basal phalloidin staining are elongated in appearance (highlighted by dashes in panel d') and present along the length of the caudal pharyngeal endoderm (white arrows panel d). N =10. Annotations: White arrowhead = basal F-actin in the endoderm, red arrowhead = apical F-actin in the endoderm , pp = pharyngeal pouch, ? = presumptive pouch, PAA = pharyngeal arch artery, dashes identify the concentration of actin filaments at the basal edge of the pharyngeal endoderm. Arrows to the left of Fig 50 illustrate the orientation of the pharyngeal apparatus sections; A = anterior, P = posterior, L = lateral, M = medial, V= ventral, D = dorsal.

Fig 51: E-cadherin and laminin are maintained in the pharyngeal endoderm of *Tbx1cKO^{Sox17}* embryos, indicative of the epithelium retaining its polarity.

Laminin staining (panels a-b') is maintained along the basal edge of *Tbx1cKO^{Sox17}* embryo's pharyngeal endoderm, the increase in stain may indicate that the endodermal cells are stacking at the basal edge of this epithelium. White arrows indicate equivalent areas of pharyngeal endoderm in the Cre negative (a and a') and *Tbx1cKO^{Sox17}* (b and b') embryos. N=3.

E-cadherin staining is unchanged in the endoderm of *Tbx1cKO^{Sox17}* embryos (compare overall E-cadherin staining in panels c and d). Small areas of enriched E-cadherin staining are visible in the endoderm of *Tbx1cKO^{Sox17}* and Cre negative embryos (white arrows in panels c' and d'). The caudal endoderm outlined in panels c and d are displayed at high magnification in panels c' and d'.

Annotations: White arrowhead = endodermal staining of interest, pp = pharyngeal pouch, ? = presumptive pouch, Ecto = ectoderm, Mesen = mesenchyme. Arrows to the left of Fig 51 illustrate the orientation of the pharyngeal apparatus sections; A = anterior, P = posterior, L = lateral, M = medial, V= ventral, D = dorsal.

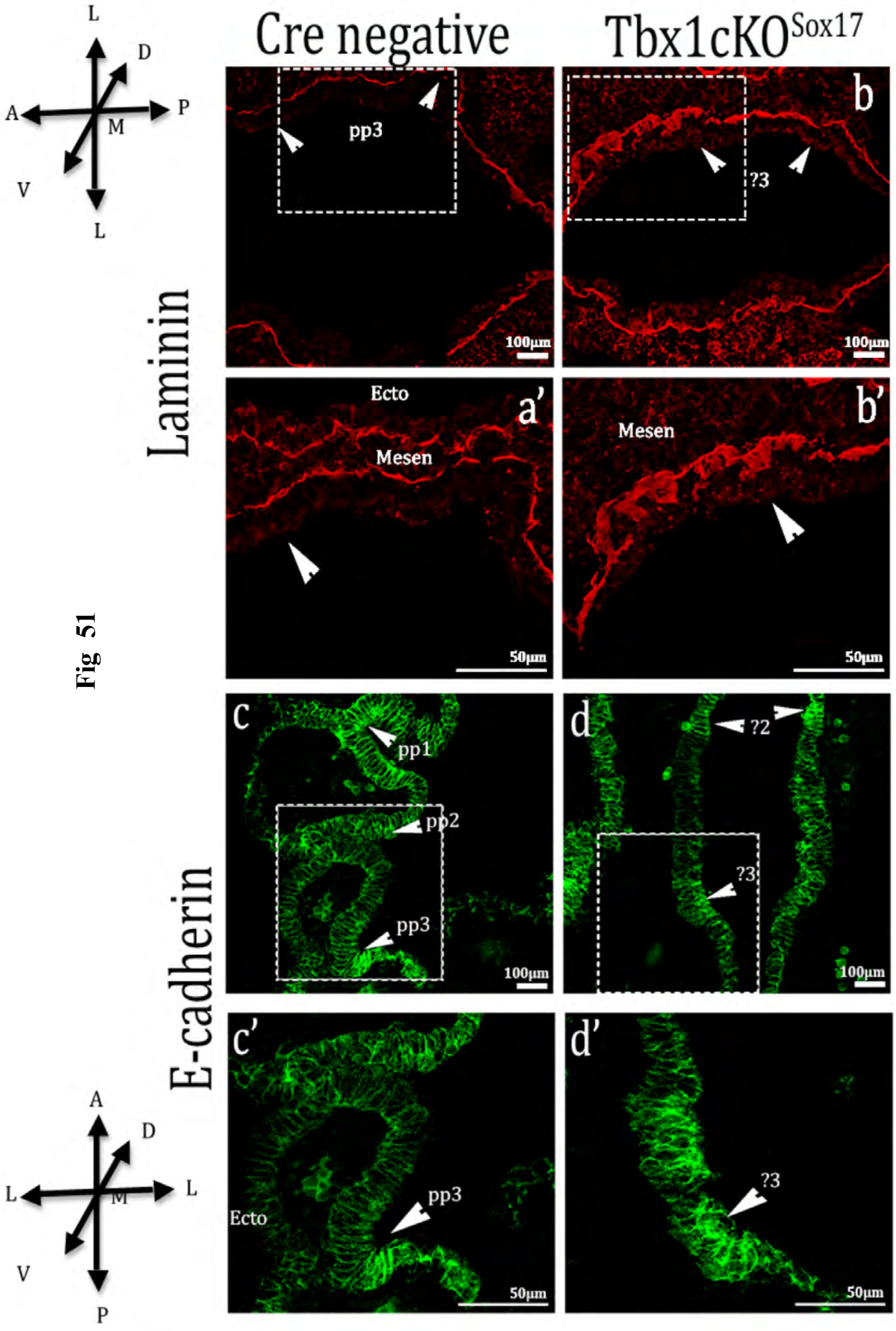
Cre negative
Tbx1cKO Sox17
Laminin
E-cadherin
L
D
A
P
M
V
L
pp3
?3
100μm
Ecto
Mesen
a'
b'
50μm
c
d
pp1
pp2
pp3
?2
?3
c'
d'
Ecto
A
D
L
M
L
V
P

Fig 51

Fig 52: The amount and location of cell proliferation is unchanged in the pharyngeal endoderm of *Tbx1cKO^{Sox17}* embryos

The average number of proliferating cells in the entire pharyngeal endoderm of *Tbx1cKO^{Sox17}* embryos is not significantly different to that of Cre negative embryos in number or place of division (n=2). Phospho-Histone 3 (PH3, red staining) marked cells were counted in serial sections throughout the pharyngeal endoderm, (delineated by E-cadherin staining, in green) and categorised as either apical or basal in location (panels a and b, arrows show an apically located PH3 positive endodermal cell). Graph C plots the mean number of apical, basal and total proliferating cells in the pharyngeal endoderm of one *Tbx1cKO^{Sox17}* and one Cre negative embryo (Error bars represent S.E.M). Unpaired T-test calculation on Graph pad show that there is no difference between the mean number of apical (p= 0.13) basal (p= 0.50) or total (p= 0.45) proliferating endodermal cells per Cre negative and *Tbx1cKO^{Sox17}* embryos.

Representative of 2 experiments.

Location of proliferating endodermal cells for each genotype	Mean number of proliferating endodermal cells/embryo	SEM
Cre negative apical	6.5	± 0.950
Tbx1cKO^{Sox17} apical	7.6	± 0.902
Cre negative basal	2.1	± 0.454
Tbx1cKO^{Sox17} basal	1.6	± 0.351
Cre negative total	8.6	± 1.24
Tbx1cKO^{Sox17} total	9.2	± 1.05

Fig 52

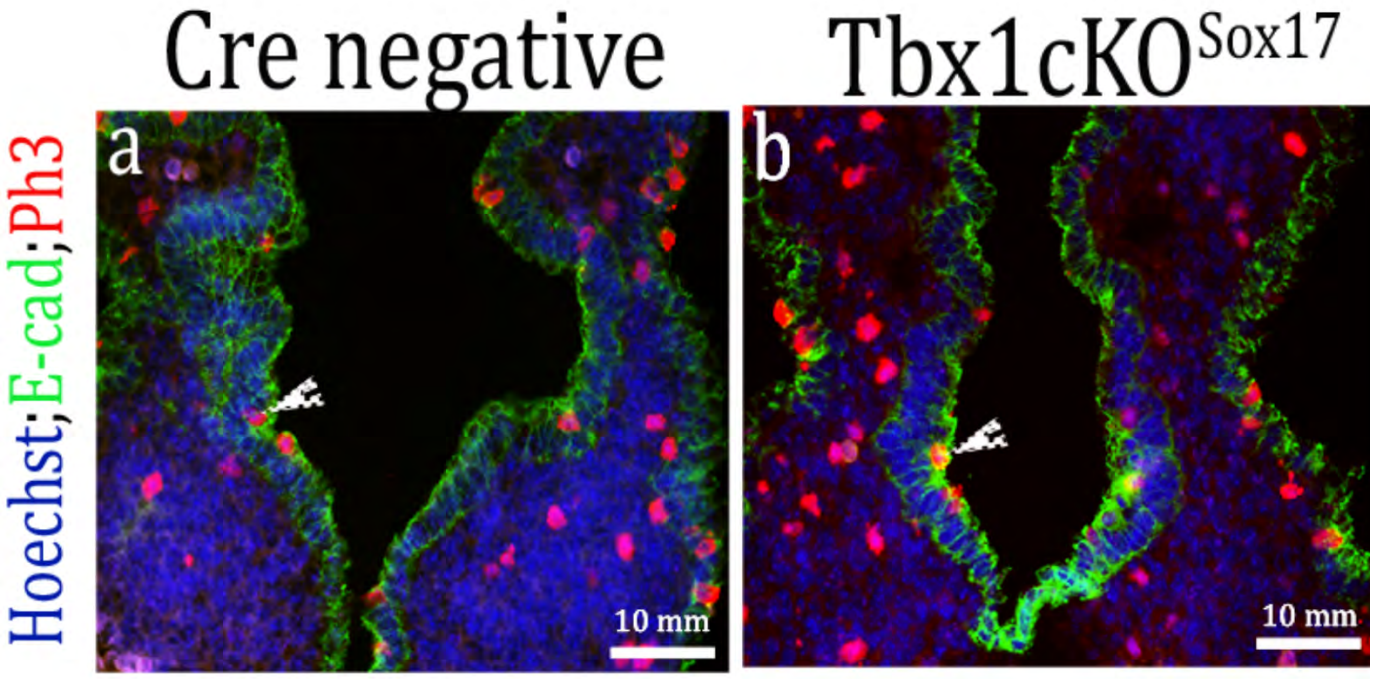
Cre negative
Tbx1cKOSox17
Hoechst;E-cad;Ph3
a
b
10 mm
10 mm

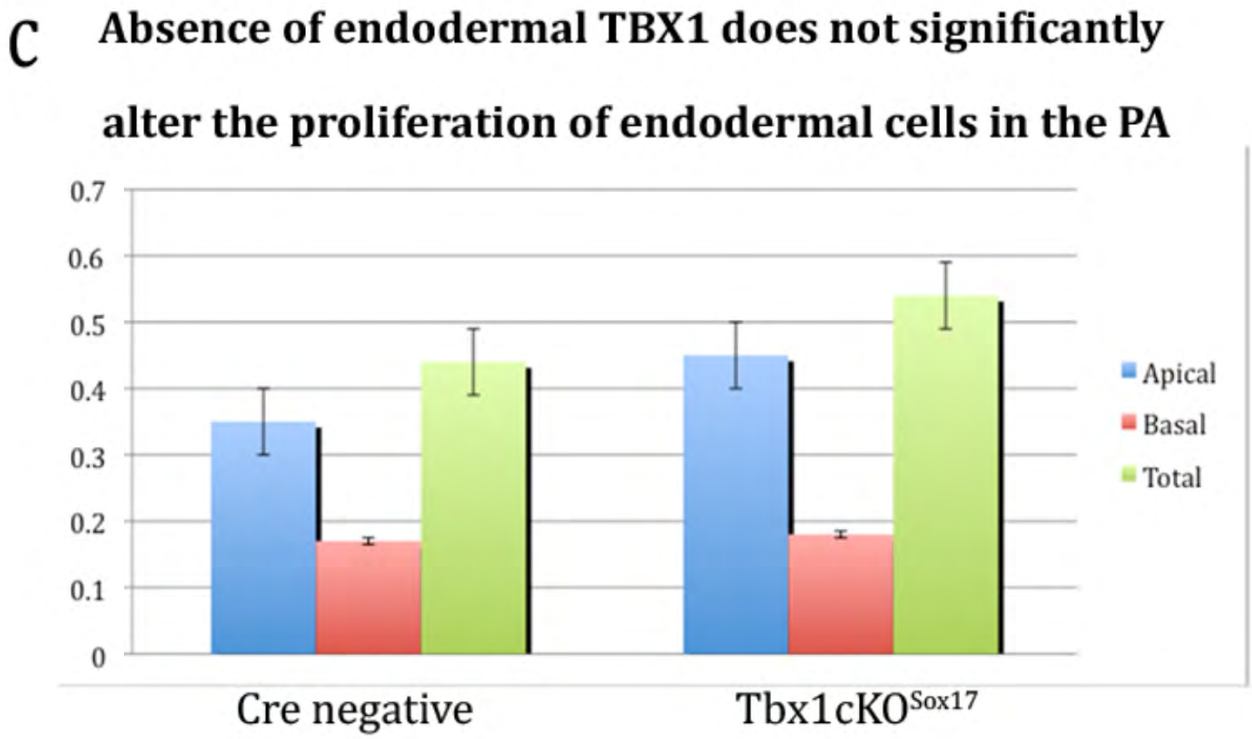
c
Absence of endodermal TBX1 does not significantly alter the proliferation of endodermal cells in the PA
0.7
0.6
0.5
0.4
0.3
0.2
0.1
0
Apical
Basal
Total
Cre negative
Tbx1cKOSox17

6.4.2 Active myosin light chain is absent from the basal edge of TBX1-deficient endoderm

Actin polarity must be established in the otic placode for invagination to occur. Polarity in the actin network is achieved by a pMLC mediated depolymerisation of F-actin at the basal edge of the otic placode (Sai and Ladher, 2008). It is possible that a lack of pMLC at the basal edge of *Tbx1cKO*^{Sox17} embryos pharyngeal endoderm may enable actin to accumulate here ectopically. Alternatively, the accumulation of F-actin along the basal edge of TBX1-deficient endoderm may be caused by the loss of a canonical actin depolymerising factor (ADF), such as cofilin (Arber et al., 1998). However, akin to the otic placode, cofilin was not detected at the basal edge of the pharyngeal endoderm of Cre negative or *Tbx1cKO*^{Sox17} embryos (Fig 53, illustrates that cofilin staining is robust in the apical but not the basal edge of the pharyngeal endoderm of all embryos [panels a and b]). Thus, the depolymerisation of actin at the basal edge of the evaginating pharyngeal pouch is unlikely to be facilitated by cofilin. In contrast, a difference in the amount of basal pMLC staining was visible in the caudal pharyngeal endoderm of the Cre negative embryo and the *Tbx1cKO*^{Sox17} embryo. At the basal edge of the *Tbx1cKO*^{Sox17} embryo's caudal pharyngeal endoderm pMLC staining is not observed (Fig 54; compare basal pMLC staining present in the endoderm of Cre negative embryos, indicated by solid arrows [panel a], with the relative area absent of pMLC indicated by unfilled arrows in the *Tbx1cKO*^{Sox17} embryo [panel b]). The loss of basal pMLC staining correlates with an increase in the extent and level of phalloidin marked actin along the same basal edge of *Tbx1cKO*^{Sox17} embryos endoderm (Fig 54, panel b' white arrowheads). Conversely, in the Cre negative embryo there is a distinct lack of phalloidin-marked actin along the pMLC positive, basal edge of the evaginating 3rd pouch, relative to the apical edge (Fig 54, panel a' unfilled

arrowheads). This trend is highlighted in the merged phalloidin and pMLC-stained images in Fig 54 (panels a'' and b''). This data suggests that the lack of caudal pouch evagination in *Tbx1cKO*^{Sox17} embryos endoderm may be attributable to the depletion of basal pMLC that disrupts the polarity of the endodermal actin network.

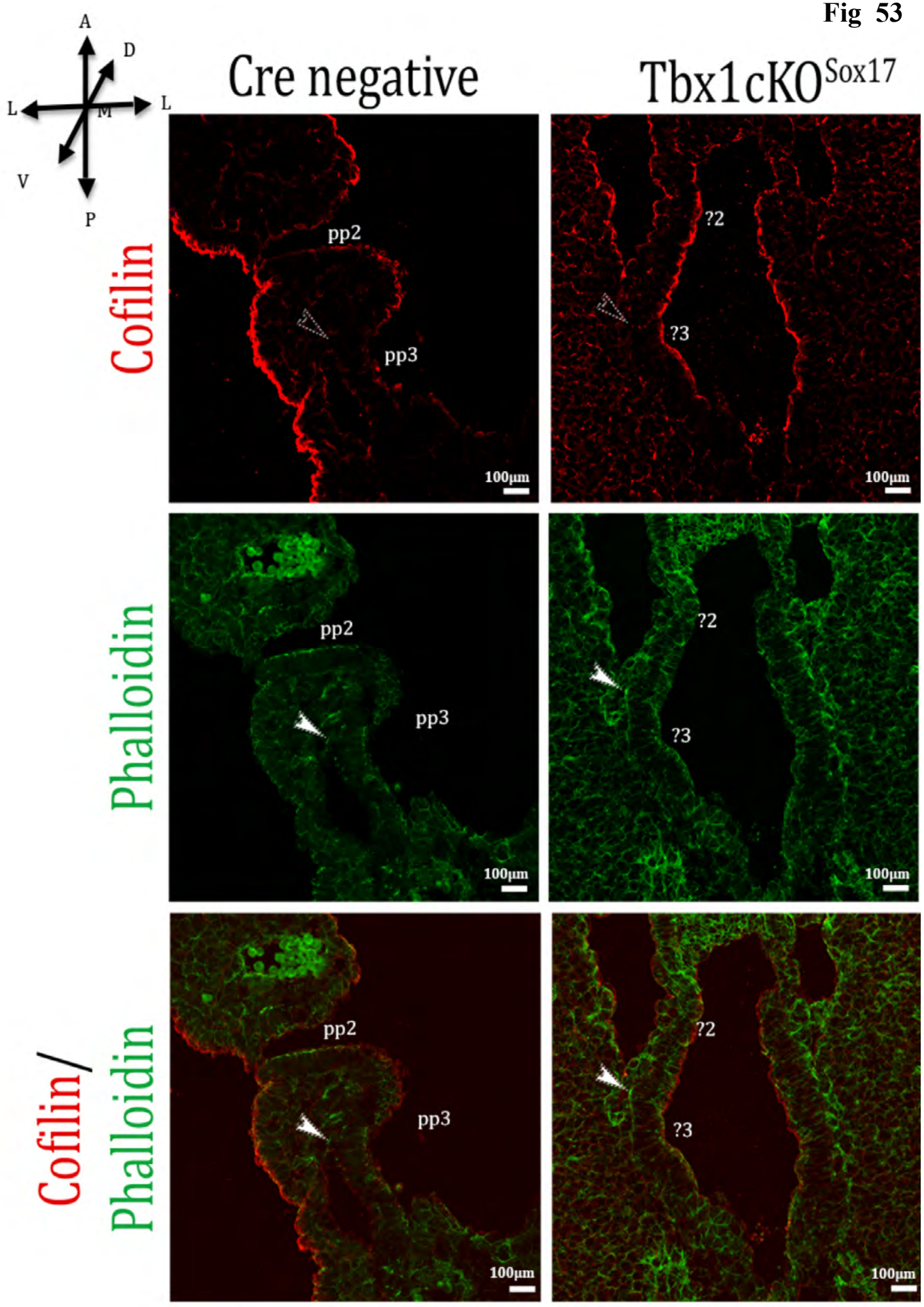
A
D
L
M
L
V
P
Cre negative
Tbx1cKO Sox17
Cofilin
Phalloidin
Cofilin/
Phalloidin
pp2
pp3
?2
?3
100µm

Fig 53: Cofilin is not detected at the basal edge of the pharyngeal endoderm of Cre negative or *Tbx1cKO^{Sox17}* embryos. Cofilin staining, (red fluorescence) in Cre negative (panels a, c and e) and *Tbx1cKO^{Sox17}* embryos (panels b, d and f) is robust at the apical edge but not visible at the basal edge of the pharyngeal endoderm, (unfilled arrows panels a and b). There does not appear to be an inverse correlation in the presence of actin (phalloidin staining, green fluorescence) and cofilin at the basal edge of the pharyngeal endoderm. Solid white arrows highlight discreet areas of basal actin in the Cre negative embryo (panels c and d) and larger areas of basal actin in *Tbx1cKO^{Sox17}* embryo (panels e and f). Cofilin staining is not enriched in the adjacent phalloidin-negative areas of basal endoderm (unfilled arrowheads). N=2.

Annotations: White arrowhead = F-actin at the basal edge of the pharyngeal endoderm, unfilled arrowhead = absence of cofilin at the basal edge of the pharyngeal endoderm. Arrows to the left of Fig 53 illustrate the orientation of the pharyngeal apparatus sections; A = anterior, P = posterior, L = lateral, M = medial, V= ventral, D = dorsal.

Fig 54: Active myosin light chain is not detected along the basal edge of *Tbx1cKO^{Sox17}* embryo's pharyngeal endoderm. Active myosin light chain (pMLC, red fluorescence) is visible at the basal edge of Cre negative embryo's pharyngeal endoderm, (panel a, solid white arrow) but is absent from the basal edge of *Tbx1cKO^{Sox17}* embryo's pharyngeal endoderm (panel b, unfilled white arrow). The presence of pMLC in the Cre negative embryos endoderm correlates with an absence of F-actin (phalloidin marked, green fluorescence) at the same location (panel a', unfilled white arrow). Conversely the absence of pMLC in *Tbx1cKO^{Sox17}* embryos correlates with the accumulation of F-actin along the basal edge of the mutant's endoderm (panel b', solid white arrow). The differences in pMLC and F-actin staining between the *Tbx1cKO^{Sox17}* and Cre negative embryos are highlighted in panels b'' and a'' respectively (red arrow in a'' highlights basal pMLC , green arrow in b'' highlights basal actin). Note that the blood cells in panel a have been removed in Photoshop because their auto-fluorescence detracted from the specific, weaker, pMLC staining. Annotations: Arrows to the left of Fig 54 illustrate the orientation of the pharyngeal apparatus sections; A = anterior, P = posterior, L = lateral, M = medial, V= ventral, D = dorsal. N = 1

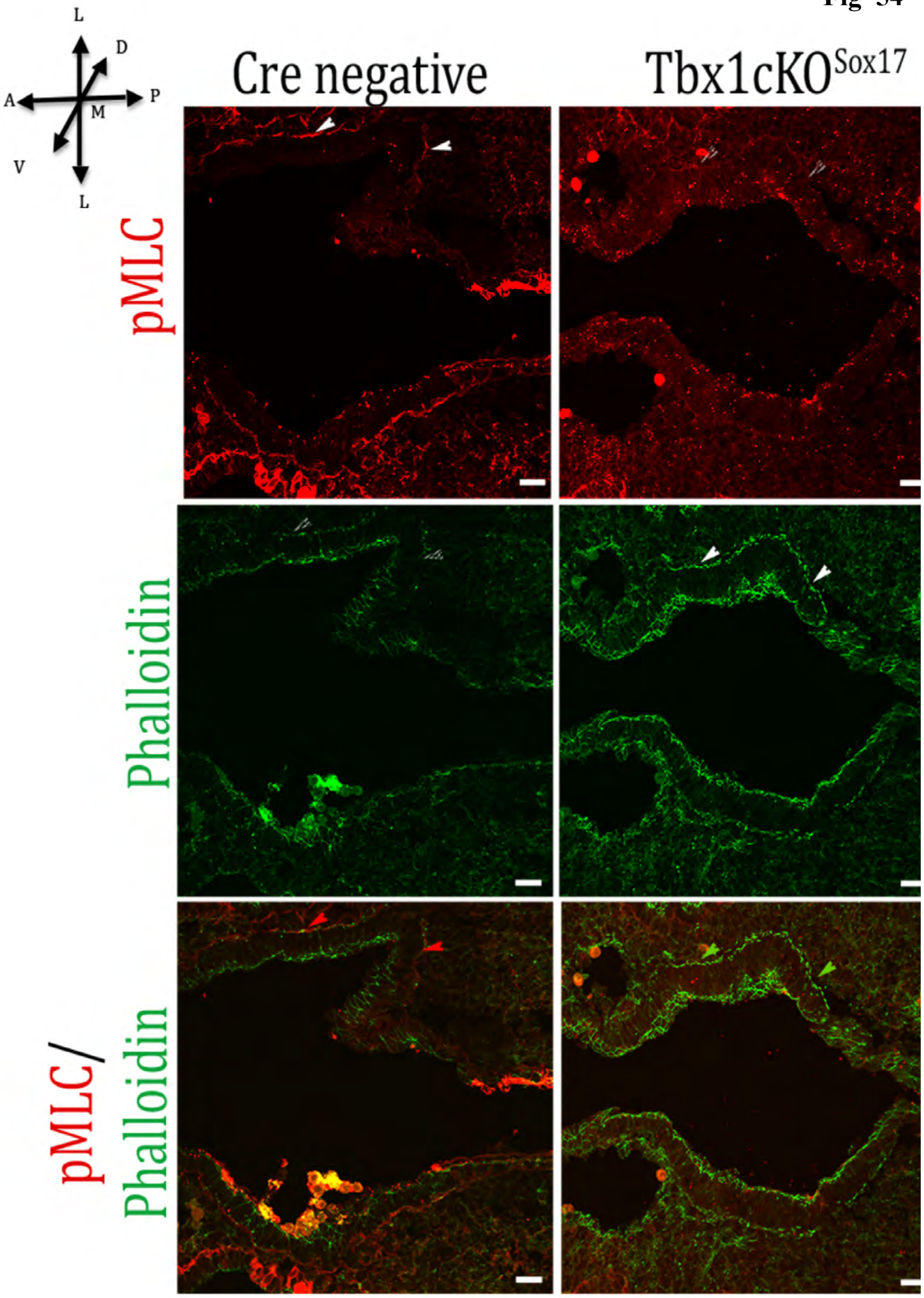
L
D
A
P
M
V
L
Cre negative
Tbx1cKO Sox17
pMLC
Phalloidin
pMLC/
Phalloidin

6.4.3 TBX1 regulates the expression of the LIM domain protein *Fhl1*, an actin effector

A microarray comparing gene expression in *Tbx1* null and control embryos revealed a number of proteins containing LIM domain proteins were down regulated in the *Tbx1*-deficient PA (Ivins et al., 2005). It is possible that a *Tbx1*-dependent change to the level or location of *Lim* gene expression in the pharyngeal endoderm may affect actin accumulation within the pouches. The expression pattern of each *Lim* protein down regulated in *Tbx1* null embryos was analysed in the PA to identify their place of expression at E9.5 within the PA. *Lim* genes expressed in the pharyngeal endoderm were then further analysed in *Tbx1cKO*^{Sox17} embryos to determine if their expression is altered in the absence of *Tbx1*.

6.4.3.1 Expression analysis of *Lim* genes in the PA of E9.5 embryos

Table 8 lists the *Lim* genes that were down regulated a microarray of *Tbx1* null embryos (Ivins et al., 2005). The expression pattern of each *Lim* gene in the PA of E9.5 wild type embryos was assessed by *in situ* hybridisation. Whilst *Lim domain only protein 4* (*Lmo4*), *Pdz and Lim domain 3* (*Pdlim3*), *Lim homeobox 2* (*Lhx2*) and *Four and a half Lim domains 2* (*Fhl2*) are all expressed in the PA, the majority of the expression appears to be in non-endodermal tissues (Fig 55). *Pdlim3* is expressed robustly throughout the mesenchyme of the pharyngeal arches but is absent from the pharyngeal epithelia (Fig 55, panel c). *Pdlim3* transcripts are also present in the heart at E9.5 (Fig 55, panel c'). *Lmo4* is also restricted to the CNCC derived mesenchyme but its expression is less ubiquitous than *Pdlim3,* being most robustly detected in the 1st arch mesenchyme (Fig 55, panel b and b'). *Lhx2* transcripts appear to be localised in the core mesoderm of each pharyngeal arch (Fig 55,

panels d and d'). *Fhl2* is present in the very anterior part of the rostral arch mesenchyme and in the forebrain (Fig 55, panels a and a') but is most robustly expressed in the mesenchyme surrounding the evaginating 3rd pouch (Fig 55, arrow in panel a). Of all the *Lim* genes analysed in the PA by *in situ* hybridisation, only *Fhl2* was detected in the endoderm in a small area within the evaginating 3rd pouch and at the lateral tips of the 1st and 2nd pouches (Fig 55, black arrowheads in panel a).

Table 8: Lim genes down regulated in a microarray of the PA of *Tbx1* null embryos

Gene bank Accession	Gene description	Relative expression to control embryos (*Dfl/+;Tbx1*$^{+/-}$)
NM_01070	*Lim homeobox protein 2 (Lhx2)*	0.653 N
NM_010212	*Four and a half LIM domains (Fhl2)*	0.713
NM_010723	*Lim domain only protein 4 (Lmo4)*	0.754
NM_016798	*PDZ and LIM domain 3 (Pdlim3)*	0.654
NM024223	*Heart LIM protein (Hlp)* *	0.714

* The mRNA probe for this gene did not generate an interpretable signal.

Fig 55: *Lim* domain genes down-regulated in *Tbx1* null embryos are not robustly expressed in the pharyngeal endoderm at E9.5. Frontal sections of E9.5 control embryo's PA displaying expression of *Fhl2* (a and a'), *Lmo4*, (b and b'), PDlim3 (c and c') and *Lhx2* (d and d') detected by *in situ* hybridization, each *in situ* n=1. Note that only *Fhl2* appears to be expressed in the pharyngeal endoderm.

Annotations: Solid black arrowhead = endodermal staining of interest (or staining in the forebrain and heart in panels a' and c' respectively), unfilled black arrowhead= lack of endodermal expression (or lack of expression in the heart on panels b and d), green arrowhead = mesenchymal staining, yellow arrowhead = mesodermal staining of interest, blue unfilled arrow = lack of ectodermal expression, red unfilled arrow panel c= lack of endodermal expression identical to black unfilled arrowhead, colour had to be changed as the black unfilled arrowhead was not visible in this area of the PA section. pp = pharyngeal pouch, Ecto = ectoderm, Fb = forebrain, Ht = heart, Mesn. = mesenchyme, Meso (x) = mesodermal core of pharyngeal arch (x). Arrows to the left of Fig 55 illustrate the orientation of the pharyngeal apparatus sections; A = anterior, P = posterior, L = lateral, M = medial, V= ventral, D = dorsal.

Fig 55

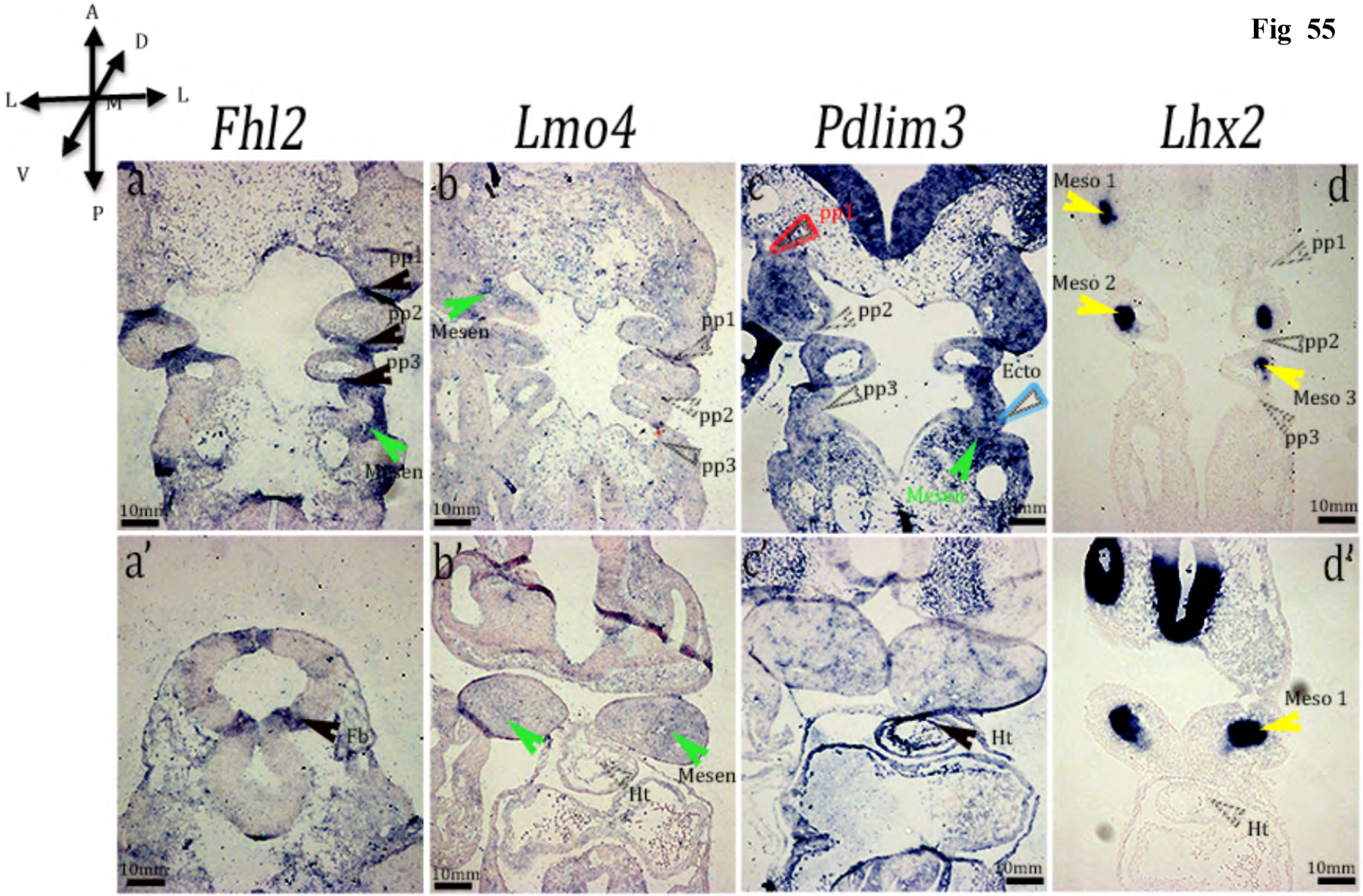
A
D
L
M
L
V
P
Fhl2
Lmo4
Pdlim3
Lhx2
a
pp1
pp2
pp3
Mesen
10mm
b
Mesen
pp1
pp2
pp3
10mm
c
pp1
pp2
pp3
Ecto
Mesen
10mm
d
Meso 1
pp1
Meso 2
pp2
Meso 3
pp3
10mm
a'
Fb
10mm
b'
Mesen
Ht
10mm
c'
Ht
10mm
d'
Meso 1
Ht
10mm

6.4.3.2 The expression of *Fhl1* is increased in the pharyngeal endoderm of *Tbx1cKO^{Sox17}* embryos

The FHL family of LIM proteins are highly conserved and a literature search revealed that, (as was revealed in Fig 55 for *Fhl2*), *Fhl1* at E10.5 is also expressed within the pharyngeal endoderm (Chu et al., 2000; Kadrmas and Beckerle, 2004). As the actin analyses in TBX1-deficient endoderm were performed at E9.5, at a time when the 3rd pouch is still 'out-pocketing' it was therefore required to establish whether *Fhl1* was expressed in the PA a day earlier at E9.5. *Fhl1* transcripts are visible in the pharyngeal endoderm at E9.5 (Fig 56, panel a). *Fhl1* is most robustly expressed in the inter-pouch regions of the pharyngeal endoderm, adjacent to the actin rich evaginating pouches (grey arrowheads in Fig 56 panel a identifies inter-pouch *Fhl1* expression, compare this to the actin staining in the pouch endoderm of Cre negative embryos, Fig 50 panels a, a', c and c'). In the absence of *Tbx1*, the expression of *Fhl1* in the pharyngeal endoderm is increased (Fig 56, panel b). The expression of *Fhl1* in the *Tbx1cKO^{Sox17}* embryo also appears to be continuous throughout the endoderm, however, the obtuse angle at which the PA of the mutant embryo was sectioned requires this to be confirmed. The FHL family of proteins are not transcription factors, however, their ability to associate with actin enables them to associate with other proteins that are able to regulate gene expression (Kadrmas and Beckerle, 2004). The observation that *Fhl1* and actin are both up-regulated in the pharyngeal endoderm of *Tbx1cKO^{Sox17}* embryos may link the changes in endoderm morphology to the observed changes in gene expression.

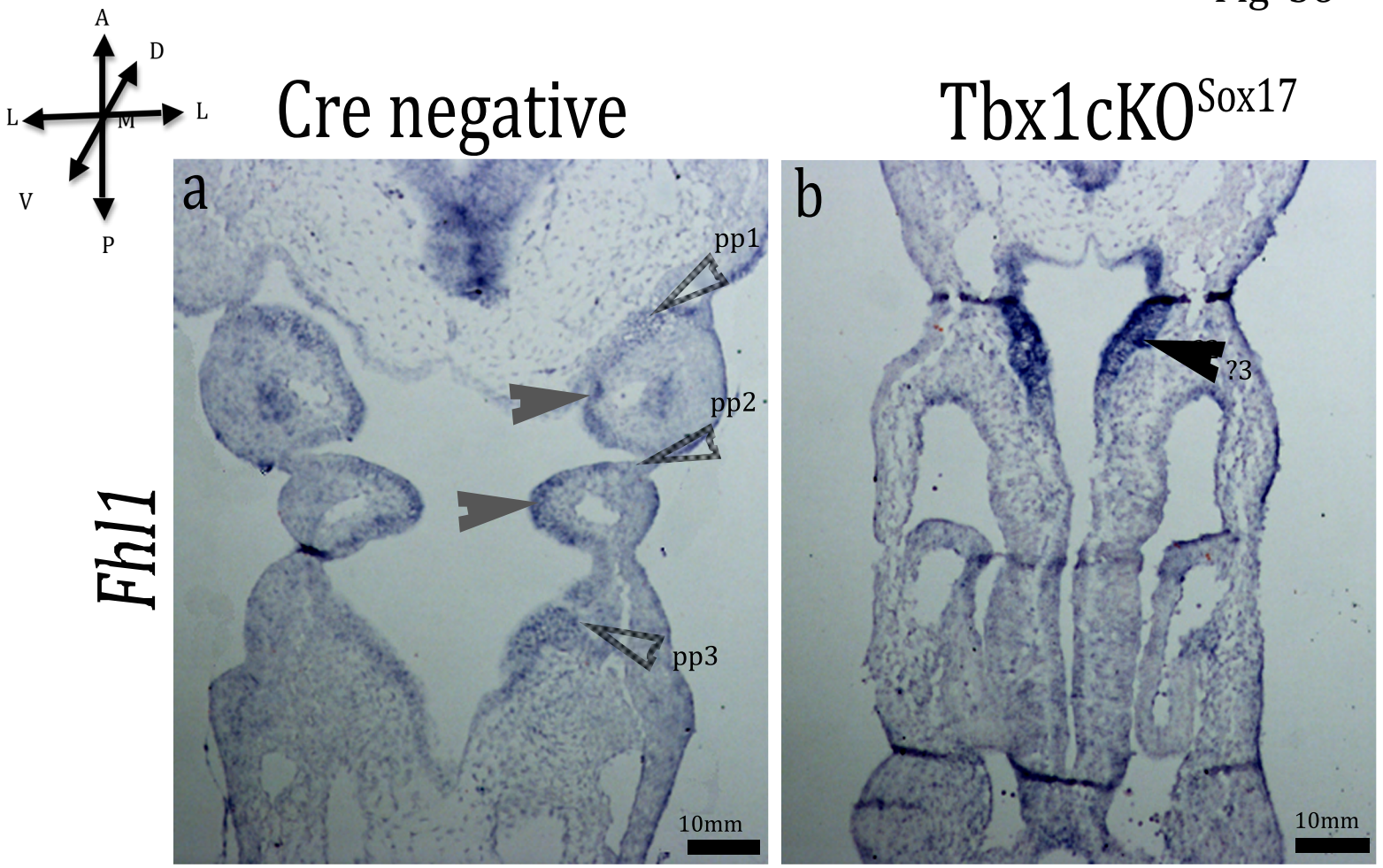

Fig 56: Fhl1 expression is increased in the pharyngeal endoderm of *Tbx1cKO*^{Sox17} embryos.

Frontal sections of E9.5 embryo's PA reveals increased *Fhl1* expression, detected by in situ hybridization, in the endoderm of *Tbx1cKO*^{Sox17} embryos (b), relative to the endodermal expression of *Fhl1* in Cre negative embryos (a) (n=1). Solid arrowheads identify relative areas of pharyngeal endoderm in the control and mutant embryo.

Annotations: Solid black arrowhead = up-regulated endodermal staining in *Tbx1*-deficient endoderm, unfilled black arrowhead= lack of endodermal expression. pp = pharyngeal pouch, ? = presumptive pouch. Arrows to the left of Fig 56 illustrate the orientation of the pharyngeal apparatus sections; A = anterior, P = posterior, L = lateral, M = medial, V= ventral, D = dorsal.

6.5 DISCUSSION

The experiments presented in Chapter 6 aimed to identify possible mechanisms that could account for the failure of caudal pouch formation in *Tbx1cKO*^{Sox17} embryos. The analysis of RA and SHH pathways in *Tbx1cKO*^{Sox17} embryos suggests that changes in endodermal gene expression may be secondary to the TBX1-dependent loss of endoderm morphology. Polymerised actin is an effector of epithelial morphology. The striking loss of actin polarity observed in TBX1-deficient endoderm likely perturbs the formation of the pharyngeal pouches. Two possible mechanisms may account for the accumulation of ectopic actin at the basal edge of the TBX1-deficient endoderm, the loss of the ADF pMLC along the basal edge of the endoderm and/or the up-regulation of *Fhl1* an actin mediator.

6.5.1 Transcriptional changes in TBX1-deficient endoderm

The anterior expansion of *Rarb* through the anterior endoderm of *Tbx1cKO*^{Sox17} embryos is in agreement with the hypothesis that TBX1 is a negative regulator of RA signalling (Guris et al., 2006). Although the expansion of *Rarb* in TBX1-deficient endoderm was not surprising, it was unexpected in context of maintained *Raldh2* and *Cyp26* gene expression. These data indicate that TBX1 in the mesoderm and/or ectoderm may be sufficient to regulate *Raldh2* expression in the mesenchyme. Moreover, it suggests that TBX1 may be a cell autonomous RA signalling antagonist, acting to regulate this pathway at the level of *Rarb* expression within the pharyngeal endoderm. The similarity in the expansion of *Cyp26b1* and *Rarb* expression in *Tbx1cKO*^{Sox17} embryos indicates that *Cyp26b1* may be a readout of RA signalling in the pharyngeal endoderm. Certainly, *Cyp26b1*

expression is induced in naïve T-cells exposed to all-*trans*-RA (Takeuchi et al., 2011). If *Raldh2* (when in excess) also negatively regulates *Cyp26b1* expression, this would explain why *Cyp26b1* expression is lost from the PA of Tbx1$^{-/-}$ embryos, (where *Raldh2* is expanded) but maintained in the *Tbx1cKO^{Sox17}* embryos (where *Raldh2* is maintained) (Guris et al., 2006). Finally, if RA is cleared to the same extent it is binding to RARB, the amount of active ectopic RA signalling in the rostral endoderm may be negligible. If the level of RA signalling is altered in the endoderm of *Tbx1cKO^{Sox17}* embryos it is not sufficient to change *Hox* gene expression.

Surprisingly, genes in the SHH signalling cascade, that are hypothesised to act upstream of *Tbx1*, were also expanded in the endoderm of *Tbx1cKO^{Sox17}* embryos (Garg et al., 2001; Yamagishi et al., 2003). One explanation may be that a feedback loop exists between TBX1 and the SHH pathway in the pharyngeal endoderm. *Shh* expression in the floorplate, (a signalling centre in the neural tube required for the specification and guidance of neural progenitors), is regulated by the binding of FOXA2 and T-BOX proteins to sites within the *Sonic hedgehog floor plate enhancer 2* (*Sfpe2*) (Jeong and Epstein, 2003). The binding of the *T-box* consensus motifs in *Sfpe2* inhibits the expression of *Shh* in specific areas of the central nervous system, such as the ventral diencephalon (Jeong and Epstein, 2003). In the pharyngeal endoderm the expression domains of *Tbx1* and *Shh* are largely complementary; *Tbx1* is expressed highly in the evaginating 3rd pouch at E9.5 whereas *Shh* is excluded from this region of endoderm. This observation indicates that TBX1 may also act to negatively regulate *Shh* expression in the pharyngeal pouches.

The expansion of the *Shh*, *Gli1* and *Ptch* expression into the caudal endoderm of

Tbx1cKO^{Sox17} embryos is ectopic. It is possible that ectopic SHH signalling in the caudal endoderm may prevent the endoderm from evaginating. Deletion of *Shh* from all tissues only mildly perturbs the formation of the caudal pouches, suggesting that this morphogen is not normally required for pouch outgrowth (Moore-Scott and Manley, 2005). Furthermore, no pouch defects were reported when *Smoothened* and *Patched* were conditionally deleted from the endoderm using NKX2.5^{Cre} (Goddeeris et al., 2007). If caudal pouch formation requires a SHH free environment, TBX1 may facilitate this by repressing *Shh* expression in the evaginating endoderm. Conserved non-coding sequences, have been identified as long-range enhancers of *Shh* expression in epithelial linings, including the pharyngeal endoderm (Sagai et al., 2009). If *T-box* consensus sites exist in these long-range enhancers, this may be a mechanism by which TBX1 can regulate the expression of *Shh* in the pharyngeal endoderm. Alternatively, TBX1 may regulate SHH signalling at the level of SHH target genes, such as *Gli1*. For instance, TBX1 family members, T-BOX 2 and T-BOX 3, have been implicated in the repression of Gli-mediated SHH signalling during Xenopus eye development (Takabatake et al., 2002). If this hypothesis is correct, pouch formation should be rescued by reducing the level of *Gli1* expression the endoderm of *Tbx1cKO*^{Sox17} embryos, (i.e. by generating *Sox17*$^{icre/+}$;*Gli1*$^{flox/-}$;*Tbx1*$^{flox/-}$ embryos).

The expression of the *Shh* agonist, *Bmp4*, is not altered in *Tbx1cKO*^{Sox17} embryos indicating that, overall, there may be no change to the amount and extent of active SHH signalling in the endoderm. A quantitative analysis of SHH signalling in the PA of *Tbx1cKO*^{Sox17} embryos by real-time quantitative PCR (qPCR) would help to clarify whether this pathway is up-regulated in the absence of *Tbx1.* Alternatively, the proposed SHH-mediated inhibition of *Bmp4* expression in the caudal

endoderm may be stage specific and thus not observed until E10.5 (Moore-Scott and Manley, 2005).

6.5.2 TBX1 affects the polarity of the actin cytoskeleton within the pharyngeal endoderm

Data presented here suggest that TBX1 may act as a tissue specific transcriptional repressor or activator of multiple genes in each of the FGF, RA and SHH pathways. However, a more parsimonious explanation may be that the expanded expression of multiple genes is a consequence of the change to the morphology of *Tbx1cKO*^{Sox17} embryo's endoderm. Actin supracables in the pharyngeal endoderm of chick embryos are thought to provide constraining forces that direct pharyngeal pouch formation (Quinlan et al., 2004). Disrupting the formation of organised actin cables in the pharyngeal endoderm causes pouches to form in a splayed or convoluted manner (Quinlan et al., 2004). The *Tbx1cKO*^{Sox17} data supports the inference that actin influences the morphogenesis of the pharyngeal endoderm into pharyngeal pouches. The deletion of *Tbx1* from the endoderm enables actin to accumulate along the basal edge of this epithelium. Presumably, the accumulation of ectopic actin at the basal edge of the pharyngeal endoderm puts an excessive constraining force on the endodermal cells that in turn prevents their evagination.

Correlating with the un-polarised accumulation of actin in the pharyngeal endoderm of *Tbx1cKO*^{Sox17} embryos was an observed up-regulation of *Fhl1* and a loss of pMLC. Active myosin is able to depolymerise F-actin (Haviv et al., 2008). Thus, the loss of basal pMLC in TBX1-deficient pharyngeal endoderm may enable actin to accumulate along the edge of this epithelia. In the otic placode the pMLC

mediated mechanism of achieving actin polarity is dependent on the phospholipase C (PLC) branch of the FGF signalling pathway (Sai and Ladher, 2008). FGF signalling appears to be maintained in the endoderm of *Tbx1cKO*^{Sox17} embryos. However, a detailed analysis of the PLC pathway specific genes is required to determine whether this branch of the FGF pathway is maintained in the absence of endodermal TBX1. Loss or reduction of the PLC pathway could also account for the loss of pMLC in TBX1-deficient pharyngeal endoderm.

The increased *Fhl1* expression may be a direct response to the loss of *Tbx1*. T-BOX proteins and LIM proteins are able to interact (Krause et al., 2004, Krcmery et al., 2010). However, to the best of my knowledge, an interaction between these factors at a transcriptional level has not been determined. An association between LMP4 and TBX5 has been established at the level of the protein, where the former mediates the shuttling of TBX5 from the nucleus to actin fibres in the cytoplasm (Krcmery et al., 2010). Yet, the interaction has only been established for the PDZ-LIM subgroup of LIM proteins. Alternatively, the increase in *Fhl1* expression may be a result of the TBX1 dependent accumulation of actin in the pharyngeal endoderm (Kadrmas and Beckerle, 2004). For instance an increase in actin polymerisation has been shown to enable myocardin-related transcription factor (MAL), a co-activator of serum response factor (SRF) to shuttle to the nucleus (Miralles et al., 2003). One of the transcriptional targets of SRF/MAL is *Fhl1*. It has been shown that the stable expression of MAL (and thus the expression of its target genes) reduces the migration of epithelial cells (Leitner et al., 2011). The inhibition of epithelial migration can be partially relieved by reducing FHL1 in the cells constitutively expressing MAL (Leitner et al., 2011). It is possible that the accumulation of F-actin at the basal edge of the pharyngeal endoderm (in the

absence of TBX1) facilitates the translocation of MAL to the nucleus where it is able to induce the expression *Fhl1*. If the same mechanism is observed *in vivo* as was observed by Lettiner et al., *in vitro*, then one would hypothesise that an increase in MAL/*Fhl1* in the pharyngeal endoderm would then prevent the migration of these epithelial cells toward the ectoderm (i.e. endodermal evagination). The latter mechanism could account for the inhibition of caudal pouch morphogenesis in *Tbx1cKO*^{Sox17} embryos pharyngeal endoderm.

Chapter 7

DISCUSSION

7.1. TBX1 regulates pharyngeal pouch morphogenesis independently from its effect on the expression of genes in the FGF signalling cascade

The PA is a transient but complex structure contributed to by four different cell types, ectoderm, endoderm, CNCC and mesoderm, the two latter cell types also differentiate into endothelial and mesenchymal tissue (Graham, 2003). The correct formation of the PA is essential for the development of many of its derivatives later in gestation, such as the thymus. It is emerging that the pharyngeal endoderm plays a prominent role in directing the morphogenesis of the PA. During PA formation, the pharyngeal endoderm evaginates toward the ectoderm to produce discreet 'slit-like' pouches (Quinlan et al., 2004). The process of pharyngeal pouch morphogenesis is perturbed by the deletion of many genes, including *Tbx1* and *Fgf8*. Caudal pharyngeal pouches do not develop in *Tbx1*$^{-/-}$, *Tbx1* hypomorphic and *Fgf8* hypomorphic embryos (Jerome and Papaioannou, 2001; Hu et al., 2004). The observation that *Fgf8* expression is lost in the pharyngeal endoderm of *Tbx1*$^{-/-}$ embryos has led to the hypothesis that FGF8 functions downstream of *Tbx1* in the endoderm to regulate pouch morphogenesis (Vitelli et al., 2002b). However, a lack of mouse models with endoderm-specific CRE activity prevented this hypothesis from being tested. This thesis addressed whether *Tbx1, Fgf8* and FGF signalling is required specifically in the endoderm during pouch morphogenesis using a new endoderm specific *Sox17*^{iCre} mouse line (Engert et al., 2009). Surprisingly, data presented in this thesis suggests that neither FGF8 not the FGF pathway acts directly downstream of *Tbx1* in the endoderm during pouch morphogenesis. In light of these findings, alternative

mechanisms by which TBX1 may regulate pouch morphogenesis within the PA were examined.

7.1.1 Pharyngeal pouch defects caused by the loss of *Tbx1* from the endoderm are distinct from the defects caused by deficiencies in endodermal FGF signalling

The deletion of *Tbx1* during development has demonstrated that this transcription factor is essential to the formation of the PA (Baldini, 2005; Scambler, 2010). Tissue-specific functions of TBX1 in the PA have begun to be elucidated through the analysis of mouse lines in which this transcription factor had been deleted from one or more cell types during development (Baldini, 2006). The studies found that the pharyngeal arch arteries and cranial nerves require a source of ectodermal *Tbx1* for their development (Zhang et al., 2005; Calmont et al., 2009). Mesodermal *Tbx1* is important for the formation of the cardiac outflow tract and the patterning of the proximal mandible (Zhang et al., 2006; Aggarwal et al., 2010). The deletion of *Tbx1* from the endoderm mediated by FOXG1^{Cre} on a Swiss-Webster (S-W) genetic background (*PE*-KO embryos) fully recapitulates the pharyngeal pouch defects observed in *Tbx1*$^{-/-}$ embryos (Arnold et al., 2006), thus indicating that the expression of *Tbx1* in the endoderm is essential for caudal pouch morphogenesis.

Surprisingly, however, the deletion of *Tbx1* from the mesoderm (*M-KO* embryos) affects pouch and thymus formation. *M-KO* embryos display pouch defects that are similar to *Tbx1*$^{-/-}$ embryos and reactivation of mesodermal *Tbx1* expression in *Tbx1* hypomorphic embryos partially rescues pouch formation (Zhang et al., 2006).

Thymus hypoplasia was also evident in *PSE-KO* embryos, although pouch defects were not documented in these mutants (Randall et al., 2009). These results, taken together with the finding that the *Foxg1Cre* is non-specifically expressed in PA tissue on genetic backgrounds other than S-W, questioned whether *Tbx1* was required specifically in the endoderm during pouch morphogenesis (Zhang et al., 2005). The data in Chapter 3 supports the conclusion that caudal pouch morphogenesis requires *Tbx1* expression in the endoderm, as *Tbx1cKO*^{Sox17} embryos display caudal pouch aplasia.

In contrast to hypotheses in the field, the data in this thesis does not provide evidence to support the prediction that TBX1 in the endoderm controls pouch morphogenesis via transcriptional regulation of the FGF pathway. Many pieces of evidence indicated that TBX1, a cell-autonomous manner, would regulate the expression of genes in the FGF pathway. The promoter elements of *Fgf8* and *Fgf10* contain *T-box* consensus sites to which TBX1 can bind. *In vitro* TBX1 has been demonstrated to activate luciferase expression driven from these FGF promoters (Hu et al., 2004; Xu et al., 2004). The observation that *Fgf3, Fgf8* and *Fgf10* are all absent from the endoderm of *Tbx1*$^{-/-}$ and *PE-KO* embryos further indicated that FGF signalling *in vivo* may be regulated by TBX1 (Vitelli et al., 2002b; Aggarwal et al., 2006; Arnold et al., 2006). Yet, data in Chapter 3 show that only *Fgf8* expression is lost from the endoderm of *Tbx1cKO*^{Sox17} embryos. The maintained expression of multiple *Fgf* ligands and *Fgf* signalling targets in *Tbx1*-deficient endoderm represents the first indication, to my knowledge, that the FGF pathway and TBX1 may only interact indirectly, within the endoderm, during pouch morphogenesis. Further evidence to support the conclusion that the FGF pathway and TBX1 do not interact directly within the endoderm during pouch morphogenesis came from the

observation that a compound deletion of *Fgf3* and *Fgf8* or *Fgfr1* and *Fgfr2* from the endoderm generates pouch defects that are distinct from those of *Tbx1cKO*^{Sox17} embryos.

The deletion of *Fgf8* from the endoderm did not have an effect on pharyngeal pouch formation (see Chapter 4). However, the compound deletion of *Fgf3* and *Fgf8* or *Fgfr1* and *Fgfr2* from the endoderm generated rostral pouch defects similar to those observed in *Fgfr1* hypomorph (Trokovic et al., 2003; Trokovic et al., 2005). This data demonstrates that FGF signalling in the endoderm, maintained by FGF ligand and FGF receptor redundancy, regulates pouch morphogenesis. The similarity of pouch defects in *R1;R2cKO*^{Sox17}, severe-*Fgf8* hypomorphs and *Fgfr1* hypomorphs and the incomplete penetrance of pouch defects in *F3;F8cKO*^{Sox17} embryos indicates that FGF signalling in the endoderm may also be elicited and maintained, in part, by FGF ligands from adjacent PA tissues. It would be interesting to determine whether it is the amount of ligand, the type of ligand or the location of the FGF ligand that is critical for directed pouch evagination. One possible approach to test the requirements of FGF ligands in the PA would be to drive the expression of *Fgf3* from the *Fgf8* promoter in an *Fgf8* hypomorphic background. If the expression of *Fgf3* in *Fgf8* expression domains did not rescue pouch morphogenesis, this would suggest that it is the FGF8 protein that is specifically required for pouch outgrowth, rather than a certain amount or location of FGF signalling that could be elicited by any FGF ligand with the same spatio-temporal expression as *Fgf8*.

Analysis of the pharyngeal endoderm of *Tbx1cKO*^{Sox17} and *R1;R2cKO*^{Sox17} embryos revealed that these mutants have distinct pouch phenotypes. The loss of *Tbx1*

prevents the caudal endoderm from evaginating laterally toward the ectoderm. Conversely, in endoderm deficient of FGF signalling, the epithelium appears to evaginate toward the ectoderm but does so without direction. In addition to the contrasting pouch phenotypes, the pharyngeal arches of each mutant also form with distinct defects. In *Tbx1cKO^{Sox17}* the lack of caudal pouch evagination prevents all but the 1st and occasionally a severely hypoplastic 2nd arch from forming. In contrast, the proximal portion of the 2nd arch is most severely affected in endodermal FGF mutants because of the disorganised evagination of the rostral endoderm. Interestingly, comparing the *Pax1* delineated pouch defects of *Fgf8*-severe hypomorphs and *Fgfr1* hypomorphs with *Tbx1* hypomorphs and *Tbx1*$^{-/-}$ embryos similar distinctions in pouch morphology are evident. The rostral pouches of *Fgf8* and *Fgfr1* hypomorphs are evident but appear splayed and fused, whereas the pharyngeal endoderm caudal to the 1st pouch is unable to evaginate in *Tbx1* null and *Tbx1* hypomorphic embryos (Jerome and Papaioannou, 2001; Abu-Issa et al., 2002; Trokovic et al., 2003; Hu et al., 2004).

7.1.2 *Tbx1* does not genetically interact with the FGF pathway, in the pharyngeal endoderm, during pouch morphogenesis

The prediction that FGF8 might act downstream of TBX1 in the endoderm during pharyngeal pouch development was also borne from the evidence that *Fgf8* and *Tbx1* genetically interact during other aspects of PA development. The combined deletion of one allele of *Tbx1* and one allele of *Fgf8* during development (*Fgf8*$^{+/-}$*;Tbx1*$^{+/-}$ embryos) results in an increased incidence of 4th PAA defects and an

incidence of aortic arch defects compared to *Tbx1*$^{+/-}$ and *Fgf8*$^{+/-}$ embryos (Aggarwal et al., 2006). Furthermore, the deletion or forced expression of *Fgf8* in the *Tbx1* expression domain modifies aortic arch and OFT phenotypes of Tbx1$^{-/-}$ embryos, respectively recapitulating or rescuing the defects observed in the mutant. *Tbx1* and *Fgf8* have also been demonstrated to interact during the organogenesis of endocrine organs derived from the pharyngeal endoderm. An increase in the incidence of thymus hypoplasia is reported in *Fgf8*$^{+/-}$;*Tbx1*$^{+/-}$ embryos relative to *Tbx1*$^{+/-}$ embryos (Brown et al., 2004; Vitelli et al., 2010). Moreover, thyroid hypoplasia manifests when *Fgf8* is deleted from *Tbx1* positive cells and is partially rescued by driving *Fgf8* transcription in *Tbx1* expression domains (Lania et al., 2009). Pouch morphogenesis has not been analysed in embryos deficient of both *Fgf8* and *Tbx1*. The observation that pouch formation in *Fgf8*;*Tbx1cHet*^{Sox17} embryos is relative to pouch formation in *Fgf8cHet*^{Sox17} and *Tbx1cHet*^{Sox17} embryos is thus a novel finding. The lack of epistasis between *Fgf8* and *Tbx1* in the endoderm during pouch morphogenesis further supports the inference that TBX1 and FGF8 function in parallel within this epithelium during pouch outgrowth. Whether *Fgf8* and *Tbx1* interact in the endoderm during pharyngeal pouch patterning or thymus organogenesis requires an analysis of *Fgf8*;*Tbx1cHet*^{Sox17} embryos later in gestation.

The data in this thesis demonstrates that it is unlikely that a loss of FGF signalling in the endoderm of *Tbx1cKO*^{Sox17} embryos is preventing caudal pouch evagination. The genetic interaction between FGF signalling and TBX1 in the endoderm was assessed by generating *Spry1;Spry2cHet;Tbx1cKO*^{Sox17} embryos and analysing the extent of pouch formation in these mutants, (see section 5.3.2). It was demonstrated that the caudal pouch aplasia of *Tbx1cKO*^{Sox17} embryos could not be

rescued by genetically de-regulating FGF signalling in the pharyngeal endoderm. This data fits with the observation that the expression of FGF target genes are maintained in the endoderm of *Tbx1cKO^{Sox17}* embryos. Aggawarl et al., found that the compound deletion of *Fgf3,Fg8* and *Tbx1* (i.e. *Fgf3$^{-/-}$;Fgf8$^{+/-}$;Tbx1$^{+/-}$* embryos) did not increase the incidence or severity of thymus defects compared to *Fgf8$^{+/-}$;Tbx1$^{+/-}$* embryos (Aggarwal et al., 2006). They hypothesised that multiple FGF ligands in the pharyngeal endoderm, in addition to *Fgf3, Fgf8* and *Fgf10*, act redundantly during thymus organogenesis (Aggarwal et al., 2006). The data in this thesis presents an alternative theory; TBX1 does not act in the same pathway as the FGF signalling cascade, within the endoderm, during pouch morhogenesis. A lack of genetic interaction between these factors within the endoderm may also occur during the organogenesis of derivatives of the pharyngeal endoderm, such as the thymus.

7.2 TBX1 may control pouch morphogenesis by regulating the activity of several signalling pathways

The present study has demonstrated that genes within the FGF, RA and SHH signalling pathways are all perturbed by the endoderm specific deletion of *Tbx1*. Whilst TBX1 may directly affect the transcription of all the anteriorly expanded genes in the pharyngeal endoderm (i.e. *Shh, Ptch, Erm, Fgf3, Rarb, Cyp26b1*), the number of genes affected and the similarity in the change to the pattern of their expression suggests that these defects may not be direct.

Alternatively it possible that TBX1 in the endoderm controls pouch morphogenesis

by positively regulating the transcription of a genes that time did not permit a full analysis of within this study. For instance, literature suggests that both *Serum response factor* (*Srf*) and homeobox domain containing (*Gbx2*) may be associated with *Tbx1* during PA development (Byrd and Meyers, 2005; Chen et al., 2009). Microarray and expression analysis has demonstrated that *Gbx2* is down regulated in the PA of *Tbx1* null embryos, including the pharyngeal endoderm (Ivins et al., 2005). However, an initial analysis of *Gbx2* in *Tbx1cKO*^{Sox17} embryos did not identify a significant loss of endodermal expression. Whilst this result needs to be confirmed, it fits with the observation that *Gbx2*$^{-/-}$ embryos appear to have normal pouch morphogenesis (Byrd and Meyers, 2005). Moreover, although *Gbx2* expression was maintained in the endoderm of the *Tbx1cKO*^{Sox17} embryos it appeared un-segmented, akin to the expression of genes in the SHH, RA and FGF pathways.

Similarly, an initial analysis of (*Eya1*) expression in *Tbx1cKO*^{Sox17} embryos also found transcripts to be expressed in an un-segmented manner throughout the pharyngeal endoderm. The expression of *Tbx1* is reduced in the pharyngeal endoderm of *Eya1* null mutants, indicating that EYA1 likely acts upstream of *Tbx1* during pouch morphogenesis (Zou et al., 2006). The latter inference was supported by microarray and *in situ* data that showed no change in the expression of *Eya1* in the pharyngeal region of embryos null for *Tbx1* (Ivins et al., 2005). Thus, like *Shh*, *Eya1* expression was not predicted to change in the endoderm of *Tbx1cKO*^{Sox17} embryos. The observation that multiple genes in the endoderm of *Tbx1cKO*^{Sox17} embryos display an un-segmented, expanded pattern of expression, (especially those predicted to act upstream of TBX1), indicates that this may be a response to the perturbed morphology of the endoderm, rather than being evidence of TBX1

acting as a transcriptional regulator of multiple genes in the pharyngeal endoderm.

7.3 TBX1 may control pouch morphogenesis by regulating the polarity of actin within the pharyngeal endoderm

The data presented in Chapter 6 indicates that TBX1 may control the morphogenesis of the pharyngeal pouches by regulating the polarity of the actin cytoskeleton within the endoderm. Disruption of the actin network has been demonstrated to perturb the morphogenesis of a number of structures in development. The formation of disorganised actin cables prevents the formation of 'slit like' pharyngeal pouches in the chick (Quinlan et al., 2004). The loss of actin polarity in the otic placode prevents the invagination of this thickened ectodermal epithelium (Sai and Ladher, 2008). Furthermore, the coordinated forward movement of epithelial cells at the leading edge during dorsal closure of *Drosophila* embryos is regulated and enabled, in part, by the constraining force of actin cables (Jacinto et al., 2002).

It is possible that TBX1 may directly affect actin dynamics and polarity within the pharyngeal endoderm. *Optomotor-blind* (*omb*) is a *Drosophila* homologue of the mammalian *Tbx2* gene family. A graded concentration of *omb* exists along the A-P axis of the *Drosophila* embryos wing disc pouch (Shen et al., 2010). The gradient influences epithelial cell shape by mediating actin dynamics, the resulting cell-shape in turn determines the affinity between neighbouring cells. The clonal loss of *omb* results in a cell-autonomous accumulation of F-actin, causing the mutant

clones to become more rounded in shape (Shen et al., 2010). As a consequence of this shape change, the rounded mutant clone retracts away from the less rounded adjacent wild type cells at their apical surface. The study by Shen et al. does not determine how the loss of *omb* function causes a rearrangement of the actin cytoskeleton. However, it does show that the clonal cytoskeleton re-arrangements are independent from the transcriptional effect *omb* has on its downstream target *sal* (Shen et al., 2010). The ability of this T-BOX homologue to maintain independent functions as a direct regulator of transcription and as a direct regulator of cytoskeletal re-arrangements may be a characteristic of all T-BOX proteins. If so, this characteristic could explain why in *Tbx1*-deficient pharyngeal endoderm the actin network is un-polarised but the expression of genes predicted to act downstream of TBX1 (i.e. *Cyp26b1*, *Erm*) are maintained.

The expanded expression of genes in the RA, SHH and FGF signalling cascade may be indirect changes caused by actin-induced alterations to the *Tbx1*-deficient endoderm. Alternatively, actin-associated proteins may actively alter the genetic profile of the pharyngeal endoderm of *Tbx1cKO*^{Sox17} embryos. It has been demonstrated that the re-distribution of myocardin-related transcription factor (MAL/MRTF), a co-activator of SRF, from the cytoplasm to the nucleus is dependent on (Rho dependent) actin treadmilling, (the polymerisation of G-actin to F-actin) (Miralles et al., 2003). For instance, endogenous MAL was prevented from accumulating in the nucleus when ß-actin was overexpressed. Conversely, the stabilisation of F-actin by the drug Jasplakinolide induces a nuclear accumulation of MAL. From this data it was predicted that the polymerisation of G-actin in the cytoplasm releases the associated MAL protein that subsequently translocates to the nucleus and forms a transcriptional complex with SRF (Miralles

et al., 2003). It is possible that the increase in F-actin in *Tbx1*-deficient endoderm may also initiate the transcription of SRF target genes, one of which is *Fhl1,* by inducing ectopic or elevated levels of MAL in the nucleus.

LIM domain proteins are also attractive candidates for actin-associated proteins that could alter the genetic profile of the pharyngeal endoderm of *Tbx1cKO*^{Sox17} embryos. LIM domain proteins are able to associate with actin and, in the case of the FHL family, can also modulate the assembly of transcriptional complexes (Kadrmas and Beckerle, 2004; Krause et al., 2004). T-BOX proteins and LIM domain proteins have been found to interact during heart and lim bud development (Krause et al., 2004; Bimber et al., 2007). Interestingly, co-transfection of *Tbx5* and *Lmp4* into COS-7 cells, (that do not express either factor), inhibited the TBX5 dependent activation of FGF10 luciferase reporters (Camarata et al., 2006; Bimber et al., 2007). This data links T-BOX mediated transcription with actin associated LIM proteins. The effect deleting T-BOX proteins has on the function of LIM domain proteins has not yet been investigated. The data in this thesis shows *Fhl1* expression is increased in the actin-rich endoderm of *Tbx1cKO*^{Sox17} embryos. Whether TBX1 associates with FHL1 at the protein level to regulate gene transcription or indeed remodelling of the actin cytoskeleton is yet to be tested.

7.4 Proposed model of pharyngeal pouch morphogenesis

The work in this thesis presents a number of novel and interesting results revealing how genes expressed in the pharyngeal endoderm interact during pouch morphogenesis. The most significant finding being that FGF signalling does not appear to act directly downstream of *Tbx1* in the pharyngeal endoderm during pouch morphogenesis. The next challenge is to identify FGF-dependent and TBX1-dependent mechanisms of endodermal evagination that, when integrated, explain how pouch morphogenesis occurs. A model for pharyngeal pouch morphogenesis is emerging based on the findings of this thesis and literature in the field. It is loosely based on the inference of Takeuchi et al. that *T-box* and *Fgf* genes are both required for limb bud outgrowth. However the role of the former is to initiate outgrowth whereas the role of the latter is to maintain growth (Takeuchi, 2003). The model below similarly proposes that TBX1 initiates pouch outgrowth by regulating actin polarity. TBX1, directly or indirectly, induces the activation of myosin (as an ADF) at the basal edge of the pharyngeal endoderm and *Fgf8* expression within the pharyngeal endoderm. The TBX1 mediated regulation of actin bundling in the 3rd pouch may also regulate the amount of *Fhl1* expression, alternatively TBX1 may directly inhibit transcription of this LIM domain factor. Endodermal evagination occurs because the cells are not constrained by the actin network. In parallel FGF signalling, induced by FGF ligands other than FGF8, is elicited in a TBX1-independent manner. The FGF signalling in the evaginating, *Tbx1* positive endoderm maintains directed pouch outgrowth.

In TBX1-deficient endoderm there is a loss of activated MLC and an up-regulation of *Fhl1* that enables actin to accumulate along the basal edge of the pharyngeal

endoderm, preventing the epithelial cells from evaginating. It is possible that the loss of TBX1 dependent *Fgf8* expression reduces signalling from the Plugs pathway of the FGF signalling cascade. The Plugs pathway has been shown to be required for pMLC accumulation at the basal edge of the otic placode. Signalling downstream of FGF3 is maintained because *Fgf3* transcription is initiated independently of TBX1 in the pharyngeal endoderm, however, this signalling cascade is not sufficient to initiate pouch evagination, only to maintain pouch outgrowth.

Fig 57

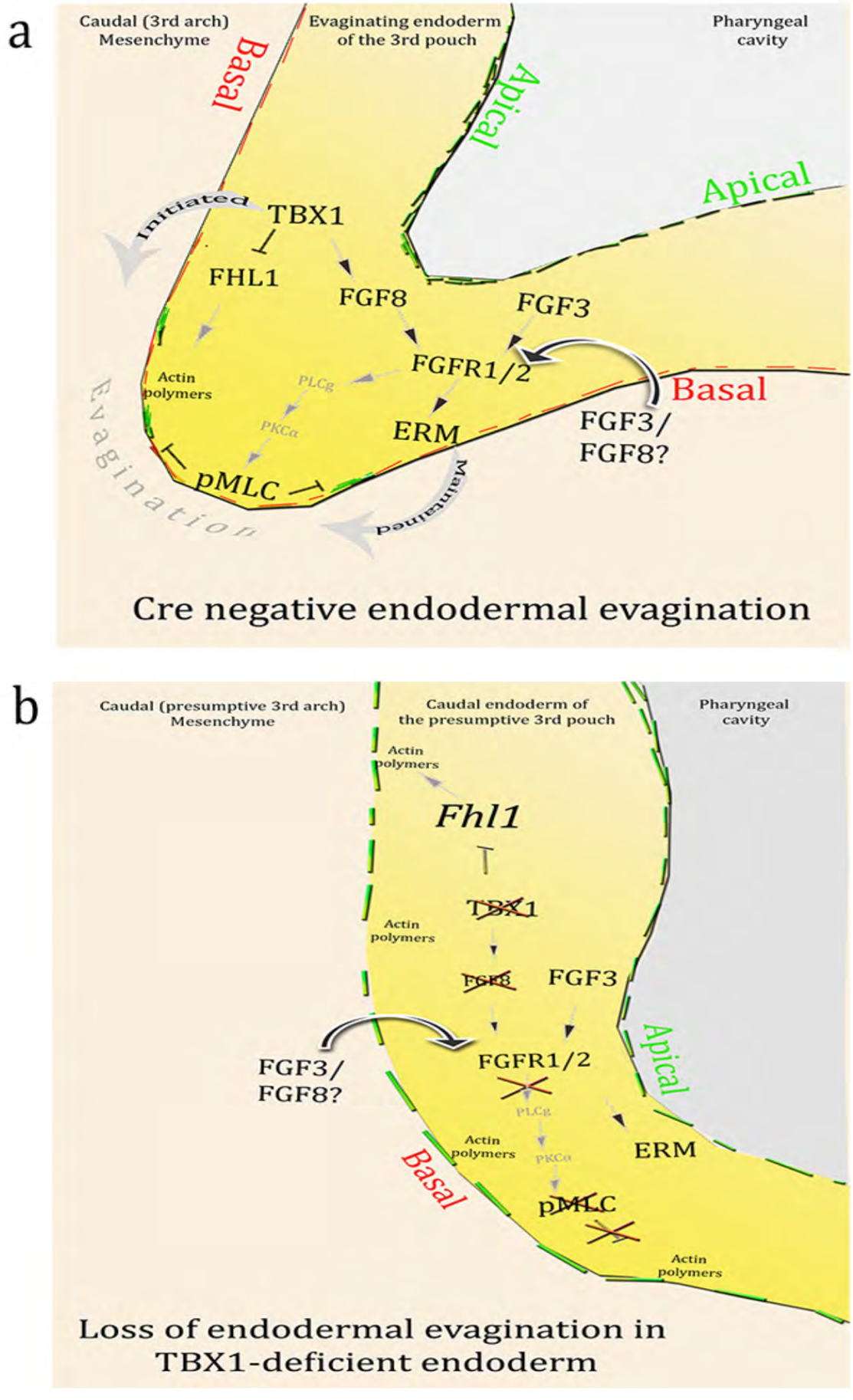
a
Caudal (3rd arch) Mesenchyme
Evaginating endoderm of the 3rd pouch
Pharyngeal cavity
Basal
Apical
Apical
Initiated
TBX1
FHL1
FGF8
FGF3
FGFR1/2
Actin polymers
PLCg
PKCa
ERM
Basal
FGF3/ FGF8?
pMLC
Evagination
Maintained
Cre negative endodermal evagination
b
Caudal (presumptive 3rd arch) Mesenchyme
Caudal endoderm of the presumptive 3rd pouch
Pharyngeal cavity
Actin polymers
Fhl1
TBX1
Actin polymers
FGF8
FGF3
FGF3/ FGF8?
FGFR1/2
Apical
PLCg
Actin polymers
PKCa
ERM
Basal
pMLC
Actin polymers
Loss of endodermal evagination in TBX1-deficient endoderm

Fig 57. A model proposing mechanisms through which pharyngeal pouch morphogenesis is regulated.

(a) The initiation of endodermal evagination is dependent on TBX1 functioning in the endoderm as a regulator of actin polarity. TBX1 may achieve this by positively influencing the activation of the ADF, pMLC, at the basal edge of the endoderm. The TBX1-dependent activation of MLC may be achieved via FGF8, a transcriptional target of TBX1. pMLC accumulation in the otic placode requires signalling from the Plugs pathway, it is possible that FGF8 activates this pathway and thus MLC in the pharyngeal endoderm. TBX1 may also control actin polymerisation by negatively regulating the actin effector FHL1. Polarised actin within the pharyngeal endoderm enables evagination to occur. This process appears to be maintained and directed by FGF signalling in the endoderm that is activated either a) independently of TBX1 e.g. through signalling elicited by FGF3, or, b) from FGF ligands present in the adjacent pharyngeal tissue, such as the mesenchyme, that could bind to FGFRs in the endoderm.

(b) In TBX1 deficient endoderm actin becomes polymerised along the apical and basal edges of the pharyngeal endoderm. The presence of unpolarised actin is correlated with an up-regulation of *Fhl1* in the endoderm and a loss of pMLC at the basal edge of the epithelium. The loss of pMLC may be attributed to the severely diminished expression of, (or absence of), *Fgf8* in the endoderm that likely would be unable to activate PLCg signalling that has been demonstrated to act upstream of pMC in the avian otic vesicle. In contrast FGF signalling is maintained in the *Tbx1*-deficient endoderm. It is possible that the expression of FGF targets such as *Erm* is elicited through either a) endodermal-FGF3 that is maintained in the absence of TBX1, or, b) from FGF ligands present in the adjacent pharyngeal tissue, such as the mesenchyme. However, in the absence of TBX1, FGF signalling is not sufficient for pharyngeal pouch morphogenesis to occur.

In a and b, yellow depicts the pharyngeal endoderm, pink is the pharyngeal mesenchyme and grey is the pharyngeal cavity. Green strands represent F-actin and red represents pMLC in the Tbx1-positive endoderm.

7.5 Future work

The data in this thesis has identified new potential mechanisms whereby loss of *Tbx1* could affect pouch outgrowth. My findings reveal that for pouch morphogenesis to occur TBX1 and FGF signalling are both required in the endoderm. FGF ligands and receptors act redundantly within the endoderm to maintain FGF signalling that drives directed pouch outgrowth. In the absence of endodermal *Tbx1*, FGF signalling is elicited through FGF ligands other than FGF8, the expression of which is TBX1-dependent. The latter indicates that FGF signalling does not act directly downstream of TBX1 in the endoderm to regulate pouch outgrowth. TBX1 appears to control pouch morphogenesis, independently from its effects on the expression of genes in the FGF signalling cascade, by regulating the polarisation of the actin cytoskeleton within the pharyngeal endoderm. To verify and expand this pouch paradigm future work should test the novel predictions that are implicit in the 'proposed model of pharyngeal pouch morphogenesis' (Fig 57).

The model assumes that the loss of endodermal-*Tbx1* has a cell autonomous effect on the morphogenesis of the pharyngeal endoderm. The data in this thesis shows that *Tbx1* is required in the endoderm for pouch formation. However, it does not demonstrate that *Tbx1* in the pharyngeal endoderm is a) sufficient to drive pharyngeal pouch morphogenesis or b) acting cell autonomously during pouch morphogenesis. The reactivation of mesodermal *Tbx1* expression in a *Tbx1* hypomorphic background (*M-KO* embryos) partially rescues pouch formation. (Zhang et al., 2006). This indicates that *Tbx1* in the mesoderm is sufficient to drive pouch outgrowth. This observation is surprising, for expression of *Tbx1* in the mesoderm is not sufficient to maintain pouch morphogenesis in *TbxcKO*^{Sox17} embryos. To prove that endodermal *Tbx1* is sufficient for pouch formation *Tbx1*

expression should be re-introduced into the endoderm of *Tbx1*$^{-/-}$ embryos in a CRE-dependent manner. The use of a mosaic CRE line to delete *Tbx1* in the endoderm would also begin to test whether TBX1 functions cell autonomously in this epithelium to regulate pouch morphogenesis. The tamoxifen inducible *Foxa2CreER*^{T2} mouse line, in our hands, displayed mosaic activity in the pharyngeal endoderm and was not used further in this project. However the mosaic activity of the *Foxa2CreER*^{T2} line could be used to delete *Tbx1* from individual cells in the pharyngeal endoderm. If TBX1 acts cell autonomously, *Tbx1* null cells should display the defects observed throughout the endoderm of *Tbx1cKO*^{Sox17} embryos, particularly an unpolarised accumulation of actin. The surrounding *Tbx1* positive cells should not be affected.

The model (based on findings from this thesis) proposes that endodermal TBX1 facilitates pouch outgrowth by regulating the polarisation of the actin in the pharyngeal endoderm. Experiments were initiated to confirm that the changes in actin dynamics were directly attributable to the loss of *Tbx1*. Gut epithelial (CACO2) cells were to be transfected with a *Tbx1* expression vector or with an expression vector carrying a dominant negative form of *Tbx1*. Subsequently phalloidin-marked changes in F-actin in the transfected cells were to be analysed by confocal microscopy. Unfortunately, this assay was not optimised in time for the completion of this thesis but it would be an effective way to begin to experimentally address whether TBX1 is able to directly facilitate changes in the actin cytoskeleton.

Alternatively, R26R expressing endodermal cells isolated by FACS from the PA of *Sox17*$^{icre/+;}$*R26R*^{2} and *Sox17*$^{icre/+;}$*Tbx1*$^{flox/-;}$*R26R*^{2} embryos may provide more

relevant cell lines to address the cell autonomous role of TBX1 as a regulator of the actin cytoskeleton. *In vitro* cultures of the FACS sorted *Tbx1* positive and *Tbx1* negative cells should, respectively, display polarised and un-polarised actin. Transfecting the *Tbx1cKO*^{Sox17} endodermal cells with a *Tbx1* expression vector should re-establish actin polarity in these mutant cells, perhaps by activating basal pMLC, if TBX1 directly regulates F-actin distributing in the pharyngeal endoderm.

The possibility that there is a link between the changes in F-actin, *Fhl1*, TBX1 and the de-regulated expression of multiple genes in the endoderm of *Tbx1cKO*^{Sox17} embryos is very speculative. To begin to address this possibility, first, a direct interaction between FHL1 and TBX1 in the pharyngeal endoderm needs to be determined. From the data in this study it appears that TBX1 may be able to regulate the transcription of *Fhl1*. If this transcriptional regulation is direct *T-box* consensus sites should be evident upstream of the *Fhl1* promoter. If TBX1 negatively regulates the transcription of *Fhl1* via the binding of such a consensus site, mutagenesis of this motif would render *Fhl1* expression insensitive to TBX1 regulation. This could be tested *in vitro* by assessing the amount of luciferase expression driven from an *Fhl1* promoter construct in the presence, or absence, of a *Tbx1* expression construct. One would hypothesise that there would be less luciferase expression in the presence of TBX1 if this protein negatively regulates *Fhl1* transcription. There should be no inhibition of luciferase expression when repeating the experiment with a *Tbx1* expression construct lacking the *T-box* domain, or, with an *Fhl1* promoter construct lacking the *T-box* consensus site. Alternatively TBX1 and FHL1 proteins may associate, as has been observed with LMP4 and TBX5. To determine whether TBX1 and FHL1 form a complex in the pharyngeal endoderm co-precipitation experiments could be performed, using

TBX1 as bait to pull down FHL1 from endodermal cells sorted by FACS from mutant and control embryos (as described above). If FHL1 and TBX1 do complex it would be interesting to determine whether the complex localises to actin (by confocal microscopy) and what affect this has on gene expression. It is possible that the expanded expression of genes such as *Shh* and *Rarb* in Tbx1-deficient endoderm may elicited downstream of FHL1. Transfecting cells absent of endogenous *Tbx1* or *Fhl1* with these expression constructs carrying these genes, singly and in combination, and subsequently analysing levels of gene expression (such as *Shh*) by qPCR would indicate whether the *in vivo* transcriptional changes are the result of unregulated FHL1.

7.5 Concluding remarks

This study has revealed a number of novel and exciting findings that further elucidate mechanisms that regulate pharyngeal pouch morphogenesis specifically within the endoderm. The observation that pharyngeal pouch morphogenesis is maintained by multiple FGF ligands and FGF receptors in the pharyngeal endoderm, highlights the importance of using conditional mouse lines to study PA development. FGF8 is clearly important for the development of the PA and the pouches within. However, surprisingly, the requirement for *Fgf8* expression within the endoderm is negligible for pouch formation. Furthermore, if *Tbx1* had not been tissue specifically analysed in the endoderm, its effect on the actin cytoskeleton may not have been revealed because the positive regulation of FGF signalling, on a 'global' scale, within the PA is so pronounced.

The observation that TBX1 mediates actin dynamics within the pharyngeal endoderm opens up new avenues of research with regards to understanding pouch morphogenesis (as highlighted in Chapter 6). The data also has a broader implication for understanding other structures that form by epithelial invagination or evagination, such as the pancreatic bud and the pronephric duct of the early kidney. Most significantly, the link between TBX1, the FHL family of LIM proteins and the actin cytoskeleton may be highly relevant for the formation of the cardiovascular system, defects of which are the main cause of morbidity in patients with DiGeorge syndrome (Scambler, 2010). An association between T-BOX proteins and LIM domain proteins has already been established during cardiogenesis. In epicardial cells (that form smooth muscle cells that line aspects of the heart, such as the myocardial wall) this interaction was related to the developmental state of the cell. TBX5 translocated from the nucleus to the

cytoplasm in epicardial cultures that were stimulated to differentiate. In the cytoplasm of the differentiated epicardial cells TBX5 co-localised to actin fibres with the LIM protein LMP4 (Camarata et al., 2006; Bimber et al., 2007). Interestingly, co-transfection of TBX5 and LMP4 into COS-7 cells, (that do not express either factor), inhibited the TBX5 dependent activation of *Fgf10* luciferase reporters. At E8.5 *Fhl1* is expressed in the OFT of the heart (Chu et al., 2000). It would be interesting to determine whether an FHL1 dependent shuttling of TBX1 is important for gene regulation, especially *Fgf10*, and thus subsequent morphogenesis of the OFT.

Appendices

APPENDIX A: Oligonucleotide sequences, requisite PCR master mixes and PCR product band size

DNA sequences were obtained from the Entrez Nucleotide database and transferred to Mac vector primer design software. Forward and reverse primer pairs with the highest efficiency and lowest duplex probability, as determined by the software, were selected. RNA polymerase promoter binding sites were added to the 3' end of forward primers used to synthesis PCR probes for RNA in situ hybridisation (see 2.4.5). If the primers were for PCR, no promoter binding sites were added. Oligonucleotides were synthesised by Millipore (MGW) and re-suspended in RNase free PCR grade H_2O to a concentration of 100mM. For working solutions dilute olio's 1:10.

APPENDIX A: Oligonucleotides and PCR parameters

Name of oligonucleotides (primers), (denote PCR probe primers)**	**Primer sequences**	**Master mix required/ PCR programme**	**Band size expected (bp)**
Fgf Receptor 1	(A)GTATTGCTGGCCCACTGTTC (B)CTGGTATCCTGTGCCTATC (C)CAATCTGATCCCAAGACCAC	Roche/AB 55 X 40	Floxed (B+C): 387 Null (C): 300 Wild Type (B+C):327
Fgf Receptor 2	(A)TGCAAGAGGCGACCAGTCAG (B) ATAGGAGCAACAGGCGG (C)CATAGCACAGGCCAGGTTG	Roche/AB 55 X 40	Floxed (A+B): 207 Null (A+C): 471 Wild Type (A+B): 327

Fhl2 (T7)	Fwd: GTAAGAAGTGCTCCCTGTCTCTGG Rev: ATTGTAATACGACTCACTATAGGGAGAA AACATCCGAATCTCTGCG	Roche/AB 55X40	138 bp
Lmo3(T7)	Fwd: TTGCCAGACAGACTACGAGGAAG Rev: ATTGTAATACGACTATAGGGGGTTATGAC AAGAACGC	Roche/AB 55X40	700 bp
Lmo4 (T7)	Fwd: AGAATGCGTGCCTTCATCTCAG Rev: ATTGTAATACGACTACGGAGCAACATCAG GACAAGAAC	Roche/AB 55X40	552bp
R262	(A)AAAGTCGCTCTGAGTTGTTAT (B)GCGAAGAGTTTGTCCTCAACC (C)GGAGCGGGAGAAATGGATATG	Roche/AB 55	R26R band (A + B): 250 Wild Type (A+C): 500
Sprouty 1	(A)GGGAAAACCGTGTTCTAAGGAGTAGC (B)GTTCTTTGTGGCAGACACTCTTCATTC (C)CTCAATAGGAGTGGACTGTGAAACTG C	Promega/ AB55 X 40	Floxed (A +C): 342 bp Null (A +B): 150 Wild Type (A +C): 311
Sprouty 2	(A)GGATGGCTCTGATCTGATCC (B)TTGAGAACATGCCTCGACC (C)GCATGGGCTATTCACAAAC	Promega/ AB57 X 40	Floxed – 500 Null - 255 Wild Type – 350
Tbx1	(A)TGACTGTGCTGAAGTGCATC (B)TCTTCTTGGGGCTGTAGACT (C)AGCGCAATGGCTTTTAAGGG	Roche (requires GC-rich)	Floxed (A+B): 580 Wild Type (A+B): 532 Null (A+C):415

PCR programme parameters:

Programme: AB55
1=94°C, 00:45
2=55°C, 00:45
3=72°C, 01:00
35 cycles
7min 72°C final elongation step

Programme : AB55 x 40/ AB57 x 40
(Lid=100˚C)

1	**T=95.0˚C**	**0:10:00**
2	**T=94.0˚C**	**0:00:45**
3	**T=55.0/57˚C**	**0:00:45**
4	**T=72.0˚C**	**0:01:00**
5	**GOTO 2**	**39 cycles**
6	**T=72.0˚C**	**0:07:00**
7	**HOLD 8.0˚C**	

APPENDIX B: Staining solutions

Protocol	Solution	Reagents	Storage conditions
X-gal staining	Xgal base	49.2mg K3Fe(CN)6 63mg K4Fe(CN)6 30mL PBS.	4°C, protect from light.
WMISH	Block 1	2% BBR diluted in MABT.	Store at -20°C, thaw at 65°C, cool before use.
WMISH	Block 2	2% BBR, 20% HI GS diluted in MABT.	Store at -20°C, thaw at 65°C, cool before use.
WMISH	10% Boehringer Blocking Reagent (BBR)	Add BBR to MAB, dissolve by heating in a microwave, cool before freezing.	Store at -20°C.
WMISH	Detergent mix	1% Igepal (Sigma), 1% SDS, 0.5% Sodium deoxycholate (Sigma), 50mM Tris-pH 8.2, 1mM EDTA and 150mM NaCl in DepC H_2O.	Store at RT°C.
WMISH	Hybridisation mix (50ml)	25ml Deionized formamide, 10ml 20x SSC, 1% Boehringer block, 1ml of 5%CHAPs, 50ul yeast tRNA (20mg/ml), 100µl heparin (50mg/ml), 0.5ml of 0.5M EDTA, 500ul Tween-20 (Sigma), make up to 50ml with DepC H_2O.	Store at -20°C, warm to 65°C before use.
WMISH	10x Maleic acid wash buffer pH7.5 (MAB)	11.6g maleic acid, 8.75g NaCl, 7.5g NaOH, top up with 800ml DepC H_2O and pH to 7.5 with maleic acid. Once at pH7.5, top up with DepC H_2O to 1L	Store at RT°C, dilute to 1x before use. *NB. pH can increase, after long term storage before use check pH is 7.5.*

		and autoclave.	
WMISH	MABT	Add 1% Tween-20 to 1x MAB post autoclaving.	Store at RT°C.
WMISH	NTMT (50ml)	1ml 5M NaCl, 1M 5ml Tris-HCL pH9.5, 5ml 1M MgCl2, 500µl Tween-20, 38.5ml H_2O.	Prepare no earlier than the day before signal detection and store at 4°C as CO_2 can alter the buffers pH.
WMISH	Solution X (250ml)	125ml Formamide, 25ml 20x SSC pH4.5, 25ml 10% SDS, 100ml sterile ddH_2O.	Store at RT°C, warm to 65°C before use.
Section ISH	Acetylation mix	625µl Triethaloamine (TEA SIGMA), 130µl 30% hydrochloric acid (sigma) in 50ml DepC H20, adding 125µl acetic anhydride (VWR) to the solution just prior to incubating with the slides.	Prepare on the day of ISH at RT°C.
Section ISH	Hybridisation mix (50ml).	25ml Deionized formamide, 10ml Dextran sulfate, 1ml 50x Denhardt's, 1.25ml yeast tRNA (10mg/ml), 3ml 5M NaCl, 1ml 1M Tris-HCL pH8, 500ul 0.5M EDTA, 500ul 1M Di-sodium hydrogen phosphate Dihydrate, 2.5ml 20% N-lauroylsarcosine, 11.5ml DepC H_2O.	Store at -20°C, warm to 65°C before use.
Section ISH	High Stringency Wash (HIS)	160ml H_2O, 40ml 20x SSC incubated	Make fresh each time.

	(200ml)	at 65°C overnight (at the end of day 1), add 200ml formamide just prior to use.	
Section ISH	N-lauroylsarcosine (Levamisole, Sigma)	For 25ml dilute 0.5g in 25ml of sterile ddH_2O (20mg/ml).	Store at 4°C.
Section ISH	NTMT (200ml)	5ml 5M NaCl, 10ml 1M Tris-HCL pH9.5, 20ml 1M $MgCl_2$, 200µl Tween-20, 2ml Levamisole, sterile ddH_2O to bring volume to 200ml.	Prepare no earlier than the day before signal detection and store at 4°C as CO_2 can alter the buffers pH.
Section ISH	RNase buffer (1L)	100ml 5M NaCl, 10ml 1M TRIS-HCL pH7.5, 10ml 0.5M EDTA. pH8.0 in 880ml H20.	Store at RT°C, incubate at 37°C prior to use.
Section ISH	Saline-sodium citrate buffer (SCC)	Dilute 20X SSC (Fisher) to 5x, 2x and 0.1x SSC with sterile ddH_2O.	Store at RT°C. At the end of day 1 incubate 5xSSC at 65°C, 2x and 0.1x SSC at 37°C.
IHC	0.5% PBT	As for PBT, (see 2.1) but add 0.5% Tween-20.	Store at RT°C.
IHC	Wax blocking solution (*)	10%GS in PBT_2	Store aliquots at -20°C.
IHC	Wax Primary/secondary antibody diluent (*)	5%GS in PBT_2	Store aliquots at -20°C.
IHC	Cryosection blocking solution (*)	10% GS, 0.5% bovine albumin serum (BSA, Sigma) in PBT.	Store aliquots at -20°C.
IHC	Cryosection Primary/secondary antibody diluent (*)	5% GS, 0.5% bovine albumin serum (BSA, Sigma) in PBT	Store aliquots at -20°C.
IHC	100mM sodium citrate		

APPENDIX C: Antibody suppliers and the dilutions used during IHC

Antibody	Company (Product No.)	Dilution
Cofilin	Sigma (C8736)	1:100
Dapi-Hoechst 33342	Invitrogen (H3570 / 23363w)	1:50,000
E-Cadherin (clone 36)	Fitzgerald (RDI-ECADHERabm)	1:200
Laminin	RDI (RDI-PRO10765)	1:100
Myosin light chain phoso-s19	GeneTex (GTX24720)	1:100
Phalloidin	Life technologies (Invitrogen) A12379	1:250
Phospho-Histone H3	Cell-signalling (9701)	1:250
Alex Fluor 568/546/488 secondary antibodies	Life technologies (Invitrogen)	All 1:250

APPENDIX D: Probes

Gene	Linearizing enzyme for antisense probes	Polymerases enzyme for antisense probes	Insert size (bp)	Reference
Bmp4	AccI	T7	1550	Unknown
Cyp26a1	Kpn1	T7	1500	Akira Imamoto
Cyp26b1	Kpn1	T3	1600	Akira Imamoto
Cyp26c1	EcoRI	T7	1000	Pete Scambler
Fgf10	BamHI RV (FL) NcoI (short)	T3 T7 (FL) Sp6 (short)		UGA
Fgf15	NotI	T7	806	John R. McWhirter
Fgf3	HindIII	T7	1000	Peters et al, Dev.Bio, 155: 423-443
Fgf8 (exon2,3)	XhoI	T7	266	Elaine Storm
Fgf8	BamHI	T7	875	Crossley and Martin, 1995 Development 121:439-451
Foxn1	AccIII	T3	1120	N. Manly
Gcm2	NcoI	SP6	926	N. Manly
Gli1	NotI	T3	1600	Harland Lab
Hoxa2	EcoRI	T7	300	Unknown
Hoxa3	XhoI	T3	650	N.Manley
Hoxb1	XbaI	T7	300	Akira Imamoto
Erm	HindIII	T3		Hippenmeyer et al.
Spry1	EcoRI	T7	1500	Minowada/G.Martin
Spry2	SacII	T3	1500	Minowada/G.Martin
Shh	EcoRI	T7	1600	Epstein, McMahon
Pea3	ApaI	SP6	500	Unknown
Pax1	XbaI	T3		Deutsch et al Cell 53:617- (1988) from N. Manley
Ptc1	BamHI	T3	841	GRM131
Raldh2	EcoRI	T3	468	Akira Imamoto (P.Dolle)
Rarb	EcoRI	T3	620	Akira Imamoto

APPENDIX E: Mouse lines utilised as tools in this thesis

Nomenclature (symbol)	MGI ID	Abbreviated Alleles	Description	Reference
Fibroblast growth factor 8; targeted mutation 1.3, Gail R Martin (Fgf8$^{tm1.3Mrt}$)	MGI:2150347	*Fgf8$^{flox/flox}$*	Double homozygous for conditional (floxed) *Fgf8* alleles	Meyers et al (1998) *Nat Genet* 18:136-41
Fibroblast growth factor receptor 1; targeted mutation 3, Chu-Xia Deng (Fgfr1^{tm3Cxd})	MGI:2181471	*Fgfr1$^{flox/flox}$*	Double homozygous for conditional (floxed) Fgfr1 alleles	Xu et al (2002) *Genesis* 32: 85-86
Fibroblast growth factor receptor 2; targeted mutation 1.1, David M Ornitz (Fgfr2$^{tm1.1Dor}$)	MGI:3044427	*Fgfr2$^{flox/flox}$*	Double homozygous for conditional Fgfr2flox alleles	Yu et al (2003) *Development* 130:3063-74
Mesoderm posterior 1; targeted mutation 2, Yumiko Saga (Mesp1$^{tm2(cre)Ysa}$)	MGI:2176467	*Mesp1$^{Cre/+}$*	Cre transgene expressed under control of *Mesp1* (core mesoderm-specific expression).	Saga et al (1999) *Development* 126:3437-47
Gene trap ROSA 26, Philippe Soriano; targeted mutation 1, Philippe Soriano (Gt(ROSA)26Sor^{tm1Sho})	MGI:1861932	*R26R^{2}*	Double homozygous for the Rosa26 lacZ Cre reporter allele	Soriano (1999) *Nat Genet* 21:70-71
Gene trap ROSA 26, Philippe Soriano; targeted mutation 1.1, Frank Costantini (Gt(ROSA)26Sor$^{tm1.1(EYFP)Cos}$)	MGI:2449041	*Rosa-YFP^{2}*	Double homozygous for the Rosa26 eYFP Cre reporter allele.	Srinivas et al (2001) *BMC Dev Biol* 1:4
Sprouty homolog 1 (Drosophila); targeted mutation 1, Jonathan D Licht (Spry1^{tm1Jdli})	MGI:3574403	*Spry1$^{flox/flox}$*	Conditional (floxed) *Spry1* allele.	Basson et al (2005) *Dev Cell* 8:229-239
Sprouty homolog 2 (Drosophila); targeted mutation 1.1, Gail R Martin (Spry2$^{tm1.1Mrt}$)	MGI:3578633	*Spry2$^{flox/flox}$*	Conditional (floxed) *Spry2* allele.	Shim et al (2005) *Dev Cell* 8: 553-564
SRY-box containing gene 17; targeted mutation 2.1, Heiko Lickert (Sox17$^{tm2.1(icre)Heli}$)	MGI:4418897	*Sox17$^{2A-icre/+}$*	A knock in of a cre transgene (precede by the self cleaving viral peptide 2A) expressed under control of *Sox17* (endoderm and endothelial cell specific expression).	Engert et al (2009) *Genesis* 47(9): 603-10
T-box 1; targeted mutation 1.1, Bernice E Morrow (Tbx1$^{tm1.1Bem}$)	MGI:3619149	*Tbx1$^{flox/flox}$*	Double homozygous for the conditional *Tbx1* (floxed) allele.	Arnold et al (2006) *Development* 133:977-87
Transgene insertion 10, David H Rowitch (Tg(Wnt1-cre/Esr1)10Rth)*	MGI:2447684	*Wnt1$^{Cre/+}$*	Cre transgene expressed under control of *Wnt1* (neural crest-specific expression).	Danielian et al (1998) *Curr Biol* 8:1323-1326

References

Abu-Issa, R., Smyth, G., Smoak, I., Yamamura, K., Meyers, E, N, (2002) 'Fgf8 is required for pharyngeal arch and cardiovascular development in the mouse', *Development* 129(1): 4613-4625.

Aggarwal, V. S., Carpenter, C., Freyer, L., Liao, J., Petti, M. and Morrow, B. E. (2010) 'Mesodermal Tbx1 is required for patterning the proximal mandible in mice', *Dev Biol* 344(2): 669-81.

Aggarwal, V. S., Liao, J., Bondarev, A., Schimmang, T., Lewandoski, M., Locker, J., Shanske, A., Campione, M. and Morrow, B. E. (2006) 'Dissection of Tbx1 and Fgf interactions in mouse models of 22q11DS suggests functional redundancy', *Hum Mol Genet* 15(21): 3219-28.

Agulnik, S. I., Garvey, N., Hancock, S., Ruvinsky, I., Chapman, D. L., Agulnik, I., Bollag, R., Papaioannou, V. and Silver, L. M. (1996) 'Evolution of mouse T-box genes by tandem duplication and cluster dispersion', *Genetics* 144(1): 249-54.

Alasti, F. and Van Camp, G. (2009) 'Genetics of microtia and associated syndromes', *J Med Genet* 46(6): 361-9.

Alexander, T., Nolte, C. and Krumlauf, R. (2009) 'Hox genes and segmentation of the hindbrain and axial skeleton', *Annu Rev Cell Dev Biol* 25: 431-56.

Arber, S., Barbayannis, F. A., Hanser, H., Schneider, C., Stanyon, C. A., Bernard, O. and Caroni, P. (1998) 'Regulation of actin dynamics through phosphorylation of cofilin by LIM-kinase', *Nature* 393(6687): 805-9.

Arman, E., Haffner-Krausz, R., Chen, Y., Heath, J. K. and Lonai, P. (1998) 'Targeted disruption of fibroblast growth factor (FGF) receptor 2 suggests a role for FGF signalling in pregastrulation mammalian development', *Proc Natl Acad Sci U S A* 95(9): 5082-7.

Arnold, J. S., Werling, U., Braunstein, E. M., Liao, J., Nowotschin, S., Edelmann, W., Hebert, J. M. and Morrow, B. E. (2006) 'Inactivation of Tbx1 in the pharyngeal endoderm results in 22q11DS malformations', *Development* 133(5): 977-87.

Bach, I. (2000) 'The LIM domain: regulation by association', *Mech Dev* 91(1-2): 5-17.

Badertscher, J. A. (1915) 'The development of the thymus in the pig. I. Morphogenesis.', *Am. J Anat.,* 17: 317-337.

Bajaj, Y., Tweedie, D., Ifeacho, S., Hewitt, R. and Hartley, B. E. (2011) 'Surgical technique for excision of first branchial cleft anomalies: how we do it', *Clin Otolaryngol* 36(4): 371-4.

Bajolle, F., Zaffran, S., Kelly, R. G., Hadchouel, J., Bonnet, D., Brown, N. A. and Buckingham, M. E. (2006) 'Rotation of the myocardial wall of the outflow tract is implicated in the normal positioning of the great arteries', *Circ Res* 98(3): 421-8.

Balczerski, B., Matsutani, M., Castillo, P., Osborne, N., Stainier, D. Y. and Crump, J. G. (2012) 'Analysis of sphingosine-1-phosphate signalling mutants reveals endodermal requirements for the growth but not dorsoventral patterning of jaw skeletal precursors', *Dev Biol* 362(2): 230-41.

Baldini, A. (2005) 'Dissecting contiguous gene defects: TBX1', *Curr Opin Genet Dev* 15(3): 279-84.

Baldini, A. (2006) 'The 22q11.2 deletion syndrome: a gene dosage perspective', *ScientificWorldJournal* 6: 1881-7.

Barnfield, P. C., Zhang, X., Thanabalasingham, V., Yoshida, M. and Hui, C. C. (2005) 'Negative regulation of Gli1 and Gli2 activator function by Suppressor of fused through multiple mechanisms', *Differentiation* 73(8): 397-405.

Bayha, E., Jorgensen, M. C., Serup, P. and Grapin-Botton, A. (2009) 'Retinoic acid signalling organizes endodermal organ specification along the entire anterio-posterior axis', *PLoS One* 4(6): e5845.

Beachy, P. A., Cooper, M. K., Young, K. E., von Kessler, D. P., Park, W. J., Hall, T. M., Leahy, D. J. and Porter, J. A. (1997) 'Multiple roles of cholesterol in hedgehog protein biogenesis and signalling', *Cold Spring Harb Symp Quant Biol* 62: 191-204.

Beenken, A., Eliseenkova, A. V., Ibrahimi, O. A., Olsen, S. K. and Mohammadi, M. (2012) 'Plasticity in interactions of fibroblast growth factor 1 (FGF1) N terminus with FGF receptors underlies promiscuity of FGF1', *J Biol Chem* 287(5): 3067-78.

Begbie, J., Brunet, J. F., Rubenstein, J. L. and Graham, A. (1999) 'Induction of the epibranchial placodes', *Development* 126(5): 895-902.

Begbie, J. and Graham, A. (2001) 'Integration between the epibranchial placodes and the hindbrain', *Science* 294(5542): 595-8.

Biddinger, P. W. and Ray, M. (1993) 'Distribution of C cells in the normal and diseased thyroid gland', *Pathol Annu* 28 Pt 1: 205-29.

Bimber, B., Dettman, R. W. and Simon, H. G. (2007) 'Differential regulation of Tbx5 protein expression and sub-cellular localization during heart development', *Dev Biol* 302(1): 230-42.

Birk, A. V., Dubovi, E. J., Cohen-Gould, L., Donis, R. and Szeto, H. H. (2008) 'Cytoplasmic vacuolization responses to cytopathic bovine viral diarrhoea virus', *Virus Res* 132(1-2): 76-85.

Blackburn, C. C. and Manley, N. R. (2004) 'Developing a new paradigm for thymus organogenesis', *Nat Rev Immunol* 4(4): 278-89.

Blentic, A., Chambers, D., Skinner, A., Begbie, J. and Graham, A. (2011) 'The formation of the cranial ganglia by placodally-derived sensory neuronal precursors', *Mol Cell Neurosci* 46(2): 452-9.

Brown, C. B., Wenning, J. M., Lu, M. M., Epstein, D. J., Meyers, E. N. and Epstein, J. A. (2004) 'Cre-mediated excision of Fgf8 in the Tbx1 expression domain reveals a critical role for Fgf8 in cardiovascular development in the mouse', *Dev Biol* 267(1): 190-202.

Bürglin, T. R. and Kuwabara, P. E. (2006) 'Homologs of the Hh signalling network in C. elegans', *Wormbook*: 1-14.

Burn, J., Takao, A., Wilson, D., Cross, I., Momma, K., Wadey, R., Scambler, P. and Goodship, J. (1993) 'Conotruncal anomaly face syndrome is associated with a deletion within chromosome 22q11', *J Med Genet* 30(10): 822-4.

Byrd, N. A. and Meyers, E. N. (2005) 'Loss of Gbx2 results in neural crest cell patterning and pharyngeal arch artery defects in the mouse embryo', *Dev Biol* 284(1): 233-45.

Calmont, A., Ivins, S., Van Bueren, K. L., Papangeli, I., Kyriakopoulou, V., Andrews, W. D., Martin, J. F., Moon, A. M., Illingworth, E. A., Basson, M. A. et al. (2009) 'Tbx1 controls cardiac neural crest cell migration during arch artery development by regulating Gbx2 expression in the pharyngeal ectoderm', *Development* 136(18): 3173-83.

Calmont, A., Thapar, N., Scambler, P. J. and Burns, A. J. (2011) 'Absence of the vagus nerve in the stomach of Tbx1$^{-/-}$ mutant mice', *Neurogastroenterol Motil* 23(2): 125-30.

Camarata, T., Bimber, B., Kulisz, A., Chew, T. L., Yeung, J. and Simon, H. G. (2006) 'LMP4 regulates Tbx5 protein subcellular localization and activity', *J Cell Biol* 174(3): 339-48.

Carey, A. H., Roach, S., Williamson, R., Dumanski, J. P., Nordenskjold, M., Collins, V. P., Rouleau, G., Blin, N., Jalbert, P. and Scambler, P. J. (1990) 'Localization of 27 DNA markers to the region of human chromosome 22q11-pter deleted in patients with the DiGeorge syndrome and duplicated in the der22 syndrome', *Genomics* 7(3): 299-306.

Carroll, S. B. (2001) 'Chance and necessity: the evolution of morphological complexity and diversity', *Nature* 409(6823): 1102-9.

Chapman, D.L, Garvey, N., Hancock, S., Alexiou, M., Agulnik, S. I., Gibson-Brown, J. J., Cebra-Thomas, J., Bollag, R.J., Silver, L.M. and Papaioannou, V.E.(1996)

'Expression of the T-box Family Genes, Tbxl-Tbx5, During Early Mouse Development', *Dev Dyn* 206(4): 379-390.

Chen, L., Fulcoli, F. G., Tang, S. and Baldini, A. (2009) 'Tbx1 regulates proliferation and differentiation of multipotent heart progenitors', *Circ Res* 105(9): 842-51.

Chen, L., Mupo, A., Huynh, T., Cioffi, S., Woods, M., Jin, C., McKeehan, W., Thompson-Snipes, L., Baldini, A. and Illingworth, E. (2010) 'Tbx1 regulates Vegfr3 and is required for lymphatic vessel development', *J Cell Biol* 189(3): 417-24.

Chiang, C., Litingtung, Y., Lee, E., Young, K. E., Corden, J. L., Westphal, H. and Beachy, P. A. (1996) 'Cyclopia and defective axial patterning in mice lacking Sonic hedgehog gene function', *Nature* 383(6599): 407-13.

Chieffo, C., Garvey, N., Gong, W., Roe, B., Zhang, G., Silver, L., Emanuel, B. S. and Budarf, M. L. (1997) 'Isolation and characterization of a gene from the DiGeorge chromosomal region homologous to the mouse Tbx1 gene', *Genomics* 43(3): 267-77.

Chu, P. H., Ruiz-Lozano, P., Zhou, Q., Cai, C. and Chen, J. (2000) 'Expression patterns of FHL/SLIM family members suggest important functional roles in skeletal muscle and cardiovascular system', *Mech Dev* 95(1-2): 259-65.

Clark, S. G., Stern, M. J. and Horvitz, H. R. (1992) 'C. elegans cell-signalling gene sem-5 encodes a protein with SH2 and SH3 domains', *Nature* 356(6367): 340-4.

Cohen, M. M., Jr. (2010) 'Hedgehog signalling update', *Am J Med Genet A* 152A(8): 1875-914.

Conway, S. J., Henderson, D. J. and Copp, A. J. (1997) 'Pax3 is required for cardiac neural crest migration in the mouse: evidence from the splotch (Sp2H) mutant', *Development* 124(2): 505-14.

Cooper, J. A. (1987) 'Effects of cytochalasin and phalloidin on actin', *J Cell Biol* 105(4): 1473-8.

Cordero, D. R., Brugmann, S., Chu, Y., Bajpai, R., Jame, M. and Helms, J. A. (2011) 'Cranial neural crest cells on the move: their roles in craniofacial development', *Am J Med Genet A* 155A(2): 270-9.

Couly, G., Creuzet, S., Bennaceur, S., Vincent, C. and Le Douarin, N. M. (2002) 'Interactions between Hox-negative cephalic neural crest cells and the foregut endoderm in patterning the facial skeleton in the vertebrate head', *Development* 129(4): 1061-73.

Crossley, P. H. and Martin, G. R. (1995) 'The mouse Fgf8 gene encodes a family of polypeptides and is expressed in regions that direct outgrowth and patterning in the developing embryo', *Development* 121(2): 439-51.

Crump, J. G., Maves, L., Lawson, N. D., Weinstein, B. M. and Kimmel, C. B. (2004) 'An essential role for Fgfs in endodermal pouch formation influences later craniofacial skeletal patterning', *Development* 131(22): 5703-16.

Culbertson, M. D., Lewis, Z. R. and Nechiporuk, A. V. (2011) 'Chondrogenic and gliogenic subpopulations of neural crest play distinct roles during the assembly of epibranchial ganglia', *PLoS One* 6(9): e24443.

Danielian, P. S., Muccino, D., Rowitch, D. H., Michael, S. K. and McMahon, A. P. (1998) 'Modification of gene activity in mouse embryos in utero by a tamoxifen-inducible form of Cre recombinase', *Curr Biol* 8(24): 1323-6.
Deng, C. X., Wynshaw-Boris, A., Shen, M. M., Daugherty, C., Ornitz, D. M. and Leder, P. (1994) 'Murine FGFR-1 is required for early postimplantation growth and axial organization', *Genes Dev* 8(24): 3045-57.

Deng, C., Wynshaw-Boris, A., Zhou, F., Kuo, A. and Leder, P. (1996) 'Fibroblast growth factor receptor 3 is a negative regulator of bone growth', *Cell* 84(6): 911-21.

Desai, R. A., Gao, L., Raghavan, S., Liu, W. F. and Chen, C. S. (2009) 'Cell polarity triggered by cell-cell adhesion via E-cadherin', *J Cell Sci* 122(Pt 7): 905-11.

Dictionaries, O. (2011) 'Concise Oxford English Dictionary' *Concise Oxford English Dictionary*: OUP Oxford.

Diman, N. Y., Remacle, S., Bertrand, N., Picard, J. J., Zaffran, S. and Rezsohazy, R. (2011) 'A retinoic acid responsive Hoxa3 transgene expressed in embryonic pharyngeal endoderm, cardiac neural crest and a subdomain of the second heart field', *PLoS One* 6(11): e27624.

Ding, Q., Fukami, S., Meng, X., Nishizaki, Y., Zhang, X., Sasaki, H., Dlugosz, A., Nakafuku, M. and Hui, C. (1999) 'Mouse suppressor of fused is a negative regulator of sonic hedgehog signalling and alters the subcellular distribution of Gli1', *Curr Biol* 9(19): 1119-22.

Dominguez-Frutos, E., Vendrell, V., Alvarez, Y., Zelarayan, L. C., Lopez-Hernandez, I., Ros, M. and Schimmang, T. (2009) 'Tissue-specific requirements for FGF8 during early inner ear development', *Mech Dev* 126(10): 873-81.

Dooley, J., Erickson, M., LaRochelle, W. J., Gillard, G. O. and Farr, A. G. (2007) 'FGFR2IIIb signalling regulates thymic epithelial differentiation', *Dev Dyn* 236(12): 3459-71.

Dorey, K. and Amaya, E. (2010) 'FGF signalling: diverse roles during early vertebrate embryogenesis', *Development* 137(22): 3731-42.

Driscoll, D. A., Salvin, J., Sellinger, B., Budarf, M. L., McDonald-McGinn, D. M., Zackai, E. H. and Emanuel, B. S. (1993) 'Prevalence of 22q11 microdeletions in

DiGeorge and velocardiofacial syndromes: implications for genetic counselling and prenatal diagnosis', *J Med Genet* 30(10): 813-7.

Drucker, B. J. and Goldfarb, M. (1993) 'Murine FGF-4 gene expression is spatially restricted within embryonic skeletal muscle and other tissues', *Mech Dev* 40(3): 155-63.

Duester, G. (2008) 'Retinoic acid synthesis and signalling during early organogenesis', *Cell* 134(6): 921-31.

Dupe, V., Ghyselinck, N. B., Wendling, O., Chambon, P. and Mark, M. (1999) 'Key roles of retinoic acid receptors alpha and beta in the patterning of the caudal hindbrain, pharyngeal arches and otocyst in the mouse', *Development* 126(22): 5051-9.

El Omari, K., De Mesmaeker, J., Karia, D., Ginn, H., Bhattacharya, S. and Mancini, E. J. (2011) 'Structure of the DNA-bound T-box domain of human TBX1, a transcription factor associated with the DiGeorge syndrome', *Proteins* 80(2): 655-660

Engert, S., Liao, W. P., Burtscher, I. and Lickert, H. (2009) 'SOX17-2A-iCre: a knock-in mouse line expressing Cre recombinase in endoderm and vascular endothelial cells', *Genesis* 47(9): 603-10.

Fagman, H., Liao, J., Westerlund, J., Andersson, L., Morrow, B. E. and Nilsson, M. (2007) 'The 22q11 deletion syndrome candidate gene Tbx1 determines thyroid size and positioning', *Hum Mol Genet* 16(3): 276-85.

Feil, R. (2007) 'Conditional somatic mutagenesis in the mouse using site-specific recombinases', *Handb Exp Pharmacol* (178): 3-28.

Finley, J.P., Collins, G.F., de Chadarévian, J.P. and Williams, R.L. (1977) 'DiGeorge syndrome presenting as severe congenital heart disease in the newborn', *Canadian Medical Association journal* 116(6): 635-640.

Frank, D. U., Fotheringham, L. K., Brewer, J. A., Muglia, L. J., Tristani-Firouzi, M., Capecchi, M. R. and Moon, A. M. (2002) 'An Fgf8 Mouse Mutant Phenocopies Human 22q11 Deletion Syndrome.', *Development* 129(19): 4591-4603.

Franklin, V., Khoo, P. L., Bildsoe, H., Wong, N., Lewis, S. and Tam, P. P. (2008) 'Regionalisation of the endoderm progenitors and morphogenesis of the gut portals of the mouse embryo', *Mech Dev* 125(7): 587-600.

Fulcoli, F. G., Huynh, T., Scambler, P. J. and Baldini, A. (2009) 'Tbx1 regulates the BMP-Smad1 pathway in a transcription independent manner', *PLoS One* 4(6): e6049.

Galili, N., Baldwin, H. S., Lund, J., Reeves, R., Gong, W., Wang, Z., Roe, B. A., Emanuel, B. S., Nayak, S., Mickanin, C. et al. (1997) 'A region of mouse

chromosome 16 is syntenic to the DiGeorge, velocardiofacial syndrome minimal critical region', *Genome Research* 7(1): 17-26.

Gardiner, J. R., Jackson, A. L., Gordon, J., Lickert, H., Manley, N. R. and Basson, M. A. (2012) 'Localised inhibition of FGF signalling in the third pharyngeal pouch is required for normal thymus and parathyroid organogenesis', *Development* 139(18): 3456-66.

Garg, V., Yamagishi, C., Hu, T., Kathiriya, I. S., Yamagishi, H. and Srivastava, D. (2001) 'Tbx1, a DiGeorge syndrome candidate gene, is regulated by sonic hedgehog during pharyngeal arch development', *Dev Biol* 235(1): 62-73.

Goddeeris, M. M., Schwartz, R., Klingensmith, J. and Meyers, E. N. (2007) 'Independent requirements for Hedgehog signalling by both the anterior heart field and neural crest cells for outflow tract development', *Development* 134(8): 1593-604.

Gomez, C. and Pourquie, O. (2009) 'Developmental control of segment numbers in vertebrates', *J Exp Zool B Mol Dev Evol* 312(6): 533-44.

Gordon, J., Bennett, A. R., Blackburn, C. C. and Manley, N. R. (2001) 'Gcm2 and Foxn1 mark early parathyroid- and thymus-specific domains in the developing third pharyngeal pouch', *Mech Dev* 103(1-2): 141-3.

Gordon, J., Patel, S. R., Mishina, Y. and Manley, N. R. (2010) 'Evidence for an early role for BMP4 signalling in thymus and parathyroid morphogenesis', *Dev Biol* 339(1): 141-54.

Graham, A. (2001) 'The development and evolution of the pharyngeal arches', *J Anat* 199: 133-141.

Graham, A. (2003) 'Development of the pharyngeal arches', *Am J Med Genet A* 119(3): 251-256.

Graham, A., Begbie, J. and McGonnell, I. (2004) 'Significance of the cranial neural crest', *Dev Dyn* 229(1): 5-13.

Grapin-Botton, A., (2008) Endoderm specification. StemBook, ed. The Stem Cell Research Community, StemBook, doi/10.3824/stembook.1.30.1, http://www.stembook.org.

Greenberg, F. (1989) 'What defines DiGeorge anomaly?', *The Journal of Pediatrics* 115(3): 412-413.

Grevellec, A., Graham, A. and Tucker, A. S. (2011) 'SHH signalling restricts the expression of Gcm2 and controls the position of the developing parathyroids', *Dev Biol* 353(2): 194-205.

Grevellec, A. and Tucker, A. S. (2010) 'The pharyngeal pouches and clefts: Development, evolution, structure and derivatives', *Semin Cell Dev Biol* 21(3): 325-32.

Griffith, A. V., Cardenas, K., Carter, C., Gordon, J., Iberg, A., Engleka, K., Epstein, J. A., Manley, N. R. and Richie, E. R. (2009) 'Increased thymus- and decreased parathyroid-fated organ domains in Splotch mutant embryos', *Dev Biol* 327(1): 216-27.

Grifone, R., Jarry, T., Dandonneau, M., Grenier, J., Duprez, D. and Kelly, R. G. (2008) 'Properties of branchiomeric and somite-derived muscle development in Tbx1 mutant embryos', *Dev Dyn* 237(10): 3071-8.

Grigorieva, I. V. and Thakker, R. V. (2011) 'Transcription factors in parathyroid development: lessons from hypoparathyroid disorders', *Ann N Y Acad Sci* 1237: 24-38.

Groth, C. and Lardelli, M. (2002) 'The structure and function of vertebrate fibroblast growth factor receptor 1', *Int J Dev Biol* 46(4): 393-400.

Guris, D. L., Duester, G., Papaioannou, V. E. and Imamoto, A. (2006) 'Dose-dependent interaction of Tbx1 and Crkl and locally aberrant RA signalling in a model of del22q11 syndrome', *Dev Cell* 10(1): 81-92.

Hanafusa, H., Torii, S., Yasunaga, T. and Nishida, E. (2002) 'Sprouty1 and Sprouty2 provide a control mechanism for the Ras/MAPK signalling pathway', *Nat Cell Biol* 4(11): 850-8.

Haviv, L., Gillo, D., BacKOuche, F. and Bernheim-Groswasser, A. (2008) 'A cytoskeletal demolition worker: myosin II acts as an actin depolymerization agent', *J Mol Biol* 375(2): 325-30.

Haworth, K. E., Wilson, J. M., Grevellec, A., Cobourne, M. T., Healy, C., Helms, J. A., Sharpe, P. T. and Tucker, A. S. (2007) 'Sonic hedgehog in the pharyngeal endoderm controls arch pattern via regulation of Fgf8 in head ectoderm', *Dev Biol* 303(1): 244-58.

Hébert, J.M. and McConnell, S.K. (2000) 'Targeting of cre to the Foxg1 (BF-1) Locus Mediates loxP Recombination in the Telencephalon and Other Developing Head Structures', *Dev Biol* 222(2): 296-306.

Hiruma, T., Nakajima, Y. and Nakamura, H. (2002) 'Development of pharyngeal arch arteries in early mouse embryo', *J Anat* 201(1): 15-29.

Hoch, R. V. and Soriano, P. (2006) 'Context-specific requirements for Fgfr1 signalling through Frs2 and Frs3 during mouse development', *Development* 133(4): 663-73.

Holzschuh, J., Wada, N., Wada, C., Schaffer, A., Javidan, Y., Tallafuss, A., Bally-Cuif, L. and Schilling, T. F. (2005) 'Requirements for endoderm and BMP signalling in sensory neurogenesis in zebrafish', *Development* 132(16): 3731-42.

Hu, D. and Helms, J. A. (1999) 'The role of sonic hedgehog in normal and abnormal craniofacial morphogenesis', *Development* 126(21): 4873-84.

Hu, T., Yamagishi, H., Maeda, J., McAnally, J., Yamagishi, C. and Srivastava, D. (2004) 'Tbx1 regulates fibroblast growth factors in the anterior heart field through a reinforcing autoregulatory loop involving forkhead transcription factors', *Development* 131(21): 5491-502.

Hunt, P., Whiting, J., Muchamore, I., Marshall, H. and Krumlauf, R. (1991) 'Homeobox genes and models for patterning the hindbrain and branchial arches', *Dev Suppl* 1: 187-96.

Hunt, P., Gulisano, M., Cook, M., Sham, M. H., Faiella, A., Wilkinson, D., Boncinelli, E. and Krumlauf, R.. (1991 b) 'A distinct Hox code for the branchial region of the vertebrate head.', *Nature* 353(6347): 861-864.

Ilagan, R., Abu-Issa, R., Brown, D., Yang, Y. P., Jiao, K., Schwartz, R. J., Klingensmith, J. and Meyers, E. N. (2006) 'Fgf8 is required for anterior heart field development', *Development* 133(12): 2435-45.

Ingham, P. W. and McMahon, A. P. (2001) 'Hedgehog signalling in animal development: paradigms and principles', *Genes Dev* 15(23): 3059-87.

Ishikawa, S. and Ito, K. (2009) 'Plasticity and regulatory mechanisms of Hox gene expression in mouse neural crest cells', *Cell Tissue Res* 337(3): 381-91.

Itoh, N. and Ornitz, D. M. (2004) 'Evolution of the Fgf and Fgfr gene families', *Trends Genet* 20(11): 563-9.

Itoh, N. and Ornitz, D. M. (2011) 'Fibroblast growth factors: from molecular evolution to roles in development, metabolism and disease', *J Biochem* 149(2): 121-30.

Ivins, S., Lammerts van Beuren, K., Roberts, C., James, C., Lindsay, E., Baldini, A., Ataliotis, P. and Scambler, P. J. (2005) 'Microarray analysis detects differentially expressed genes in the pharyngeal region of mice lacking Tbx1', *Dev Biol* 285(2): 554-69.

Jacinto, A., Wood, W., Woolner, S., Hiley, C., Turner, L., Wilson, C., Martinez-Arias, A. and Martin, P. (2002) 'Dynamic analysis of actin cable function during Drosophila dorsal closure', *Curr Biol* 12(14): 1245-50.

Janknecht, R., Monte, D., Baert, J. L. and de Launoit, Y. (1996) 'The ETS-related transcription factor ERM is a nuclear target of signalling cascades involving MAPK and PKA', *Oncogene* 13(8): 1745-54.

Jeong, Y. and Epstein, D. J. (2003) 'Distinct regulators of SHH transcription in the floor plate and notochord indicate separate origins for these tissues in the mouse node', *Development* 130(16): 3891-902.

Jerome, L. A. and Papaioannou, V. E. (2001) 'DiGeorge syndrome phenotype in mice mutant for the T-box gene, Tbx1', *Nature genet* 27 (3): 286-91.

Kadrmas, J. L. and Beckerle, M. C. (2004) 'The LIM domain: from the cytoskeleton to the nucleus', *Nat Rev Mol Cell Biol* 5(11): 920-31.

Kam, R. K., Deng, Y., Chen, Y. and Zhao, H. (2012) 'Retinoic acid synthesis and functions in early embryonic development', *Cell Biosci* 2(1): 11.

Kaufman, M. H. (1992) *The Atlas of Mouse Development* United States, San Diego: Elsevier Science Publishing Co Inc.

Kelly, R. G., Brown, N. A. and Buckingham, M. E. (2001) 'The arterial pole of the mouse heart forms from Fgf10-expressing cells in pharyngeal mesoderm', *Dev Cell* 1(3): 435-40.

Kelly, R. G., Jerome-Majewska, L. A. and Papaioannou, V. E. (2004) 'The del22q11.2 candidate gene Tbx1 regulates branchiomeric myogenesis', *Hum Mol Genet* 13(22): 2829-40.

Kingsbury, B. F. (1915) 'THE DEVELOPMENT OF THE HUMAN PHARYNX', *The American Journal of Anatomy.* 18(3): 329-397.

Kirby, M. L. (2008) 'Pulmonary atresia or persistent truncus arteriosus: is it important to make the distinction and how do we do it?', *Circ Res* 103(4): 337-9.

Kirby, M. L. and Waldo, K. L. (1995) 'Neural crest and cardiovascular patterning', *Circ Res* 77(2): 211-5.

Kispert, A., Koschorz, B. and Herrmann, B. G. (1995) 'The T protein encoded by Brachyury is a tissue-specific transcription factor', *EMBO J* 14(19): 4763-72.

Kochilas, L., Merscher-Gomez, S., Lu, M. M., Potluri, V., Liao, J., Kucherlapati, R., Morrow, B. and Epstein, J. A. (2002) 'The Role of Neural Crest during Cardiac Development in a Mouse Model of DiGeorge Syndrome', *Dev Biol* 251(1): 157-166.

Korzh, V. and Grunwald, D. (2001) 'Nadine Dobrovolskaia-Zavadskaia and the dawn of developmental genetics', *Bioessays* 23(4): 365-71.

Kouhara, H., Hadari, Y. R., Spivak-Kroizman, T., Schilling, J., Bar-Sagi, D., Lax, I. and Schlessinger, J. (1997) 'A lipid-anchored Grb2-binding protein that links FGF-receptor activation to the Ras/MAPK signalling pathway', *Cell* 89(5): 693-702.

Krause, A., Zacharias, W., Camarata, T., Linkhart, B., Law, E., Lischke, A., Miljan, E. and Simon, H. G. (2004) 'Tbx5 and Tbx4 transcription factors interact with a new chicken PDZ-LIM protein in limb and heart development', *Dev Biol* 273(1): 106-20.

Krcmery, J., Camarata, T., Kulisz, A. and Simon, H. G. (2010) 'Nucleocytoplasmic functions of the PDZ-LIM protein family: new insights into organ development', *Bioessays* 32(2): 100-8.

Kusakabe, T., Hoshi, N. and Kimura, S. (2006) 'Origin of the ultimobranchial body cyst: T/ebp/Nkx2.1 expression is required for development and fusion of the ultimobranchial body to the thyroid', *Dev Dyn* 235(5): 1300-9.

Ladher, R. K., O'Neill, P. and Begbie, J. (2010) 'From shared lineage to distinct functions: the development of the inner ear and epibranchial placodes', *Development* 137(11): 1777-85.

Langston, A. W., Thompson, J. R. and Gudas, L. J. (1997) 'Retinoic acid-responsive enhancers located 3' of the Hox A and Hox B homeobox gene clusters. Functional analysis', *J Biol Chem* 272(4): 2167-75.

Lania, G., Zhang, Z., Huynh, T., Caprio, C., Moon, A. M., Vitelli, F. and Baldini, A. (2009) 'Early thyroid development requires a Tbx1-Fgf8 pathway', *Dev Biol* 328(1): 109-17.

Lee, J. J., Ekker, S. C., von Kessler, D. P., Porter, J. A., Sun, B. I. and Beachy, P. A. (1994) 'Autoproteolysis in hedgehog protein biogenesis', *Science* 266(5190): 1528-37.

Leitner, L., Shaposhnikov, D., Mengel, A., Descot, A., Julien, S., Hoffmann, R. and Posern, G. (2011) 'MAL/MRTF-A controls migration of non-invasive cells by upregulation of cytoskeleton-associated proteins', *J Cell Sci* 124(Pt 24): 4318-31.

Li, S., Edgar, D., Fassler, R., Wadsworth, W. and Yurchenco, P. D. (2003) 'The role of laminin in embryonic cell polarization and tissue organization', *Dev Cell* 4(5): 613-24.

Liao, J., Kochilas, L., Nowotschin, S., Arnold, J. S., Aggarwal, V. S., Epstein, J. A., Brown, C. M., Adams, J. and Morrow, B. E. (2004) 'Full spectrum of malformations in velocardio-facial syndrome/DiGeorge syndrome mouse models by altering Tbx1 dosage.', *Hum Mol Genet* 13(15): 1577–1585.

Liao, W. P., Uetzmann, L., Burtscher, I. and Lickert, H. (2009) 'Generation of a mouse line expressing SOX17-driven Cre recombinase with specific activity in arteries', *Genesis* 47(7): 476-83.

Lindsay, E. A., Botta, A., Jurecic, V., Carattini-Rivera, S., Cheah, Y. C., Rosenblatt, H. M., Bradley, A. and Baldini, A. (1999) 'Congenital heart disease in mice deficient for the DiGeorge syndrome region', *Nature* 401(6751): 379-83.

Lindsay, E. A. (2001) 'Chromosomal microdeletions: dissecting del22q11 syndrome', *Nat Rev Genet* 2(11): 858-68.

Lindsay, E. A., Vitelli, F., Su, H., Morishima, M., Huynh, H., Pramparo, T., Jurecic, V., Ogunrinu, G., Sutherland, H.F., Scambler, P.J., Bradley, A. and Baldini, A. (2001b) 'Tbx1 haploinsufficiency in the DiGeorge syndrome region causes aortic arch defects in mice', *Nature* 410(1): 97-101.

Liu, W., Selever, J., Wang, D., Lu, M. F., Moses, K. A., Schwartz, R. J. and Martin, J. F. (2004) 'Bmp4 signalling is required for outflow-tract septation and branchial-arch artery remodelling', *Proc Natl Acad Sci U S A* 101(13): 4489-94.

Lowenstein, E. J., Daly, R. J., Batzer, A. G., Li, W., Margolis, B., Lammers, R., Ullrich, A., Skolnik, E. Y., Bar-Sagi, D. and Schlessinger, J. (1992) 'The SH2 and SH3 domain-containing protein GRB2 links receptor tyrosine kinases to ras signalling', *Cell* 70(3): 431-42.

Macatee, T. L., Hammond, B. P., Arenkiel, B. R., Francis, L., Frank, D. U. and Moon, A. M. (2003) 'Ablation of specific expression domains reveals discrete functions of ectoderm- and endoderm-derived FGF8 during cardiovascular and pharyngeal development', *Development* 130(25): 6361-74.

Mahmood, R., Mason, I. J. and Morriss-Kay, G. M. (1996) 'Expression of Fgf-3 in relation to hindbrain segmentation, otic pit position and pharyngeal arch morphology in normal and retinoic acid-exposed mouse embryos', *Anat Embryol (Berl)* 194(1): 13-22.

Mallo, M. and Gridley, T. (1996) 'Development of the mammalian ear: coordinate regulation of formation of the tympanic ring and the external acoustic meatus', *Development* 122(1): 173-179.

Manley, N. R. and Capecchi, M. R. (1995) 'The role of Hoxa-3 in mouse thymus and thyroid development', *Development* 121(7): 1989-2003.

Manley, N. R., Selleri, L., Brendolan, A., Gordon, J. and Cleary, M. L. (2004) 'Abnormalities of caudal pharyngeal pouch development in Pbx1 knock out mice mimic loss of Hox3 paralogs', *Dev Biol* 276(2): 301-12.

Marigo, V., Davey, R. A., Zuo, Y., Cunningham, J. M. and Tabin, C. J. (1996) 'Biochemical evidence that patched is the Hedgehog receptor', *Nature* 384(6605): 176-9.

Maroon, H., Walshe, J., Mahmood, R., Kiefer, P., Dickson, C. and Mason, I. (2002) 'Fgf3 and Fgf8 are required together for formation of the otic placode and vesicle', *Development* 129(9): 2099-108.

Maroto, M., Bone, R. A. and Dale, J. K. (2012) 'Somitogenesis', *Development* 139(14): 2453-6.

Matt, N. (2003) 'Retinoic acid-induced developmental defects are mediated by RARbeta/RXR heterodimers in the pharyngeal endoderm', *Development* 130(10): 2083-2093.

McDonald-McGinn, D. M. and Sullivan, K. E. (2011) 'Chromosome 22q11.2 deletion syndrome (DiGeorge syndrome/velocardiofacial syndrome)', *Medicine (Baltimore)* 90(1): 1-18.

Meyers, E. N., Lewandoski, M. and Martin, G. R. (1998) 'An Fgf8 mutant allelic series generated by Cre- and Flp-mediated recombination', *Nat Genet* 18(2): 136-41.

Miner, J. H. and Yurchenco, P. D. (2004) 'Laminin functions in tissue morphogenesis', *Annu Rev Cell Dev Biol* 20: 255-84.

Minguillon, C. and Logan, M. (2003) 'The comparative genomics of T-box genes', *Brief Funct Genomic Proteomic* 2(3): 224-33.

Minowada, G., Jarvis, L. A., Chi, C. L., Neubüser, A., Sun, X., Hacohen, N., Krasnow, M. A. and Martin, G. R. (1999) 'Vertebrate Sprouty genes are induced by FGF signalling and can cause chondrodysplasia when overexpressed', *Development* 126(20): 4465-4475.

Miralles, F., Posern, G., Zaromytidou, A. I. and Treisman, R. (2003) 'Actin dynamics control SRF activity by regulation of its coactivator MAL', *Cell* 113(3): 329-42.

Moffat, D. B. (1959) 'Developmental changes in the aortic arch system of the rat', *Am J Anat* 105: 1-35.

Mohammadi, M., Olsen, S. K. and Goetz, R. (2005) 'A protein canyon in the FGF-FGF receptor dimer selects from an a la carte menu of heparan sulfate motifs', *Curr Opin Struct Biol* 15(5): 506-16.

Moon, A. M., Guris, D. L., Seo, J. H., Li, L., Hammond, J., Talbot, A. and Imamoto, A. (2006) 'Crkl deficiency disrupts Fgf8 signalling in a mouse model of 22q11 deletion syndromes', *Dev Cell* 10(1): 71-80.

Moore-Scott, B. A. and Manley, N. R. (2005) 'Differential expression of Sonic hedgehog along the anterior-posterior axis regulates patterning of pharyngeal pouch endoderm and pharyngeal endoderm-derived organs', *Dev Biol* 278(2): 323-35.

Moraes, F., Novoa, A., Jerome-Majewska, L. A., Papaioannou, V. E. and Mallo, M. (2005) 'Tbx1 is required for proper neural crest migration and to stabilize

spatial patterns during middle and inner ear development', *Mech Dev* 122(2): 199-212.

Moses, K. A., DeMayo, F., Braun, R. M., Reecy, J. L. and Schwartz, R. J. (2001) 'Embryonic expression of an Nkx2-5/Cre gene using ROSA26 reporter mice', *Genesis* 31(4): 176-80.

Mulay, A. V. and Watterson, K. G. (1997) 'Isolated right subclavian artery, interrupted aortic arch, and ventricular septal defect', *Ann Thorac Surg* 63(4): 1163-5.

Murone, M., Rosenthal, A. and de Sauvage, F. J. (1999) 'Sonic hedgehog signalling by the patched-smoothened receptor complex', *Curr Biol* 9(2): 76-84.

Nechiporuk, A., Linbo, T., Poss, K. D. and Raible, D. W. (2007) 'Specification of epibranchial placodes in zebrafish', *Development* 134(3): 611-23.

Nechiporuk, A., Linbo, T. and Raible, D. W. (2005) 'Endoderm-derived Fgf3 is necessary and sufficient for inducing neurogenesis in the epibranchial placodes in zebrafish', *Development* 132(16): 3717-30.

Niederreither, K. (2003) 'The regional pattern of retinoic acid synthesis by RALDH2 is essential for the development of posterior pharyngeal arches and the enteric nervous system', *Development* 130(11): 2525-2534.

Niederreither, K. and Dolle, P. (1998) 'In situ hybridization with 35S-labeled probes for retinoid receptors', *Methods Mol Biol* 89: 247-67.

Niederreither, K., McCaffery, P., Drager, U. C., Chambon, P. and Dolle, P. (1997) 'Restricted expression and retinoic acid-induced downregulation of the retinaldehyde dehydrogenase type 2 (RALDH-2) gene during mouse development', *Mech Dev* 62(1): 67-78.

Nissen, R. M. (2003) 'Zebrafish foxi one modulates cellular responses to Fgf signalling required for the integrity of ear and jaw patterning', *Development* 130(11): 2543-2554.

Nusslein-Volhard, C. and Wieschaus, E. (1980) 'Mutations affecting segment number and polarity in Drosophila', *Nature* 287(5785): 795-801.

Ohuchi, H., Hori, Y., Yamasaki, M., Harada, H., Sekine, K., Kato, S. and Itoh, N. (2000) 'FGF10 acts as a major ligand for FGF receptor 2 IIIb in mouse multi-organ development', *Biochem Biophys Res Commun* 277(3): 643-9.

Ornitz, D. M. (2000) 'FGFs, heparan sulfate and FGFRs: complex interactions essential for development', *Bioessays* 22(2): 108-12.

Ornitz, D. M. and Itoh, N. (2001) 'Fibroblast growth factors', *Genome Biol* 2(3): REVIEWS3005.

Orr-Urteger, A., Bedford, M. T., Burakova, T., Arman, E., Zimmer, Y., Yayo, A., Givol, D. and Lonai, P. (1993)' Developmental localization of the splicing alternatives of fibroblast growth factor receptor-2 (FGFR-2)', *Dev Biol* 158; 474-486.

Park, E. J., Ogden, L. A., Talbot, A., Evans, S., Cai, C. L., Black, B. L., Frank, D. U. and Moon, A. M. (2006) 'Required, tissue-specific roles for Fgf8 in outflow tract formation and remodelling', *Development* 133(12): 2419-33.

Partanen, J., Schwartz, L. and Rossant, J. (1998) 'Opposite phenotypes of hypomorphic and Y766 phosphorylation site mutations reveal a function for Fgfr1 in anteroposterior patterning of mouse embryos', *Genes Dev* 12(15): 2332-2344.

Patel, S. R., Gordon, J., Mahbub, F., Blackburn, C. C. and Manley, N. R. (2006) 'Bmp4 and Noggin expression during early thymus and parathyroid organogenesis', *Gene Expr Patterns* 6(8): 794-9.

Pepinsky, R. B., Zeng, C., Wen, D., Rayhorn, P., Baker, D. P., Williams, K. P., Bixler, S. A., Ambrose, C. M., Garber, E. A., Miatkowski, K. et al. (1998) 'Identification of a palmitic acid-modified form of human Sonic hedgehog', *J Biol Chem* 273(22): 14037-45.

Plotnikov, A. N., Hubbard, S. R., Schlessinger, J. and Mohammadi, M. (2000) 'Crystal structures of two FGF-FGFR complexes reveal the determinants of ligand-receptor specificity', *Cell* 101(4): 413-24.

Pomies, P., Macalma, T. and Beckerle, M. C. (1999) 'Purification and characterization of an alpha-actinin-binding PDZ-LIM protein that is up-regulated during muscle differentiation', *J Biol Chem* 274(41): 29242-50.

Prescott, K., Ivins, S., Hubank, M., Lindsay, E., Baldini, A. and Scambler, P. (2005) 'Microarray analysis of the Df1 mouse model of the 22q11 deletion syndrome', *Hum Genet* 116(6): 486-96.

Qiu, M., Bulfone, A., Ghattas, I., Meneses, J. J., Christensen, L., Sharpe, P. T., Presley, R., Pedersen, R. A. and Rubenstein, J. L. (1997) 'Role of the Dlx homeobox genes in proximodistal patterning of the branchial arches: mutations of Dlx-1, Dlx-2, and Dlx-1 and -2 alter morphogenesis of proximal skeletal and soft tissue structures derived from the first and second arches', *Dev Biol* 185(2): 165-184.

Quinlan, R., Gale, E., Maden, M. and Graham, A. (2002) 'Deficits in the posterior pharyngeal endoderm in the absence of retinoids', *Dev Dyn* 225(1): 54-60.

Quinlan, R., Martin, P. and Graham, A. (2004) 'The role of actin cables in directing the morphogenesis of the pharyngeal pouches', *Development* 131(3): 593-9.

Raible, F. and Brand, M. (2001) 'Tight transcriptional control of the ETS domain factors Erm and Pea3 by Fgf signalling during early zebrafish development', *Mech Dev* 107(1-2): 105-17.

Randall, V., McCue, K., Roberts, C., Kyriakopoulou, V., Beddow, S., Barrett, A. N., Vitelli, F., Prescott, K., Shaw-Smith, C., Devriendt, K. et al. (2009) 'Great vessel development requires biallelic expression of Chd7 and Tbx1 in pharyngeal ectoderm in mice', *J Clin Invest* 119(11): 3301-10.

Ray, M. K., Fagan, S. P. and Brunicardi, F. C. (2000) 'The Cre-loxP system: a versatile tool for targeting genes in a cell- and stage-specific manner', *Cell Transplant* 9(6): 805-15.

Rebustini, I. T., Patel, V. N., Stewart, J. S., Layvey, A., Georges-Labouesse, E., Miner, J. H. and Hoffman, M. P. (2007) 'Laminin alpha5 is necessary for submandibular gland epithelial morphogenesis and influences FGFR expression through beta1 integrin signalling', *Dev Biol* 308(1): 15-29.

Revest, J. M., DeMoerlooze, L. and Dickson, C. (2000) 'Fibroblast growth factor 9 secretion is mediated by a non-cleaved amino-terminal signal sequence', *J Biol Chem* 275(11): 8083-90.

Rizzoti, K. and Lovell-Badge, R. (2007) 'SOX3 activity during pharyngeal segmentation is required for craniofacial morphogenesis', *Development* 134(19): 3437-48.

Roberts, C., Ivins, S., Cook, A. C., Baldini, A. and Scambler, P. J. (2006) 'Cyp26 genes a1, b1 and c1 are down-regulated in Tbx1 null mice and inhibition of Cyp26 enzyme function produces a phenocopy of DiGeorge Syndrome in the chick', *Hum Mol Genet* 15(23): 3394-410.

Roberts, C., Ivins, S. M., James, C. T. and Scambler, P. J. (2005) 'Retinoic acid down-regulates Tbx1 expression in vivo and in vitro', *Dev Dyn* 232(4): 928-38.

Roehl, H. and Nusslein-Volhard, C. (2001) 'Zebrafish pea3 and erm are general targets of FGF8 signalling', *Curr Biol* 11(7): 503-507.

Rogers, W. M. (1927) 'The fate of the ultimobranchial body in the white rat (Mus Norvegucus Albinus)', *Am. J. Anat* 38: 349-377.

Ryan, A. K., Goodship, J. A., Wilson, D. I., Philip, N., Levy, A., Seidel, H., Schuffenhauer, S., Oechsler, H., Belohradsky, B., Prieur, M. et al. (1997) 'Spectrum of clinical features associated with interstitial chromosome 22q11 deletions: a European collaborative study', *J Med Genet* 34(10): 798-804.

Ryckebusch, L., Bertrand, N., Mesbah, K., Bajolle, F., Niederreither, K., Kelly, R. G. and Zaffran, S. (2010) 'Decreased levels of embryonic retinoic acid synthesis accelerate recovery from arterial growth delay in a mouse model of DiGeorge syndrome', *Circ Res* 106(4): 686-94.

Saga, Y., Miyagawa-Tomita, S., Takagi, A., Kitajima, S., Miyazaki, J. and Inoue, T. (1999) 'MesP1 is expressed in the heart precursor cells and required for the formation of a single heart tube', *Development* 126(15): 3437-47.

Sagai, T., Amano, T., Tamura, M., Mizushina, Y., Sumiyama, K. and Shiroishi, T. (2009) 'A cluster of three long-range enhancers directs regional SHH expression in the epithelial linings', *Development* 136(10): 1665-74.

Sai, X. and Ladher, R. K. (2008) 'FGF signalling regulates cytoskeletal remodeling during epithelial morphogenesis', *Curr Biol* 18(13): 976-81.

Santagati, F., Minoux, M., Ren, S. Y. and Rijli, F. M. (2005) 'Temporal requirement of Hoxa2 in cranial neural crest skeletal morphogenesis', *Development* 132(22): 4927-36.

Sato, A., Scholl, A. M., Kuhn, E. B., Stadt, H. A., Decker, J. R., Pegram, K., Hutson, M. R. and Kirby, M. L. (2011) 'FGF8 signalling is chemotactic for cardiac neural crest cells', *Dev Biol* 354(1): 18-30.

Sauka-Spengler, T. and Bronner-Fraser, M. (2008) 'A gene regulatory network orchestrates neural crest formation', *Nat Rev Mol Cell Biol* 9(7): 557-68.

Scambler, P. J. (2000) 'The 22q11 deletion syndromes', *Hum Mol Genet* 9(16): 2421-6.

Scambler, P. J. (2010) '22q11 deletion syndrome: a role for TBX1 in pharyngeal and cardiovascular development', *Pediatr Cardiol* 31(3): 378-90.

Scholpp, S. and Brand, M. (2004) 'Endocytosis controls spreading and effective signalling range of Fgf8 protein', *Curr Biol* 14(20): 1834-41.

Serbedzija, G. N., Bronner-Fraser, M. and Fraser, S. E. (1992) 'Vital dye analysis of cranial neural crest cell migration in the mouse embryo', *Development* 116(2): 297-307.

Sharrocks, A. D. (2001) 'The ETS-domain transcription factor family', *Nat Rev Mol Cell Biol* 2(11): 827-37.

Shen, J., Dahmann, C. and Pflugfelder, G. O. (2010) 'Spatial discontinuity of optomotor-blind expression in the Drosophila wing imaginal disc disrupts epithelial architecture and promotes cell sorting', *BMC Dev Biol* 10: 23.

Shprintzen, R. J., Goldberg, R. B., Young, D. and Wolford, L. (1981) 'The velo-cardio-facial syndrome: a clinical and genetic analysis', *Pediatrics* 67(2): 167-72.

Simrick, S., Szumska, D., Gardiner, J. R., Jones, K., Sagar, K., Morrow, B., Bhattacharya, S. and Basson, M. A. (2012) 'Biallelic expression of Tbx1 protects

the embryo from developmental defects caused by increased receptor tyrosine kinase signalling', *Dev Dyn* 241(8): 1310-24.

Stone, D. M., Hynes, M., Armanini, M., Swanson, T. A., Gu, Q., Johnson, R. L., Scott, M. P., Pennica, D., Goddard, A., Phillips, H. et al. (1996) 'The tumour-suppressor gene patched encodes a candidate receptor for Sonic hedgehog', *Nature* 384(6605): 129-34.

Sun, X., Meyers, E. N., Lewandoski, M. and Martin, G. R. (1999) 'Targeted disruption of Fgf8 causes failure of cell migration in the gastrulating mouse embryo', *Genes Dev* 13(14): 1834-46.

Sutherland, H. F., Kim, U. J. and Scambler, P. J. (1998) 'Cloning and comparative mapping of the DiGeorge syndrome critical region in the mouse', *Genomics* 52(1): 37-43.

Takabatake, Y., Takabatake, T., Sasagawa, S. and Takeshima, K. (2002) 'Conserved expression control and shared activity between cognate T-box genes Tbx2 and Tbx3 in connection with Sonic hedgehog signalling during Xenopus eye development', *Dev Growth Differ* 44(4): 257-71.

Takeuchi, H., Yokota, A., Ohoka, Y. and Iwata, M. (2011) 'Cyp26b1 regulates retinoic acid-dependent signals in T cells and its expression is inhibited by transforming growth factor-beta', *PLoS One* 6(1): e16089.

Takeuchi, J. K. (2003) 'Tbx5 and Tbx4 trigger limb initiation through activation of the Wnt/Fgf signalling cascade', *Development* 130(12): 2729-2739.

Tamarin, A. and Boyde, A. (1977) 'Facial and visceral arch development in the mouse embryo: a study by scanning electron microscopy', *J Anat* 124(Pt 3): 563-80.

Tekin, M., Ozturkmen Akay, H., Fitoz, S., Birnbaum, S., Cengiz, F. B., Sennaroglu, L., Incesulu, A., Yuksel Konuk, E. B., Hasanefendioglu Bayrak, A., Senturk, S. et al. (2008) 'Homozygous FGF3 mutations result in congenital deafness with inner ear agenesis, microtia, and microdontia', *Clin Genet* 73(6): 554-65.{Tekin, 2008 #189}

Theveniau-Ruissy, M., Dandonneau, M., Mesbah, K., Ghez, O., Mattei, M. G., Miquerol, L. and Kelly, R. G. (2008) 'The del22q11.2 candidate gene Tbx1 controls regional outflow tract identity and coronary artery patterning', *Circ Res* 103(2): 142-8.

Thisse, B. and Thisse, C. (2005) 'Functions and regulations of fibroblast growth factor signalling during embryonic development', *Dev Biol* 287(2): 390-402.

Tickle, C. (2006) 'Making digit patterns in the vertebrate limb', *Nat Rev Mol Cell Biol* 7(1): 45-53.

Trainor, P. A., Ariza-McNaughton, L. and Krumlauf, R. (2002) 'Role of the isthmus and FGFs in resolving the paradox of neural crest plasticity and prepatterning', *Science* 295(5558): 1288-91.

Trainor, P. A. and Krumlauf, R. (2001) 'Hox genes, neural crest cells and branchial arch patterning', *Curr Opin Cell Biol* 13(6): 698-705.

Tremblay, K. D. and Zaret, K. S. (2005) 'Distinct populations of endoderm cells converge to generate the embryonic liver bud and ventral foregut tissues', *Dev Biol* 280(1): 87-99.

Trokovic, N., Trokovic, R., Mai, P. and Partanen, J. (2003) 'Fgfr1 regulates patterning of the pharyngeal region', *Genes Dev* 17(1): 141-53.

Trokovic, N., Trokovic, R. and Partanen, J. (2005) 'Fibroblast growth factor signalling and regional specification of the pharyngeal ectoderm', *Int J Dev Biol* 49(7): 797-805.

Trumpp, A., Depew, M. J., Rubenstein, J. L., Bishop, J. M. and Martin, G. R. (1999) 'Cre-mediated gene inactivation demonstrates that FGF8 is required for cell survival and patterning of the first branchial arch', *Genes Dev* 13(23): 3136-48.

Tulin, S. and Stathopoulos, A. (2010) 'Analysis of Thisbe and Pyramus functional domains reveals evidence for cleavage of Drosophila FGFs', *BMC Dev Biol* 10: 83.

Tumpel, S., Wiedemann, L. M. and Krumlauf, R. (2009) 'Hox genes and segmentation of the vertebrate hindbrain', *Curr Top Dev Biol* 88: 103-37.

Tzahor, E. and Evans, S. M. (2011) 'Pharyngeal mesoderm development during embryogenesis: implications for both heart and head myogenesis', *Cardiovasc Res* 91(2): 196-202.

Veitch, E., Begbie, J., Schilling, T. F., Smith, M. M. and Graham, A. (1999) 'Pharyngeal arch patterning in the absence of neural crest', *Curr Biol* 9(24): 1481-4.

Vermot, J., Niederreither, K., Garnier, J. M., Chambon, P. and Dolle, P. (2003) 'Decreased embryonic retinoic acid synthesis results in a DiGeorge syndrome phenotype in newborn mice', *Proc Natl Acad Sci U S A* 100(4): 1763-8.

Vesterhus, P., Eide, J., Froland, S. S., Haneberg, B. and Jacobsen, K. B. (1975) 'Case report: maldescent of the thymus in a hypoparathyroid infant with Pharyngeal Pouch Syndrome', *Acta Paediatr Scand* 64(3): 555-8.

Vincentz, J. W., McWhirter, J. R., Murre, C., Baldini, A. and Furuta, Y. (2005) 'Fgf15 is required for proper morphogenesis of the mouse cardiac outflow tract', *Genesis* 41(4): 192-201.

Vitelli, F., Morishima, M., Taddei, I., Lindsay, E.A. and Baldini, A. (2002) 'Tbx1 mutation causes multiple cardiovascular defects and disrupts neural crest and cranial nerve migratory pathways', *Hum Mol Genet* 11(8): 915–922.

Vitelli, F., Taddei, I., Morishima, M., Meyers, E. N., Lindsay, E. A and Baldini, A. (2002b) 'A genetic link between Tbx1 and fibroblast growth factor signalling', *Development* 129(19): 4605-4611.

Vitelli, F., Zhang, Z., Huynh, T., Sobotka, A., Mupo, A. and Baldini, A. (2006) 'Fgf8 expression in the Tbx1 domain causes skeletal abnormalities and modifies the aortic arch but not the outflow tract phenotype of Tbx1 mutants', *Dev Biol* 295(2): 559-570.

Vitelli, F., Lania, G., Huynh, T. and Baldini, A. (2010) 'Partial rescue of the Tbx1 mutant heart phenotype by Fgf8: genetic evidence of impaired tissue response to Fgf8', *J Mol Cell Cardiol* 49(5): 836-40.

Waldo, K. L., Kumiski, D. H., Wallis, K. T., Stadt, H. A., Hutson, M. R., Platt, D. H. and Kirby, M. L. (2001) 'Conotruncal myocardium arises from a secondary heart field', *Development* 128(16): 3179-88.

Wallin, J., Eibel H, Neubüser A, Wilting J, Koseki H, Balling R. (1996) 'Pax1 is expressed during development of the thymus epithelium and is required for normal T-cell maturation.', *Development* 122(1): 23-30.

Walshe, J., Maroon, H., McGonnell, I. M., Dickson, C. and Mason, I. (2002) 'Establishment of hindbrain segmental identity requires signalling by FGF3 and FGF8', *Curr Biol* 12(13): 1117-23.

Walshe, J. and Mason, I. (2000) 'Expression of FGFR1, FGFR2 and FGFR3 during early neural development in the chick embryo.', *Mech Dev* 90(1): 103-10.

Wang, F., Kan, M., Xu, J., Yan, G. & McKeehan, W. L. (1995) 'Ligand-specific structural domains in the fibroblast growth factor receptor.'
J. Biol . Chem. 270: 10222–10230

Watanabe, Y., Miyagawa-Tomita, S., Vincent, S. D., Kelly, R. G., Moon, A. M. and Buckingham, M. E. (2010) 'Role of mesodermal FGF8 and FGF10 overlaps in the development of the arterial pole of the heart and pharyngeal arch arteries', *Circ Res* 106(3): 495-503.

Wendling, O. D. C., Chambon, P. and Mark, M. (2000) 'Retinoid signalling is essential for patterning the endoderm of the third and fourth pharyngeal arches.', *Development* 127(8): 1553-15562.

Wilson, D. I., Burn, J., Scambler, P. and Goodship, J. (1993) 'DiGeorge syndrome: part of CATCH 22', *J Med Genet* 30(10): 852-6.

Wurdak, H., Ittner, L. M. and Sommer, L. (2006) 'DiGeorge syndrome and pharyngeal apparatus development', *Bioessays* 28(11): 1078-86.

Xu, H., Cerrato, F. and Baldini, A. (2005) 'Timed mutation and cell-fate mapping reveal reiterated roles of Tbx1 during embryogenesis, and a crucial function during segmentation of the pharyngeal system via regulation of endoderm expansion', *Development* 132(19): 4387-95.

Xu, H., Morishima, M., Wylie, J. N., Schwartz, R. J., Bruneau, B. G., Lindsay, E. A. and Baldini, A. (2004) 'Tbx1 has a dual role in the morphogenesis of the cardiac outflow tract', *Development* 131(13): 3217-27.

Yamagishi, C., Yamagishi, H., Maeda, J., Tsuchihashi, T., Ivey, K., Hu, T. and Srivastava, D. (2006) 'Sonic hedgehog is essential for first pharyngeal arch development', *Pediatr Res* 59(3): 349-54.

Yamagishi, H., Maeda, J., Hu, T., McAnally, J., Conway, S. J., Kume, T., Meyers, E. N., Yamagishi, C. and Srivastava, D. (2003) 'Tbx1 is regulated by tissue-specific forkhead proteins through a common Sonic hedgehog-responsive enhancer', *Genes Dev* 17(2): 269-81.

Yamagishi, H. and Srivastava, D. (2003b) 'Unraveling the genetic and developmental mysteries of 22q11 deletion syndrome',*TRENDS in Molecular Medicine* 9(9): 383-389.

Yamaguchi, T. P., Harpal, K., Henkemeyer, M. and Rossant, J. (1994) 'Fgfr-1 is required for embryonic growth and mesodermal patterning during mouse gastrulation', *Genes Dev* 8(24): 3032-44.

Yeh, B. K., Igarashi, M., Eliseenkova, A. V., Plotnikov, A. N., Sher, I., Ron, D., Aaronson, S. A. and Mohammadi, M. (2003) 'Structural basis by which alternative splicing confers specificity in fibroblast growth factor receptors', *Proc Natl Acad Sci U S A* 100(5): 2266-71.

Zhang, Z., Cerrato, F., Xu, H., Vitelli, F., Morishima, M., Vincentz, J., Furuta, Y., Ma, L., Martin, J. F., Baldini, A. and Lindsay, E. A. (2005) 'Tbx1 expression in pharyngeal epithelia is necessary for pharyngeal arch artery development', *Development* 132(23): 5307-15.

Zhang, Z, Huynh, T. and Baldini, A. (2006) 'Mesodermal expression of Tbx1 is necessary and sufficient for pharyngeal arch and cardiac outflow tract development.', *Development* 133(18): 3587–3595.

Zhu, X., Komiya, H., Chirino, A., Faham, S., Fox, G. M., Arakawa, T., Hsu, B. T. and Rees, D. C. (1991) 'Three-dimensional structures of acidic and basic fibroblast growth factors', *Science* 251(4989): 90-3.

Zorn, A. M. and Wells, J. M. (2009) 'Vertebrate endoderm development and organ formation', *Annu Rev Cell Dev Biol* 25: 221-51.

Zou, D., Silvius, D., Davenport, J., Grifone, R., Maire, P. and Xu, P. X. (2006) 'Patterning of the third pharyngeal pouch into thymus/parathyroid by Six and Eya1', *Dev Biol* 293(2): 499-512.